ON THERMAL TRANSPORT BY PHONONS IN BULK AND NANOSTRUCTURED SEMICONDUCTOR MATERIALS

Ph.D. Thesis

A dissertation submitted in satisfaction of the requirements for the degree of Doctor in Physics in the Postgraduate School of the

Universitat Autònoma de Barcelona

at the

Department of Physics

15th September 2014

by

Carla de Tomás Andrés

under the direction of

Dr. Francesc Xavier Àlvarez Calafell

and

Dr. Andrés Cantarero Sáez

Agradecimientos Durante estos tres años de doctorado se ha acumulado un gran numero de personas que, directa o indirectamente, han colaborado en la culminación de este trabajo, y por lo cuál les estoy muy agradecida. En primer lugar quiero agradecer a mis directores de tesis Xavier Àlvarez y Andrés Cantarero su dedicación, su implicación, la confianza que han depositado en mi, y su aporte imprescindible de "Física" sin la cuál este trabajo no habría visto la luz. En segundo lugar, quiero dar las gracias a todos los profesores del Grupo de Física Estadística porque en tres aos me ha dado tiempo de llamar a sus puertas con alguna pregunta muchas veces, y en especial, quiero darle las gracias a David Jou, porque tanto la cuantía de su ayuda como su calidez humana han sido inestimables desde principio. También doy las gracias al grupo de Nanomateriales de la UAB, en especial a Javier Rodríguez, por su implicación en el proyecto y su paciencia con los teóricos. A Miguel Muñoz Rojo del Instituto de Microelectrónica de Madrid, por su colaboración con las simulaciones de bismuto de telurio, sin su ayuda y sus sugerencias el Capítulo 7 estaría incompleto. A Dan Blake del Servei de Llenguas de la UAB, por revisar el manuscrito en inglés. A mi hermano Ignacio de Tomás por el diseo de la portada. Gracias a Dani Möller, que ha sido mi compaero de faenas y además, su maestría informática le ha valido para que reclamase muchas veces su tiempo, sin su ayuda, aún estaría lidiando con algún error de Gnuplot. Thanks to Sweta Banshali for being not only a Ph.D. colleague, but a true friend. Fuera del ámito científico quiero agradecer a Anna Soler sus cuidados y su ayuda en el día a día, a Graziella Vernetti y a Eugenia y Pep porque ofrecerme un hogar durante mi primera etapa de doctorante nómada. A Alexandre tengo tantas cosas que agradecerle, que simplemente, gracias por todo. Y finalmente quiero agradecer a mis padres y mis abuelos el cariño y el apoyo que me han brindado desde el otro lado de la Península.

Este trabajo ha sido posible gracias a la financiación del Ministerio de Innovacion y Ciencia a través de los proyectos NanoTHERM CSD2010-00044 y FIS2009-13370-C02-01, y de la Direcció General de Recerca de la Generalitat de Catalunya a través del proyecto 2009-SGR00164.

RESUMEN

La presente tesis doctoral versa sobre el transporte de calor llevado a cabo por los fonones en sólidos cristalinos semiconductores. La motivación de este trabajo es doble. En primer lugar, se pretende contribuir a entender mejor cómo funciona el transporte de calor a distintas escalas de tamaño: desde semiconductores con tamaño bulk (del orden de milímetros o mayores) hasta semiconductores nano-estructurados, como por ejemplo nanocables o láminas finas, cuyos tamaños característicos están en la escala nanométrica. La intención es describir dicho transporte de calor en estas escalas en un amplio rango de temperaturas, prestando especial atención a las colisiones entre fonones, pues son la causa intrínseca de la propagación del calor en los sólidos cristalinos semiconductores. En segundo lugar, se pretende mejorar la capacidad de predicción a la hora de describir el comportamiento de la conductividad térmica de los semiconductores más comunes por su implicación en procesos termoeléctricos, como son el silicio, el diamante, el germanio y el bismuto de telurio.

Para lograr alcanzar estos objetivos, es necesario formular un nuevo modelo que nos permita superar las dificultades asociadas a los modelos ya existentes, con el objetivo de cumplir dos condiciones muy deseables. Por un lado, obtener una expresión general para la conductividad térmica válida para diferentes materiales, que pueda ser aplicada a muestras de dichos materiales con diferentes composiciones isotópicas, diferentes tamaños (desde la macro hasta la nano-escala) y con diferentes geometrías. Por otro lado, dicha expresión deberá tener el menor número posible de parámetros ajustables para asegurar la fiabilidad del modelo. La potencialidad de dicho modelo radicaría en servir como herramienta a la hora de guiar el diseño de dispositivos termoeléctricos más eficientes.

La presente tesis se organiza en 8 capítulos ordenados de la siguiente manera:

En el capítulo 1 se contextualiza el tema en el que está enmarcado el presente trabajo de investigación y se presentan los conceptos físicos necesarios para trabajar con el transporte fonónico. En el segundo capítulo se desarrolla la dinámica de la red para los distintos materiales que serán objeto de estudio en el presente trabajo, en particular se aplica el modelo Bond-charge para obtener las relaciones de dispersión y la densidad de estados de los semiconductores del grupo IV (silicio, germanio, diamante y estaño gris) y análogamente se aplica el modelo Rigid-ion sobre el bismuto de telurio para obtener sus relaciones de

dispersión y densidad de estados. Los tiempos de relajación apropiados para dichos materiales se discutirán en detalle en el capítulo 3, proponiendo nuevas expresiones empíricas para describir las interacciones fonón-fonón. En el capítulo 4 se introducen y discuten los modelos de conductividad térmica más representativos de la literatura y a continuación se presenta un nuevo modelo para predecir la conductividad térmica: el modelo Kinetic-collective, cuya principal característica consiste en interpretar el transporte de calor en dos regímenes diferentes, el primero de ellos de tipo cinético donde los fonones son tratados como partículas libres y el segundo de tipo colectivo donde todos los fonones que participan en el transporte pierden su individualidad y se comportan como una colectividad de partículas. En el capítulo 5 el modelo Kinetic-collective se aplica a silicio bulk con diferentes composiciones isotópicas, y a varias muestras de silicio nanoestructuradas con diferentes geometrías y tamaños efectivos. Se obtienen predicciones de la conductividad térmica en un amplio intervalo de temperaturas que concuerdan satisfactoriamente con las medidas experimentales y se discuten diversos aspectos novedosos sobre el transporte fonónico. En el capítulo 6 el modelo Kinetic-collective se aplica al resto de materiales componentes del grupo IV de semiconductores y se obtiene una relación teórica que nos permite predecir los valores de los parámetros libres asociados a los tiempos de relajación de dichos materiales y así poder predecir sus conductividades térmicas sin la necesidad de añadir nuevos parámetros. En el capítulo 7 vamos un paso más allá y aplicamos el modelo a bismuto de telurio, obteniendo predicciones de la conductividad térmica para nanocables con diferentes diámetros y discutimos los resultados en vista a posibles aplicaciones termoeléctricas. Finalmente, el capítulo 8 está dedicado a recoger las principales conclusiones de este trabajo de investigación y a indicar posibles líneas futuras de trabajo surgidas a consecuencia de los resultados obtenidos.

Contents

Introduction **15**

1 Heat transport in solids **17**

1.1 Introduction 17

1.2 Phonons I: Mechanical properties 20

1.2.1 Dispersion relations 21

1.2.2 Density of states 23

1.3 Phonons II: Thermal properties in equilibrium 26

1.3.1 Distribution function 26

1.3.2 Internal energy 27

1.3.3 Specific heat 27

1.4 Phonons III: Transport properties in local-equilibrium 29

1.4.1 Thermal conductivity in simple kinetic theory 29

1.4.2 The Boltzmann transport equation 31

1.4.3 Standard Relaxation-time approximation 33

2 Lattice dynamics **35**

2.1 General problem of Lattice Dynamics 36

2.1.1 The equation of motion and the force constants 38

2.1.2 Dynamical matrix: dispersion relations 38

2.2 Interatomic forces and Phonon dispersion relations 39

2.3 The adiabatic Bond-charge model 40

2.3.1 The diamond structure 41

2.3.2 Bond-charges in the diamond structure 45

2.3.3 Short-range interactions 45

2.3.4 Force constants 46

2.3.5 The dynamical matrix within the bond-charge model 47
2.3.6 Dispersion relations and density of states of group IV semiconductors . 48
2.4 Rigid-ion model 49
2.4.1 Crystal structure of Bi_2Te_3 52
2.4.2 Interatomic Potentials and the Dynamical matrix 52
2.4.3 Dispersion relations and density of states of Bi_2Te_3 56

3 Phonon relaxation times 59
3.1 Fermi Golden Rule 60
3.2 Phonon scattering processes 61
3.2.1 Three-phonon processes: Normal and Umklapp scattering 62
3.2.2 Mass-defect scattering 75
3.2.3 Boundary scattering and the associated size effect 78
3.3 Matthiessen rule 82

4 Thermal conductivity 85
4.1 Discussion on the approaches to solve the Boltzmann transport equation . . . 85
4.2 Relaxation-time approach: Kinetic methods 86
4.2.1 The Callaway model 87
4.2.2 Some Callaway-based models 90
4.3 Variational method 94
4.4 Note on ab-initio methods 95
4.5 Guyer-Krumhansl model 96
4.6 Kinetic-collective model: A generalization of the Guyer-Krumhansl model . . . 102
4.6.1 Resistive vs Normal scattering 103
4.6.2 Thermal conductivity regimes 104
4.6.3 Kinetic regime 104
4.6.4 Collective regime 106
4.6.5 Thermal conductivity in terms of frequency and relaxation times 107
4.6.6 Size-effects on the kinetic and collective terms 110
4.6.7 Total thermal conductivity in the Kinetic-Collective Model: a simple expression 111
4.7 Kinetic-Collective vs. Ballistic-Diffusive transport 112

5 Applying the Kinetic-Collective model to silicon 113
5.1 Inputs for the calculations 113
5.2 Silicon thermal conductivity 115
5.2.1 Bulk thermal conductivity: Kinetic and collective behavior 117
5.2.2 Predicting the effect of the isotopic composition on the thermal conductivity 119
5.2.3 Predicting the effect of shape and size on the thermal conductivity: Thin-films and Nanowires 120
5.2.4 Transition from the kinetic to the collective regime: 122
5.2.5 Size-effects in the collective regime: $F(L_{\text{eff}})$ 122
5.2.6 Global overview of the thermal conductivity 125
5.2.7 Comparison between standard RTA, Callaway and Kinetic-collective models 127
5.2.8 Effect of N-processes on the thermal conductivity 128
5.3 Behavior of the relaxation times with frequency 131
5.4 Spectral thermal conductivity 134

6 Applying the Kinetic-Collective model to group-IV semiconductors. 141
6.1 Relations between phonon-phonon relaxation times expressions 142
6.2 Inputs for the calculations 144
6.3 Thermal conductivity of group-IV semiconductors 147
6.3.1 Transition from the kinetic to the collective regime: 150
6.3.2 Comparison with other models 152

7 Applying the Kinetic-collective model to Bi_2Te_3 155
7.1 Inputs for the calculations 156
7.1.1 Relaxation times expressions 156
7.2 Bi_2Te_3 thermal conductivity 158
7.3 Thermoelectric applications 160

8 Conclusions 165

Appendix A 169

Appendix B 174

Appendix C **176**

References **177**

List of Figures

1.1 Sketch of the Debye dispersion relation 22
1.2 Sketch of the transversal section of the $\boldsymbol{q}$-mesh showing a surface of constant energy and its elementary area dS_ω. 24
1.3 Sketch of the Debye density of states compared with a real density of the states 25
1.4 Heat capacity of silicon as a function of the cubic temperature: experimental measurements vs Debye model 28
1.5 Sketch for the heat flux evaluation in simple kinetic theory 30

2.1 Equilibrium and displaced atomic positions vectors of a pair of ions 37
2.2 Diamond structure 42
2.3 Brillouin zone of a FCC lattice 43
2.4 BCM scheme of the unit cell of the diamond 44
2.5 Phonon dispersion relations and density of sates for diamond calculated with the BCM 49
2.6 Phonon dispersion relations and density of sates for silicon calculated with the BCM 50
2.7 Phonon dispersion relations and density of sates for germanium calculated with the BCM 50
2.8 Phonon dispersion relations and density of sates for -Sn calculated with the BCM 51
2.9 Specific heat of Si, Ge, C and $-$Sn calculated with the BCM dispersion relations and density of states. 51
2.10 Crystal structure of Bi_2Te_3 53
2.11 Dispersion relations of Bi_2Te_3 calculated in the present work using the RIM, in the crystallographic direction [110]. 56

2.12 Comparison between experimental and theoretical dispersion relations of Bi_2Te_3 in the crystallographic direction [111]: (a) experiment by Ref. [1], (b) calculated using Morse interatomic potential with the RIM by Qiu and Ruan [2], (c) calculated in the present work using the RIM. 57
2.13 Density of states of Bi_2Te_3 calculated from the RIM. 57
2.14 Specific heat of Bi_2Te_3 calculated from the RIM. 58

3.1 Scheme of the general behavior of the phonon thermal conductivity with temperature for a non-metallic crystal. The dominant resistive scattering process in each range of temperature is depicted qualitatively. 62
3.2 Feynman diagrams for the possible three-phonon interactions 64
3.3 Sketch of a general three-phonon process 66
3.4 Sketch of the cross-section of the energy conservation surface in the $\mathbf{q}$-space . . 70
3.5 Comparison of several temperature functions $g_i(T)$ intervening in τ_U 74
3.6 Feynman diagrams for the phonon-impurity interaction 76
3.7 Sketch of the atoms arranged in a lattice with the presence of impurities . . . 77
3.8 Phonon thermal conductivity measurements of silicon and germanium bulk samples with several isotopic compositions 79
3.9 Experimental measurements of phonon thermal conductivity for several diameters silicon nanowires 81
3.10 Experimental measurements of phonon thermal conductivity of a 115 nm diameter silicon nanowire and a 110 nm thickness silicon thin-film 82

4.1 Thermal conductivity of naturally occurring Ge and isotopically enriched Ge calculated by Callaway 91
4.2 Thermal conductivity normalized by its value at T=320 K for Si nanowires of several widths, calculated by the Callaway formula with different cut-offs in the integrals 93
4.3 Phonon behavior in the kinetic and collective regime 105

5.1 Total thermal conductivity as a function of temperature in a double logarithmic plot for ^{na}Si and the prediction for ^{iso}Si. Pure kinetic $_{kin}$ and collective $_{coll}$ thermal conductivity regimes for ^{na}Si are also shown 118
5.2 Thermal conductivity predictions for Si TFs with several thicknesses and several diameter Si NWs 121

5.3 Switching factor as a function of temperature in a semilogarithmic plot for ^{na}Si and ^{iso}Si bulk, 830 nm TF and 115 nm NW. 123
5.4 Predicted thermal conductivity as a function of temperature for the 115 nm NW compared with experimental data. The pure kinetic $_{kin}$ and the collective $_{coll}$ regimes are also shown. 123
5.5 Size-effects in the collective flux 124
5.6 Thermal conductivity of all the silicon samples studied in this work (Bulk, thin films and nanowires) 126
5.7 Thermal conductivity as a function of temperature for ^{na}Si and ^{iso}Si bulk, and the 115 nm NW. We show the best fit provided by the standard RTA and the Callaway models against the Kinetic-Collective model. 129
5.8 Thermal conductivity for the three representative samples ^{na}Si and ^{iso}Si bulk, and 115nm NW calculated using: (I) the RTA model and (II) the Callaway model, with and without τ_N 130
5.9 Behavior of phonon relaxation times τ_N, τ_U, τ_I and τ_B with the frequency for the LA branch at several temperatures 132
5.10 Behavior of phonon relaxation times τ_N, τ_U, τ_I and τ_B with the frequency for the LO branch at several temperatures 133
5.11 Kinetic and collective phonon diffusion coefficients in terms of frequency for ^{na}Si and 115nm NW at low and room temperature 136
5.12 Spectral thermal conductivity contributions in terms of frequency of both regimes at low $T = 30$K and room temperature $T = 300$K for Si bulk (a),(b) and 115nm NW (c),(d), respectively. In all the plots pure kinetic $_k$ and collective $_c$ regimes (shortened in the legend as $_k$ and $_c$ respectively) are shown in dashed-lines, the reduction due to is shown for each regime with filled curves. For the NW the effect of $F(L_{\text{eff}})$ in the collective regime is also shown (solid line), for the bulk is omitted for the sake of simplicity, since $F(L_{\text{eff}}) = 1$ at both temperatures (see Fig. 5.5). Note that in (a) and (b) the peaks of $_k$ appear cut because are out of scale. 138
5.13 Normalized thermal conductivity contribution due to optical phonons for several sample sizes. 139

6.1 Thermal conductivity predictions for the set of samples of group-IV semiconductors 148

6.2 Thermal conductivity kinetic and collective regimes for the set of natural occurring samples of group-IV semiconductors 149
6.3 Switching factor as a function of temperature in a semilogarithmic plot for the naturally occurring samples. 151
6.4 Switching factor as a function of temperature in a semilogarithmic plot for the set of germanium samples with several isotopic compositions. 151
6.5 Thermal conductivity of natural and enriched germanium and silicon samples calculated with Morelli's model 152
6.6 Thermal conductivity of natural and enriched diamond samples, calculated with Morelli's model 153

7.1 Thermal conductivity of bulk Bi_2Te_3 and NWs with several diameters 159
7.2 Bi_2Te_3 thermal properties for 350 nm and 100 nm NWs at several temperatures. S and are taken from bulk as it is not expected to change for these NWs' diameter range. is calculated with the BCM. ZT calculated with Eq. (7.8) Courtesy of M.M. Rojo. 161
7.3 Voltage vs temperature difference for the several NWs with diameters ranging from 350 nm to 100nm. Courtesy of M.M. Rojo. 162
7.4 ZT calculated with with Eq. (7.8 entering the values shown in Fig. 7.2 with T being the average temperature corresponding to the temperature difference generated by the corresponding voltage, for the set of NWs with diameters ranging from 350 nm to 100nm.Courtesy of M.M. Rojo. 163

List of Tables

2.1 Lattice parameters for group-IV semiconductors ordered from the lower to the higher value. The lower the value of a, the higher the frequencies in the dispersion curves [3]. 42

2.2 BCM parameters for group-IV semiconductors given in units e^2/V_a. The BCM for diamond has one additional parameter $a = 0.51r^0/16$. These values are those found by Weber in [4] after fitting to experimental dispersion relations from neutron scattering data. 48

2.3 Parameters for first and second-neighbors interactions of Morse potential (2.43) for Bi_2Te_3, from Qiu and Ruan [2]. 55

3.1 Summary of most relevant expressions for Umklapp and normal scattering rates that can be found in the literature for silicon and germanium. Subindex $i = \mathrm{L}, \mathrm{T}$ denotes longitudinal or transversal polarization for the acoustic branches. 73

5.1 Relaxation times for non-resistive and resistive scattering processes. τ_N and τ_U are original contributions of the present thesis, while τ_I and τ_B are widely used in the literature 115

5.2 Values of several properties for naturally occurring and for isotopically enriched Si bulk samples and several thin-films and nanowires 116

5.3 Best-fit parameters for ^{na}Si bulk. 119

5.4 Best-fit parameters for ^{na}Si bulk with the standard RTA, Callaway and Kinetic-collective model. 128

6.1 Relaxation times for non-resistive and resistive scattering processes for group-IV semiconductors. 143

6.2 Materials properties: Debye temperature $_D$, atomic mass M, atomic volume V, mean zone-center velocity $\bar{v}$, and Umklapp extinction temperature $_U$. . . 145
6.3 Conversion factors f_x and f_x 146
6.4 Values of Γ, cross-section A and effective size L_{eff} for Si, Ge, C and -Sn samples with natural and enriched isotopic compositions. 146
6.5 Best-fit parameters for ^{na}Si bulk 147

7.1 Bi_2Te_3 properties: Debye temperature $_D$, atomic mass M, atomic volume V, and Umklapp extinction temperature $_U$. 156
7.2 Values of Γ, diameter d for NWs, and the effective size L_{eff} for naturally occurring Bi_2Te_3 samples. 156
7.3 Fitting parameters for Bi_2Te_3 bulk. 158

Introduction

The aim of this theoretical work is twofold. First, to contribute to a better understanding of phonon heat transport in bulk and nanostructured semiconductors, like thin-films or nanowires, in a wide range of temperatures, paying special attention to phonon-phonon collisions. Second, to improve the prediction capability of the thermal conductivity of the most common semiconductors. To achieve this, it becomes necessary the formulation of a new model allowing us to overcome the difficulties associated to the existing models, with the aim to fulfill two desirable conditions: to provide a general expression for the thermal conductivity, valid for several materials with different size-scales and geometries in a wide range of temperatures, and to have the smallest number of free adjustable parameters to assure the reliability of the model. The potentiality of such model would be to serve as a useful tool to design more efficient thermoelectric devices.

The fruit of our study is the Kinetic-collective model which is developed in the framework of the Boltzmann transport equation as a natural generalization of the Guyer-Krumhansl model. Since phonon interactions are the source of thermal resistance, they deserve a special discussion in any thermal conductivity study. Precisely, the keystone in our work is the treatment of phonon-phonon collisions regarding their different nature.

The prediction capability of the model need to be tested on several materials. In particular, we study five materials with thermoelectric interest. In first place, silicon, because it is an ideal test material due to the considerable amount of experimental data available in the literature, and because of its inherent scientific and technological importance. Secondly, we extend our study to other materials with the same lattice structure as silicon, that is the family of group IV element semiconductors (germanium, diamond, silicon and gray-tin), which also have been object of intense study, specially germanium, due to the recent and fast development of SiGe alloys and superlattices. Finally, we finish our study with a more complicated material regarding its lattice structure, bismuth telluride, which is known to be a very efficient thermoelectric material due to its high figure of merit.

The Thesis is arranged in eight Chapters. The lay out is as follows: Chapter 1 contextualizes the topic of the work and briefly introduces the basic physics related to phonon transport. In Chapter 2 the fundamental quantity necessary for considering any thermal property, the phonon dispersion relations, have been obtained for the materials under study. For this purpose, two lattice dynamics models are used: the Bond-charge model for group-IV semiconductors (silicon, germanium, diamond and gray-tin), and the Rigid-ion model for bismuth telluride (Bi_2Te_3). Along with their corresponding phonon dispersion relations, phonon density of states and specific heat results are also presented. The phonon relaxation times that suit these materials are discussed in Chapter 3, where new expressions to account for the phonon-phonon collisions are also presented. In the first part of Chapter 4 the most representative thermal conductivity models to date are introduced and discussed, in the second part, a new model to predict the thermal conductivity, the Kinetic-collective model, is presented and its conceptual differences and advantages with respect to previous similar models are discussed. In Chapter 5 the Kinetic-collective model is applied to silicon bulk samples with different isotopic composition and several nanostructured samples with different geometries (thin-films and nanowires) obtaining predictions for their thermal conductivity in a wide interval of temperatures. Some novel aspects of phonon transport arising from these results are discussed. In Chapter 6 the Kinetic-collective model is applied to the other group-IV materials using theoretical expressions to predict their relaxation times and, eventually, their thermal conductivity. Results for several samples with different isotopic compositions in a wide range of temperature are presented and discussed. In Chapter 7 the Kinetic-collective model is applied to Bi_2Te_3, providing thermal conductivity predictions for nanowires with several diameter values, and the results are discussed in view of possible applications in thermoelectricity. Finally, in Chapter 8 the main conclusions of this Thesis are summarized and possible future lines of work stemming from its several results are discussed.

Chapter 1

Heat transport in solids

La chaleur pénètre, comme la gravité, toutes les substances de l'univers, ses rayons occupent toutes les parties de l'espace. Le but de notre ouvrage est d'exposer les lois mathématiques que suit cet élèment. Cette théorie formera désormais une des branches les plus importantes de la physique générale.

J. Fourier, "*Théorie analytique de la chaleur*". (1822)

1.1 Introduction

Heat transfer is a process whereby thermal energy is transferred from place to place in response to a temperature gradient. There are three ways of heat transfer: conduction, convection, and radiation. In solids, heat transport at room or low temperatures is mainly due to conduction, since the bonding between atoms avoids convection, and in general radiation is only important at very high temperatures. Thermal conduction in solids can be explained as the combination of two main mechanisms: atomic lattice vibrations, *i.e.* phonons, and translational motion of electrons or holes. Then, the carriers of the transferred energy are lattice waves and free electrons. When there is a temperature difference in a body, the transport occurs spontaneously, in absence of external forces, from the hot part to the cold part of the solid and also, when two bodies at different temperature are in contact, it flows from the hot end to the cold end, until thermal equilibrium is reached.

Heat conduction is described through the well known Fourier's law, published by J. Fourier

in 1822 in his classical work *Théorie analytique de la chaleur* [5]. It is written as

$$\mathbf{j} = - \quad T, \tag{1.1}$$

which states that the local heat flux density, $\mathbf{j}$, is proportional to the negative local temperature gradient $- \quad T$. The proportionality constant is called thermal conductivity and it is an intrinsic property of each material, denoting how easily heat is transported through the material.

Although Fourier's law describes correctly heat conduction in macroscopic systems, it fails when applied to systems with reduced characteristic dimensions. The pioneering works on heat transport by R. E. Peierls in 1929 [6], and later by H. B. G. Casimir [7], showed that collisions of the energy carriers against the sample's boundaries decrease its thermal conductivity when the size of the sample is reduced. This situation is worsened with the miniaturization of the systems. In fact, on theoretical grounds, such reduction was already studied in the 1920's, but the results at that time were more academic than practical. With the technology of our time, experimentalists have been able to grow wires and thin-films with diameters within the nanometer scale, and this has allowed us to observe that, indeed, the thermal conductivity of a material is severely reduced when it is nanostructured. For instance, in the well-known experiment by Li *et al.* in 2003, where silicon nanowires (NWs) were grown with diameters between 115 nm and 22 nm, the measured thermal conductivities at room temperature were found to be between 40 W/mK for the 115 nm NW and 9 W/mK for the 22 nm NW, about two orders of magnitude lower than that of the bulk (140W/m K) [8]. In the recent experiment by Wignert et al. (2011), they grew very tiny germanium nanowires with diameters of 15 nm and 19 nm, measuring a thermal conductivity of 1.54 and 2.26 W/mK respectively, around 7 times smaller than that of 62 nm diameter NW (13W/mK) [9]. However, if the size of the system is further reduced, below a couple of nanometers, quantum confinement effects can also modify and may lead to a surprisingly increase. As show by Ponomareva *et al.* with Molecular Dynamics simulations, the thermal conductivity of silicon NWs with diameters between 8 nm and 1 nm decreases as diameter also does, but at a certain size-threshold, found to be 1.5 nm, begins to increase [10]. This striking behavior has also been seen experimentally with graphene layers [11].

Another limitation of the macroscopic theories, like Fourier law, relies on the consideration of the medium as a continuum and that there is local thermodynamic equilibrium everywhere. The continuum assumption breaks downs when the characteristic size of the system is comparable to or smaller than the "mechanistic length", that is, the carrier mean free path.

The presence of high temperature gradients at small scales or during short periods of time leads to non-equilibrium situations, where the local equilibrium hypothesis is not applicable. Furthermore, there are other phenomena at the micro/nanoscale that reduce thermal conductivity, for instance discontinuous carrier velocities, temperature boundary conditions, wave interferences, or tunneling of electrons and phonons [12, 13].

Thus, Fourier's law with a size-independent thermal conductivity can no longer be used, since it is not able to describe these observations, and the theories developed within the macroscopic framework are no longer suitable to understand the heat transport behavior. A microscopic formulation is clearly needed. The most widely used microscopic models are based on a statistical physics framework and start from the Boltzmann transport equation. Besides, between macro and microscopic models, there are also mesoscopic models for generalized transport equations. In this framework, usually under a thermodynamic perspective, heat transport equations are modified mainly through the inclusion of terms related to memory and non-local effects, leading to size and form-dependent effective thermal transport properties [14]. It is important to recall that macro, meso and microscopic models are not at all unbridgeable, and sometimes combining them appropriately may help to provide simplified modeling of the complex microscopic heat transport.

The main result of this thesis is the development of a microscopic model to account for the phonon thermal conductivity within the Boltzmann transport equation framework, able to give some physical insights on the phonon contribution to heat transport in solids from the macro to the nanoscale, enabling reliable predictions of the thermal conductivity for several bulk and nanostructured materials. Since this work is devoted to the understanding of phonon thermal transport, it will be restricted to semiconductors materials, where phonons are the main heat carriers and the electronic contribution to thermal conductivity is very small. Heat transport in other solids, like metals or even degenerate semiconductors, where electrons are the main heat carriers and the phononic conduction is swamped by the electronic conduction, is out of the scope of the present work. Note that the phonon contribution to thermal conductivity is usually called lattice thermal conductivity, but here and onwards we refer to it simply as thermal conductivity, for the sake of simplicity.

Previous to any attempt to model thermal conductivity in a microscopic approach, it is important to know the mechanical and thermal properties of carriers present in the system, as well as their interactions and some properties of the atomic movement in a semiconductor crystal. In the next Sections we briefly introduce the necessary physical concepts to deal with phonon transport.

1.2 Phonons I: Mechanical properties

A crystal lattice is a solid structure in which the atoms, or ions, are arranged in periodic arrays, with translational symmetry in three non-coplanar directions of the real space. The primitive unit cell represents the minimum arrangement of atoms that will be repeated periodically along the real space. It is conventional when defining a real structure in terms of its atomic coordinates in real space to also define a set of vectors which corresponds to reciprocal space, which is also called momentum or $\boldsymbol{q}$-space. The unit cell in reciprocal space is called the Brillouin zone.

The vibrational motion of the atoms around their equilibrium positions is considered harmonic. When solving the equation of motion of the lattice we seek a solution representing a wave with angular frequency ω and wave vector $\boldsymbol{q}$ with components (q_x, q_y, q_z) parallel to the principal axes of the lattice, such that the displacement of the jth atom is

$$\boldsymbol{u}_j \quad e^{i(qja-\omega t)} \,. \tag{1.2}$$

where a is the interatomic distance, and ja is the discrete equilibrium location of atom j. The use of a discrete lattice coordinate is because the vibrations are only possible at the atomic sites. Then, an infinitely divisible continuum coordinate x used in a continuos medium has no sense. The wave vectors corresponding to the allowable vibrations are given by the Born-von Karman periodic boundary conditions [15–17], yielding

$$q = \frac{2\pi m}{N} \,, m = 0, \pm 1, \pm 2, \ldots \tag{1.3}$$

where N is the number of atoms in the crystal. The total number of modes in the crystal is equal to the number of atoms in the primitive cell n times the number of atoms in the crystal. Thus, in a 3-dimensional crystal the number of modes is equal to $3nN$, since the vibrations can be emitted in the three directions of the space. The energies of the normal modes of a crystal are quantized. A phonon is a quantum of energy $\hbar\omega$ of the normal modes of vibration. Clearly, in the harmonic approximation we have non-interacting phonons, and the anharmonic terms (cubic and quartic expansion of the lattice potential) are latter introduced as phonon renormalization or phonon-phonon interactions. Due to translational symmetry, in general the calculations are restricted to the first Brillouin zone, which contains all the possible modes within a range $q \quad [-\pi/a, \pi/a]$. Let us know describe two important properties arising from the study of the dynamics of the lattice: the dispersion relations and the density of states.

1.2.1 Dispersion relations

The amount of thermal energy that a phonon with wave vector $\mathbf{q}$ can transport through the crystal lattice is related to its frequency and velocity. The functional relations between the frequency and the wave vector for each branch ν are called dispersion relations $\omega_\nu(\mathbf{q})$[1].

When carrying energy from a hot region to a cold region, as in the case of the electron movement in a band, phonons move with a group velocity given by

$$\mathbf{v}_{\mathbf{q}\nu} = \quad {}_{\mathbf{q}}\omega_\nu(\mathbf{q})\,. \tag{1.4}$$

At the edge of the Brillouin zone the group velocity of the phonons approaches zero, creating a standing wave, this is reflected in the dispersion relations when the curves flatten for values of $\mathbf{q}$ belonging to the edge of the Brillouin zone, also called boundary zone.

For each wave vector we have multiple allowed frequencies, depending on the number of degrees of freedom of the primitive unit cell, that is, $3n$, n being the number of atoms in the unit cell. For instance, a lattice with one atom per unit cell will have 3 dispersion curves in a given $\mathbf{q}$-direction, which are, regarding polarization, one longitudinal acoustic (LA) and two transversal acoustic (TA1 and TA2); if we have a lattice with 2 atoms per unit cell, as in the case of silicon, as well as in germanium, diamond, and most III-V compounds, we will have $\nu = 6$ phonon branches, which are, three optic branches, one longitudinal (LO) and two transversal (TO1 and TO2), different in the different directions of the space, in addition to the three acoustic branches. If there are more than 2 atoms per unit cell, we still have the three acoustic branches and the others are optic branches. Generally, the split between acoustic and optic branches is given by the range of the frequencies: we classify as optic modes those with high frequencies, and acoustic modes those with low frequencies ranging from zero upwards. We can find the frequencies of a given wave vector by solving the equations of motion of the crystal lattice, since the frequencies, or more accurately the square of the frequencies, are the solutions of the eigenvalue equation for a given $\mathbf{q}$. This will be described in detail in the next Chapter. The dispersion relations can be very complex, and it is common to use the linearized expression provided by Debye [18, 19], which was originally proposed in 1912 to describe the dependence of the specific heat on the temperature, especially at low temperatures (the well known T^3 dependence of the specific heat at low temperatures), to improve the simpler but pathbreaking model proposed by A. Einstein in 1907 [20], which described for the first time

[1]Note on usage: for the sake of simplicity, along this work we will drop, in most of the cases, the branch subindex in any quantity A depending on the wave vector, such that $A_{\boldsymbol{q}\nu}$ may be found as $A_{\boldsymbol{q}}$.

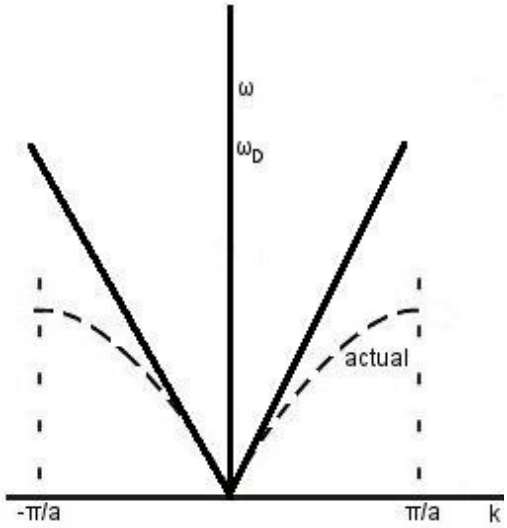

Figure 1.1: Sketch of the Debye dispersion relation given by Eq. (1.5) represented as solid lines. Dashed lines stand for a real dispersion relation for a simplified model of crystal, where it can be observed how the curve flattens at the Brillouin zone boundary, i. e. at the highest values of wavevector (denoted "k" in this sketch by Bruesch [21]) in the Brillouin zone.

a vanishing specific heat at $T \quad 0$ but with a wrong temperature dependence. The Debye approximation assumes a linear relation between the frequency and the wavevector, such that

$$\omega = c|\boldsymbol{q}| = cq \quad , \tag{1.5}$$

where c is a constant corresponding to the sound velocity in the crystal. The Debye approximation (1.5) implies that all the modes are approximated by three identical acoustic branches, this means that the medium is considered isotropic, *i. e.* all phonon branches have the same velocity in all directions.

However, this approximation is only valid at low enough frequencies, because a difference with respect to this behavior is observed as the wavevectors increase their value. In other words, the Debye approximation assumes a non-zero group velocity at the boundary of the first Brillouin zone (BZ), while experimentally it is observed that close to the border of the BZ the dispersion relation flattens and the group velocity tends to zero, as shown in Fig. 1.1. Furthermore, it is also not suitable for optic phonons, which are neglected. Nevertheless, (1.5) is a good approximation at low temperatures, because most of the phonons have low energy, or equivalently, low frequency, and the acoustic branches are the main heat carriers.

Many models used to calculate the thermal conductivity to the date are based on the

Debye model or a modified version of it [22–27]. However, some authors have stressed that using actual dispersion relations is crucial in order to predict thermal conductivity of micro/nanostructured systems [28]. Nowadays, the most active trend in research is to calculate the complete phonon dispersion relations for the material under study using either *ab initio* techniques or an appropriate model to account for lattice dynamics, both providing successful results. Following this trend, we devote the next Chapter to find the actual dispersion relations of the materials under study in this work using suitable lattice dynamics models.

1.2.2 Density of states

Once all the information about the modes present on a material is known thank to the dispersion relations, we can calculate another interesting property of the crystals, the density of states. The phonon density of states gives us the number of normal modes per unit volume in a frequency interval $[\omega, \omega + d\omega]$.

The general expression is

$$D(\omega) = \sum_{\nu} D_{\nu}(\omega) = \sum_{\nu} \frac{1}{V} \frac{dN_{\nu}}{d\omega} \quad . \tag{1.6}$$

being dN_{ν} the number of states between ω_{ν} and $\omega_{\nu} + d\omega_{\nu}$ in the phonon branch ν, but the form of the constant energy surfaces (ω_{ν}=cte and $\omega_{\nu} + d\omega_{\nu}$=cte) in a real crystal is far from trivial. We can write the number of states between these surfaces as

$$dN_{\nu} = \frac{V}{8\pi^3} \int_{\omega_{\nu}}^{\omega_{\nu}+d\omega_{\nu}} d\boldsymbol{q} \tag{1.7}$$

where we can express $d\boldsymbol{q} = dS_{\omega} dq$ (see Fig. (1.2)). Since $\nabla_{\boldsymbol{q}}\omega$ is perpendicular to the ω_{ν} =cte surface, we have $d\omega = |\nabla_{\boldsymbol{q}}\omega_{\nu}| dq$. Then

$$dN_{\nu} = \frac{V}{8\pi^3} \int_{\omega_{\nu}}^{\omega_{\nu}+d\omega_{\nu}} dS_{\omega} \frac{d\omega}{|\nabla_{\boldsymbol{q}}\omega_{\nu}|} \tag{1.8}$$

and substituting in (1.6) we have

$$D(\omega) = \frac{1}{8\pi^3} \sum_{\nu} \int_{\omega} \frac{dS_{\omega}}{|\nabla_{\boldsymbol{q}}\omega_{\nu}|} \quad . \tag{1.9}$$

In regions where the dispersion relation is very flat (commonly in the borders of the BZ or in the case of optical modes), the density of states can be very high. In the case we consider de density of states per branch $D(\omega_{\nu})$ we call it partial density of states.

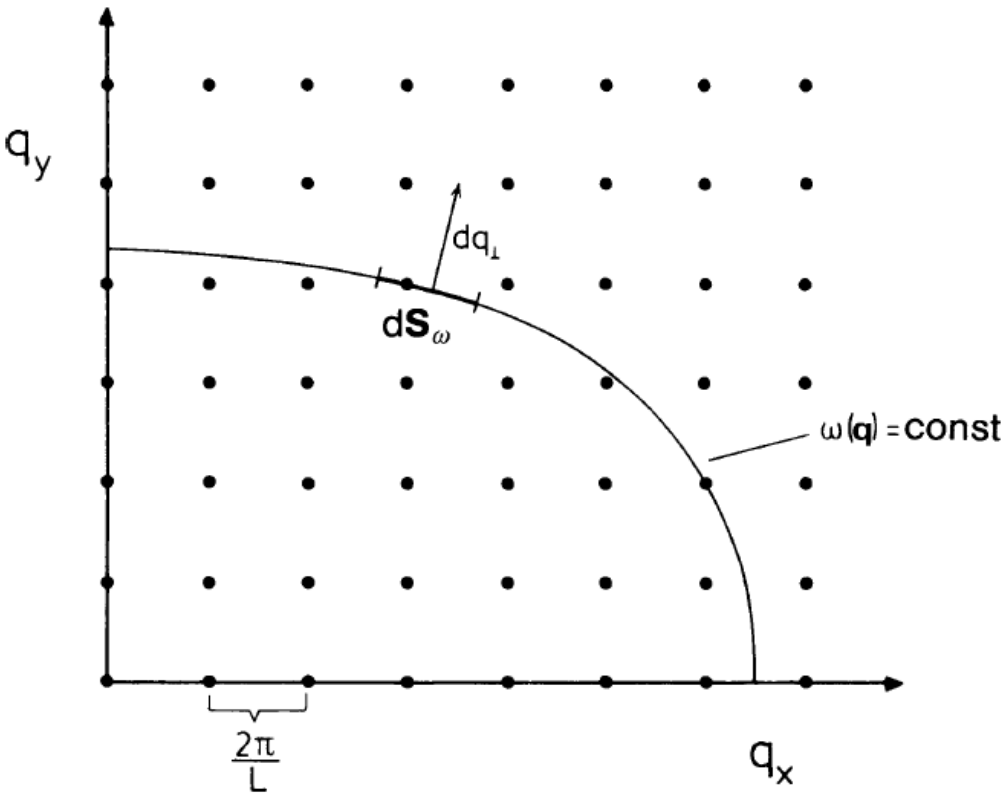

Figure 1.2: Sketch of the transversal section of the $\boldsymbol{q}$*-mesh showing a surface of constant energy and its elementary area* dS_ω*.*

Integration of Eq. (1.9) requires, in first place the knowledge of the dispersion relations , and secondly a realistic integration over the whole Brillouin zone of the crystal under study. Therefore, we need to calculate $D(\omega)$ with a numerical method. For this purpose, we will use the root sampling method [17]. In this picture, the density of states (1.9) can be expressed as

$$D(\omega) = \frac{1}{8\pi^3} \sum_{\boldsymbol{q}\nu} \quad (\omega - \omega_\nu(\mathbf{q})) \tag{1.10}$$

using a large mesh of points in the $\boldsymbol{q}$-space within the irreducible part of the Brillouin zone. With this, we can compute $D(\omega)$ by replacing the Dirac delta in (1.10) by a function such that

$$D(\omega) = \frac{1}{V_{BZ}} \sum_{\boldsymbol{q}\nu} \quad (\omega - \omega_\nu(\mathbf{q})) \tag{1.11}$$

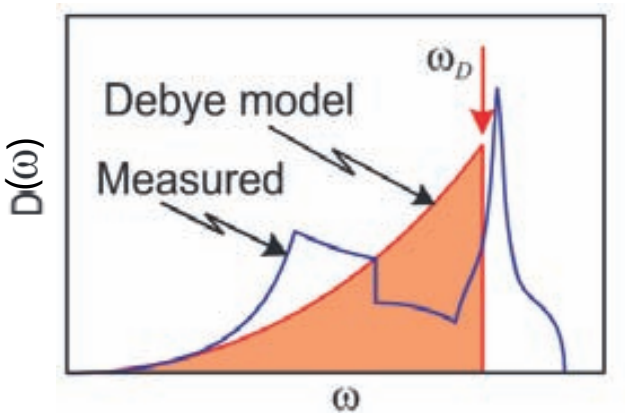

Figure 1.3: Sketch of the Debye density of states compared with a real density of the states (Extracted from [29]).

where

$$(\omega - \omega_\nu(\mathbf{q})) = \begin{array}{ll} 1 & \text{if} \quad |\omega - \omega_\nu(\mathbf{q})| \quad \Delta\omega/2 \\ 0 & \text{otherwise} \end{array} \tag{1.12}$$

with a suitable small frequency width $\Delta\omega$, and being V_{BZ} the volume of the Brillouin zone.

Nevertheless, it is worthy to compute the density of states in the Debye model (isotropic approximation), since the problem simplifies considerably by assuming that the constant energy surfaces are spheres. Then $d\boldsymbol{q} = 4\pi q^2 dq$ and $\quad_{\boldsymbol{q}}\omega_\nu$ is the sound velocity in the branch ν, considering only 3 acoustic branches with identical velocity. From (1.9) we obtain the Debye density of states

$$D(\omega) = \frac{3}{2\pi^2 c^3}\omega^2 \ . \tag{1.13}$$

Since the total number of states in a three-dimensional lattice is $3nN$, the Debye model considers a cut-off frequency ω_D defined from the expression

$$3nN = \frac{V}{2\pi^2}\frac{3}{c^3} \quad {}_0^{\omega_D} \omega^2 d\omega = \frac{V}{2\pi^2}\frac{\omega_D}{c^3} \tag{1.14}$$

It is more convenient to define the Debye temperature $\quad_D$ by equating $\hbar\omega_D = k_B \quad_D$.

The Debye temperature is a very useful amount that works as a threshold. If $T < \quad_D$ the solid behaves a a quantum system, while in the case where $T > \quad_D$ we recover the Dulong and Petit law for the specific heat, as we shall see in the next Section, and the solid behaves as a classical system.

In Fig. 1.3 we represent schematically the Debye density of states in comparison with a more realistic density of states. As we will see in the next Sections, $D(\omega)$ is directly linked to

the calculation of the specific heat, and eventually of the thermal conductivity. The accuracy of the calculation of $D(\omega)$ for a given material is tested by successfully predicting its measured specific heat. In the next Chapter, we show, along with the dispersion relations, the calculated density of states for the materials under study in this thesis.

1.3 Phonons II: Thermal properties in equilibrium

Once that the mechanical information of phonons has been obtained through the dispersion relations, we need to take into account the thermodynamic information they can provide.

In a thermalized system, the states, or modes, with higher energies are necessarily populated. This information is provided by the distribution function, which determines the probability of a specific state to be occupied in terms of its energy (frequency) and temperature. From this function, we are able to calculate the thermodynamic information of the crystal, like the internal energy or the specific heat.

1.3.1 Distribution function

Since the energy of the vibrational field of the lattice is quantized, the allowable energy levels in a mode of frequency $\omega_{\boldsymbol{q}}$ are $(n + 1/2)\hbar\omega_{\boldsymbol{q}}$, where n is any positive integer. In addition, phonons are bosons, they obey the Bose-Einstein statistics, so that their average occupation number in the $\mathbf{q}$-th mode in thermal equilibrium at temperature T is given by the Bose-Einstein distribution function

$$n^0_{\mathbf{q}} = \frac{1}{e^{\hbar\omega_{\mathbf{q}}/k_B T} - 1} \tag{1.15}$$

where $\hbar$ is the Planck constant and k_B is the Boltzmann constant. From expression (1.15), we can observe that at low temperatures $\hbar\omega_{\boldsymbol{q}} \quad k_B T$, thus $n^0_{\mathbf{q}} \quad \exp(-\hbar\omega_{\boldsymbol{q}}/k_B T)$, this means that the probability for a mode to be populated is exponentially small. At high temperatures $\hbar\omega_{\boldsymbol{q}} \quad k_B T$, and now $n^0_{\mathbf{q}} \quad k_B T/\hbar\omega_{\boldsymbol{q}}$, the modes get populated linearly with temperature. At absolute zero temperature the phonon population is not zero, since the zero-point energy is $\frac{1}{2}\hbar\omega_{\boldsymbol{q}}$. Therefore, the phonon population in a crystal is determined by the temperature. The phonon chemical potential is zero, at least not very far from equilibrium, since far from equilibrium some authors [30] have proposed that phonons could have a non-vanishing chemical potential, but here we will leave aside this topic, which is usually ignored in the analysis of heat transport.

1.3.2 Internal energy

The mean internal energy density of the crystal is the mean internal energy E per unit volume V and it is defined in terms of the density of states $D(\omega)$, the distribution function $n^0(\omega)$ and the energy $\hbar\omega$ of each mode as

$$\equiv \frac{E}{V} = \sum_{\nu} \hbar\omega\, n^0(\omega_\nu)\, D(\omega_\nu)\mathrm{d}\omega \quad . \tag{1.16}$$

If we use the Debye model, we find, by substituting Eq. (1.13) in Eq. (1.16), that at high temperatures $= 3Nk_BT$.

1.3.3 Specific heat

One way of studying the modes in a crystal is to analyze its heat capacity. This quantity accounts for how fast a system increases its energy when the system temperature is raised, and it is defined as the variation of the internal energy E with temperature T at constant volume V, this is

$$C_v = \left.\frac{E}{T}\right|_V \quad . \tag{1.17}$$

It is directly related to the number of modes present in the system. If the system has a high number of allowed modes, it will have a high heat capacity, while in the opposite situation, the heat capacity will be low.

The specific heat c_v is the heat capacity per unit volume

$$c_v = \frac{C_v}{V} \quad . \tag{1.18}$$

We can obtain the specific heat from the internal energy density of a solid . Hence, substituting Eq.(1.16) in Eqs. (1.17) and (1.18) the phonon specific heat is calculated as

$$c_v = \sum_{\nu} \hbar\omega_\nu \frac{n^0(\omega_\nu)}{T} D(\omega_\nu)\mathrm{d}\omega \quad . \tag{1.19}$$

Notice that $D(\omega)$ does not depend on the temperature.

Experimental observations in semiconductor crystals show us that at low-intermediate temperatures C_v behaves as T^3. However, when the temperature of the system increases and reaches a certain value, the Debye temperature, above which most normal modes are excited, the heat capacity C_v approaches a constant value $C_v \quad 3Nk_B$, where N is the number

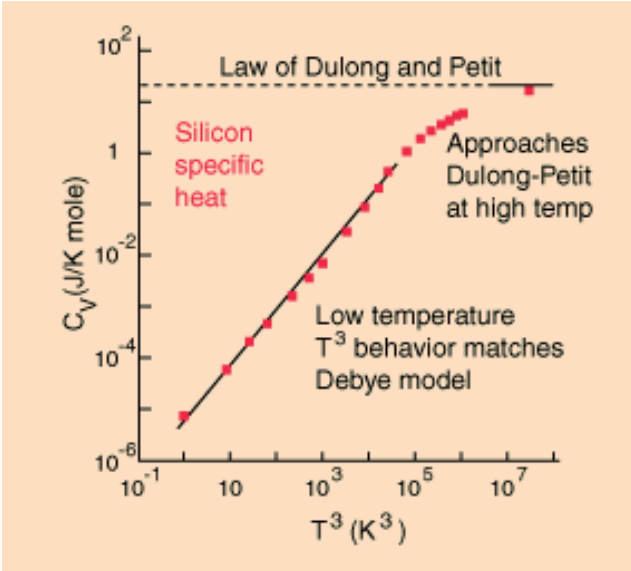

Figure 1.4: Heat capacity of silicon as a function of the cubic temperature: experimental measurements (symbols) and Debye model (solid line) from Rohlf [32]. The Dulong-Petit limit is plotted in dashed-line. (Figure extracted from [33]).

of atoms in the crystal, in agreement with the Dulong and Petit law. Well above the Debye temperature all the permitted states are occupied. The behavior of C_v, or analogously c_v, with temperature can be generally interpreted in terms of the Debye model [15, 19]. Considering the Debye dispersion relations (1.5) and density of states (1.13) in the integral expression (1.20) and using dimensionless variables $x = \hbar\omega/k_B T$ and $x_D = \ _D/T$, we can express the specific heat capacity as

$$C_v = 9Nk_B \ \frac{T}{\ _D}^{\ 3} \ \int_0^{x_D} \frac{x^4 e^x}{(e^x - 1)^2} \mathrm{d}x \ . \tag{1.20}$$

At high temperatures $x \quad 1$, $e^x - 1 \quad x$, so $C_v = 3Nk_B$. At low temperatures $x \quad 1$ and $x_D \quad$, so integrating we obtain $C_v = \frac{12\pi^4}{5} Nk_B \left(T/\ _D\right)^3$ which holds the T^3 behavior observed experimentally and an excellent fit to measurements at low temperatures has been found for many materials (see Fig.1.4). Nevertheless, we must keep in mind that $\ _D$ is an empiric parameter extracted from the fit to experiments [31], and when dealing with a real crystal a more accurate treatment of the heat capacity is required in terms of real dispersion relations provided by a realistic lattice dynamics model.

1.4 Phonons III: Transport properties in local-equilibrium

The next step in a thermal transport study is to break the equilibrium condition used in the previous Section, and apply a temperature gradient on the crystal. The thermal conductivity is a transport property, characteristic of each crystal, raised from this non-equilibrium situation. To study the phonon transport in this situation, the simplest approach consists of using the local-equilibrium hypothesis. This implies to assume that the thermodynamic variables change their values from point to point, but smoothly enough to consider that nearly in each point of the crystal we are able to define all the thermodynamic variables as we were in equilibrium.

1.4.1 Thermal conductivity in simple kinetic theory

Despite of the limitations of the Fourier law, it describes correctly the average behavior of the heat flow if we average the microscopic motion of the heat carriers in a region large enough and over a long enough time interval. This is the basis of the simple kinetic theory, where the thermal conductivity defined from the Fourier law is expressed in microscopic terms which allows us to obtain concrete values of for a given system [16, 34].

Let us consider a system as sketched in Fig. 1.5, where the crystal is heated by being in contact with a hot thermal bath at temperature T_{hot} in one extreme, while the other extreme has a colder temperature $T_{\text{cold}} < T_{\text{hot}}$, and according to the Fourier law, a phonon diffusion current is originated transporting the heat energy from the hot to the cold side. We can calculate the net heat flow j_x in a certain direction x across some surface S as the difference between the energy fluxes the carriers transport while crossing S in the positive and the negative direction before they scatter:

$$j_x = \frac{1}{2} n E v_x|_{x+v_x\tau} - \frac{1}{2} n E v_x|_{x-v_x\tau} \tag{1.21}$$

where n is the number of carriers per unit volume, E the energy of each carrier, and v_x the random velocity of the carrier in the x direction, and τ is the relaxation time or collision time (the average time between two successive collisions). Since the motion of the heat carriers is random, we take half of them moving in the positive direction and the other half in the opposite direction. The mean-free path is then $= v_x\tau$.

As we are in the neighborhood of S, x 0 and we can make a Taylor expansion

$$j_x = -v_x\tau \frac{d(nEv_x)}{dx} \quad . \tag{1.22}$$

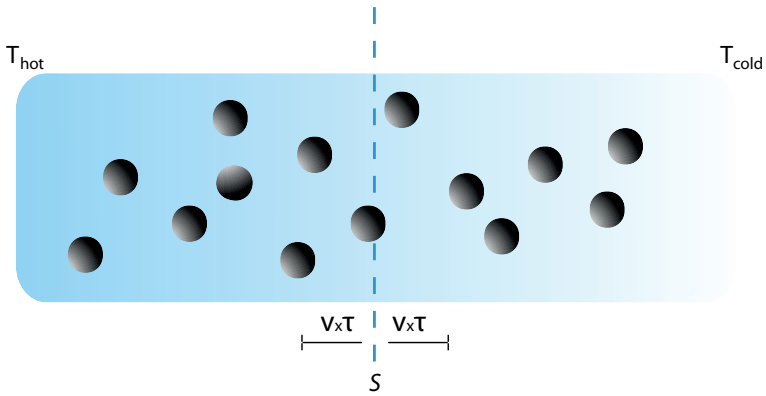

Figure 1.5: Sketch for the heat flux evaluation in simple kinetic theory. (After [16])

Assuming isotropy , that is, v_x independent of the direction, we have the mean velocity of the carriers v as $v_x^2 = v_y^2 = v_z^2 = \frac{1}{3}v^2$, then

$$j_x = -\frac{1}{3}v^2\tau\frac{d}{dx} \quad , \tag{1.23}$$

where $= nE$ is the internal energy density, and according to (1.17,1.18, 1.16) we can express the net heat flux in terms of the temperature gradient and the specific heat

$$j_x = -\frac{1}{3}v^2\tau c_v\frac{dT}{dx} \quad . \tag{1.24}$$

Comparing with the Fourier law

$$j_x = -\frac{dT}{dx} \quad , \tag{1.25}$$

we obtain the thermal conductivity in the simple kinetic approach

$$= \frac{1}{3}v^2\tau c_v \tag{1.26}$$

which represents a useful tool and a widely used first approximation in thermal conductivity modeling because of its simplicity. This expression relates the thermal conductivity to the specific heat c_v, the square of the average particle velocity v^2, which in the Debye model for phonons would be c^2, and the collision time τ. The specific heat is well known from thermal measurements at equilibrium, c is the average speed of elastic waves,that is, the sound velocity in the solid, but τ, or equivalently is unknown. Of course, unless τ is known for each temperature, expression (1.26) is not useful to obtain the thermal conductivity. In such a case, the knowledge of leads to the knowledge of τ (or equivalently), rather than

the opposite way. However, reasonable estimates of τ or can be made using (1.26) when we know the experimental value of at a certain temperature. An accurate knowledge of the relaxation times related to several scattering mechanism phonons may suffer and their microscopic understanding is a subtle matter, as it will be discussed at length in Chapter 3, and all along this thesis. This is a key-point in the microscopic models developed to find from an approximate solution of the Boltzmann transport equation. The main analytical approach derived to solve the BTE in a first stage, is the Relaxation-time approximation (RTA), which constitutes the equivalent of the simple kinetic theory providing the well known integral version of (1.26). This and further microscopic models will be discussed in Chapter 4.

Let us notice, eventually, that for high temperature gradients or non linear gradients, the expansion of Eq. (1.21) cannot be truncated to the lowest order and higher-order contributions should be considered in Eq. (1.22), leading to expressions going beyond the Fourier law, like

$$j = - \quad T - \ ^{2} \ _{1} \ ^{2}(\ T) - \dots \tag{1.27}$$

In this case, description of thermal transport becomes considerably more complex than with Fourier law. Therefore, here and onward, we will implicitly consider only small and linear temperature gradients in our study[2]. In situations when $^{2} \ ^{2}T \quad T$, however, additional terms like that in (1.27) could not be ignored. This is the case of the so-called Burnett approximation to the solutions of the Boltzmann equation, and is the subject of active interest in some groups looking for generalized heat transport equations going beyond Fourier law.

1.4.2 The Boltzmann transport equation

The Boltzmann transport equation (BTE) is the usual starting point in a microscopic study of the thermal conductivity. Its mathematical form and the physical interpretation of its terms in thermal transport applications have been widely discussed in the literature [35–37].

[2]The experimental techniques used to measure the thermal conductivity assumes, in general, small thermal gradients and it is in agreement with most of the theoretical approaches. An example is the 3ω method, which requires to establish small gradients in the sample (roughly in the range T [1mK-1K]) to avoid heat transfer between both thermal baths in contact with the sample due to the usually reduced size of the sample, and to avoid a local temperature raising able to destroy the sample by thermal evaporation. If the sample is big enough or is suspended between two thermal baths then it could be possible to put it under bigger thermal gradients, always restricted to the sensitivity of the measurement set up.

It was first introduced by L. Boltzmann in 1872 for monoatomic gasses [38] and here it can be briefly explained in the case of phonons.

In the presence of a temperature gradient T, phonons bring thermal energy from the hot to the cold side of a sample. The temperature in each region of the sample will determine the phonon population in that region. This is described through the distribution function $n_{\mathbf{q}}$, which is temperature dependent and varies from place to place in the sample, but its form is unknown *a priori*, unlike in the equilibrium situation (absence of thermal gradients), where the distribution function in equilibrium $n^0_{\boldsymbol{q}}$ is given by Eq. (1.15).

As hotter regions are more populated than colder ones, a phonon diffusion current is generated which will tend to equilibrate this situation. That is, the system tends to thermal equilibrium. In their travel through the system, phonons will scatter with other phonons, with impurities present in the material, electrons, defects or even the boundary of the system. During the scattering process phonons gain or loose part of their energy, and the system approaches towards thermal equilibrium.

The BTE relates the phonon diffusion and the phonon scattering by equating the rate of change of the phonon distribution out of thermal equilibrium $n_{\mathbf{q}}$ due to both of these processes, namely,

$$\frac{dn_{\mathbf{q}}}{dt}_{\text{diff}} = \frac{dn_{\mathbf{q}}}{dt}_{\text{scatt}} . \tag{1.28}$$

The general form of the diffusion term is

$$\frac{dn_{\mathbf{q}}}{dt}_{\text{diff}} \equiv \frac{n_{\mathbf{q}}}{t} + \boldsymbol{v}_{\boldsymbol{q}} \cdot \frac{n_{\boldsymbol{q}}}{\mathbf{r}} + \frac{\mathbf{F}}{m} \cdot \frac{n_{\mathbf{q}}}{\boldsymbol{v}_{\boldsymbol{q}}} , \tag{1.29}$$

where $\mathbf{r}$ is the position vector, $\mathbf{F}$ the total external force acting on the particles, and m their mass. In our case, it is usual to assume steady-state ($n_{\mathbf{q}}/\ t = 0$) and no external forces ($\mathbf{F} = \mathbf{0}$), then we obtain the diffusion term directly in terms of the phonon group velocity and the spatial gradient of the phonon distribution as

$$\frac{dn_{\mathbf{q}}}{dt}_{\text{diff}} \equiv \boldsymbol{v}_{\boldsymbol{q}} \cdot \frac{n_{\mathbf{q}}}{\mathbf{r}}. \tag{1.30}$$

Under these assumptions the BTE is

$$\boldsymbol{v}_{\boldsymbol{q}} \cdot \frac{n_{\mathbf{q}}}{\mathbf{r}} = \frac{dn_{\mathbf{q}}}{dt}_{\text{scatt}} \tag{1.31}$$

However, the scattering term is unknown *a priori*, and it is necessary to make approximations to derive it on physical grounds, and to solve (1.31) analytically.

A good approximation to solve (1.31) is by using numerical methods. The computational power nowadays allows the numerical solution of the BTE in combination with density functional theory obtaining remarkable results in particular intervals of temperature. In spite of this, the computational cost at low temperatures or for very small systems, like nanowires, is out of the computational capability [39]. Furthermore, the complexity of this method may mask the underlying physics in phonon transport. Then, phenomenological approaches to provide analytic solutions are still a useful and desirable tool to study the thermal transport properties in a crystal.

Let us now introduce the first and simplest approximation to solve analytically the BTE: the standard relaxation-time approximation.

1.4.3 Standard Relaxation-time approximation

The relaxation-time approximation is the simplest approach to formulate and solve the BTE and obtain an integral expression for the thermal conductivity. It states that, when the phonon distribution remains near equilibrium, the rate of change of the phonon distribution $n_{\boldsymbol{q}}$ due to collisions depends inversely on the relaxation time τ, that is

$$\frac{dn_{\boldsymbol{q}}}{dt}\bigg|_{\text{scatt}} = -\frac{n_{\boldsymbol{q}} - n^0_{\boldsymbol{q}}}{\tau}. \tag{1.32}$$

It means that a perturbation in the distribution function will decay exponentially with a relaxation time τ, that, unlike in the standard RTA, can depend on the phonon frequency.

Recalling the Eq. (1.31), the BTE in steady-state and in absence of external forces can be written as

$$\boldsymbol{v}_{\boldsymbol{q}} \quad n_{\boldsymbol{q}} = \quad \frac{dn_{\boldsymbol{q}}}{dt}\bigg|_{\text{scatt}}, \tag{1.33}$$

using the relaxation time approximation (4.2) we can express the BTE as

$$\boldsymbol{v}_{\boldsymbol{q}} \quad n_{\boldsymbol{q}} = -\frac{n_{\boldsymbol{q}} - n^0_{\boldsymbol{q}}}{\tau} \quad . \tag{1.34}$$

This assumption allows us to obtain an approximate expression for the non-equilibrium distribution $n_{\boldsymbol{q}}$ in terms of the equilibrium distribution $n^0_{\boldsymbol{q}}$, making the assumption that the displacements are small $\quad n_{\boldsymbol{q}} \qquad n^0_{\boldsymbol{q}}$, since we are not far from equilibrium. Thus

$$n_{\boldsymbol{q}} \quad n^0_{\boldsymbol{q}} - \tau \boldsymbol{v}_{\boldsymbol{q}} \quad n^0_{\boldsymbol{q}} = n^0_{\boldsymbol{q}} - \tau v_{\boldsymbol{q}} \cos\,, \frac{n^0_{\boldsymbol{q}}}{T} \quad T \tag{1.35}$$

The thermal conductivity can be obtained from this last expression by using the microscopic definition of the energy flux $\mathbf{j}$, that is, the average over the phonon population of the phonon energy $\hbar\omega$ times the group velocity in the direction of the thermal gradient $\mathrm{v_g}\cos\,,\ ,$ that is

$$\mathbf{j} =< \hbar\omega v_{\boldsymbol{q}} \cos\,,\ >= \sum_{\nu} \quad \hbar\omega\, v_{\boldsymbol{q}} \cos\,,\ n_{\boldsymbol{q}} \frac{d^3\boldsymbol{q}}{(2\pi)^3} \tag{1.36}$$

Substituting Eq. (1.35) into Eq. (1.36) and considering that the integration of the first term of (1.35) is zero because of the symmetry of the equilibrium distribution function, we have

$$\mathbf{j} = - \sum_{\nu} \quad \hbar\omega\tau v_{\boldsymbol{q}}^2 \cos^2\,, \frac{n_{\boldsymbol{q}}^0}{T} \frac{d^3\boldsymbol{q}}{8\pi^3} \qquad T \tag{1.37}$$

that, after the identification of this expression with the Fourier law (1.1), leads to an integral expression of the thermal conductivity

$$= \sum_{\nu} \quad \hbar\omega\tau v_{\boldsymbol{q}}^2 \cos^2\,, \frac{n_{\boldsymbol{q}}^0}{T} \frac{d^3\boldsymbol{q}}{8\pi^3} \quad , \tag{1.38}$$

where we are integrating in $d^3\boldsymbol{q} \equiv dqd, d\ \ ,$ and after performing the angular integral, we can re-express the remaining dq integral in terms of the angular frequency of the phonons, since $dq/8\pi^3 = D(\omega)d\omega$. This leads to the well-known expression of the thermal conductivity in the standard RTA approximation

$$= \frac{1}{3} \sum_{\nu} \quad \hbar\omega v_{\boldsymbol{g}}^2 \tau \frac{n^0(\omega)}{T} D(\omega)\mathrm{d}\omega \tag{1.39}$$

This expression is, in fact, a refinement of the simple kinetic theory expression (1.26), and similarly, its advantage is being simple and easy to implement, and able to provide good general trends of the behavior of with the temperature. Despite of the fact that this approach takes into account the whole phonon collectivity through the distribution function and the density of states, the phonon collisions are deficiently described through a single relaxation time. Chapter 3 is devoted to discuss phonon collisions, and further approaches based on the RTA with a different treatment of phonon collisions will be presented in Chapter 4.

Chapter 2

Lattice dynamics

The general problem of lattice dynamics in a crystal is focused on obtaining the characteristic dispersion relations of the crystal, namely, the relations between ω and $\mathbf{q}$, as explained in Chapter 1, and it can be summarized with the following steps:

- To choose a suitable interaction potential for the crystal considered, according to the type of binding between atoms in the crystal and built the Lagrangian or the Hamiltonian (the second Newton law can also be used).
- To obtain the force constants by calculating the second derivative of the potential with respect to the position.
- To use a wave expansion in order to transform the $3nN$ equations in $3n$ equations in a Fourier space. We find the so called dynamical matrix.
- To obtain the eigenvalues (the frequency square for a given wavevector) and eigenvector (given the atomic movement of the different atoms and thus giving the polarization) of the dynamical matrix. The relationship between ω_ν and q_j in three non-coplanar directions of the space are the so called dispersion relations.

In the next Sections 2.1 and 2.2, we elaborate these steps giving the mathematical detail of the general problem. Afterwards, in Secs. 2.3 and 2.4 we obtain the dispersion relations and density of states of certain materials related to this research by using two main lattice dynamics models suitable for these materials. Firstly, the Bond-charge Model, which describes very well several element and compound semiconductor materials and we will apply it to calculate the dispersion relations of silicon, germanium, diamond and gray-tin. These materials are

used in this thesis for their thermal conductivity study, as we will see in Chapters 5 and 6. Secondly, the Rigid-ion Model which is suitable to obtain the dispersion relations of Bi_2Te_3, whose thermal conductivity study will be presented in Chap. 7. It is our intention to be concise, so in the following Sections we present only the main steps in the calculations for each model. Further mathematical details on the models can be found in Ref. [21].

2.1 General problem of Lattice Dynamics

Let us suppose a crystal with n atoms, or ions, per unit cell. We will use $= 1, 2 \ldots n$ to number the atoms within the unit cell l. These atoms have a mass given by M_κ. The equilibrium position of any atom in the unit cell l is given by the vector

$$\boldsymbol{r}^0_{l\kappa} = \boldsymbol{r}_{\boldsymbol{l}} + \boldsymbol{r}_\kappa \quad , \tag{2.1}$$

where $\boldsymbol{r}^0_\kappa$ is the equilibrium position vector of the atom within the unit cell l, and

$$\boldsymbol{r}^0_{\boldsymbol{l}} = l_1\boldsymbol{a}_1 + l_2\boldsymbol{a}_2 + l_3\boldsymbol{a}_3 \quad , \tag{2.2}$$

is the equilibrium position vector of the l unit cell relative to an origin located at any atom, $\boldsymbol{a}_i$ being the primitive lattice vectors defining the primitive unit cell, and l_1, l_2, l_3 being integers. These atoms are not in equilibrium, but vibrating around their equilibrium positions as a result of thermal fluctuations in the crystal. Therefore, the actual position of any atom ($\boldsymbol{l}$) is given by

$$\boldsymbol{r}_{l\kappa} = \boldsymbol{r}^0_{l\kappa} + \boldsymbol{u}_{l\kappa} \quad , \tag{2.3}$$

where $\boldsymbol{u}_{l\kappa}$ are the small displacement of the ion ($\boldsymbol{l}$) around equilibrium (see Fig. 2.1). The kinetic energy of the vibrating crystal is

$$\mathcal{T} = \frac{1}{2}\sum_{l\kappa} M_\kappa \dot{\boldsymbol{u}}^2_{l\kappa} \quad , \tag{2.4}$$

and the potential energy is assumed to be a function depending on the position of all ions in the unit cell

$$U = U(\{\boldsymbol{l}\ \}). \tag{2.5}$$

Then, the Lagrangian of the system is

$$\mathcal{L} = \frac{1}{2}\sum_{l\kappa} M_\kappa \dot{\boldsymbol{u}}^2_{l\kappa} - U(\{\boldsymbol{l}\ \}) \quad . \tag{2.6}$$

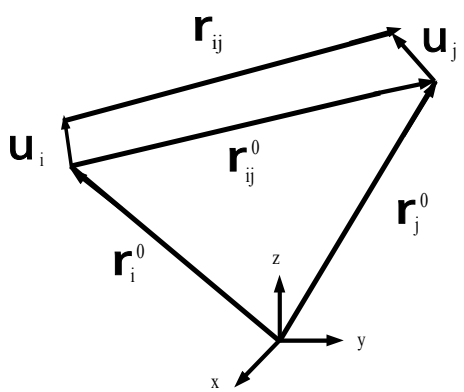

Figure 2.1: Equilibrium (r_i^0 and r_j^0) and displaced (u_i and u_j) atomic positions vectors of a pair of ions $i = (\boldsymbol{l}\ \ )$ and $j = (\boldsymbol{l}\ \ \ )$.

In order to arrive to the equation of motion, if the displacements of the atoms around their equilibrium position are small compared with the interatomic distances, it is enough to consider the harmonic approximation. It consists of expanding the potential energy U about its equilibrium positions in terms of the small displacements $\boldsymbol{u}$ and cut the Taylor expansion at second order.

Let us write

$$U(\{\boldsymbol{l}\ \ \}) = U_0 + \sum_{\boldsymbol{l}\kappa,\alpha} \ \ {}_{\alpha}(\boldsymbol{l}\ \ )u_{\boldsymbol{l}\kappa,\alpha} + \frac{1}{2}\sum_{\substack{\boldsymbol{l}\kappa,\alpha \\ \boldsymbol{l}'\kappa',\beta}} \ \ {}_{\alpha\beta}(\boldsymbol{l}\ \ ;\boldsymbol{l}\ \ \ )u_{\boldsymbol{l}\kappa,\alpha}u_{\boldsymbol{l}'\kappa',\beta} \tag{2.7}$$

where and . are Cartesian components and

$${}_{\alpha}(\boldsymbol{l}\ \ ) = \frac{U}{u_{\boldsymbol{l}\kappa,\alpha}}\Big|_{\boldsymbol{u}=0} \tag{2.8}$$

and

$${}_{\alpha\beta}(\boldsymbol{l}\ \ ;\boldsymbol{l}\ \ \ ) = \frac{{}^2U}{u_{\boldsymbol{l}\kappa,\alpha}\ \ u_{\boldsymbol{l}'\kappa',\beta}}\Big|_{\boldsymbol{u}=0} \quad . \tag{2.9}$$

The term U_0 is the energy of the crystal without considering the atomic motion and it can be considered as the origin of energies *i.e.*, U_0 =0. The second term in the expansion yields the

forces around equilibrium. But the total force on a given atom is zero in equilibrium (there is a minimum in the potential energy, *i.e.* the atoms move around the equilibrium position). Thus,

$$_{\boldsymbol{l}\kappa,\alpha} = 0 \qquad (\boldsymbol{l} \ , \ ) \quad . \tag{2.10}$$

After this simplification, the potential energy can be written, in the harmonic approximation, as

$$U = \frac{1}{2} \sum_{\substack{\boldsymbol{l}\kappa,\alpha \\ \boldsymbol{l}'\kappa',\beta}} \ _{\alpha\beta}(\boldsymbol{l} \ ; \boldsymbol{l} \ )u_{\boldsymbol{l}\kappa,\alpha} u_{\boldsymbol{l}'\kappa',\beta} \tag{2.11}$$

and the Lagrangian of the system becomes

$$\mathcal{L} = \frac{1}{2} \sum_{\boldsymbol{l}\kappa} M_\kappa \dot{\boldsymbol{u}}^2_{\boldsymbol{l}\kappa} - \frac{1}{2} \sum_{\substack{\boldsymbol{l}\kappa,\alpha \\ \boldsymbol{l}'\kappa',\beta}} \ _{\alpha\beta}(\boldsymbol{l} \ ; \boldsymbol{l} \ )u_{\boldsymbol{l}\kappa,\alpha} u_{\boldsymbol{l}'\kappa',\beta} \tag{2.12}$$

If we need to solve the equation of motion, an explicit mathematical form of the potential is needed. A suitable potential will be chosen depending on the crystal we are studying, this will be detailed in the next sections, where we introduce the lattice dynamics models required for the present work.

2.1.1 The equation of motion and the force constants

The Lagrange equations of motion are

$$\frac{d}{dt} \frac{\mathcal{L}}{\dot{u}_{\boldsymbol{l}\kappa,\alpha}} = \frac{\mathcal{L}}{u_{\boldsymbol{l}\kappa,\alpha}} \quad . \tag{2.13}$$

Taking the derivative of Eq. (2.12), it is found

$$M_\kappa \ddot{u}_{\boldsymbol{l}\kappa,\alpha} = - \sum_{\boldsymbol{l}'\kappa',\beta} \ _{\alpha\beta}(\boldsymbol{l} \ ; \boldsymbol{l} \ )u_{\boldsymbol{l}'\kappa',\beta} \qquad (\boldsymbol{l} \ , \ ) \quad , \tag{2.14}$$

this is a set of $3nN$ equations, where the coefficients $_{\alpha\beta}(\boldsymbol{l} \ ; \boldsymbol{l} \ )$ given by Eq. (2.9) are called *atomic force constants.*

2.1.2 Dynamical matrix: dispersion relations

We are looking for wave solutions for the displacements. Thus, the atomic displacement must have the form

$$\boldsymbol{u}_{\boldsymbol{l}\kappa}(\omega_{\mathbf{q}}, \boldsymbol{q}) = \frac{1}{2 \ \sqrt{NM_\kappa}} A_{\boldsymbol{q}} \boldsymbol{e}_{\boldsymbol{q}\kappa} e^{i(\boldsymbol{q}\cdot\boldsymbol{r}_{\boldsymbol{l}\kappa} - \omega_{\boldsymbol{q}} t)} + \text{c.c.} \tag{2.15}$$

Here, $A_{\boldsymbol{q}}$ is an amplitude (which can depend on the temperature and, of course, on the physical properties of the material) and $\boldsymbol{e}_{\boldsymbol{q}\kappa}$ is the polarization vector, that is, an unitary vector which indicates the direction of the atomic motion (longitudinal or transversal). Note that, although the branch index has been omitted for simplicity, whenever we introduce a parameter depending on $\mathbf{q}$, the dependence can be substituted by $\boldsymbol{q}, \nu$, *e. g.* $\omega_{\boldsymbol{q},\nu}$, $A_{\boldsymbol{q},\nu}$ and $\boldsymbol{e}_{\boldsymbol{q},\nu,\kappa}$. Introducing expression (2.15) into the equation of motion (2.14) yields

$$\omega_{\boldsymbol{q}}^2 M_\kappa \frac{1}{2\sqrt{NM_\kappa}} A_{\boldsymbol{q}} e_{\boldsymbol{q}\kappa,\alpha} e^{i\boldsymbol{q}\cdot\boldsymbol{r}_{\boldsymbol{l}\kappa}} = \sum_{\boldsymbol{l}'\kappa',\beta} \frac{1}{2\sqrt{NM_{\kappa'}}} \quad {}_{\alpha\beta}(\boldsymbol{l} \ ;\boldsymbol{l} \quad) A_{\boldsymbol{q}} e_{\boldsymbol{q}\kappa',\beta} e^{i\boldsymbol{q}\cdot\boldsymbol{r}_{\boldsymbol{l}'\kappa'}} \tag{2.16}$$

Simplifying, one obtains

$$\omega_{\boldsymbol{q}}^2 e_{\boldsymbol{q}\kappa,\alpha} = \sum_{\boldsymbol{l}'\kappa',\beta} \frac{1}{\sqrt{M_\kappa M_{\kappa'}}} \quad {}_{\alpha\beta}(\boldsymbol{l} \ ;\boldsymbol{l} \quad) e_{\boldsymbol{q}\kappa',\beta} e^{i\boldsymbol{q}\cdot(\boldsymbol{r}_{\boldsymbol{l}'\kappa'}-\boldsymbol{r}_{\boldsymbol{l}\kappa})} \tag{2.17}$$

By introducing the dynamical matrix

$$D_{\alpha\beta}(\boldsymbol{q}; \quad) = \frac{1}{\sqrt{M_\kappa M_{\kappa'}}} \sum_{\boldsymbol{l}'} \quad {}_{\alpha\beta}(\boldsymbol{l} \ ;\boldsymbol{l} \quad) e^{i\boldsymbol{q}\cdot(\boldsymbol{r}_{\boldsymbol{l}'\kappa'}-\boldsymbol{r}_{\boldsymbol{l}\kappa})} \quad , \tag{2.18}$$

we can write (2.17) as an eigenvalue equation

$$\omega_{\boldsymbol{q}}^2 e_{\boldsymbol{q}\kappa,\alpha} = \sum_{\kappa',\beta} D_{\alpha\beta}(\boldsymbol{q}; \quad) e_{\boldsymbol{q}\kappa',\beta} \quad , \tag{2.19}$$

which can be re-written as

$$\sum_{\kappa',\beta} D_{\alpha\beta}(\boldsymbol{q}; \quad) - \quad {}_{\kappa\kappa'} \quad {}_{\alpha\beta}\omega_{\boldsymbol{q}}^2 \ e_{\boldsymbol{q}\kappa',\beta} = 0 \quad . \tag{2.20}$$

This equation can be written in terms of a determinant of order $3n \quad 3n$, giving $3n$ solutions for a given $\boldsymbol{q}$. These solutions are the dispersion relations of the crystal, *i. e.* the $3n$ eigenmodes, or eigenfrequencies, corresponding to a given $\boldsymbol{q}$. The *Lattice Dynamical* problem consists of finding the solutions of the eigenvalue equation for a given $\boldsymbol{q}$. For this purpose, we need, in first place, to define the potential energy of our crystal taking into account some considerations, as explained in the following Section.

2.2 Interatomic forces and Phonon dispersion relations

Generally, to define the potential energy of our crystal, we will suppose that U is originated by a two-body interaction among all possible pairs of ions $i = (\boldsymbol{l} \ ), j = (\boldsymbol{l} \quad)$, although

some times we will need to consider a three-body interaction, as it is the case of the Keating potential. The interaction energy between two ions usually can contain two terms and can be written as

$$U = U^{Short-range} + U^{Long-range} \tag{2.21}$$

The first term is a short-range interaction of Van der Waals type, which accounts for the repulsive forces. The basic short-range forces are stretching and bending forces between ions in the crystal. The second term is the electrostatic interaction or Coulomb term, which accounts for the long-range interactions and has an attractive and a repulsive component.

To deal with the short-range interactions it is necessary to chose a suitable potential for the type of binding between the atoms in the crystal under study, some of the most used potentials are Lennard-Jones, Keating, Morse or Stillinger-Weber potentials. We also need a model to account for these interactions between first, second, or even third-neighboring atoms in the crystal. In the next Sections, we particularize the lattice dynamics problem to study two different types of materials, each one with the appropriate short-range potential within the appropriate lattice dynamics model. The way of dealing with the long-range Coulomb interaction is something general to all the crystals. The usual approach in a three dimensional crystal is given by the Ewald's method [40, 41] and it has been summarized in Appendix A.

2.3 The adiabatic Bond-charge model

The adiabatic Bond-charge model (BCM) was developed by Weber [4, 42] to account for the lattice dynamics of covalent crystals. It deals with the short-range interaction between atoms in a crystal by including a set of massless charges called bond-charges, which presumably are located at the position corresponding to the maximum density of charge in the bond between atoms. These bond-charges account for the electrons shared by the atoms participating in the covalent bond, which tend to be partially localized between the bonding atoms. The number of bond-charges depends, thus, on the number of bonds. The long-range interactions are treated from the usual Ewald's method (see Appendix A).

As shown by Weber [42], the BCM provides accurate and complete dispersion relations for the group of materials we are interested in: the group-IV element semiconductors, that consist of silicon (Si), germanium (Ge), diamond (C) and gray-tin (-Sn). These materials have the same lattice structure as the diamond lattice, which is a double interpenetrated FCC lattice, where each atom in the crystal forms a covalent bond with other 4 atoms providing

a tetragonal bond (see Figs. (2.2) and (2.4)). The covalent bond is usually formed from two electrons, one from each atom participating in the bond. The bond-charge is constituted by these two electrons, because they tend to be partially localized between the bonding atoms. In our case, we deal with monoatomic crystals (Si, Ge, C and -Sn), so the equilibrium site of the bond-charge is in the middle of the two bonding atoms. The model has also been extended to groups III-V compound semiconductors and to group II-VI, which are covalent compounds of different atoms, (for instance GaN). In this case, the bond-charge equilibrium site would be shifted toward the most electronegative atom.

One of the advantages of the BCM against other more simple models, like the rigid-ion model we will present in the next Section, is that the dispersion relations can be obtained with a minimum set of force constants, actually 4 parameters for diamond-like semiconductors and 5 in the case of III-V or II-VI compounds [43]. Furthermore, the covalent semiconductors with diamond or sphearalite structure (except diamond itself) have very low frequencies in the transversal acoustic branches, and present a drastic change in the tendency of the curves: the slope of the $\omega(\boldsymbol{q})$ acoustic curves at $\boldsymbol{q}$ 0 (the zone center of the Brillouin zone) has high values, while at $\boldsymbol{q}$ π/a (the border of the Brillouin zone) the curves are very flat. The BCM reproduces very well this behavior of the transversal acoustic branches, while other models with more parameters are not able to do it, *e.g.* the valence-force-field model which needs 6 parameters as shown in [44]; the shell model with 5 parameters for germanium according to [21], or the rigid-ion model which needs usually 11 parameters, as shown in [17,45]. Another advantage is that the optic branches are also well reproduced within the BCM [46], what allows us, eventually, to includes the contribution of optical phonons on the thermal conductivity, neglected in the Debye approximation.

2.3.1 The diamond structure

The lattice structure of the group IV semiconductors is the diamond structure, which consist of two FCC structures shifted $(1/4, 1/4, 1/4)a$ along the diagonal, being a the lattice parameter. The only difference between these materials is, precisely, the value of a, indicated in Table 2.1. Therefore, we will elaborate the model using silicon as reference, being analogous for the other materials.

The usual setting is shown in Fig. 2.2, with two atoms forming the basis of the lattice: one Si atom at (0,0,0) (Si_1), and another in

$(1/4, 1/4, 1/4)a$ (Si_2). The bonding around a given atom is tetragonal and all bonds have

Table 2.1: Lattice parameters for group-IV semiconductors ordered from the lower to the higher value. The lower the value of a, the higher the frequencies in the dispersion curves [3].

Material	Diamond	Silicon	Germanium	-Tin
a (Å)	3.57	5.45	5.66	6.49

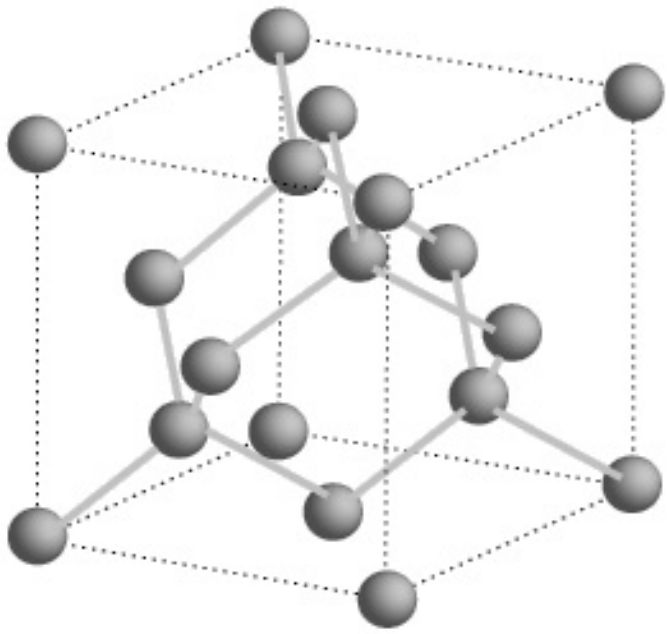

Figure 2.2: Diamond structure. It consist of a interpenetrated FCC lattice, or in other words, two FCC lattices, one of them shifted $(1/4, 1/4, 1/4)a$ *along the diagonal from the other.*

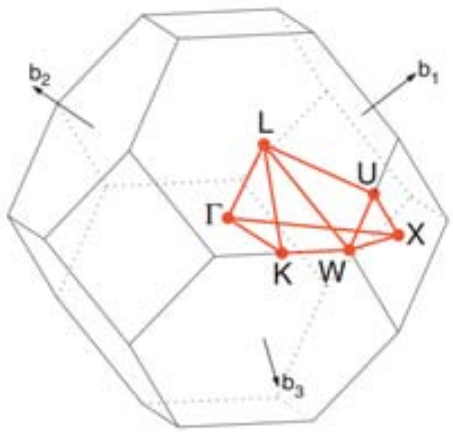

Figure 2.3: Brillouin zone of a FCC lattice, with high-symmetry $\mathbf{q}$ *points* $L = \frac{2\pi}{a}(\frac{1}{2}, \frac{1}{2}, \frac{1}{2})$, $X = \frac{2\pi}{a}(1, 0, 0)$, $K = \frac{2\pi}{a}(\frac{3}{4}, \frac{3}{4}, 0)$ *and* $\Gamma = (0, 0, 0)$ *being* a *the lattice parameter,* Γ *is the center of the BZ and the other points label the most important points in the BZ; the vectors* $\mathbf{b}_i$ *are the reciprocal lattice vectors. From Setyawan and Curtarolo [47].*

the same length. The primitive cell is trigonal, with primitive vectors

$$\boldsymbol{a}_1 = \quad \frac{1}{2}, \frac{1}{2}, 0 \quad a \quad ; \quad \boldsymbol{a}_2 = \quad 0, \frac{1}{2}, \frac{1}{2} \quad a \quad ; \quad \boldsymbol{a}_3 = \quad \frac{1}{2}, 0, \frac{1}{2} \quad a \tag{2.22}$$

The volume of the unit cell is

$$V_a = \boldsymbol{a}_1 \quad \boldsymbol{a}_2 \quad \boldsymbol{a}_3 = \begin{matrix} \frac{1}{2} & \frac{1}{2} & 0 \\ 0 & \frac{1}{2} & \frac{1}{2} \\ \frac{1}{2} & 0 & \frac{1}{2} \end{matrix} \quad a^3 = \frac{a^3}{4} \quad . \tag{2.23}$$

It is convenient to write the atomic position of the ions as a function of the primitive vectors, thus

$$\begin{matrix} \mathrm{Si}_1 & 0 \\ \mathrm{Si}_2 & \frac{1}{4}\boldsymbol{a}_1 + \frac{1}{4}\boldsymbol{a}_2 + \frac{1}{4}\boldsymbol{a}_3 \quad . \end{matrix} \tag{2.24}$$

so they are separated a distance $d_0 = a \quad \overline{3}/4$, which is the bond length. The directions of the bonds, arising in Si_1 are:

$$\boldsymbol{a}_1 + \boldsymbol{a}_2 + \boldsymbol{a}_3; \quad -\boldsymbol{a}_1 - \boldsymbol{a}_2 + \boldsymbol{a}_3; \quad \boldsymbol{a}_1 - \boldsymbol{a}_2 - \boldsymbol{a}_3; \quad -\boldsymbol{a}_1 + \boldsymbol{a}_2 - \boldsymbol{a}_3 \tag{2.25}$$

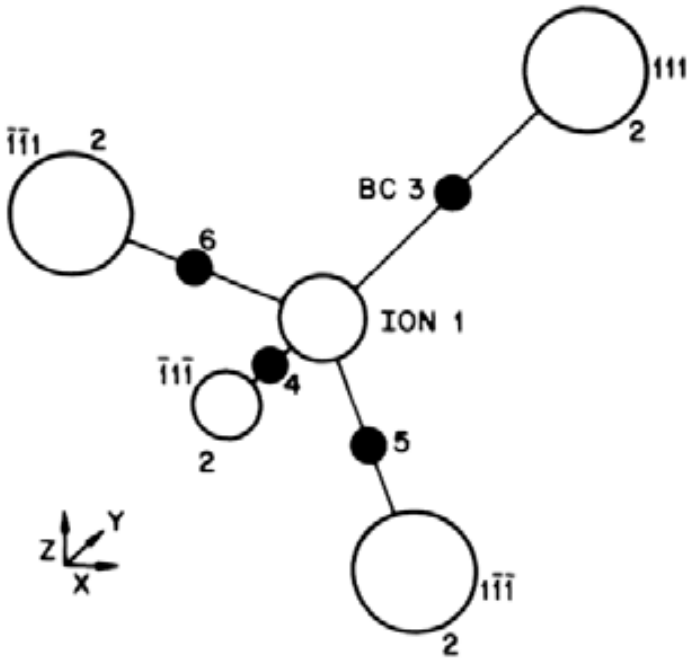

Figure 2.4: Scheme of the unit cell of the diamond structure with ions 1 and 2 (open circles) and bond-charges 3-6 (solid circles). (Reproduced from [42]).

while the bonds arising in Si_2 are directed along

$$-\boldsymbol{a}_1 - \boldsymbol{a}_2 - \boldsymbol{a}_3; \quad \boldsymbol{a}_1 + \boldsymbol{a}_2 - \boldsymbol{a}_3; \quad -\boldsymbol{a}_1 + \boldsymbol{a}_2 + \boldsymbol{a}_3; \quad \boldsymbol{a}_1 - \boldsymbol{a}_2 + \boldsymbol{a}_3 \tag{2.26}$$

Obviously, they have opposite sign as compared to the previous bond directions. As it is well known, the reciprocal lattice of a FCC is a BCC structure. The corresponding first Brillouin zone is shown in Fig. 2.3, where the vectors from the $2\pi-$reciprocal lattice are

$$\boldsymbol{b}_1 = \frac{2\pi}{a}(11\bar{1}) \quad ; \quad \boldsymbol{b}_2 = \frac{2\pi}{a}(\bar{1}11) \quad ; \quad \boldsymbol{b}_3 = \frac{2\pi}{a}(1\bar{1}1) \quad . \tag{2.27}$$

The center of the BZ is denoted by the point $\Gamma = (0, 0, 0)$ and the high-symmetry directions in the $\boldsymbol{q}$-space correspond to the paths between the points $\Gamma, \mathrm{X}, \mathrm{L}, \mathrm{U}, \mathrm{K}, \mathrm{W}$ shown with red lines in the figure.

2.3.2 Bond-charges in the diamond structure

The unit cell of the diamond structure is shown in Fig. 2.4, where we have added the bond-charges. Let us call d_0 the Si_1–Si_2 bond length. The bond-charge is located in the middle of them, that is, at $d_0/2$ from the Si_1 atom. There are four bond-charges in the unit cell, the four around the Si_1 and Si_2atoms, which means there are two bond-charges per atom.

We need to number the bond-charges and to know their position in the lattice preferably in terms of the primitive vectors, given by

$$\begin{aligned}
\mathrm{bc}_1 &: \frac{1}{8}(\boldsymbol{a}_1+\boldsymbol{a}_2+\boldsymbol{a}_3)\\
\mathrm{bc}_2 &: \frac{1}{8}\boldsymbol{a}_1+\frac{3}{8}\boldsymbol{a}_2+\frac{3}{8}\boldsymbol{a}_3\\
\mathrm{bc}_3 &: \frac{3}{8}\boldsymbol{a}_1+\frac{1}{8}\boldsymbol{a}_2+\frac{3}{8}\boldsymbol{a}_3\\
\mathrm{bc}_4 &: \frac{3}{8}\boldsymbol{a}_1+\frac{3}{8}\boldsymbol{a}_2+\frac{1}{8}\boldsymbol{a}_3
\end{aligned} \tag{2.28}$$

2.3.3 Short-range interactions

We have considered three types of interactions: (1) a central potential $/_{ii}$ between nearest-neighbor ions, which is a bond-stretching type; (2) a central potential $/_{i-bc}$ between nearest-neighbor ions and bond-charges (bc), which is also a bond-stretching type; and (3) the interactions between two adjacent bonds, that is, two bond-charges bonding a common ion, which is a bond-bending (bb) type and it is described by Keating's potential, given by

$$V_{bb} = \frac{\cdot}{{}_2}\ (\boldsymbol{r}_{\boldsymbol{l}'\kappa'}-\boldsymbol{r}_{\boldsymbol{l}\kappa})\cdot(\boldsymbol{r}_{\boldsymbol{l}''\kappa''}-\boldsymbol{r}_{\boldsymbol{l}\kappa}) + \quad {}^2\ {}^2 \tag{2.29}$$

where ${}^2 = |(\boldsymbol{r}_{\boldsymbol{l}'\kappa'}-\boldsymbol{r}_{\boldsymbol{l}\kappa})\cdot(\boldsymbol{r}_{\boldsymbol{l}''\kappa''}-\boldsymbol{r}_{\boldsymbol{l}\kappa})|$.

The ions interact between them and with the bond-charges via central potentials. Let us denote these potential as $/_{ii}$ for the ion1-ion2 interaction (bond-streching type), and $/_{i-bc}$ for the ion-bc interaction (also bond-stretching type). The bond-charges bonding a common ion interact between them via a three-body Keating potential (bond-bending type).

We have limited the short-range ion-BC and BC-BC interactions to nearest neighbors.

According to the adiabatic correction introduced by Weber, the bond-charges are not fixed, but they are allowed to move adiabatically between the bonded atoms [4]. To stabilize the bond-charges in their site we need to introduce short-range forces between the bond-charges and the atoms.

Thus, the short-range potential energy is the combination of taking into account all the these possible interactions between the ions and the bond-charges

$$U^{Short-range} = 4[/_{ii}(d_0) + /_{i-bc}(d_0)] + 6[V_{bb}(d_0, ,) + \quad _1] \tag{2.30}$$

The mathematical detail can be followed from the works by Weber [4, 42]. Along these Sections we only summarize the main steps.

2.3.4 Force constants

According to (2.9) we can calculate the force constants for the three types of interactions. The mathematical detail can be followed from the works by Weber [4, 42].

Ion-ion interaction

The interaction potential in case of ion-ion interaction is $/_{ii}$. Thus, according to (2.9) we can calculate the force constants as

$$\begin{smallmatrix}\text{i-i}\\ \alpha\beta\end{smallmatrix}(\boldsymbol{q}, \quad , \quad) \equiv \frac{^2/_{ii}}{x_{\boldsymbol{l}'\kappa',\alpha} \quad x_{\boldsymbol{0}\kappa,\beta}} = \frac{}{x_{\boldsymbol{0}\kappa,\beta}} \quad /_{ii}\frac{|\boldsymbol{r}_{\boldsymbol{l}'\kappa} - \boldsymbol{r}_{\boldsymbol{0}\kappa}|}{x_{\boldsymbol{l}'\kappa',\alpha}} \quad = \frac{}{x_{\boldsymbol{0}\kappa,\beta}} \quad /_{ii}\frac{x_{\boldsymbol{l}'\kappa',\beta} - x_{\boldsymbol{0}\kappa,\beta}}{|\boldsymbol{r}_{\boldsymbol{l}'\kappa} - \boldsymbol{r}_{\boldsymbol{0}\kappa}|} \tag{2.31}$$

where $|\boldsymbol{r}_{\boldsymbol{l}'\kappa} - \boldsymbol{r}_{\boldsymbol{0}\kappa}| \equiv d_0$ is the ion-ion distance, that is, the bond length. After operating and simplifying we obtain an expression of $\begin{smallmatrix}\text{i-i}\\ \alpha\beta\end{smallmatrix}(\boldsymbol{q}, \quad , \quad)$ in terms of the first $/_{ii}$ and second $/_{ii}$ derivative of the interaction potential

$$\begin{smallmatrix}\text{i-i}\\ \alpha\beta\end{smallmatrix}(\boldsymbol{q}, \quad , \quad) = - \quad _{\alpha\beta}\frac{/_{ii}}{d_0} - \quad /_{ii} + \frac{/_{ii}}{t} \quad \frac{1}{d_0^2}\sum_{\boldsymbol{l}'}(x_{\boldsymbol{l}'\kappa',\alpha} - x_{\boldsymbol{0}\kappa,\alpha})(x_{\boldsymbol{l}'\kappa',\beta} - x_{\boldsymbol{0}\kappa,\beta}) \tag{2.32}$$

The condition of stable equilibrium relates the first derivatives of the short-range potentials with the Madelung energy of the system [4]. Thus, $/_{ii}/d_0$ can be written as

$$\frac{/_{ii}}{d_0} = - \quad _M\frac{z^2}{} \frac{e^2}{2d_0^3} \tag{2.33}$$

being $\quad _M$ the Madelung constant, z the charge of the bond-charge, e the electron charge and the dielectric constant, where substituting the value of the bond length $d_0 = a \quad \overline{3}/4$ in terms of the unit cell volume V_a according to (2.23) we obtain

$$\frac{/_{ii}}{d_0} = -\frac{8}{3} \quad _M\frac{z^2}{} \frac{e^2}{V_a} \quad . \tag{2.34}$$

The terms $/_{ii}$ and $\frac{z^2}{}$ remain as free adjustable parameter.

Ion–bond-charge interaction

The potential related to the ion-bond-charge $/_{i-bc}$ for the ion-bond-charge situated at a distance $d_0/2$. Let us calculate the related force constants from (2.9). First,

$$ {}^{\mathrm{i-bc}}_{\alpha\beta}(\boldsymbol{q}, \quad , \quad) = \frac{{}^{2}/_{i-bc}}{x_{\boldsymbol{l}'\kappa',\alpha} \quad x_{\boldsymbol{0}\kappa,\beta}} = \frac{}{x_{\boldsymbol{0}\kappa,\beta}} \quad /_{i-bc} \frac{|\boldsymbol{r}_{\boldsymbol{l}'\kappa} - \boldsymbol{r}_{\boldsymbol{0}\kappa}|}{x_{\boldsymbol{l}'\kappa',\alpha}} \quad = \frac{}{x_{\boldsymbol{0}\kappa,\beta}} \quad /_{i-bc} \frac{x_{\boldsymbol{l}'\kappa',\beta} - x_{\boldsymbol{0}\kappa,\beta}}{|\boldsymbol{r}_{\boldsymbol{l}'\kappa} - \boldsymbol{r}_{\boldsymbol{0}\kappa}|} \tag{2.35} $$

where $|\boldsymbol{r}_{\boldsymbol{l}'\kappa} - \boldsymbol{r}_{\boldsymbol{0}\kappa}| \equiv d_0/2$ is the ion-bond-charge distance. After a little algebra we find

$$ {}^{\mathrm{i-bc}}_{\alpha\beta}(\boldsymbol{q}, \quad , \quad) = - \quad {}_{\alpha\beta} \frac{/_{i-bc}}{d_0/2} - \quad /_{i-bc} + \frac{/_{i-bc}}{d_0/2} \quad \frac{1}{(d_0/2)^2} \sum_{\boldsymbol{l}'} (x_{\boldsymbol{l}'\kappa',\alpha} - x_{\boldsymbol{0}\kappa,\alpha}) (x_{\boldsymbol{l}'\kappa',\beta} - x_{\boldsymbol{0}\kappa,\beta}) \tag{2.36} $$

where the firs derivative of the potential is assumed to be zero $/_{i-bc} = 0$ according to [4, 42]. The term $/_{i-bc}$ is a free adjustable parameters.

Bond-charge–bond-charge interaction

The contribution to the bond-charge–bond-charge force constants comes from the second derivative of (2.29) according to (2.9),

$$ \begin{aligned} {}^{\mathrm{bc-bc}}_{\alpha\beta}(\boldsymbol{q}, \quad , \quad) &= \frac{{}^{2}V_{bb}}{x_{\boldsymbol{l}'\kappa',\alpha} \quad x_{\boldsymbol{0}\kappa,\beta}} = \\ &= \frac{B_1}{4a_1^2} \sum_{\boldsymbol{l}'\boldsymbol{l}''\kappa} (\boldsymbol{r}_{\boldsymbol{l}'\kappa'} - \boldsymbol{r}_{\boldsymbol{0}\kappa}) (\boldsymbol{r}_{\boldsymbol{l}''\kappa''} - \boldsymbol{r}_{\boldsymbol{0}\kappa}) + a_1^2 \quad {}_{\alpha\beta} \\ &+ \frac{B_1}{4a_1^2} \sum_{\boldsymbol{l}'\boldsymbol{l}''\kappa} (x_{\boldsymbol{l}'\kappa',\alpha} - x_{\boldsymbol{0}\kappa,\alpha}) (x_{\boldsymbol{l}''\kappa'',\beta} - x_{\boldsymbol{0}\kappa,\beta}) \end{aligned} \tag{2.37} $$

2.3.5 The dynamical matrix within the bond-charge model

If we return to the equations of motion (2.14), namely

$$ M_\kappa \ddot{u}_{\boldsymbol{l}\kappa,\alpha} = - \sum_{\boldsymbol{l}'\kappa',\beta} \quad {}_{\alpha\beta}(\boldsymbol{l} \quad ; \boldsymbol{l} \quad) u_{\boldsymbol{l}'\kappa',\beta} \qquad (\boldsymbol{l} \quad , \quad) \tag{2.38} $$

and we separate the contribution of ions (denoting their corresponding displacement hypervector $\boldsymbol{u}[1:2]$)and bond-charges (denoting their corresponding displacement hypervector $\boldsymbol{u}[3:6]$), we get

$$ \begin{aligned} \boldsymbol{M}\omega^2 \boldsymbol{u}[1:2] &= (\boldsymbol{R} + \boldsymbol{C}_R) \boldsymbol{u}[1:2] + (\boldsymbol{T} + \boldsymbol{C}_T) \boldsymbol{u}[3:6] \\ 0 &= \boldsymbol{T}^\dagger + \boldsymbol{C}_T^\dagger \quad \boldsymbol{u}[1:2] + (\boldsymbol{S} + \boldsymbol{C}_S) \boldsymbol{u}[3:6] \end{aligned} \tag{2.39} $$

Table 2.2: BCM parameters for group-IV semiconductors given in units e^2/V_a. The BCM for diamond has one additional parameter $a = 0.51r^0/16$. These values are those found by Weber in [4] after fitting to experimental dispersion relations from neutron scattering data.

	C	Si	Ge	-Sn
$\frac{1}{3}/_{ii}$	-10.0	6.21	6.61	7.43
$z^2/$	0.885	0.180	0.162	0.163
$\frac{1}{3}/_{i-bc}$	50.0	6.47	5.71	5.59
.	12.56	8.60	8.40	7.80

where $\boldsymbol{M}$ is a diagonal matrix with the masses of the ions, note that the adiabatic approximation is expressed by having put the mass of the bond-charges equal to zero in (2.39). The bond-charge coordinates $\boldsymbol{u}[3:6]$ can be eliminated, obtaining

$$\boldsymbol{M}\omega^2\boldsymbol{u}[1:2] = \quad (\boldsymbol{R}+\boldsymbol{C}_R) - (\boldsymbol{T}+\boldsymbol{C}_T)\,(\boldsymbol{S}+\boldsymbol{C}_S)^{-1} \quad \boldsymbol{T}^\dagger + \boldsymbol{C}_T^\dagger \quad \boldsymbol{u}[1:2] \tag{2.40}$$

with the dynamical matrix being

$$\boldsymbol{D} = \boldsymbol{M}^{-1/2} \quad (\boldsymbol{R}+\boldsymbol{C}_R) - (\boldsymbol{T}+\boldsymbol{C}_T)\,(\boldsymbol{S}+\boldsymbol{C}_S)^{-1} \quad \boldsymbol{T}^\dagger + \boldsymbol{C}_T^\dagger \tag{2.41}$$

according to the definition (2.18), where $\boldsymbol{R}$, $\boldsymbol{T}$ and $\boldsymbol{S}$ are the dynamical matrices for the short range ion-ion, ion-bc and bc-bc interactions; and $\boldsymbol{C}_R$, $\boldsymbol{C}_T$ and $\boldsymbol{C}_S$ are the corresponding Coulomb matrices which are evaluated by Ewalds method described in Appendix A.

2.3.6 Dispersion relations and density of states of group IV semiconductors

We have applied the described adiabatic Bond-charge model to diamond, silicon, germanium and gray tin, belonging to group-IV semiconductors. According to the procedure described in the previous Sections and finding the eigenvalues of the dynamical matrix (2.41) for each material, with the values of the parameters indicated in Table 2.2, we have obtained their dispersion relations.

In Figs. 2.5 (a)-2.8 (a) we show the obtained dispersion relations for each material along high-symmetry directions in $\boldsymbol{q}-$space and compare them with data from neutron scattering experiments. Note that there are 6 dispersion curves or branches, in some directions degenerated, according to $\nu = 3n$ with $n = 2$ for these materials, corresponding to 3 acoustic branches

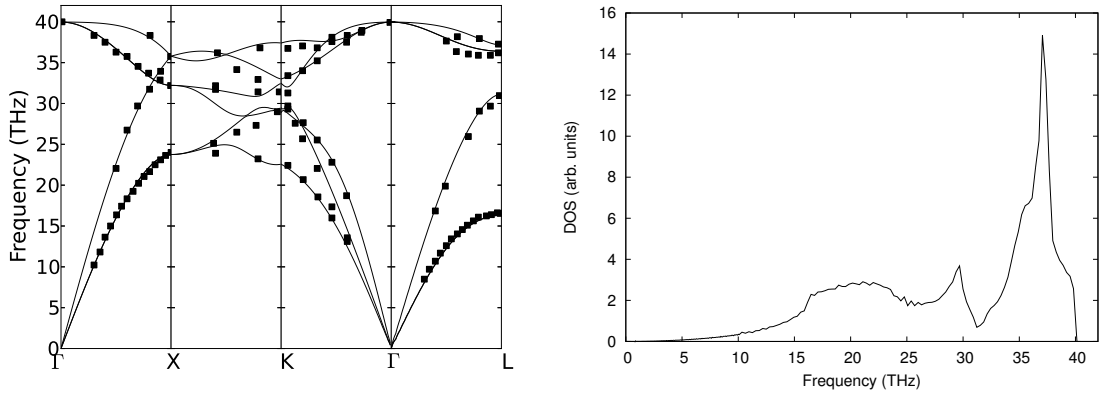

(a) (b)

Figure 2.5: Phonon dispersion relations and density of sates for diamond (C). (a) Solid lines: theoretical dispersion relations obtained with the BCM along high-symmetry axes. Symbols: data from neutron scattering experiments [48]. (b) Density of states calculated from BCM dispersion relations.

and 3 optic branches. It can be observed that the predictions are in very good agreement with data from such experiments. Particularly, transversal acoustic phonon branches close to the border of the Brillouin zone (X,K and L points) are very well reproduced, as we discussed in 2.3. In figures 2.5(b)-2.8 (b) we show the corresponding density of states in terms of the frequency for each material calculated according to Eq. (1.11) using the obtained dispersion relations. Note that the curve exhibits the peaks at the frequencies corresponding to the limit of the BZ of each branch. The reliability of the calculation of the density of states lies in the accuracy of prediction of the specific heat as a function of the temperature. We show in Fig. 2.9 the obtained specific heat as a function of temperature for the group-IV materials, where the Debye temperature is marked with a grid.

2.4 Rigid-ion model

The rigid-ion model (RIM) is one of the simplest and usual approaches, together with the shell model, to account for the atomic interactions in a crystal [21]. As we will see, its degree of complexity is much lower than the Bond-charge model. In the RIM, the ionic charges of the crystalline lattice are taken as point charges centered at the nuclei of the atoms. In fact,

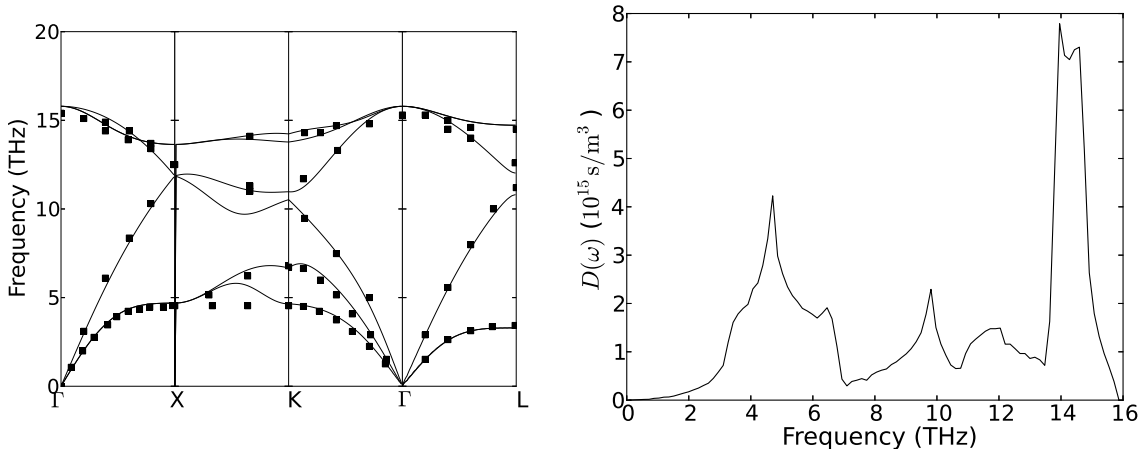

(a) (b)

Figure 2.6: Phonon dispersion relations and density of sates for silicon (Si). (a) Solid lines: theoretical dispersion relations obtained with the BCM along high-symmetry axes. Symbols: data from neutron scattering experiments [49]. (b) Density of states calculated from BCM dispersion relations.

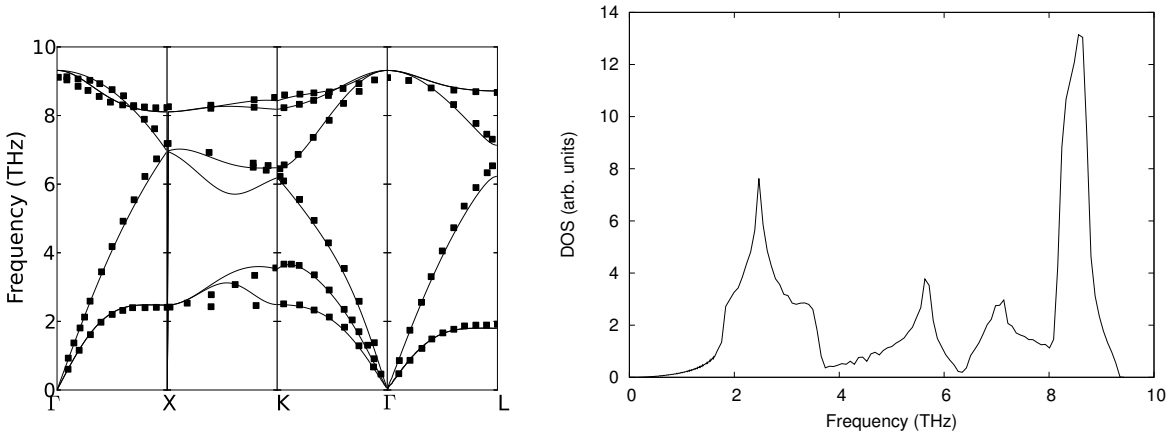

(a) (b)

Figure 2.7: Phonon dispersion relations and density of sates for germanium (Ge). (a) Solid lines: theoretical dispersion relations obtained with the BCM along high-symmetry axes. Symbols: data from neutron scattering experiments [49]. (b) Density of states calculated from BCM dispersion relations.

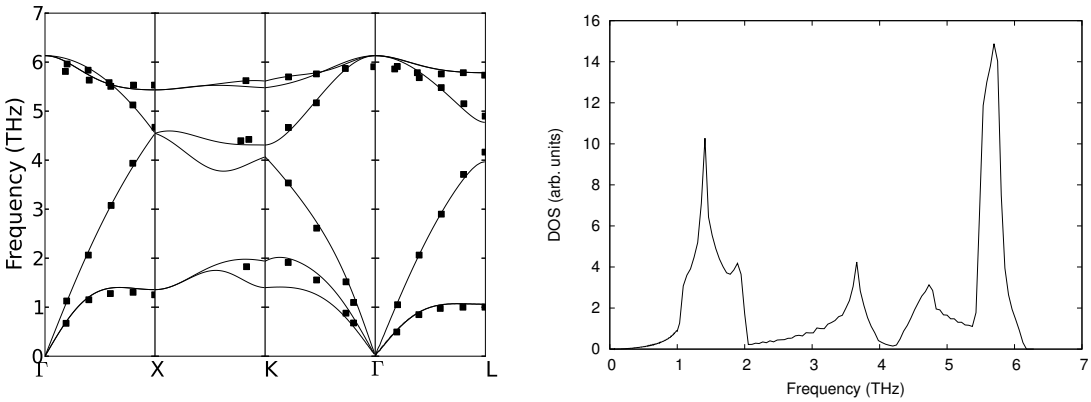

(a) (b)

Figure 2.8: Phonon dispersion relations and density of sates for -Sn. (a) Solid lines: theoretical dispersion relations obtained with the BCM along high-symmetry axes. Symbols: data from neutron scattering experiments [50]. (b) Density of states calculated from BCM dispersion relations.

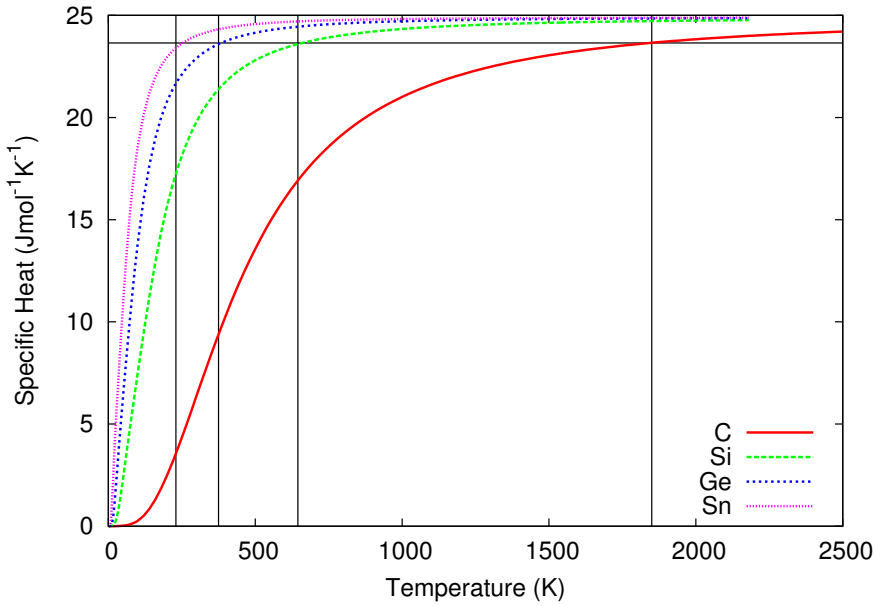

Figure 2.9: Specific heat of Si, Ge, C and −Sn calculated with the BCM dispersion relations and density of states.

ions are polarizable, but with this rigid approximation we avoid the effects of the electronic polarizability over the electric field generated by the ions displacements and the effective dynamic charges, that eventually affect the phonon frequencies. Despite of this simplification, this model is believed to be the most suitable one, using the Morse potential to obtain the dispersion relations of the material we are interested in, the bismuth telluride (Bi_2Te_3) [2,51]. Here, we follow the steps by Qiu and Ruan [2] to find the force constants from the second derivative of the Morse potential, and eventually find the eigenvalues of the dynamical matrix.

2.4.1 Crystal structure of Bi_2Te_3

The Bi_2Te_3 has a rhombohedral lattice structure, although sometimes it is also represented with the hexagonal structure, as it is shown in Fig. 2.10 (left). It can be seen that the rhombohedral unit cell contains five atoms along the trigonal axis following the sequence Te1-Bi-Te2-Bi-Te1. The lattice parameter of the rhombohedral unit cell is $a_R = 10.473$ Å, and the rotational symmetry angle is , $_R = 24.159$; the corresponding parameters of the hexagonal unit cell are $a = 10.473$ Å and $c = 30.487$ Å. In the rhombohedral structure, the Te1 atoms have coordinates $(\pm u, \pm u, \pm u)$, while Bi atoms have $(\pm v, \pm v, \pm v)$ where $u = 0.4001$ and $v = 0.2095$ [52]. According to [51–53] the bond length of the Te1-Bi bond is 3.07 Å, which is shorter than that of the Bi-Te2 bond (3.25 Å), indicating that they may be of different bond types, actually, the Te1-Bi bond has a higher bond energy and a higher force constant than the Bi-Te2 bond, this indicates that the Te1-Bi bond is more ionic than the Te2-Bi bond. On the other hand, the Te1-Te1 bond is the longest (3.64 Å) and is considered to be a Van der Waals interaction, therefore with bond energy lower than that of a typical ionic or covalent bond. The first BZ of the rhomboedral lattice is shown in Fig. 2.10 (right).

2.4.2 Interatomic Potentials and the Dynamical matrix

Let us now call $U(r_{ij})$ the interaction energy between two ions $i \equiv (\boldsymbol{l}k)$ at position $\mathbf{r}_i$ and $j \equiv (\boldsymbol{l}\, k\,)$ at position $\mathbf{r}_j$ separated a distance $r_{ij} = |\mathbf{r}_j - \mathbf{r}_i|$. According to (2.21) $U(r_{ij})$ is obtained taking into account two contributions: the short-range interactions described by a suitable potential, which for Bi_2Te_3 is usually taken the Morse potential because it is a good approximation of the vibrational structure of molecules, and the long-range interactions are, as usual, the coulombian ones, thus

$$U(r_{ij}) = U_{Morse}(r_{ij}) + U_{Coulomb}(r_{ij}) \quad . \tag{2.42}$$

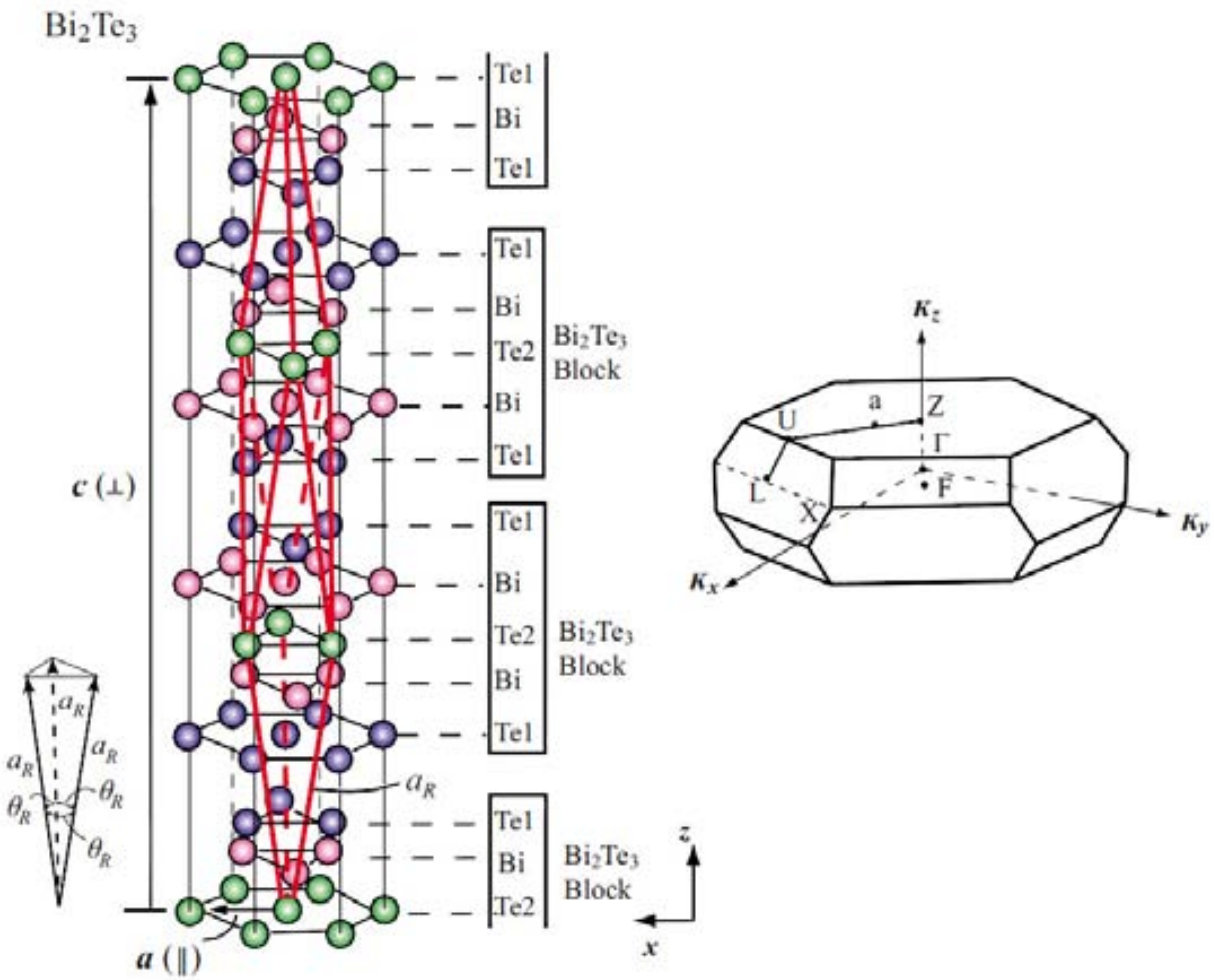

Figure 2.10: Crystal structure of Bi_2Te_3 showing the rhombohedral and hexagonal unit cells. Left: hexagonal structure is made of Te1-Bi-Te2-Bi-Te1 five-layer blocks. Right: The first Brillouin zone for the rhombohedral cell with some high-symmetry axes and points. The crystallographic direction [111] corresponds to the $\Gamma - Z$ axis, and [110] corresponds to $\Gamma - F$. Extracted from Ref. [51].

Short-range interactions

Following the simplified proposal by Qiu and Ruan [2], we will extend the short-range interactions to first and second-neighbors, since considering third-neighbors would complicate considerably the calculations, and the resulting dispersion relations and density of states would not differ significantly [2]. The Morse potential is given by

$$U_{Morse}(r_{ij}) = D[(1 - e^{-A(r_{ij} - r_{ij}^0)})^2 - 1] \tag{2.43}$$

where for each type of interaction i-j, D is the potential depth, A the bond elasticity, and r_{ij}^0 the equilibrium bond distance between atoms i and j, namely

$$r_{ij}^0 = \sqrt{\sum_{\alpha} (x_{i\alpha}^0 - x_{j\alpha}^0)^2} \tag{2.44}$$

being $x_{i\alpha}$ the Cartesian coordinates ($= 1, 2, 3$) of atom i and

$$r_{ij} = \sqrt{\sum_{\alpha} (x_{i\alpha} - x_{j\alpha})^2} = \sqrt{\sum_{\alpha} (x_{i\alpha}^0 - x_{j\alpha}^0 + u_{i\alpha} - u_{j\alpha})^2} \tag{2.45}$$

where $\mathbf{u}_i$ and $\mathbf{u}_j$ are the displacement vectors respect to the equilibrium position of atoms i and j for each possible interaction, (see Fig. 2.1). The values of these parameter for the bismuth telluride are given in Table 2.3.

Long-range interaction energy in (2.42) is given by the Coulomb potential energy

$$U_{Coulomb}(r_{ij}) = \frac{z_i z_j e^2}{r_{ij}} \tag{2.46}$$

where $z_i e$ and $z_j e$ are the point charges of ions i and j, respectively, and $e = 1.6 \quad 10^{-19}$C is the electron charge. The sum over all atomic positions r_{ij} should be performed by the Ewald's method, as indicated in Appendix A.

Now, we can calculate the force constants as

$$_{\alpha\beta}(ij) = \ _{\alpha\beta}^{M}(ij) + \ _{\alpha\beta}^{C}(ij) \tag{2.47}$$

where $_{\alpha\beta}^{M}(ij)$ and $_{\alpha\beta}^{C}(ij)$ are the force constants derived from the Morse and Coulomb energy, (2.43) and (2.46) respectively, and the subindex referring to the Cartesian coordinates $, . = x, y, z$ of the interaction between i, j.

Table 2.3: Parameters for first and second-neighbors interactions of Morse potential (2.43) for Bi_2Te_3, from Qiu and Ruan [2].

Interaction	A (Å^{-1})	D (eV)	r_0 (Å)
Bi-Bi	2.212	0.085	4.203
Te1-Te1	1.675	0.076	3.642
Te2-Te2	2.876	0.066	4.312
Bi-Te1	1.285	0.975	3.098
Bi-Te2	1.257	0.582	3.251
Te1-Te2	0.731	0.807	4.497

As explained before, the force constants are generally calculated as the second derivatives of the potential, according to Eq. (2.9). The force constants of the Morse potential for the interaction $i-j$, between different ions, is

$$\overset{M}{\alpha\beta}(ij) = \frac{{}^2U^M}{r_{ij}^2} =$$

$$= -2DAe^{[-A(r_{ij}-r_0)]} \quad A\left(2e^{[-A(r_{ij}-r_0)]}-1\right)\frac{r_{ij}^{\alpha}r_{ij}^{\beta}}{r_{ij}^2} + \quad {}_{\alpha\beta} - \frac{r_{ij}^{\alpha}r_{ij}^{\beta}}{r_{ij}^2} \quad \frac{\left(1-e^{[-A(r_{ij}-r_0)]}\right)}{r_{ij}} \tag{2.48}$$

and for the interaction $i-i$ it is found as

$$\overset{M}{\alpha\beta}(ii) = -\sum_j \overset{M}{\alpha\beta}(ij) \tag{2.49}$$

and the force constant of the Coulomb potential is

$$\overset{C}{\alpha\beta}(ij) = \frac{{}^2U^C}{r_{ij}^2} = z_i z_j e^2 \frac{{}_{\alpha\beta} r_{ij}^2}{r_{ij}^5} \tag{2.50}$$

and similarly

$$\overset{C}{\alpha\beta}(ii) = -\sum_j \overset{C}{\alpha\beta}(ij) \tag{2.51}$$

The equations of motion, according to Eq. (2.14), can be now written as

$$\boldsymbol{M}\omega^2\boldsymbol{u} = \boldsymbol{D}\boldsymbol{u} \tag{2.52}$$

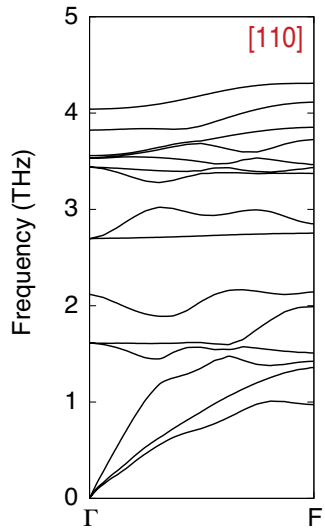

Figure 2.11: Dispersion relations of Bi_2Te_3 calculated in the present work using the RIM, in the crystallographic direction [110].

with $\boldsymbol{M}$ being the mass-matrix and D being the dynamical matrix, which is calculated, according to (2.18), for a given $\boldsymbol{q}$ as

$$D^{(\kappa\kappa')}_{\alpha\beta}(\boldsymbol{q}) = \sum_{\boldsymbol{l}'} \quad {}_{\alpha\beta}(\boldsymbol{l} \;\; ; \boldsymbol{l} \quad) \exp\left[i\boldsymbol{q}(\boldsymbol{r}_{\boldsymbol{l}\kappa} - \boldsymbol{r}_{\boldsymbol{l}'\kappa'})\right] =$$

$$= \sum_{\boldsymbol{l}'} (\; {}^{M}_{\alpha\beta}(\boldsymbol{l} \;\; ; \boldsymbol{l} \quad) + \; {}^{C}_{\alpha\beta}(\boldsymbol{l} \;\; ; \boldsymbol{l} \quad)) \exp\left[i\boldsymbol{q}(\boldsymbol{r}_{\boldsymbol{l}\kappa} - \boldsymbol{r}_{\boldsymbol{l}'\kappa'})\right] \tag{2.53}$$

2.4.3 Dispersion relations and density of states of Bi_2Te_3

By finding the eigenvalues of the dynamical matrix (2.53), we have obtained the dispersion relations of Bi_2Te_3 shown in Figs. 2.11-2.12

Note that the agreement between theoretical and experimental dispersion relations along [111] is not completely satisfactory. In first place, we must notice that the available experimental dispersion relations are obtain from a sample of polycrystalline powder of Bi_2Te_3 according to [1], this may induce some discrepancies with the theoretical models, where implicitly monocrystallinity is considered. These discrepancies are mainly associated to the optical modes, for instance the crossing optical branches near a 2 THz frequency, that can be observed in Fig. 2.12 (a) are not possible to be reproduced within the classical interatomic

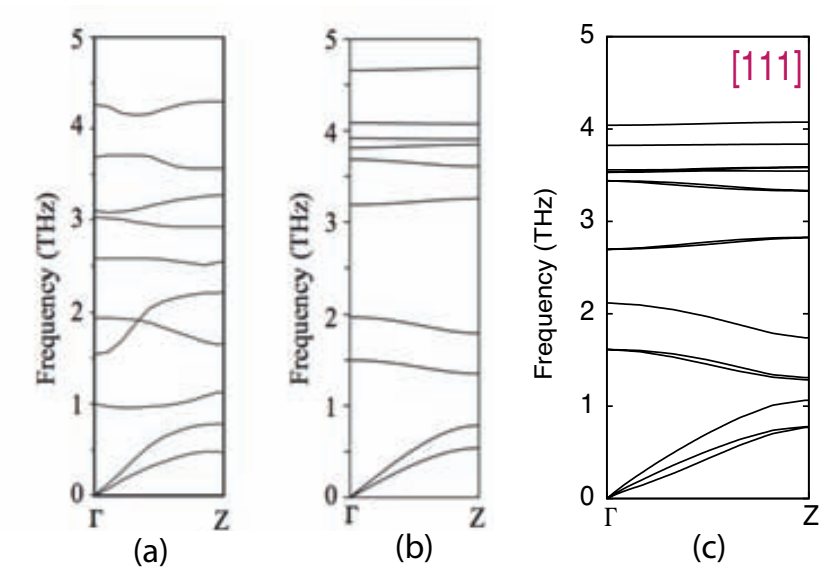

Figure 2.12: Comparison between experimental and theoretical dispersion relations of Bi_2Te_3 in the crystallographic direction [111]: (a) experiment by Ref. [1], (b) calculated using Morse interatomic potential with the RIM by Qiu and Ruan [2], (c) calculated in the present work using the RIM.

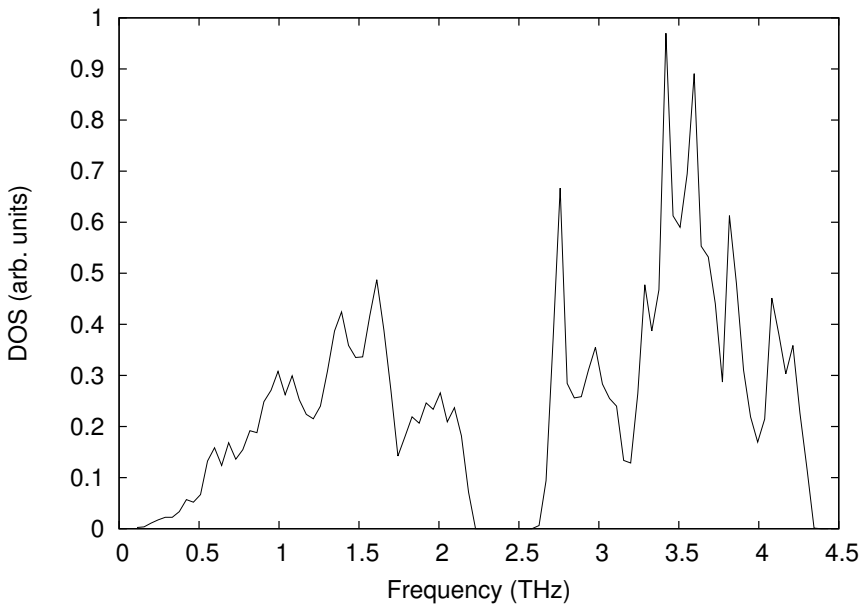

Figure 2.13: Density of states of Bi_2Te_3 calculated from the RIM.

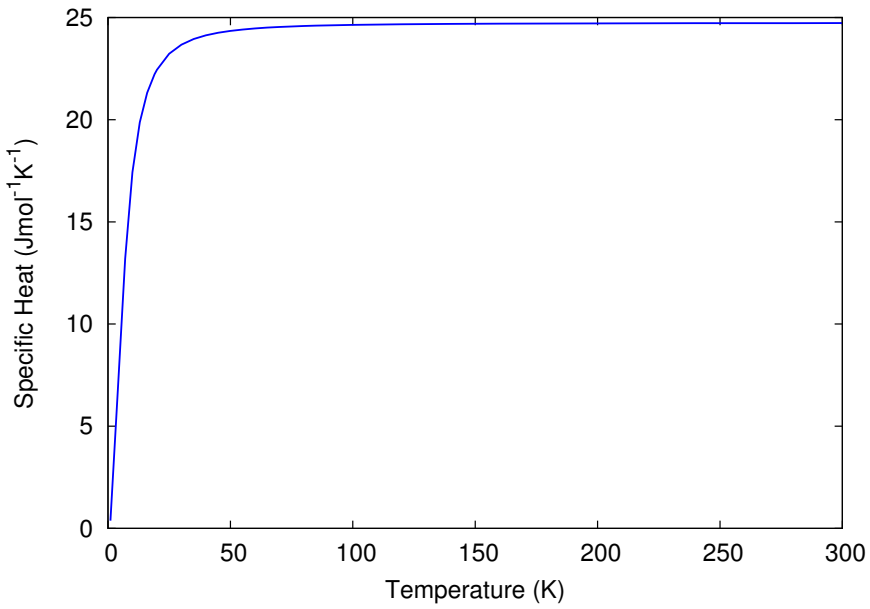

Figure 2.14: Specific heat of Bi_2Te_3 calculated from the RIM.

potential models, as shown in the works [2,51]. Furthermore, the overestimated height of the optical modes is one of the weak points of the rigid-ion model, since the polarization in Bi and Te atoms is neglected. Nevertheless, acoustic branches are in good agreement with the experimental curves, and since the acoustic modes are the dominating modes in the thermal transport, the dispersion relations found within this model are usually considered an enough good approximation to study the thermal transport in such a complex material [2,51]. In Fig. 2.13 we show the density of states in terms of the frequency corresponding to the obtained dispersion relations and calculated according to Eq. (1.11). The curve is in agreement with previous calculations [2,51]. Once the dispersion relations and the density of states is known, we can calculate the specific heat according to Eq. (1.20), which is shown as a function of the temperature in Fig. 2.14. Note that the Debye temperature for the Bi_2Te_3 that can be found in the literature is typically 160 K, which slightly higher to that arising from our calculations, around 120 K, as it can be extracted from the plot.

Chapter 3

Phonon relaxation times

In the previous Chapter, we have presented the dynamics of the crystal lattice in the harmonic approximation, corresponding to a quadratic potential. This first approximation is valid to calculate quantities related to thermal equilibrium, for instance as we have done with the specific heat. However, to study of the thermal conductivity we need the knowledge of phonon interactions, which require to consider anharmonic terms in the potential.

Above the absolute zero temperature, the atomic displacements in the lattice give raise to third, quartic and higher-order terms in the potential. If we keep only the harmonic (second-order) term and neglect the anharmonic terms, the lattice waves, obeying the superposition principle, will travel without interactions. In such case, they would never decay and the thermal energy will be carried with no resistance. This yields, as first indicated by Debye [54], an infinite thermal conductivity, contrary to experimental evidence. Then, the anharmonicities result, fundamentally, into phonon-phonon interactions which are the source of the intrinsic thermal resistance in a non metallic material.

Furthermore, the introduction of a displacement field in the crystal lattice as a result of an external force or a lattice defect or impurity also leads to scattering processes experienced by phonons. Besides, the finite size of a real crystal induces the moving phonons to collide against the crystal boundaries.

These three scattering processes, phonon-phonon scattering, phonon-impurity scattering and phonon-boundary scattering, are the fundamental mechanisms present in any real crystal giving raise to thermal resistance. Other processes could be phonon collisions against geometrical defects, such as dislocations, against electrons or holes, or they may interact with photons, but we will not deal with them here, since they are out of the scope of this thesis. In

the present Chapter, we examine the particular form of the relaxation time for each of these scattering processes and its influence on the thermal conductivity.

3.1 Fermi Golden Rule

Generally, the scattering problem is treated within the standard time-dependent perturbation theory [35]. The anharmonic terms of the potential, despite of their important effects, are significantly smaller than the harmonic term, so they can be considered as a perturbation to an ideal harmonic crystal[1]. This method allows us to calculate the transition rates between the interacting modes.

In this approach, the Hamiltonian of a real crystal can be split into two terms

$$H = H_0 + H \qquad , \tag{3.1}$$

where H_0 is the harmonic Hamiltonian of a perfect crystal, and H is the perturbation Hamiltonian, whose form depends on the phonon interaction, *i.e.* scattering process, we want to study. When we deal with the scattering problem, it is usual to express the Hamiltonian in the language of quantum field theory. Thus, the harmonic Hamiltonian $H_0 = \mathcal{T} + \mathcal{U}$, with the kinetic energy $\mathcal{T}$ and the harmonic potential energy $\mathcal{U}$ given in Sec. 2.1 (Eqs. (2.4) and (2.7) respectively), can be expressed in terms of phonon creation and annihilation operators, $a^+_{\mathbf{q}\nu}$ and $a_{\mathbf{q}\nu}$ respectively, depending on the phonon wave vector $\mathbf{q}$ and branch ν. The final expression is

$$H_0 = \frac{1}{2}\sum_{\mathbf{q},\nu} \hbar\omega^2_{\mathbf{q}} \quad a^+_{\mathbf{q}\nu} a_{\mathbf{q}\nu} + \frac{1}{2} \tag{3.2}$$

The eigenstates of H_0 are $|n_{\boldsymbol{q}\nu}$, which denotes a state with n phonon of wavevector $\boldsymbol{q}$ in the branch ν. The operators $a^+_{\mathbf{q}\nu}$ and $a_{\mathbf{q}\nu}$ act on the eigenstate by increasing or decreasing in one unit the number of phonons, such that

$$\begin{aligned} a^+_{\boldsymbol{q}\nu}|n_{\boldsymbol{q}\nu} &= \overline{n_{\boldsymbol{q}\nu}+1}|n_{\boldsymbol{q}\nu}+1 \\ a_{\boldsymbol{q}\nu}|n_{\boldsymbol{q}\nu} &= \overline{n_{\boldsymbol{q}\nu}}|n_{\boldsymbol{q}\nu}-1 \quad . \end{aligned} \tag{3.3}$$

[1]Note that in the case of anharmonic scattering this approach is not strictly correct since we are facing a many-body problem, that is, the potential extends all over the crystal volume, but still, it is a good approximation. However, in the case of scattering with lattice impurities, standard perturbation theory is adequate, since impurities act as scattering centers. Further discussion can be found in [55, 56].

Thus,

$$a^{+}_{\mathbf{q}\nu} a_{\mathbf{q}\nu} |n_{\boldsymbol{q}\nu} \rangle = n_{\boldsymbol{q}\nu} |n_{\boldsymbol{q}\nu} \rangle \quad . \tag{3.4}$$

Then, one can easily find the eigenvalues $_{\boldsymbol{q}\nu}$ of the harmonic Hamiltonian, as

$$H_0 |n_{\boldsymbol{q}\nu} \rangle = \sum_{\boldsymbol{q}\nu} {}_{\boldsymbol{q}\nu} |n_{\boldsymbol{q}\nu} \rangle \tag{3.5}$$

with

$$_{\boldsymbol{q}\nu} = \hbar\omega_{\boldsymbol{q}\nu} \quad n_{\boldsymbol{q}\nu} + \frac{1}{2} \quad , \tag{3.6}$$

where $\frac{1}{2}\hbar\omega_{\boldsymbol{q}\nu}$ is the zero-point energy corresponding to $T = 0$ K.

To calculate the effect of the perturbation H on an system in the initial state $|i\rangle$ of energy E_i after a certain time t, we use the Fermi Golden rule. It states that the transition probability to a final state $|f\rangle$ due to that perturbation is given by

$$P_i^f = \frac{2\pi}{\hbar} |\langle f|H|i\rangle|^2 \, (E_f - E_i) \quad , \tag{3.7}$$

where $(E_f - E_i)$ is the Dirac delta indicating that only the energy conserving transitions are allowed to happen, and $\langle f|H|i\rangle$ is the so-called scattering matrix.

Calculation of the scattering matrix $\langle f|H|i\rangle$ is a formidable task, but eventually leads to find expressions for the scattering rates associated to the transition $i \quad f$.

In the following Section, we detail the main aspects of the transition rates of the three types of phonon interactions considered in this work. This will lead us to find analytical expressions for the relaxation times that we will use in the following Chapters in the thermal conductivity calculations.

3.2 Phonon scattering processes

As we have previously introduced, phonons may suffer several types of interactions. The importance of these different mechanisms depends on the characteristics of the material under study. Since the present work is focused on semiconductor crystals, we will deal only with the main scattering processes which are nearly always present in this type of materials. These processes are the boundary scattering due to the finite size of the crystal, mass-defect scattering due to the presence of impurities, and three-phonon processes due to the crystal anharmonicities, which can be classified into momentum conservative (normal scattering) or non-conservative (Umklapp scattering) processes. We have depicted in Fig. 3.1 the general

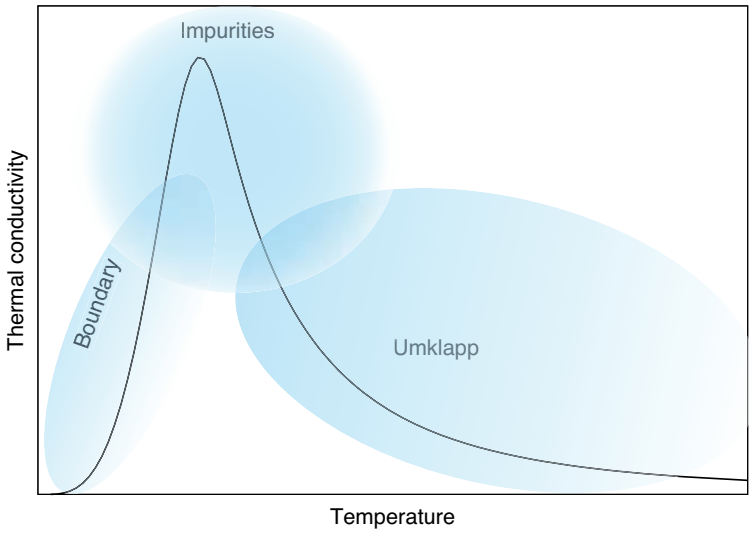

Figure 3.1: Scheme of the general behavior of the phonon thermal conductivity with temperature for a non-metallic crystal. The dominant resistive scattering process in each range of temperature is depicted qualitatively.

behavior of the thermal conductivity with temperature for a bulk sample, showing the dominant scattering mechanism in each range of temperatures. At low temperatures the boundary scattering is the main dominant process, as the temperature raises the thermal conductivity reaches a maximum governed by the impurity scattering, and after the peak the thermal conductivity decreases due to the Umklapp scattering. The role of normal process deserves a deep discussion and represents one of the milestones of the present thesis. In the following sections we explain the nature of each of these mechanisms and their contribution to thermal resistance.

3.2.1 Three-phonon processes: Normal and Umklapp scattering

Even in a perfect crystal there is an intrinsic scattering process that avoids an infinite thermal conductivity. This is the phonon-phonon interaction related to the third-order term in the energy potential of the crystal, as pointed out by Peierls (1929) [6]; it allows two classes of processes involving three phonons:

- Class 1 processes: Two phonons of wavevector and frequency ($\mathbf{q}_1$, ω_1) and ($\mathbf{q}_2$, ω_2) collide turning into another one ($\mathbf{q}_3$, ω_3), being possible the reverse process.

- Class 2 processes: One phonon ($\mathbf{q}_1$, ω_1) splits into two other phonons ($\mathbf{q}_2$, ω_2) and ($\mathbf{q}_3$, ω_3), being also possible the reverse process.

These processes are illustrated with the Feynman diagrams in Fig. 3.2. There are also scattering processes involving four or more phonons (corresponding to quartic or higher terms in the Hamiltonian), but as shown by Pomeranchuk [57], they mainly occur at temperatures comparable to or higher than the Debye temperature. So let us focus our attention on three-phonon processes. This interaction can exhibit different natures depending on the conservation laws they fulfill. According to Peierls [6] these laws are, for Class 1 processes

$$\omega_1 + \omega_2 = \omega_3 \tag{3.8}$$

which represents energy conservation between the initial and the final states, since $\hbar\omega$ is the quantum of energy for a mode of frequency ω, and

$$\mathbf{q}_1 + \mathbf{q}_2 = \mathbf{q}_3 + \mathbf{G} \tag{3.9}$$

with $\mathbf{G}$ a reciprocal lattice vector. For a vibrational mode, $\hbar\mathbf{q}$ is treated as a momentum. Thus, Eq. (3.11) is interpreted as a momentum conservation law with $\mathbf{G} = 0$. Analogously, these laws for Class 2 processes are

$$\omega_1 = \omega_2 + \omega_3 \tag{3.10}$$

$$\mathbf{q}_1 = \mathbf{q}_2 + \mathbf{q}_3 + \mathbf{G} \quad . \tag{3.11}$$

Now one must distinguish between normal scattering (N-processes) if momentum is conserved ($\mathbf{G} = 0$) and Umklapp scattering (U-processes) if momentum is not conserved ($\mathbf{G} = 0$), but transferred to the lattice (see the sketch in Fig. (3.3)).

The perturbation hamiltonian H due to three-phonon processes is expressed as

$$H = \frac{1}{3!} \sum_{\mathbf{q_1},\nu_1;\mathbf{q_2},\nu_2;\mathbf{q_3},\nu_3} \mathbf{q_1}+\mathbf{q_2}+\mathbf{q_3},\boldsymbol{G}\, \mathcal{F}_{\mathbf{q_1},\nu_1;\mathbf{q_2},\nu_2;\mathbf{q_3},\nu_3} (a^+_{\mathbf{q_1},\nu_1} - a_{-\mathbf{q_1},\nu_1})(a^+_{\mathbf{q_2},\nu_2} - a_{-\mathbf{q_2},\nu_2})(a^+_{\mathbf{q_3},\nu_3} - a_{-\mathbf{q_3},\nu_3}) \tag{3.12}$$

where $\mathcal{F}_{\mathbf{q_1},\nu_1;\mathbf{q_2},\nu_2;\mathbf{q_3},\nu_3}$ are scalar quantities proportional to the average of the Fourier transformed anharmonic tensor projected over the directions of the polarization vectors[2]. In principle, the sum of Eq. (3.12) is over the three modes participating in the scattering, but one should consider only those events that are compatible with energy conservation (3.10) and

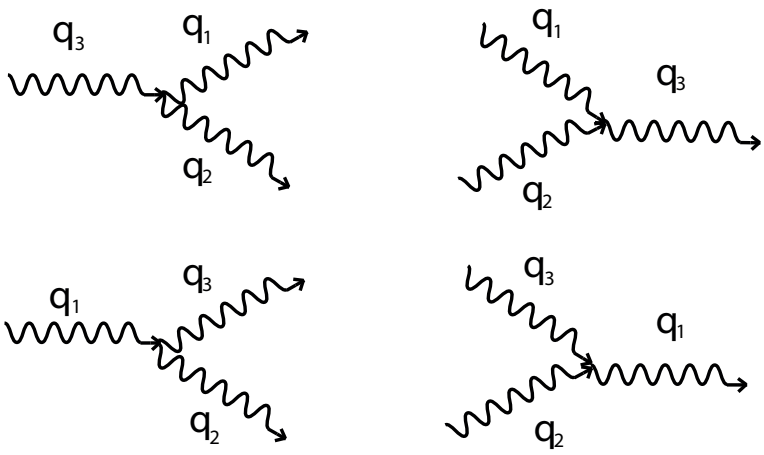

Figure 3.2: Feynman diagrams for the possible three-phonon interactions. Top diagrams represent Class 1 processes and bottom diagrams correspond to Class 2 processes.

momentum conservation (3.11) with $\mathbf{G} = 0$ or $\mathbf{G} = 0$ in the case of N-processes or U-processes, respectively, as we shall see.

Invoking the Fermi golden rule (3.7) we can calculate the transition probability for three-phonon processes, given that the initial state is

$$|i \ \equiv |n_{\mathbf{q_1},\nu_1}, n_{\mathbf{q_2},\nu_2}, n_{\mathbf{q_3},\nu_3} \tag{3.13}$$

and the final state is, for Class 1 processes

$$|f \ \equiv |n_{\mathbf{q_1},\nu_1} - 1, n_{\mathbf{q_2},\nu_2} - 1, n_{\mathbf{q_3},\nu_3} + 1 \tag{3.14}$$

and for Class 2 processes

$$|f \ \equiv |n_{\mathbf{q_1},\nu_1} - 1, n_{\mathbf{q_2},\nu_2} + 1, n_{\mathbf{q_3},\nu_3} + 1 \quad . \tag{3.15}$$

Let us first calculate the transition probability for Class 1 processes:

$$P^{\mathbf{q_3}\nu_3}_{\boldsymbol{q}_1\nu_1,\mathbf{q_2},\nu_2} = \frac{2\pi}{\hbar}|\ n_{\mathbf{q_1},\nu_1} - 1, n_{\mathbf{q_2},\nu_2} - 1, n_{\mathbf{q_3},\nu_3} + 1|H\ |n_{\mathbf{q_1},\nu_1}, n_{\mathbf{q_2},\nu_2}, n_{\mathbf{q_3},\nu_3}\ |^2\ \ (\hbar\omega_3 - \hbar\omega_2 + \hbar\omega_1) \quad . \tag{3.16}$$

where substituting (3.12) and after a little algebra we find

$$P^{\mathbf{q_3}\nu_3}_{\boldsymbol{q}_1\nu_1,\mathbf{q_2},\nu_2} = \frac{2\pi}{\hbar} n_{\mathbf{q_1},\nu_1} n_{\mathbf{q_2},\nu_2}(n_{\mathbf{q_3},\nu_3} + 1)|\mathcal{F}_{\mathbf{q_1},\nu_1;\mathbf{q_2},\nu_2;\mathbf{q_3},\nu_3}|^2\ \ {}_{\mathbf{q_1}+\mathbf{q_2}+\mathbf{q_3},\boldsymbol{G}}\ \ (\hbar\omega_3 - \hbar\omega_2 + \hbar\omega_1) \quad . \tag{3.17}$$

[2]We skip the complete expression of $\mathcal{F}_{\mathbf{q_1},\nu_1;\mathbf{q_2},\nu_2;\mathbf{q_3},\nu_3}$ and related mathematical details for the sake of brevity and simplicity, but they can be consulted in Refs. [17, 36].

Note that the delta functions

$$(\omega_3 + \omega_2 - \omega_1) \tag{3.18}$$

and

$$(\mathbf{q}_3 + \mathbf{G} + \mathbf{q}_2 - \mathbf{q}_1) \tag{3.19}$$

assure that the transition probability vanishes for those processes which do not fulfill the energy and momentum conservation laws.

On the other hand, for the sake of simplicity, we can denote

$$Q^{\mathbf{q_3}\nu_3}_{\boldsymbol{q}_1\nu_1,\mathbf{q_2}\nu_2} = \frac{2\pi}{\hbar}|\mathcal{F}_{\mathbf{q_1},\nu_1;\mathbf{q_2},\nu_2;\mathbf{q_3},\nu_3}|^2 \;\; {}_{\mathbf{q_1}+\mathbf{q_2}+\mathbf{q_3},\boldsymbol{G}} \;\; (\hbar\omega_3 - \hbar\omega_2 + \hbar\omega_1) \quad . \tag{3.20}$$

the *intrinsic transition probability*, which is independent of the phonon distribution, and so (3.17) can be expressed in a simplified way

$$P^{\mathbf{q_3}\nu_3}_{\boldsymbol{q}_1\nu_1,\mathbf{q_2}\nu_2} = n_{\mathbf{q_1},\nu_1} n_{\mathbf{q_2},\nu_2}(n_{\mathbf{q_3},\nu_3} + 1) Q^{\mathbf{q_3}\nu_3}_{\boldsymbol{q}_1\nu_1,\mathbf{q_2},\nu_2} \quad . \tag{3.21}$$

Analogously, we can obtain the transition probability for Class 2 processes, given by

$$P^{\mathbf{q_3}\nu_3,\mathbf{q_2}\nu_2}_{\boldsymbol{q}_1\nu_1} = (n_{\mathbf{q_1},\nu_1} + 1) n_{\mathbf{q_2},\nu_2} n_{\mathbf{q_3},\nu_3} Q^{\mathbf{q_3}n_3,\mathbf{q_2}\nu_2}_{\boldsymbol{q}_1\nu_1} \quad . \tag{3.22}$$

Since the intrinsic transition probability does not depend on the number of phonons $n_{\mathbf{q}\nu}$, by the principle of microscopic reversibility we have, for Class 1 processes

$$Q^{\mathbf{q_3}\nu_3}_{\boldsymbol{q}_1\nu_1,\mathbf{q_2},\nu_2} = Q^{\boldsymbol{q}_1\nu_1,\mathbf{q_2},\nu_2}_{\boldsymbol{q}_3\nu_3} \tag{3.23}$$

and analogously for Class 2 processes. Thus, similarly we can obtain the transition probabilities for the Class 1 and Class 2 reverse processes, $P^{\boldsymbol{q}_1\nu_1,\boldsymbol{q}_2\nu_2}_{\boldsymbol{q}_3\nu_3}$ and $P^{\boldsymbol{q}_1\nu_1}_{\boldsymbol{q}_2\nu_2,\boldsymbol{q}_3\nu_3}$ respectively.

The total probability of mode $\boldsymbol{q}_1$ suffering a scattering can be obtained as

$$P^{\nu_3}_{\boldsymbol{q}_1\nu_1,\nu_2} = \quad P^{\mathbf{q_3}\nu_3}_{\boldsymbol{q}_1\nu_1,\mathbf{q_2}\nu_2} d\boldsymbol{q}_2 d\boldsymbol{q}_3 = \quad n_{\mathbf{q_1},\nu_1} n_{\mathbf{q_2},\nu_2}(n_{\mathbf{q_3},\nu_3} + 1) Q^{\mathbf{q_3}\nu_3}_{\boldsymbol{q}_1\nu_1,\mathbf{q_2},\nu_2} d\boldsymbol{q}_2 d\boldsymbol{q}_3 \tag{3.24}$$

Actually, this complicated integral with six degrees of freedom (each of $\boldsymbol{q}_2$ and $\boldsymbol{q}_3$ has three) is reduced to a single integral with two degrees of freedom. This is thanks to the four equations of the conservation conditions (3.8, 3.9), which let us fix four degrees of freedom out of the six. The remaining two degrees of freedom define a surface S_2 in the reciprocal space, on which $\boldsymbol{q}_2$ must lie for the process in Eq. (3.9) to take place. The complete and detailed mathematical description can be found in [17, 36, 58]. Still, this surface integral can be quite complex. If we are using the Debye model for the dispersion relations (dispersionless

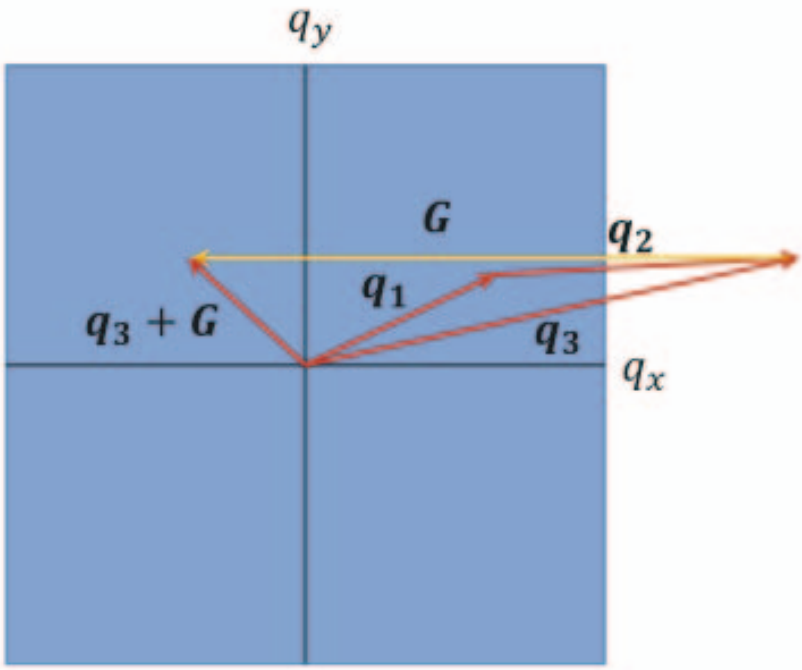

Figure 3.3: Sketch of a general three-phonon process $\mathbf{q}_1 + \mathbf{q}_2 = \mathbf{q}_3 + \mathbf{G}$. *The blue square represents the first Brillouin zone. With the center as origin, two vectors* $\mathbf{q}_1$ *and* $\mathbf{q}_2$ *are drawn and their sum is represented* $\mathbf{q}_3$. *In the case of U-process* $\mathbf{q}_3$ *falls outside the Brillouin zone, as indicated in the figure. To bring vector* $\mathbf{q}_3$ *inside the Brillouin zone it is necessary adding or subtracting to it a reciprocal lattice vector* $\mathbf{G}$, *yielding* $\mathbf{q}_3 + \boldsymbol{G}$. *The N-process is the particular case when* $\boldsymbol{G} = 0$, *that is,* $\mathbf{q}_3$ *falls inside the Brillouin zone.*

model), the surface S_2 degenerates into a line of zero area, because all the lattice waves are considered to have the same phase velocity regardless polarization, then the conservation laws (3.11) and (3.10) are satisfied by taking $\mathbf{q}_1, \mathbf{q}_2, \mathbf{q}_3$ in the same straight line.

However, in the general case, dispersion in the phonon branches and anisotropy in the crystal must be considered, and it leads to more complicated constructions, as discussed by Herring [58]. To illustrate this, in Fig. 3.4 we show the curves representing the cross-section of the energy conservation surface S obtained by Herring for two particular situations depending on the wavevector of the interacting modes in the normal process $\mathbf{q}_1 + \mathbf{q}_2 = \mathbf{q}_3$; in the top sketch are represented the curves for the case $\mathbf{q_2}$ much larger than $\mathbf{q_1}$ and in the bottom for the case where $\mathbf{q_2}$ is comparable to $\mathbf{q_1}$. In the figures solid lines represent the cross-section of the surface $\omega(\mathbf{q}) \equiv \omega_2$ with origin at O_1, dashed lines stand for the cross-section of the surface $\omega(\mathbf{q}) \equiv \omega_1 + \omega_2 = \omega_3$ with origin at O_2 displaced from O_1 by $-\mathbf{q}_1$. From the plots we can observe in the top one, that in this case ($\mathbf{q_1}$ small) degeneracy is possible, that is, two frequencies correspond to a single mode, as can be appreciated in actual dispersion relations (see for instance the plots of the silicon dispersion relations presented in the previous Chapter, Fig.2.6 (a)). This degeneracy is represented by the points Q and P, where solid lines cross. On the other hand, in the bottom figure, when $\mathbf{q_1} \quad \mathbf{q_2}$, we can observe a tangent F point between ω_2-surface and ω_3 surface in the direction $\mathbf{q}_1$ occurring when ω_2 is small enough to neglect dispersion. This is not likely to happen in the other case (top), represented by point R. From these examples, that we have explained *grosso modo* here, it is easy to see that there are some sort of "selection rules" for the allowed three-phonon processes, which make even more complex to find a solution of (3.24).

Although general expressions for the relaxation times associated to N- and U-processes, τ_N and τ_U, have not been derived to date, this thorough study by Herring [58] has provided us at least with a rule for the frequency and temperature dependence of τ_N in two temperature limits, always under the Debye temperature, to consider that the probability of four-phonon processes is negligible.

According to Herring, when considering long-wavelength modes, or equivalently short-frequency modes, we have three modes $\mathbf{q}_1, \mathbf{q}_2, \mathbf{q}_3$ interacting through normal scattering such that they belong to acoustic branches. Then, only Class 1 events are the most likely, since Class 2 events implies that higher frequency modes are participating in the collision. Therefore, these modes satisfy

$$\mathbf{q}_1 + \mathbf{q}_2 = \mathbf{q}_3 \quad , \tag{3.25}$$

and since we are dealing with low-frequency modes, we can consider $\omega(\boldsymbol{q}) \quad q$. This way, the intrinsic transition probability (3.20) is found to be proportional to the wave numbers of the interacting modes, such that the transition probability (3.21) can be expressed as

$$P^{\mathbf{q_3}\nu_3}_{\boldsymbol{q}_1\nu_1,\mathbf{q_2}\nu_2} \quad q_1 q_2 q_3 n_{\mathbf{q_1},\nu_1} n_{\mathbf{q_2},\nu_2}(n_{\mathbf{q_3},\nu_3}+1) \tag{3.26}$$

and similarly for the reverse process

$$P^{\boldsymbol{q}_1\nu_1,\mathbf{q_2}\nu_2}_{\mathbf{q_3}\nu_3} \quad q_1 q_2 q_3 n_{\mathbf{q_3},\nu_3}(n_{\mathbf{q_1},\nu_1}+1)(n_{\mathbf{q_2},\nu_2}+1) \tag{3.27}$$

Note that, even if $\mathbf{q}_2$ and $\mathbf{q}_3$ are high-energy modes where the approximation $\omega(\boldsymbol{q}) \quad q$ is not valid (due to dispersion), while $\boldsymbol{q}_1$ belongs to an acoustic branch, we still have the proportionality $q_1 n_{\mathbf{q_1},\nu_1}$ in (3.26) and $q_1(n_{\mathbf{q_1},\nu_1}+1)$ in (3.27). According to Klemens [59] the relaxation time associated to mode $\boldsymbol{q}_1$ is defined as

$$\tau^{-1}(\boldsymbol{q}_1) = -\lim_{n_{\boldsymbol{q}_1} \quad n^0_{\mathbf{q_1}}} \frac{(dn_{\boldsymbol{q}_1}/dt)_{\text{scatt}}}{n_{\boldsymbol{q}_1} - n^0_{\mathbf{q_1}}} \tag{3.28}$$

where $n^0_{\boldsymbol{q}_1}$ is the value of the occupation number $n_{\boldsymbol{q}_1}$ in thermal equilibrium, and $(dn_{\boldsymbol{q}_1}/dt)_{\text{scatt}}$ is the total rate of change of $n_{\boldsymbol{q}_1}$ due to phonon-phonon collisions when it departs from equilibrium but all other modes have equilibrium occupation, and it can be expressed as the sum of the transition probabilities

$$\frac{dn_{\boldsymbol{q}_1}}{dt}_{\text{scatt}} = P^{\mathbf{q_3}\nu_3}_{\boldsymbol{q}_1\nu_1,\mathbf{q_2}\nu_2} - P^{\boldsymbol{q}_1\nu_1,\mathbf{q_2}\nu_2}_{\mathbf{q_3}\nu_3} d\boldsymbol{q}_2 d\boldsymbol{q}_3 \tag{3.29}$$

By evaluating integral (3.29) according to (3.26) and (3.27), and substituting it in (3.30) we obtain

$$\tau^{-1}(\boldsymbol{q}_1) \quad q_1 q_2 q_3 (n^0_{\boldsymbol{q}_2,\nu_2} - n^0_{\boldsymbol{q}_3,\nu_3})(\ \Delta\omega/\ q_2\ )^{-1} dS_2 \tag{3.30}$$

where $\Delta\omega = \omega(\boldsymbol{q}_1+\boldsymbol{q}_2) - \omega(\boldsymbol{q}_1) - \omega(\boldsymbol{q}_2)$ measures the departure from energy conservation and q_2 is the component of $\boldsymbol{q}_2$ perpendicular to the surface dS_2. To determine the behavior of the integral of (3.30) it is necessary to determine first the form of the energy conservation surface S_2 and the magnitude of the normal derivative of $\Delta\omega$ on it. However, it is possible to derive two scaling laws for $\tau^{-1}(\boldsymbol{q}_1)$ without this information, in the range of low and high temperatures. Performing the limit in (3.30) in each temperature range, we have:

- **Low-temperatures:**
  At temperatures low enough the temperature variance of (3.30) is given by

$$\tau^{-1}(\boldsymbol{q}_1) \quad q_1^a T^{5-a} \tag{3.31}$$

where a is found depending on the crystal lattice geometry as

$$a = -\lim_{\boldsymbol{q}\ \ 0} \frac{d \ln \tau(\boldsymbol{q}, T)}{d \ln q} \tag{3.32}$$

This is to the so-called fifth-power law, which is usually written in terms of frequency with the general expression

$$\tau^{-1}(\omega) \quad \omega^a T^b \text{ with } a + b = 5\,. \tag{3.33}$$

Herring also provided a table with the values of a calculated for several lattice geometries according to crystallographic considerations [58].

- **High-temperatures:**
  In this limit all the modes are highly excited, the transition probabilities (3.26) and (3.27) in (3.30) contain T only through a term linear in the n^0's. Thus,

$$\tau^{-1}(\boldsymbol{q}_1) \quad T^{-1}\,. \tag{3.34}$$

Effect of normal and Umklapp processes on the thermal conductivity

Regarding the role of the three-phonon processes on the thermal conductivity, it is very important to point out that Umklapp scattering is a resistive process, that is, it adds resistance to heat transport since phonons lose momentum in the collision. In addition, after an Umklapp collision the direction of the group velocity of the resulting phonon is very different from those of the initial phonons, and since thermal energy is carried in the direction of the phonon group velocity, the net effect is to make the phonon distribution relax to equilibrium. In other words, U-processes increase thermal resistance, and therefore reduce the thermal conductivity. In contrast, normal scattering is the only non-resistive process, *i.e.* it does not contribute to thermal resistance, because phonons conserve the initial momentum after colliding. This prevents the phonon distribution to relax to equilibrium. Instead, the phonon distribution is relaxed to a distribution displaced from equilibrium [34]. Because of this feature, the role of N-processes in thermal transport has often been dismissed [25, 28]. Recently, the scientific community seems to agree on the crucial role they play in some relevant aspects of thermal transport. However, it is still under debate which is the right way to account for this non-resistive process and how it exactly affects thermal conductivity. As we will discuss in the following Chapters, an appropriate treatment of normal and Umklapp scattering events together with suitable analytical expressions is indeed crucial step in thermal conductivity modeling.

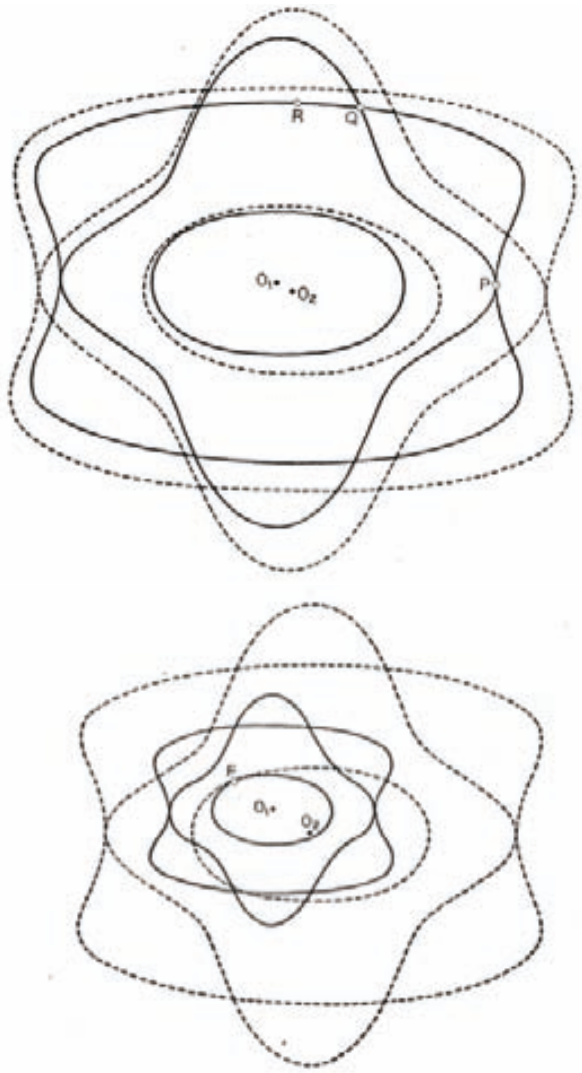

Figure 3.4: Sketch of the cross-section of the energy conservation surface in the $\mathbf{q}$*-space for a general model (with dispersion), for two typical cases depending on the wavevector of the interacting modes in the process* $\mathbf{q}_1 + \mathbf{q}_2 = \mathbf{q}_3$*: (top) A longitudinal mode with* $\mathbf{q}_2$ *larger than* $\mathbf{q}_1$*; (bottom) A longitudinal mode with* $\mathbf{q}_2$ *comparable to* $\mathbf{q}_1$*. Solid lines represent the cross-section of the surface* $\omega(\mathbf{q}) \equiv \omega_2$ *with origin at* O_1*, dashed lines stand for the cross-section of the surface* $\omega(\mathbf{q}) \equiv \omega_1 + \omega_2 = \omega_3$ *with origin at* O_2 *displaced from* O_1 *by* $-\mathbf{q}_1$*. (Top)* Q *and* R *are points of degeneracy. Point* F *is the tangent point between* ω_2*-surface and* ω_3*-surface in the direction* $\mathbf{q}_1$ *occurring when* ω_2 *is small enough to neglect dispersion. Reproduced from Herring [58].*

Expressions for Normal and Umklapp scattering

As we have already pointed out, finding a formal equation for the scattering rate associated to N- and U-processes is far from trivial. It is known that they are strongly frequency and temperature dependent, but to the date there is no standardized equation to account for this dependence. Furthermore, each material should exhibit a characteristic dependence, since the lattice type is directly related to the anharmonicities.

Many expressions for τ_N and, similarly for τ_U, based on Herring's work have been proposed since then. In order to have a better perspective of the diversity of expressions for τ_N and τ_U, we have summarized chronologically in Table 3.1 the expressions proposed in the most relevant works on silicon thermal conductivity from the last decades to the date. Note that for τ_U the is no agreement between the expressions, but for τ_N, when considered, the tendency is to use $\tau_N \quad \omega^2 T^3$ according to Herring's calculations for the exponents [58]. Regarding the parameters appearing in the expressions, usually denoted as B with a subindex indicating the type of process (N for normal, U for Umklapp) and sometimes also the phonon branch (L for longitudinal, T for transversal), they are usually treated as fitting parameters. Although there have been attempts to find empirical expressions to calculate them in terms of some materials properties, like atomic volume, atomic mass, Grüneisen parameter or group velocity [60]. This will be further discussed in Chapter 6.

From this picture one can notice two things: first, the lack of agreement on how three-phonon scattering should behave with frequency and temperature in a given material, and second, the lack of direct experimental measurements on relaxation times in terms of frequency and temperature that could shed light to this controversy.

Nevertheless, *ab-initio* methods have remarkably contributed to provide valuable information about the frequency and temperature dependence of τ_N and τ_U in certain intervals of temperature. With this technique, Ward and Broido [61] have recently proposed the following expressions

$$\tau_N^{-1} = B_N \omega^2 T[1 - \exp(-3T/ \quad _D)] \tag{3.35}$$

$$\tau_U^{-1} = B_U \omega^4 T[1 - \exp(-3T/ \quad _D)] \tag{3.36}$$

for silicon and germanium valid in the temperature interval $[100 - 300]$ K. Note that the expression of τ_N^{-1} provided by Ward and Broido does not follow the Herring's fifth-power law. According to Herring, for diamond-like materials, such is the case of silicon and germanium, it is found the exponent $a = 2$ (see [58]), so there is an agreement between the frequency

dependence ω^2 predicted by Herring and that obtained by Ward and Broido in (3.35). However, to fulfill the Herring's fifth law at low temperatures (3.35) should exhibit a T^3 behavior, and a term suitable for high temperatures should be also taken into account, as other authors have indicated [23]. Since the *ab-initio* calculations are restricted to a certain range of temperatures, a whole description of the behavior of τ_N with temperature might not be found with this method.

Since one of the objectives of this work is studying the thermal transport in a wide range of temperatures, we propose to modify the *ab-initio* expression of τ_N in order to extend it to both lower and higher temperature regimes, respectively. In (3.35), we have corrected the exponent of the temperature according to Herring's fifth-power law (now T^3) and we have added an additional term $1/(B_N T)$ to account for high-temperature intervals according to (3.34). In this way, our final expression for τ_N is

$$\tau_N = \frac{1}{B_N T^3 \omega^2 [1 - \exp(-3T/\ \ _D)]} + \frac{1}{B_N T} \quad , \tag{3.37}$$

and so it is expected to be valid in the whole temperature range.

Concerning U-processes, following the argument provided by Ziman [36], at low temperatures the scattering of two phonons with wave vectors $\boldsymbol{q}_1$ and $\boldsymbol{q}_2$ cannot provide $\boldsymbol{q}_3 + \boldsymbol{G}$, with $\boldsymbol{G} = 0$, since low temperature means low energy or low $\boldsymbol{q}$. In other words, U-processes are not possible at low temperatures. Therefore, we have established a temperature limit assuming that 1/3 of the limit of the Brillouin zone, corresponding to a wave vector $q_U = 2\pi/3a$ (a being the lattice parameter), the probability of U-processes to happen decreases exponentially. We have denoted this temperature limit $\ \ _U$, referring to it as the Umklapp extinction temperature, and it can be calculated from the dispersion relations through the expression $\hbar\omega_{\boldsymbol{q}_U} \quad k_B \ \ _U$. For silicon we have obtained $\ \ _U = 140$ K. Then, we propose to add an exponential factor $\exp(\ \ _U/T)$ in the *ab-initio* expression of τ_U to account for this behavior at the limit of low temperatures, such that our final expression for U-processes is:

$$\tau_U = \frac{\exp(\ \ _U/T)}{B_U \omega^4 T [1 - \exp(-3T/\ \ _D)]} \quad . \tag{3.38}$$

Note that at high enough temperatures, the numerator of Eq. (3.38) is 1 and the Ward and Broido's expression (3.36) is recovered.

In addition, we have studied how the temperature exponentials influence the behavior of τ_U with T in (3.38). Let us rewrite Eq. (3.38) as

$$\tau_U = \frac{g_i(T)}{B_U \omega^4} \tag{3.39}$$

Table 3.1: Summary of most relevant expressions for Umklapp and normal scattering rates that can be found in the literature for silicon and germanium. Subindex $i = \mathrm{L}, \mathrm{T}$ denotes longitudinal or transversal polarization for the acoustic branches.

Work	Ref.	τ_U^{-1}	τ_N^{-1}
Callaway (1959)	[22]	$B\omega^2 T^3$	$B\omega^2 T^3$
Holland (1963)	[23]	$B_i\omega^2/\sinh(k_B T/\hbar\omega)$	$B_{\mathrm{T}}\omega T^4$
		$i = \mathrm{L}, \mathrm{T}$	$B_{\mathrm{L}}\omega^2 T^3$
Morelli et al. (2002)	[27]	$B_i\omega^2 T e^{\theta_i/3T}$	$B_{\mathrm{T}}\omega T^4$
		$i = \mathrm{L}, \mathrm{T}$	$B_{\mathrm{L}}\omega^2 T^3$
Mingo (2003)	[28]	$B\omega^2 T e^{-C/T}$	neglected
Chantrenne et al. (2005)	[26]	$B_{\mathrm{L}}\omega^2 T^{1.5}$	neglected
		$B_{\mathrm{T}}\omega T^4$	neglected
Kazan et al. (2010)	[62]	$B_i\omega^2 T e^{-\theta_{D,i}/3T}$	$B_{\mathrm{L}}\omega^2 T^3$
		$i = \mathrm{L}, \mathrm{T}$	$B_{\mathrm{T}}\omega T^4$
Ward & Broido (2010)	[61]	$B_U\omega^4 T \;\; 1 - e^{(-3T/\Theta_D)}$	$B_N\omega^2 T \;\; 1 - e^{(-3T/\Theta_D)}$

with $i = 1, 2, 3, 4$, being

$$g_1(T) = \frac{1}{T} \tag{3.40}$$

$$g_2(T) = \frac{1}{T(1 - \exp(-3T/\quad_D))} \tag{3.41}$$

$$g_3(T) = \frac{1}{T}\exp(\quad_U/T) \tag{3.42}$$

and

$$g_4(T) = \frac{\exp(\quad_U/T)}{T(1 - \exp(-3T/\quad_D))} \quad . \tag{3.43}$$

Introducing $g_2(T)$ in Eq. (3.39) yields the *ab-initio* expression (3.36), and $g_4(T)$ in Eq. (3.39) yields the expression (3.38) we have proposed in this work; $g_1(T)$ accounts for the temperature dependence of τ_U without the correction of any exponential term, and $g_3(T)$ accounts for the effect of the term $\exp(\quad_U/T)$ alone, standing for the Umklapp extinction temperature that we have suggested in this work. In Fig. 3.5 we show the curves corresponding to the four possible combinations $g_1(T), g_2(T), g_3(T)$ and $g_4(T)$ for silicon. We can observe that above room temperature all the curves have the same behavior, which can be modulated in strength through the fitting parameter B_U in (3.39). At very low temperatures the behavior is different

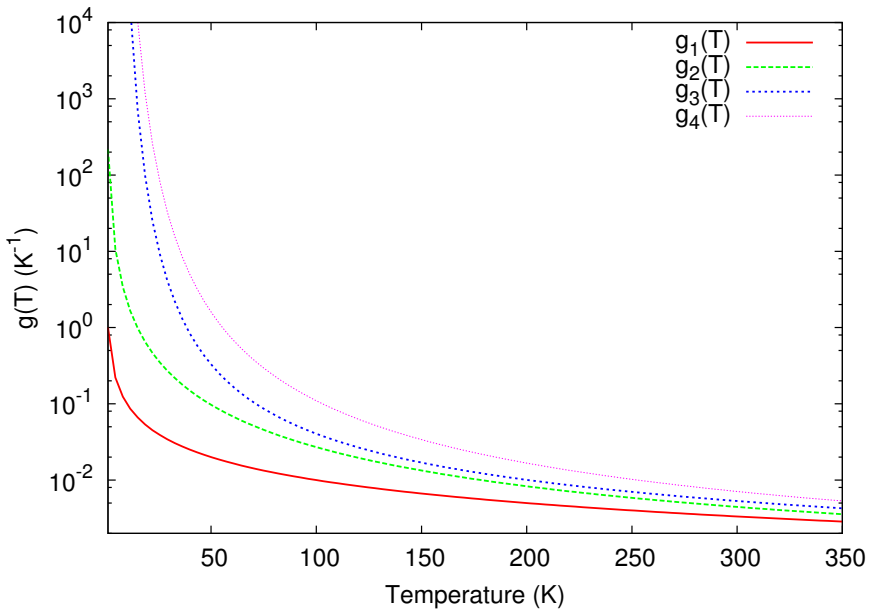

Figure 3.5: Comparison of several temperature functions $g_i(T)$ intervening in $_U$. It can be observed that the curves differ from each other specially under room temperatures, and that the combinations of the exponential factors in $g_2(T), g_3(T), g_4(T)$ provides a smoother transition from the behavior at high-temperatures towards the $g(T)$ behavior at low temperatures. Curves are compute for silicon with Θ_D=650 K and Θ_U=140 K.

for each function. Since the modes do not have enough energy to collide in a way such that they generate a higher energy mode able to jump out of the first Brillouin zone, the Umklapp processes cannot occur. This is translated as a divergence with temperature in the expression of τ_U. We can observe in the plot that the effect of the exponential terms in $g_i(T)$ is to smooth this transition towards the divergence, or in other words, to increase the temperature at which the transition from the high-temperatures behavior towards divergence at low-temperatures ($g(T)$) behavior occurs. Note that $g_1(T)$, that is, the terms without exponential factors correction, shows an abrupt divergence when T 0, while $g_4(T)$ provides the smoothest transition in agreement with a realistic extinction temperature.

The expressions (3.37) and (3.38) for τ_N and τ_U respectively, will be used to calculated the thermal conductivity of the diamond-like materials under study in Chapters 5 and 6 and will be further discussed in Chapter 7. As last remark, we wish to highlight that we have obtained (3.37) and (3.38) following Herring's work to avoid the thermal conductivity results could be influenced by introducing *ad hoc* or empirical frequency and temperature dependences.

3.2.2 Mass-defect scattering

The point-defect scattering is a general term referring to all possible scattering processes between a phonon and a lattice defect, which can be due to several factors, for instance, a difference of mass between the lattice atom and the defect, a difference in the binding between the defect and their neighbors, or anharmonic effects of the distortion about the defect. Although many substances can be obtained very pure chemically, it is difficult to separate the various isotopes from their natural composition. Therefore, this type of "impurity" is the most common and hardest to eliminate. Other defects may also be vacancies, or disclinations, or more complex topological structures, requiring a more complicated analysis than that presented here (see Fig. 3.7). In the case of a difference in mass, we call it mass-defect scattering, which is, therefore, the process where a phonon scatters with a point of the lattice containing a different atom, impurity or isotope, due only to the mass difference. Some representative examples are alloys, doped materials and isotopically enriched materials, respectively. In most of the cases, the mass-defect scattering is the only one usually considered, since the composition of a sample is normally well known, and the theory related to this process is more precise than in the other cases (distortion and misfit scattering) [63]. Therefore, let us consider in this work only the relaxation time related to the mass-defect scattering due to isotopic disorder in the crystal composition, often named in the literature impurity scattering, for simplification, and denoted as τ_I. In the present work we will focus on the effect of mass-defect scattering in the thermal conductivity as the results of different isotopic abundances in a given material.

In 1951, Klemens derived an expression for the mass-defect scattering rate using perturbation theory described in Sec. 3.1.

According to Klemens [59, 63], in a mass-defect scattering process, the kinetic energy of the crystal would be altered due to a mass difference ΔM between an atom of the crystal and the impurity. Then, the perturbed hamiltonian H is given by

$$H = \frac{1}{2}\Delta M \quad \frac{du}{dt} \quad ^{2} \tag{3.44}$$

being $\mathbf{u}(\mathbf{x}) = \frac{1}{N^{1/2}} \sum_{\boldsymbol{q}} a_{\boldsymbol{q}\nu} \boldsymbol{p}_{\boldsymbol{q}} \exp(i\boldsymbol{q} \cdot x)$ the displacement vector of an atom at the lattice-site $\boldsymbol{x}$, with N the number of atoms in the crystal, and $\boldsymbol{p}_{\boldsymbol{q}}$ the polarization vector. If the impurity atom belongs to a different chemical element, (for instance SiGe alloys) the potential energy of the crystal would also be altered by its presence, but this can be disregarded in our case, since we will study the effect of the impurity scattering on the thermal conductivity as a result

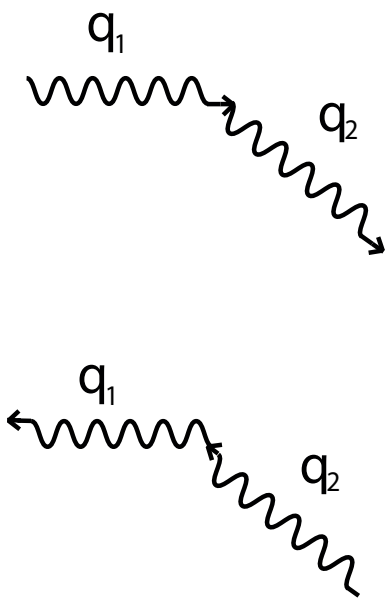

Figure 3.6: Feynman diagrams for the phonon-impurity interaction. Note that this is an elastic scattering, where the modulus is conserved $q_1 = q_2$ but not the direction.

of isotopic disorder in single element crystals (group-IV semiconductors[3]).

Following the works by Klemens [59, 63] and later by Tamura [64], using the Fermi golden rule, the scattering rate due to phonon-impurity scattering is expressed as

$$\tau_I^{-1} = \sum_{\nu_2} \quad \frac{\pi}{2}\omega_{1,\nu_1}^2(\mathbf{q_1})|\ \mathbf{q_2}|H\ |\mathbf{q_1}\ |^2\ \ (\omega - \omega_{2,\nu_2}(\mathbf{q_2}))d\mathbf{q_2} \tag{3.45}$$

where energy and momentum are conserved, that is

$$\omega_1 = \omega_2, \quad q_1 = q_2 \tag{3.46}$$

since this type of scattering is an elastic collision (see the Feynman diagrams in Fig. 3.6). After a little algebra (where we have also considered a cubic symmetry in the lattice)[4] we can find that

$$\tau_I^{-1} = \frac{\pi}{12}\omega_{1,\nu_1}^2(\mathbf{q_1})\Gamma \sum_{\nu_2} \quad (\omega - \omega_{2,\nu_2}(\mathbf{q_2}))d\mathbf{q_2} \tag{3.47}$$

[3]Note that in the case of bismuth telluride (see Chap. 7), we will deal only with naturally occurring samples.

[4]The full mathematical description can be found in the work by Tamura [64].

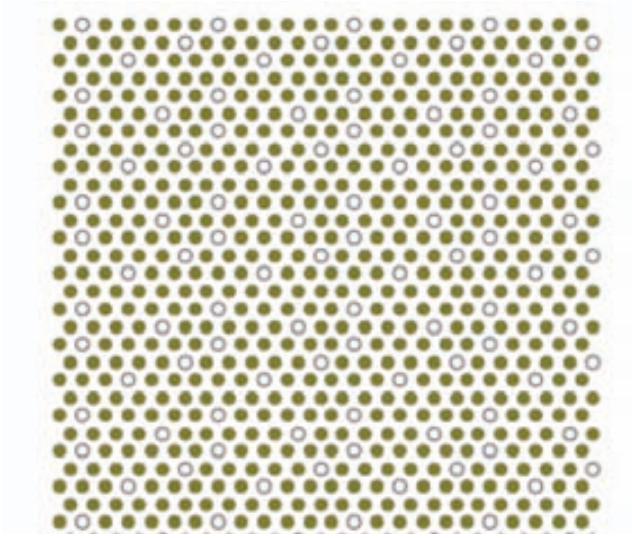

Figure 3.7: Sketch of the atoms arranged in a lattice (filled circles) with the presence of impurities (empty circles).

where

$$\Gamma = \sum_i f_i \left(\Delta M/\bar{M}\right)^2 \tag{3.48}$$

is the mass-fluctuation factor, being f_i the isotopic fraction of the i-th isotope and $\bar{M} = \sum_i f_i M_i$ the mean mass, and the mass-difference is $\Delta M = M_i - \bar{M}$. From (3.47) it is found that the relaxation time depends on the wave vector only through the frequency and then no spatial anisotropy nor polarization dependence take place. Therefore, we can delete the suffix ν and the variable $\boldsymbol{q}$, and re-express (3.47) in terms of the density of states $D(\omega)$

$$\tau_I^{-1} = \frac{\pi}{6} V \Gamma D(\omega) \omega^2 \quad , \tag{3.49}$$

where V is the atomic volume. If one substitutes in the expression derived by Tamura (3.49) the Debye density of states (see Sec. 2.1), we obtain the well-known expression first given by Klemens[5]

$$\tau_I^{-1} = \frac{V\Gamma}{4\pi v^3} \omega^4. \tag{3.50}$$

This expression has been widely used in the literature and has become, in some way, standardized [22–28, 61, 62, 65]. Despite the expression is obtained under Debye model assumptions,

[5]Note that in the Klemens' expression the ω^4 dependence is the well-known Rayleigh scattering, applied since 1895 to photon-molecule scattering in atmospheric optics, and it explains why the sky is blue.

it has provided remarkable results in a wide variety of materials. However, we must recall that, usually, the quantity $A \equiv V\Gamma/(4\pi v^3)$ has been neglected, using it instead as a fitting parameter [22, 23, 28].

Although both equations (3.49) and (3.50) can provide calculated values for τ_I, the advantage of the Klemens' equation (3.50) is that it is a very good approximation even using a real dispersion relation model, because in the temperature interval this scattering is dominating the transport, short-wavelength modes (large $\boldsymbol{q}$) are not populated and one can approximate with small error the region of long-wavelength modes in the real dispersion relation by the Debye linear dispersion (1.5), so little error is induced. On the other hand, the advantage of Tamura's expression (3.49) is that, since it depends explicitly on the density of states, it can provide a more precise description of the modes intervening in the impurity scattering for each material under the considered symmetry.

Regarding the influence of mass-defect scattering on thermal transport, it has been observed experimentally that the smaller the mass-fluctuation factor Γ, the higher the peak in the thermal conductivity as a function of temperature (*i. e.* the maximum of Fig. 3.1). As shown in Fig. 3.8, several samples of germanium and silicon with different isotopic composition exhibit peaks of different height in the thermal conductivity. One can observe that the peak occurs at a certain interval of temperatures characteristic for each material. This means that in this interval the mass-defect scattering is dominating. Before the peak, the dominant scattering mechanism is the boundary scattering, since the samples have the identical structure and dimension, as reported by Inyushkin [65, 66], the thermal conductivity is the same. After the peak, the three-phonons processes begin to dominate the transport and therefore, are the cause for the lowering of the thermal conductivity, and as the temperature increases all the samples tend to the same values of thermal conductivity. This information is very valuable to tailoring the thermal conductivity of semiconductors.

3.2.3 Boundary scattering and the associated size effect

In a finite size sample, there is a certain temperature below which the thermal conductivity decreases as temperature reduces, as sketched in Fig. 3.1. This is due to the boundary scattering, which is the process where a phonon scatters with the boundaries of the sample when it arrives at the surface. The temperature at which boundary scattering is the leading scattering mechanism will depend on the size and geometry of the sample. In samples characteristic sizes of the order of millimeters the boundary scattering dominance is restricted to a low

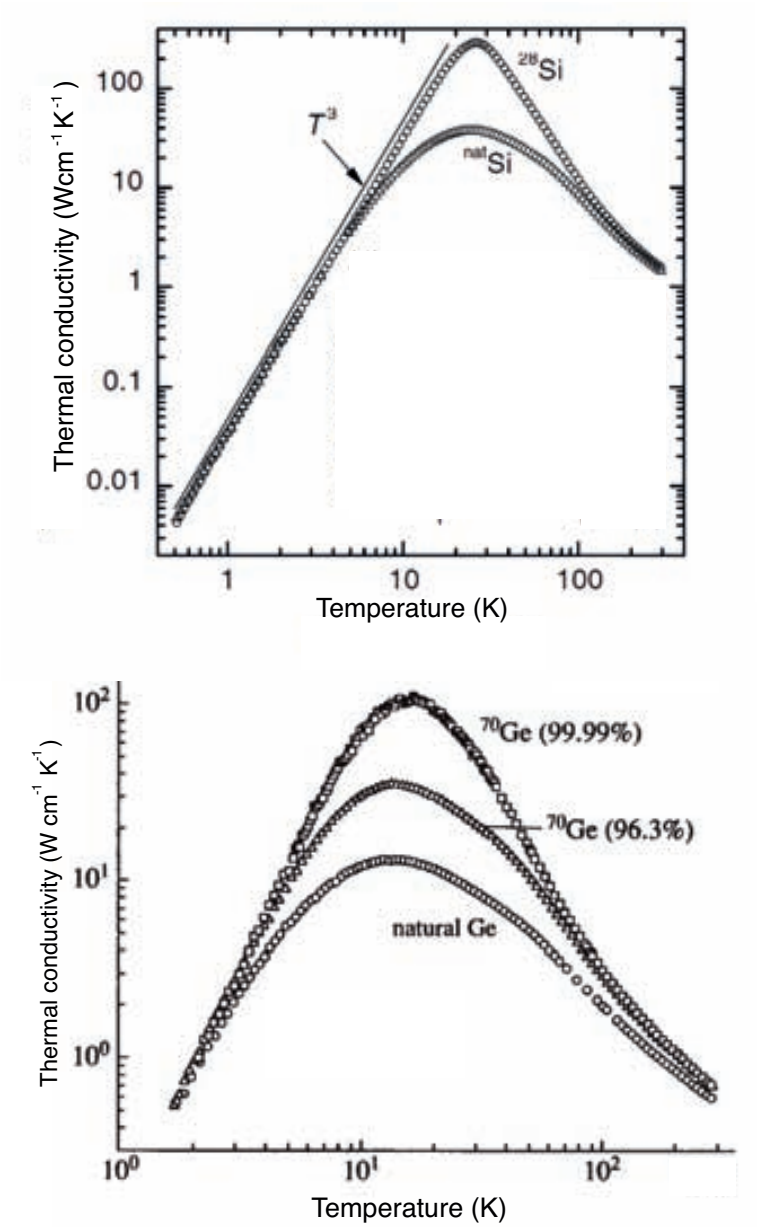

Figure 3.8: Phonon thermal conductivity measurements of silicon and germanium bulk samples with several isotopic compositions: (a) Naturally occurring silicon $^{\mathrm{nat}}Si$ *(92.2%*^{28}Si*, 4.7%*^{29}Si*, 3.1%*^{30}Si*) and isotopically enriched silicon* ^{28}Si *(99.983%*$^{2}8Si$*, 0.014%*$^{2}9Si$*, 0.003%*$^{3}0Si$*) from Ref. [65] and (b) naturally occurring germanium* $^{\mathrm{nat}}Ge$ *(20.5%*^{70}Ge*, 27.4%*^{72}Ge*,7.8%*^{73}Ge*,36.5%*^{74}Ge*,7.8%*^{76}Ge*) and isotopically enriched germanium with two different abundances* ^{70}Ge*(99.99%) (99.99%*^{70}Ge*, 0.01%*^{73}Ge*) and* ^{70}Ge*(96.3%) (96.3%*^{70}Ge*, 2.1%*^{72}Ge*, 0.1%*^{73}Ge*, 1.2%*^{74}Ge*, 0.3%*^{76}Ge*) from Ref. [66]. Since all the samples in (a) and (b) are the same size and shape, the effect of the impurity scattering is highlighted: the less concentration of impurities, the less impurity scattering and the higher the peak of the curve.*

temperature range, while at the nanoscale the influence of the boundary scattering reaches even room temperatures. This is highlighted by the drastic thermal conductivity decrease observed, for instance, in silicon nanowires (see Fig. 3.9 (a)). Note the differences in the shape of between these nanowires and the millimetric Si samples shown in Fig. 3.8 (a). In addition, the thermal conductivity behavior with temperature exhibits a T^3 tendency at low temperatures (see Figs. 3.8 and 3.9), *i.e.* the same temperature dependence as the specific heat.

As the size of the system reduces drastically, we can observe that this slope smooths. Experimentally, it has been observed a T^1 slope in very thin silicon nanowires (with diameter 22nm, and surface considered smooth) [8] (see Fig. 3.9 (a)). This could be interpreted on the basis that, in this case, phonon motion is one-dimensional (implying C_v T), instead of three-dimensional (implying C_v T^3), but in the thicker nanowire the behavior is more similar to T^3, as shown in Fig. 3.9 (b), where appears a zoom of the data in a logarithmic scale, it can be observed how the slope of the conductivity of the nanowires smoothes as the diameter reduces. This still it is a very puzzling result that suggests some confinement quantum effects may be involved in the drastic reduction of the thermal conductivity of very thin nanowires [10].

Furthermore, the geometry of the system also affects to the reduction of the thermal conductivity [67, 68], since thin-films (two-dimensional system) and nanowires (one-dimensional system) with equivalent effective size have different thermal conductivity at the same temperature, as shown by the experimental measurements in Fig. 3.10, where it can be seen that a thin-film with thickness slightly smaller than the diameter of a nanowire, exhibits a higher thermal conductivity.

Surprisingly, the boundary scattering is characterized by the following simple relaxation rate given by Casimir (1938) [7]

$$\tau_B^{-1} = \frac{v}{L_{\text{eff}}} \tag{3.51}$$

where L_{eff} represents the effective dimension of the system, and v is the phonon group velocity. Note that τ_B is frequency-dependent through the group velocity, although in the original expression by Casimir, it was used instead a constant value, the velocity of the sound in the solid. Usually, the features of the surface, whether it is smooth or rough, are normally taken into account through a correction factor F multiplying the effective length [36]. For the sake of simplicity, in the present work we restrict ourselves to the case of smooth surfaces, where $F = 1$, since in the case of rough surfaces more complicated mechanisms, such as backscattering, may occur. Although in nanowires with very rough surfaces this mechanisms

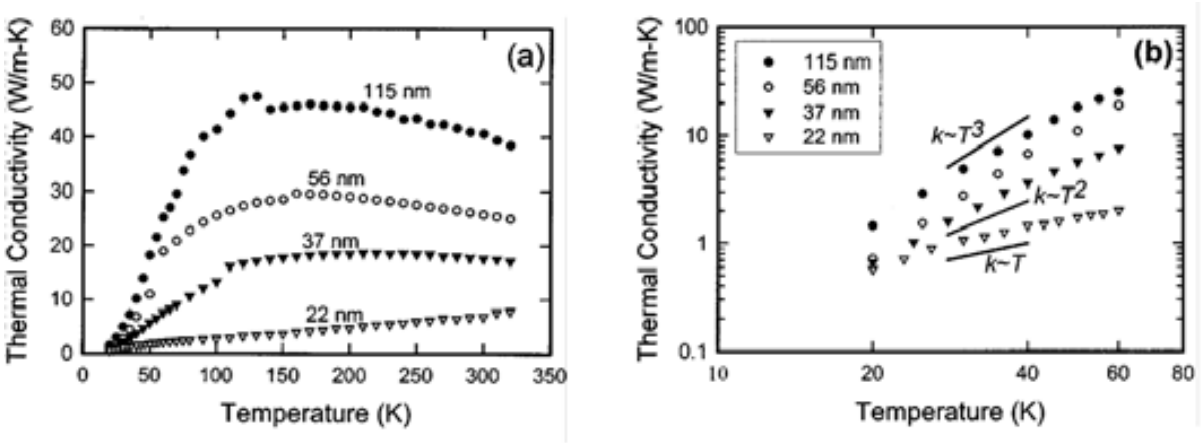

Figure 3.9: (a) Experimental measurements of phonon thermal conductivity for several diameters silicon nanowires. (b) Zoom at low temperatures where the curves T^3, T^2 and T are plotted for comparison. (Figures reproduced from Ref. [8]).

has revealed as a useful tool to drastically reduce the thermal conductivity [69,70], to account for it is out of the scope of this thesis. As such, we will use the expression (3.51) which has become standard in the literature. On the other hand, with an appropriate effective size L_{eff} entering into Eq. (3.51), the size and geometry effects should be correctly described. For this purpose, L_{eff} needs to be calculated regarding the geometry of the system. This way, following Zhang [12], with a little algebra one can obtain for samples with square cross-section

$$L_{\text{eff}} = 1.12 \quad \overline{A} \tag{3.52}$$

where $A = l_1 \quad l_2$ is the cross-section of the sample, with l_1 and l_2 the width and thickness. For cylindrical wires of diameter d we have

$$L_{\text{eff}} = d \tag{3.53}$$

and

$$L_{\text{eff}} = 2.25h \tag{3.54}$$

for thin-films of thickness h.

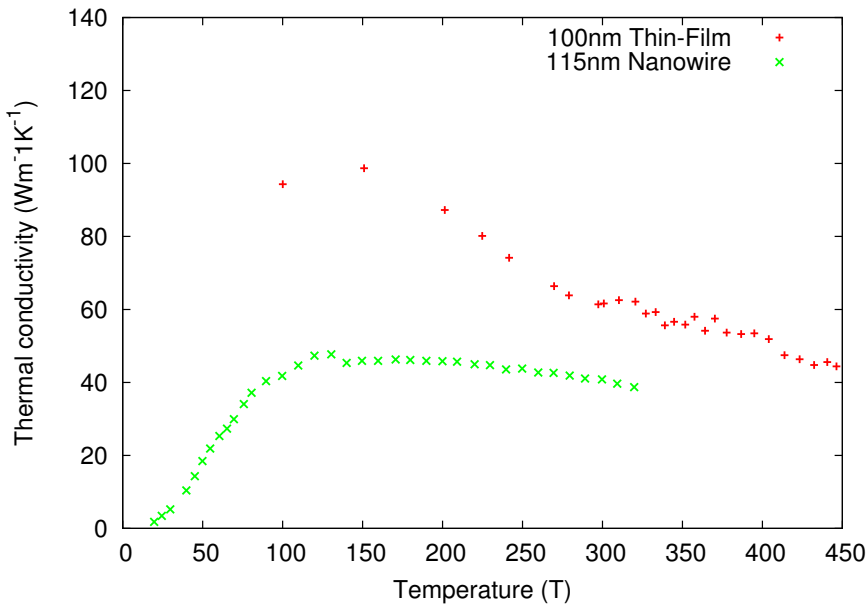

Figure 3.10: Experimental measurements of phonon thermal conductivity of a 115 nm diameter silicon nanowire [8] and a 110 nm thickness silicon thin-film [71].

3.3 Matthiessen rule

When there are several scattering processes taking place at the same time in the crystal, we have to determine how they can be combined to yield an effective scattering rate. The simplest approach is to assume that the probability of scattering associated to each mechanism does not depend on the other mechanisms, and then the frequencies corresponding to each collision can be added, obtaining an effective frequency given by

$$f_{\text{eff}} = f_1 + f_2 + \dots f_n \tag{3.55}$$

where the f_i is the scattering frequency of the i scattering mechanism. This is called the Matthiessen rule. As the relaxation times are the reciprocal of the scattering frequencies, we have

$$\frac{1}{\tau_{\text{eff}}} = \frac{1}{\tau_1} + \frac{1}{\tau_2} + \cdots + \frac{1}{\tau_n} \tag{3.56}$$

where τ_{eff} is the effective relaxation time. In other words, if the phonons suffer various scattering processes, each process contributes additively to $1/\tau$. Here, it is crucial to remark that this is only valid for resistive processes, and therefore, N-processes, which do not contribute

directly to thermal resistance, should not be included in the Matthiessen rule, but require a special treatment [36, 72], which will be discussed in Chapters 4 and 5.

Chapter 4

Thermal conductivity

As we have seen in the previous Chapter, several phonon scattering processes are the source of the thermal resistance in a crystal. Therefore, they must be considered in a microscopic study of the lattice thermal conductivity in solids, which is carried out mainly under three different approaches: relaxation-time approach, variational approach, and Green's function or density matrix approach. Both the relaxation-time and the variational approach assume that the lattice thermal conductivity can be studied from a solution of the linearized Boltzmann transport equation, while the Green's function approach uses the quantum statistics framework. Other possible techniques may be based on fluctuation-dissipation approaches, as in the Green-Kubo relations.

Since our framework is the Boltzmann transport equation, in this work we will focus on both the relaxation-time and variational approaches. With the aim of bridging up these two approaches, we will present in this Chapter a new model on thermal conductivity developed after discussing the main precedent models that have been devoted to provide an analytical expression of the thermal conductivity within these approaches.

4.1 Discussion on the approaches to solve the Boltzmann transport equation

As we have introduced in Chapter 1, the BTE is a usual starting point in thermal conductivity modeling. Summarizing, when a small temperature difference T is applied on a system, the phonon distribution $n_{\boldsymbol{q}}$ moves from equilibrium at a linear rate. On the other hand, collisions turn the phonon distribution back to equilibrium at a rate that depends on the scattering

transition rate. The BTE allows to obtain the resulting phonon distribution function by relating both rates

$$\frac{n_{\boldsymbol{q}}}{t}_{\text{driff}} = \frac{n_{\boldsymbol{q}}}{t}_{\text{scatt}} . \tag{4.1}$$

As we have already discussed in Sec. 1.3, its exact analytical solution is unknown, both because the form of the right-hand term is very complicated from the physical point of view, and because of the mathematical complexity of the resulting equation when the scattering term is specified.

Within the analytical framework, there are roughly two main approaches to solve the BTE: the the relaxation-time approach or kinetic methods (KM) and the variational methods (VM). KM can be applied when the distribution function is expected to be very close to equilibrium. In this case, the collision term is usually simplified by assuming that it is proportional to the inverse of a relaxation time, this is the relaxation-time approximation (RTA) presented in Sec. 1.4.3, where the several phonon modes are assumed to behave independently of each other. Finding relaxation times for reduced regions of temperature and sizes is not difficult. The problem appears if one wants to extend the region of applicability to wider intervals using the KM approach with the same RTA expression. In the last decades, the miniaturization has worsened this situation, showing dramatic divergences between KM-RTA predictions and the experimental results when bulk and nanoscale samples are simulated with the same relaxation time expressions, as we will detail in the next Section.

In contrast, when the system is not so close to equilibrium, VM provide a better way to solve the BTE. In general, the collision term in VM cannot be expressed analytically, instead it has to be obtained by integration using a trial function. This trial function should be close to the actual solution to have a good convergence. The main drawback of VM is that the trial function is not necessarily the same at every temperature interval. In conclusion, this approach is only useful in regions where the form of the phonon distribution is known to some extent.

4.2 Relaxation-time approach: Kinetic methods

As we have shown in Sec. 1.4.3, the relaxation-time approximation (RTA) is the simplest approach in order to formulate and solve the BTE and obtain an integral expression for the thermal conductivity (see Eq. (1.39)). This approach assumes that, when the phonon distribution remains near equilibrium, the rate of change of the phonon distribution $n_{\boldsymbol{q}}$ due

to collisions depends inversely on the relaxation time $\tau_{\boldsymbol{q}}$, that is

$$\left.\frac{dn_{\boldsymbol{q}}}{dt}\right|_{\text{scatt}} = -\frac{n_{\boldsymbol{q}} - n_{\boldsymbol{q}}^0}{\tau_{\boldsymbol{q}}}. \tag{4.2}$$

It means that a perturbation in the distribution function will decay exponentially with a relaxation time $\tau_{\boldsymbol{q}}$. This relaxation time $\tau_{\boldsymbol{q}}$ should account for the scattering processes giving raise to thermal resistance by adding their scattering rates through the Matthiessen rule (see Sec. 3.3). Therefore, the role of non-resistive processes is not clear, since their only perspective within this picture is whether to be neglected, or to be treated as another resistive process being added in the Matthiessen rule. In words of J. Callaway *"It is well known that normal processes (scattering processes which conserve the total crystal momentum) cannot by themselves lead to a finite thermal conductivity. Consequently, it cannot be legitimate just to add reciprocal relaxation times for the normal processes to those which do not conserve the crystal momentum"* [22]. With this in mind, he made the first attempt to improve the RTA taking into account the special nature of N-processes. Let us see in the following Section the formulation of his model.

4.2.1 The Callaway model

To improve the results provided by the standard RTA, in 1959 Callaway published his well-known model for phonon heat transfer [22], becoming the most used expression in the literature for calculating phonon thermal conductivity. Since then, the Callaway model has been deeply studied and it has suffered some variations and corrections [17, 23, 73].

The main contribution of Callaway consisted in taking into account the different character of normal scattering processes. The model takes their role under consideration by splitting the collision term of the Boltzmann equation in the RTA into two expressions, one depending on resistive scattering that relaxes the phonon distribution $n_{\boldsymbol{q}}$ to the equilibrium distribution $n_{\boldsymbol{q}}^0$ (see Eq. (1.15)), and a second one depending on normal scattering that relaxes $n_{\boldsymbol{q}}$ to another distribution denoted by $n_{\boldsymbol{q}}(\mathbf{a})$, which is displaced from the equilibrium one, this is

$$\left.\frac{dn_{\boldsymbol{q}}}{dt}\right|_{\text{scatt}} = -\frac{n_{\boldsymbol{q}} - n_{\boldsymbol{q}}^0}{\tau_{\boldsymbol{q}_R}} - \frac{n_{\boldsymbol{q}} - n_{\boldsymbol{q}}(\mathbf{a})}{\tau_{\boldsymbol{q}_N}} \tag{4.3}$$

where $\tau_{\boldsymbol{q}_N}$ is the relaxation time for normal processes, and $\tau_{\boldsymbol{q}_R}$ is obtained through the Matthiessen rule (3.56) by adding reciprocal relaxation times of all the resistive processes

participating in thermal transport in the system considered. Due to the non-resistive nature of normal scattering, $n_{\boldsymbol{q}}(\mathbf{a})$ must be a Bose-Einstein distribution function centered in a non-zero momentum $\mathbf{a}\cdot\mathbf{q}$ in the direction of propagation, thus

$$n_{\boldsymbol{q}}(\mathbf{a}) = \frac{1}{\exp\ \frac{\hbar\omega-\mathbf{a}\cdot\mathbf{q}}{\mathrm{k_B T}}\ -1}\quad \frac{1}{\exp\ \frac{\hbar\omega}{\mathrm{k_B T}}\ -1} + \frac{\mathbf{a}\cdot\mathbf{q}}{k_B T}\frac{\exp\ \frac{\hbar\omega}{\mathrm{k_B T}}}{\exp\ \frac{\hbar\omega}{\mathrm{k_B T}}\ -1}^{2}\ . \tag{4.4}$$

where $\mathbf{a}$ is a constant vector in the direction of the temperature gradient.

The BTE with scattering term given by (4.3) is

$$\boldsymbol{c}\cdot\quad T\frac{dn_{\boldsymbol{q}}}{dT} = -\frac{n_{\boldsymbol{q}}-n^0_{\boldsymbol{q}}}{\tau_R} - \frac{n_{\boldsymbol{q}}-n_{\boldsymbol{q}}(\mathbf{a})}{\tau_N} \tag{4.5}$$

where $\boldsymbol{c}$ is the phonon velocity in the Debye approximation. If we define $n_1 = n_{\boldsymbol{q}} - n^0_{\boldsymbol{q}}$, and using (4.4) we can express (4.5) as

$$-\frac{\hbar\omega}{k_B T^2}\boldsymbol{c}\cdot\quad T\frac{e^{\hbar\omega/k_B T}}{(e^{\hbar\omega/k_B T}-1)^2} + \frac{\mathbf{a}\cdot\mathbf{q}}{\tau_N k_B T}\frac{e^{\hbar\omega/k_B T}}{(e^{\hbar\omega/k_B T}-1)^2} - \left(\tau_N^{-1}+\tau_R^{-1}\right)n_1 = 0 \tag{4.6}$$

where a combined relaxation time τ_C^{-1} is defined as

$$\tau_C^{-1} = \tau_R^{-1} + \tau_N^{-1}\,. \tag{4.7}$$

We obtain n_1 as follows:

$$n_1 = -\quad \boldsymbol{c}\cdot\quad T\frac{\hbar\omega}{k_B T}\frac{e^{\hbar\omega/k_B T}}{\left(e^{\hbar\omega/k_B T}-1\right)^2} \tag{4.8}$$

Now we need to determine $\quad_{\boldsymbol{q}}$ in terms of τ_C and τ_N, since after using (4.8), with the Fourier law and the usual algebra (see Sec. 1.4.3), the thermal conductivity expression is

$$= \frac{1}{3}\quad \hbar\omega c^2\ \ D(\omega)\frac{dn^0_{\boldsymbol{q}}}{dT}d\omega \tag{4.9}$$

If we substitute (4.7) and (4.8) into (4.6) we obtain

$$\frac{\hbar\omega}{\tau_C T}\boldsymbol{c}\cdot\quad T + \frac{\boldsymbol{a}\cdot\boldsymbol{q}}{\tau_N} = \frac{\hbar\omega}{T}\boldsymbol{c}\cdot\quad T\,. \tag{4.10}$$

Recall that $\boldsymbol{a}$ is a constant vector in the direction of $\quad T$, so if we define a parameter . with dimension of a relaxation time, such that we can write

$$\boldsymbol{a} = -\frac{\hbar}{T}.\ c^2\quad T \tag{4.11}$$

and given by the Debye approximation that $\boldsymbol{q} = \boldsymbol{c}\omega/c^2$, we obtain

$$\boldsymbol{a} \cdot \boldsymbol{q} = -\frac{\hbar}{T}. \; \boldsymbol{c} \cdot \quad T \tag{4.12}$$

and then (4.10) simplifies yielding

$$\frac{}{\tau_C} - \frac{\cdot}{\tau_N} = 1 \tag{4.13}$$

Now, using the Debye dispersion relations and density of states and substituting from (4.13) in (4.9), we obtain the following expression for thermal conductivity

$$= \frac{k_B}{2\pi^2 c}(I_1 + . \; I_2) \tag{4.14}$$

which is split into two contributions, a first one

$$I_1 = \int_0^{k_B\theta_D/\hbar} \tau_C \frac{\hbar^2\omega^2}{k_B^2 T^2} \frac{e^{\hbar\omega/k_B T}}{(e^{\hbar\omega/k_B T} - 1)^2} d\omega \tag{4.15}$$

and a second one

$$I_2 = \int_0^{k_B\theta_D/\hbar} \frac{\tau_C}{\tau_N} \frac{\hbar^2\omega^2}{k_B^2 T^2} \frac{e^{\hbar\omega/k_B T}}{(e^{\hbar\omega/k_B T} - 1)^2} d\omega \tag{4.16}$$

Finally, we only need to determine . . For this purpose, we make use of the momentum conserving nature of the N-processes. Since the rate of change of the total momentum due to normal collisions is set equal zero, we can write

$$\frac{dn_{\boldsymbol{q}}}{dt}\Big|_N \boldsymbol{q} d\boldsymbol{q} = \int \frac{n_{\boldsymbol{q}}(\boldsymbol{a}) - n_{\boldsymbol{q}}}{\tau_N} \boldsymbol{q} d\boldsymbol{q} = 0 \tag{4.17}$$

Substituting (4.4), (4.8) and (4.12) into (4.17), we obtain

$$. = \frac{\int_0^{\theta_D/T} \frac{\tau_C}{\tau_N} x^4 \frac{e^x}{(e^x - 1)^2} dx}{\int_0^{\theta_D/T} \frac{1}{\tau_N} \quad 1 - \frac{\tau_C}{\tau_N} \quad x^4 \frac{e^x}{(e^x - 1)^2} dx} \tag{4.18}$$

where $x = \hbar\omega/k_B T$. In the first term I_1 the normal processes are considered resistive through the combined relaxation time τ_C, which involves resistive and non-resistive (normal) scattering processes.

Note that, as pointed by Ziman [36] and Callaway itself [22], the N-processes treatment as if they were resistive processes and their inclusion into the Matthiessen sum (4.7) is not strictly

correct. Thus, the second term of the thermal conductivity . I_2 represents the correction due to the effect of N-processes to the first term I_1. So, in fact, I_1 is the standard RTA expression including N-processes, whose inclusion is counterbalanced by . I_2. Actually, in the case of neglecting the N-processes $\tau_N =$, or when the transport is dominated by the resistive processes τ_R τ_N, we have $\tau_C = \tau_R$ and $\tau_C/\tau_N = 1/(1 + \tau_N/\tau_R) = 0$, therefore we recover the integral expression of in the standard RTA Eq.(1.39) with a purely resistive relaxation time.

The Callaway model provides a good approximation of the thermal conductivity behavior in bulk samples below room temperatures, as shown by Callaway for Ge [22] (see Fig.4.1), and shown in [74,75] for other materials, and Eq. (4.7), though incorrect, is assumed as a first approach to deal with N-processes. Nevertheless, the predictive capability of the Callaway model is low. It has been shown that when applying the Callaway model to nanoscale samples, it leads to an overestimation of the thermal conductivity. Although several authors believe that this drawback may be improved by using suitable expression of the relaxation times or including other scattering mechanisms, like dislocation scattering or the decay of optic phonons into acoustic, it is still not clear if the low predictive capability may be linked, instead, to the treatment of N-processes in the model. Let us discuss next some of the most relevant Callaway model derivatives that have been proposed in the last years with the aim of improving thermal conductivity predictions.

4.2.2 Some Callaway-based models

The Callaway model has been the subject of many studies related to lattice thermal conductivity and usually taken as the standard model to calculate it. Here, we will briefly discuss some of the works based in the Callaway model that have been proposed to improved the thermal conductivity predictions in certain samples. The first refinement is provided by Holland [23] a few years after the publication of the Callaway model. He improved the thermal conductivity results on bulk silicon and germanium using the Callaway model, but this time considering the polarizations of the acoustic modes (one longitudinal and two transversal), this implies considering the sound velocity values in each polarization, as well as different Debye temperatures and parameters in τ_U and τ_N for the transversal and longitudinal branches (see Table 3.1). In addition, to improve the predictions at high temperatures, firstly, he modifies the expressions of τ_U and τ_N to account for this temperature regime, and secondly, splits the transversal contribution to the thermal conductivity with a threshold in the frequency

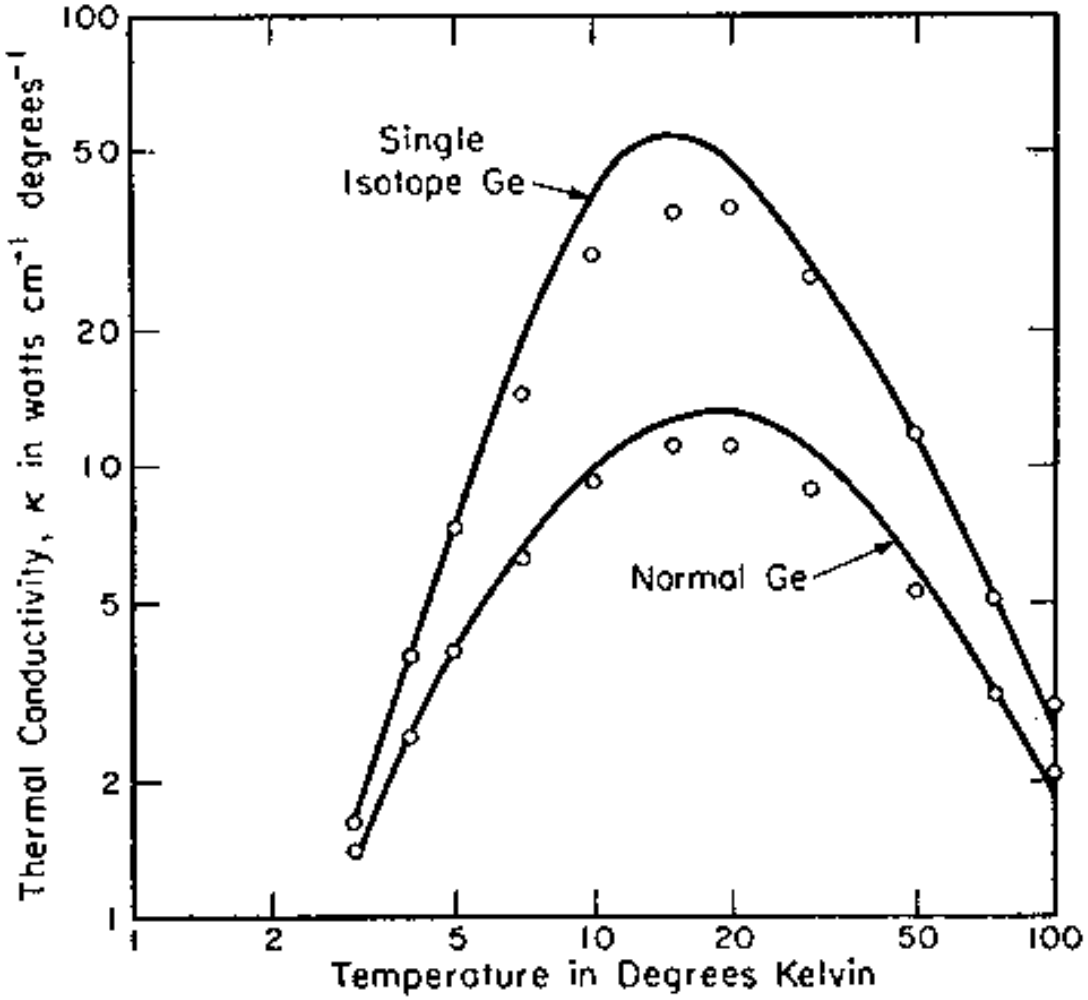

Figure 4.1: Thermal conductivity of naturally occurring (normal) Ge and isotopically enriched Ge calculated by Callaway with Eq. (4.14). Experimental results from Ref. [76]. (Reproduced from Ref. [22])

spectrum, one for low temperatures, and another for hight temperatures. This way, Holland's results on germanium were significantly improved respect to those provided by Callaway, but at the expense of multiplying the number of free adjustable parameters appearing in the relaxation times expressions.

When experimental data for thermal conductivity from micro and nanoscale samples became available in the late 90's, the Callaway model failed in the prediction of these new data, above certain temperature interval, and especially around room temperature. Since

then, there has been a proliferation of several Callaway-like models introducing some changes in order to fit bulk and micro or nanoscale data with a single thermal conductivity expression [24, 27, 28, 62].

As shown by Mingo [28] (see Fig. 4.2(a)), the predictions made with the Callaway model for silicon nanowires with several diameters are overestimated. To improve this, Mingo proposed to use real dispersion relations calculated atomistically for a wire, instead of the non-dispersive relations given by the Debye model which are employed in the Callaway model [28]. The reason is that integration up to the limit given by the Debye frequency may increase artificially the importance of the high-frequency phonons. In Fig. 4.2(b) we can see the theoretical predictions made by Mingo [28] with the Callaway formula using a cut-off frequency ω_C smaller than the Debye frequency ω_D, and a different set of expressions for the relaxation times. We can observe that the predictions lower reasonably. However, there are two important drawbacks i) this cut-off is obtained by adjusting to experimental data, therefore it is not predictive, and ii) the boundary relaxation times includes a fitted correction factor, and since τ_B is the main scattering involved in the size-effects, the predictive power lowers drastically. Actually, in Fig. 4.2 we observe several curves corresponding to aleatory values of the correction factor. Furthermore, τ_N is used for bulk calculations, but neglected for the nanowires. So in fact, Mingo is using the RTA formula (1.39). The main contribution of Mingo is to advise that more accurate dispersion relations must be used to get better descriptions of the thermal conductivity in systems with different scales. Nevertheless, it has been shown that using bulk actual dispersion relations is enough to describe nanowires with diameters wider than 30 nm [77], rather than calculate complex dispersion curves that should take into account surface features, like the cross-sectional shape of the wires, the roughness of the surface, the coating etc.

Furthermore, confinement effects are expected in the smallest (sub 30 nm) samples as shown by Srivastava [10] and, when these effects are important, we should observe a change in the thermal conductivity slope at low temperatures from a T^3 dependence in larger samples to a T^1 slope in the thinnest samples. Although in extremely reduced silicon nanowires this change in the slope has been observed [8], in samples within 30-100 nm of diameter the slope is closer to the T^3 behavior than to the T^1 expected for confined (effectively one-dimensional) systems. Therefore, a modification of the bulk dispersion relations and density of states should not be, in principle, the main cause of reduction of the thermal conductivity in this interval of sizes. To date, the general trend in thermal conductivity modeling is using bulk dispersion relations calculated either with lattice dynamics, or with *ab-initio* techniques, since both are

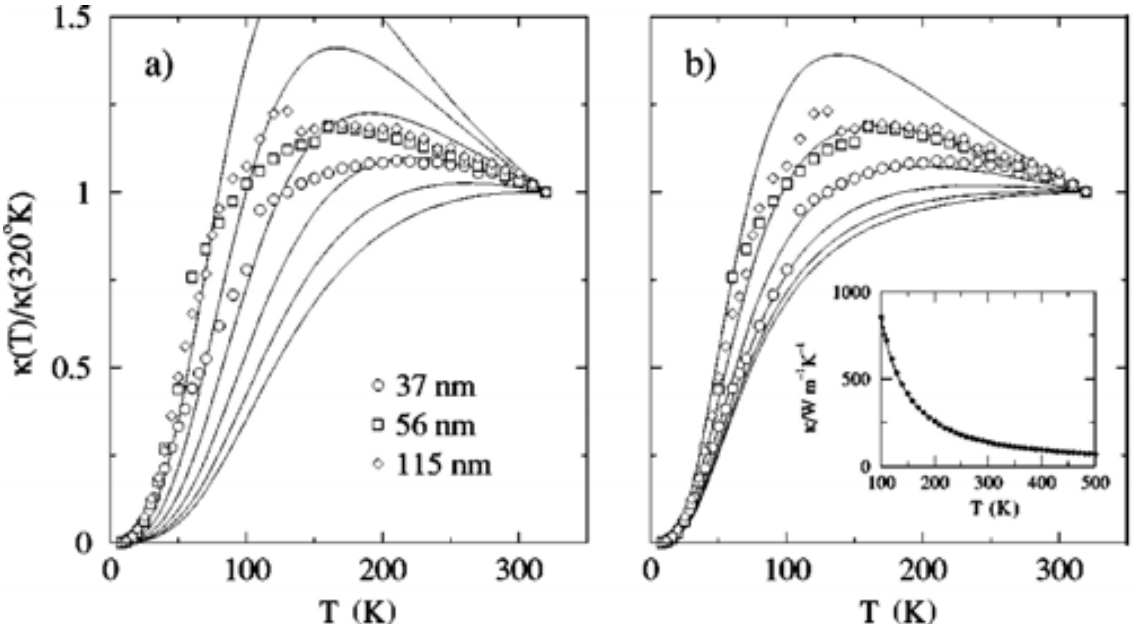

Figure 4.2: Thermal conductivity normalized by its value at T=320 K for Si nanowires of several widths, calculated by the Callaway formula with cut-off in the integrals at (a) Debye frequency $\omega_D = 86 \quad 10^{12}$ *rad/s, and (b) an adjustable cut-off* $\omega_C = 42 \quad 10^{12}$ *rad/s. Experimental results from Ref. [8] appear in symbols as indicated in the legend. Inset: bulk Si thermal conductivity for the two cases (overlapping almost complete) and experimental data from Ref. [23] (dots). (Reproduced from Ref. [28])*

in excellent agreement with measured data from neutron scattering experiments, as shown in Chapter 2.

Another usually studied modification of the Callaway model is related to relaxation times, either considering different scattering rate expressions for transversal and longitudinal polarizations, as first indicated by Holland [23], or including additional scattering mechanisms, like the decay of optical phonons into acoustic phonons [62] or roughness in the surface [26]. Some authors have also suggested that in order to predict nanoscale transport parameters, memory and non-localities should be taken into account [14, 78].

Nevertheless, what all these models have in common as a heritage of the Callaway model, is that the N-processes have been either neglected or treated as if they had a resistive nature in the Callaway fashion.

This perspective has motivated a recent work by Allen [73], where the Callaway model is corrected by a more rigorous rethinking of the Callaway model itself, paying particular

attention to the introduction of the normal scattering relaxation time into the expression of the thermal conductivity. He found that in fact, I_2 should contain τ_C instead of τ_C/τ_N, and that . should contain τ_C/τ_U in the denominator instead of $\frac{1}{\tau_N}\ \ 1-\frac{\tau_C}{\tau_N}$, but still τ_N remains in the integrals in combination with τ_R.

Despite of this variety of models, none of them has achieved the goal of describing bulk, micro and nanostructured systems thermal conductivity without making some additional assumptions depending on the studied system. Maybe this fact has stimulated, afterwards, the activity on other modeling strategies, like *ab-initio* methods, Green-Kubo integral or density functional theory [61]. The lack of generality and agreement related to the relaxation times plus the special conservative nature of the N-processes, has led us to believe that a more adequate treatment of N-processes in the thermal conductivity model may be the key point to clarify this complex situation.

4.3 Variational method

The variational method gives and approximate calculation of a functional by using a trial function, which is a first-order solution of a given equation. Since the BTE is a linear inhomogeneous integral equation, it is a good candidate to find a solution constructed formally by applying the variational method to a general trial function. This was first developed by Kohler [79, 80] and Sondheimer [81], and latter applied to lattice thermal conductivity by Ziman [36] and Leibfried and Schlömann [60], as we briefly indicate next.

The distribution function is obtained as a function of $/_{\boldsymbol{q}}$, such that

$$n_{\boldsymbol{q}} = n^0_{\boldsymbol{q}} - /_{\boldsymbol{q}} \frac{n^0_{\boldsymbol{q}}}{(\hbar\omega_{\boldsymbol{q}})} \tag{4.19}$$

where $/_{\boldsymbol{q}}$ represents a measure of the deviation from equilibrium in the phonon distribution, weighted by a factor which depends on the form of the distribution. In fact, it is the average extra energy that the phonons have because of the transport process. Operating on $n^0_{\boldsymbol{q}}$, given by Bose-Einstein distribution (1.15), we can rewrite (4.19) as

$$n_{\boldsymbol{q}} = n^0_{\boldsymbol{q}} - /_{\boldsymbol{q}} \frac{1}{k_B T} n^0_{\boldsymbol{q}}(n^0_{\boldsymbol{q}} + 1)\,. \tag{4.20}$$

Following the derivation by Ziman [36], it is found the inverse of the thermal conductivity

given by

$$\frac{1}{} = \frac{1}{2k_B T^2} \frac{(/_{\boldsymbol{q}} + /_{\boldsymbol{q}'} - /_{\boldsymbol{q}''})^2 Q^{\boldsymbol{q}''}_{\boldsymbol{q}\boldsymbol{q}'} d\boldsymbol{q} d\boldsymbol{q}\, d\boldsymbol{q}}{\boldsymbol{v}_{\boldsymbol{q}} /_{\boldsymbol{q}} \frac{n^0_{\boldsymbol{q}}}{T} d\boldsymbol{q}^{\;2}} . \tag{4.21}$$

must be a minimum when $/_{\boldsymbol{q}}$ satisfies the Boltzmann equation.

In the case of N-processes dominating, the form of the trial function $/_{\boldsymbol{q}}$ is usually taken as

$$/_{\boldsymbol{q}} = \boldsymbol{q} \cdot \boldsymbol{u} \tag{4.22}$$

with $\boldsymbol{u}$ a fixed unit vector in the direction of the thermal gradient. It is easy then to see, that (4.21) has its minimum value. In fact, the numerator vanishes and (4.21) is zero, since

$$/_{\boldsymbol{q}} + /_{\boldsymbol{q}'} - /_{\boldsymbol{q}''} = (\boldsymbol{q} + \boldsymbol{q} \;\; - \boldsymbol{q} \;\;) \cdot \boldsymbol{u} \tag{4.23}$$

vanishes for N-processes (momentum is conserved) and yields infinite thermal conductivity. This is a good starting point to obtain (4.21) for U-processes, since now, (4.21) takes the value $\boldsymbol{G} \cdot \boldsymbol{u}$, with $\boldsymbol{G}$ a reciprocal lattice vector (momentum is not conserved), and in the integrand of (4.21) will only remain unknown the terms related to the scattering matrix $Q^{\boldsymbol{q}''}_{\boldsymbol{q}\boldsymbol{q}'}$, which are related to geometrical factors depending on polarization, dispersion, lattice structure, etc. This complicates considerably a practical application of this method, and it is unavoidable to make some approximations in terms of crystal properties, as suggested by Leibfried and Schlömann [60]. Another drawback, is that (4.21) yields values of as a results of the three-phonon resistive processes, therefore its application is valid in the temperature range where this scattering mechanism is dominating the transport.

4.4 Note on ab-initio methods

Recent works have focused their attention on the calculation of phonon scattering rates by *ab initio* techniques [39, 61, 82–84]. These works suggest that the main reason for the poor adjustment of current theories arises from the use of empirical potentials with adjustable parameters or the use of empirical or analytical expressions for the relaxation times. The *ab initio* method is a numerical method to find an approximate solution of the BTE by using recursive iterations, that is, we need to start with a trial form of the distribution function. This first trial function yields expressions for the scattering rates. These scattering rates expressions are used to obtain a more accurate form of the distribution function, which is

used again to obtain better expressions for the scattering rates, and so on, until a minimum of certainty in the solutions is reached. With the obtained solutions, one can calculate the thermal conductivity by using the integral expression (1.39).

The thermal conductivity of several materials has been calculated from this approach (see Ref. [85] and references therein). In these works, the theoretical predictions agree very well with experimental measurements of bulk materials in particular intervals of temperature, normally above 50 or 100K for Si and Ge, since for lower temperatures the required computational power and time is too high [39]. Therefore, the peak of the thermal conductivity is usually not shown. Furthermore, predictions for nanowires have not been able to stand comparison with experiments since they provide larger values of , according to Ref. [39]. To date, this kind of approach has not been able to obtain a single thermal conductivity solution valid at all ranges of temperatures and sample sizes. Then, a combination between analytical models and *ab initio* techniques is desirable. In this line of thought, recently, Fugallo *et al.* [84] have calculated the thermal conductivity of natural diamond and isotopically enriched diamond by solving the BTE using the variational principle and the conjugate gradient scheme. To account for the interval of low temperatures, they introduced the scattering due to boundary effects with a shape factor to fit this temperature range. The model of Fugallo *et al.* [84] is a good example where analytical and numerical methods are combined to provide results in a wide range of temperatures.

In spite of these advances, the models based on *ab initio* techniques lose some of the thermodynamic features involved in the heat transport mechanisms, hidden behind the numerical complexity of the models. At this stage, a phenomenological model is always desirable when the physical processes can be clearly described.

4.5 Guyer-Krumhansl model

Returning to the contemporaries of Callaway, we can find in the literature a parallel approach developed by Krumhansl and coworkers [86–88]. They were also motivated to offer a solution of the BTE accounting correctly for the different natures of the resistive and normal processes. Surprisingly, this model seems to have been ignored by the scientific community, maybe because of its complex formulation, and it has been mainly applied to the research of second sound, with successful results in Helium [89, 90].

In the outstanding works published by Guyer and Krumhansl in the 60's, they developed a formal solution of the linearized BTE in terms of the eigenvectors of the normal process

collision operator [87, 88]. They also provided an alternative expression for the thermal conductivity to that given by Callaway, showing that the Callaway expression (4.14) is found as a special case after some approximations. As Guyer and Krumhansl discussed in their original papers, and other contemporary authors indicated [34, 36], one of the drawbacks of the Callaway model is that normal scattering process, despite its non-resistive nature, is interpreted as a resistive contribution appearing inside the thermal conductivity integrals, and this leads, according to [88], to the inclusion of spurious terms in the equations.

The method followed by Guyer and Krumhansl was first indicated by Peierls [6, 35], who remarked the special nature of the N-processes, different to the resistive processes, and suggested to split the distribution function into different components accounting for this fact.

The formulation of Guyer and Krumhansl deals with the phonon transport problem in an operator form and assumes that the phonon distribution depends on both position and time $n(\boldsymbol{q}, \boldsymbol{r}, t)$. It is also formulated using the isotropic dispersionless approximation (Debye model). Then, the BTE is expressed as

$$\mathbf{D}n(\boldsymbol{q}, \boldsymbol{r}, t) = \mathbf{C}n(\boldsymbol{q}, \boldsymbol{r}, t) \tag{4.24}$$

where $\mathbf{D} = (\ \ / \ \ \mathbf{t}) + \mathbf{c} \cdot \ \ _{\mathbf{r}}$ is the drift operator, being $\mathbf{c}$ the mean group velocity in the Debye model, and $\mathbf{C}$ the linearized collision operator, which must account for N-processes and R-processes, then it may be split into two terms $\mathbf{C} = \mathbf{N} + \mathbf{R}$, with $\mathbf{N}$ the normal processes collision operator and $\mathbf{R}$ the resistive processes collision operator. Thus,

$$\mathbf{D}n(\boldsymbol{q}, \boldsymbol{r}, t) = (\mathbf{N} + \mathbf{R})n(\boldsymbol{q}, \boldsymbol{r}, t) \tag{4.25}$$

and when the inverse of the collision operator is known, the solution of Eq.(4.24) is

$$n(\boldsymbol{q}, \boldsymbol{r}, t) = \mathbf{C}^{-1}\mathbf{D}n(\boldsymbol{q}, \boldsymbol{r}, t) \tag{4.26}$$

Their method to solve the equations was based on collecting the lower moments on the heat flux (first-order moment), leaving only energy and heat flux as final quantities requiring specific equations. The combination of the high-order moments is made by simple matrix operations[1]. In this representation, they obtain a basis where the first terms are eigenstates with null eigenvalue and the operator corresponding to normal collisions $\mathbf{N}$ is diagonal, so

[1] It is not our intention to detail this formulation in the present work and, for the sake of simplicity, the notation has been modified and simplified. A complete mathematical picture of the operator representation can be found in Refs. [86–88]

that, in this basis, the equation

$$(\mathbf{D} - \mathbf{N} - \mathbf{R})n(\boldsymbol{q}, \boldsymbol{r}, t) = 0 \tag{4.27}$$

takes the form

$$\begin{matrix} D_{00} & D_{01} & 0 \\ D_{10} & D_{11} & D_{12} \\ 0 & D_{21} & D_{22} \end{matrix} - \begin{matrix} 0 & 0 & 0 \\ 0 & 0 & 0 \\ 0 & 0 & N_{22} \end{matrix} - \begin{matrix} 0 & 0 & 0 \\ 0 & R_{11} & R_{12} \\ 0 & R_{21} & R_{22} \end{matrix} \begin{matrix} a_0 \\ \mathbf{a}_1 \\ \mathbf{a}_2 \end{matrix} = \begin{matrix} 0 \\ 0 \\ 0 \end{matrix} \tag{4.28}$$

where a_0, $\boldsymbol{a}_1$ and $\boldsymbol{a}_2$ are the eigenvectors of $\boldsymbol{N}$, a_0 is the zero-order moment related to T, $\boldsymbol{a}_1$ is the first-order moment related to the heat flux $\boldsymbol{j}$ and $\boldsymbol{a}_2$ is the second-order moment related to the flux of the heat flux. The mean values of the operators are

$$\mathbf{D} = \begin{matrix} D_{00} & D_{01} & 0 \\ D_{10} & D_{11} & D_{12} \\ 0 & D_{21} & D_{22} \end{matrix} \qquad \begin{matrix} / \ t & \mathbf{c} \cdot \ _{\mathbf{r}} & 0 \\ \mathbf{c} \cdot \ _{\mathbf{r}} & / \ t & D_{12} \\ 0 & D_{21} & / \ t \end{matrix} \tag{4.29}$$

$$\mathbf{R} = \begin{matrix} 0 & 0 & 0 \\ 0 & R_{11} & R_{12} \\ 0 & R_{21} & R_{22} \end{matrix} \qquad \begin{matrix} 0 & 0 & 0 \\ 0 & \tau_R^{-1} & R_{12} \\ 0 & R_{21} & \tau_R^{-1} \end{matrix} \tag{4.30}$$

$$\mathbf{N} = \begin{matrix} 0 & 0 & 0 \\ 0 & 0 & 0 \\ 0 & 0 & N_{22} \end{matrix} \qquad \begin{matrix} 0 & 0 & 0 \\ 0 & 0 & 0 \\ 0 & 0 & 1/ \ \tau_N \end{matrix} \tag{4.31}$$

where the brackets stand for averaging, which is calculated generally for a i process as

$$\tau_i = \frac{\hbar\omega\tau_i(\omega)\dfrac{n^0(\omega)}{T}D(\omega)d\omega}{\hbar\omega\dfrac{n^0(\omega)}{T}D(\omega)d\omega}. \tag{4.32}$$

As it can be seen in (4.28) a_0 (scalar) is an eigenstate with zero eigenvalue either for normal and resistive scattering, while $\mathbf{a}_1 = (a_1x, a_1y, a_z)$ has zero value for normal scattering but not for resistive scattering. From (4.28) we can write the set of equations

$$\begin{aligned} D_{00}a_0 + D_{01}\boldsymbol{a}_1 &= 0 \\ -D_{11}\boldsymbol{a}_1 - D_{10}a_0 &= -R_{11}\boldsymbol{a}_1 - (R_{12} - D_{12})\boldsymbol{a}_2 \\ (N_{22} + R_{22} - D_{22})\boldsymbol{a}_2 &= -(R_{21} - D_{21})\boldsymbol{a}_1 \end{aligned} \tag{4.33}$$

where $\boldsymbol{a}_2$ can be eliminated reducing the set from three to two equations

$$\begin{aligned} D_{00}a_0 + D_{01}\boldsymbol{a}_1 &= 0 \\ -D_{11}\boldsymbol{a}_1 - D_{10}a_0 &= [R_{11} - (R_{12} - D_{12})(N_{22} + R_{22} - D_{22})^{-1}(R_{21} - D_{21})]\,\boldsymbol{a}_1 \end{aligned} \tag{4.34}$$

where the quantity in brackets is defined as the phonon momentum relaxation operator, namely

$$\hat{\tau} = \ (R_{11} - D_{11}) - (R_{21} - D_{21})(R_{22} - D_{22} + N_{22})^{-1}(R_{12} - D_{12})\ ^{-1}\ . \tag{4.35}$$

The physical identification of a_0, $\boldsymbol{a}_1$ and $\boldsymbol{a}_2$ for an isotropic dispersionless medium is found to be

$$E(\boldsymbol{x}, t) = c_v\ T(\boldsymbol{x}, t) = \frac{k_B T}{\mu} a_0 \tag{4.36}$$

and

$$\boldsymbol{j}(\boldsymbol{x}, t) = \frac{k_B T \hbar c^2}{{}_x} a_{1x} \tag{4.37}$$

and analogously for a_{1y}, a_{1z}, where μ and are renormalization constants. Identifying the terms appearing in Eqs. (4.34), we can rewrite them as

$$\begin{aligned} E/\ t + \ {}_{\boldsymbol{r}}\boldsymbol{j} &= 0 \\ \boldsymbol{j}/\ t + (\mu\hbar c^2/\ )\ E &= -(\hat{\tau}^{-1})\mathbf{j} \end{aligned} \tag{4.38}$$

and we can re-express the last equation in terms of the specific heat as

$$-\frac{1}{3}c_v c^2\ \ {}_{\mathbf{r}}T = \frac{\boldsymbol{j}}{t} + (\hat{\tau}^{-1})\boldsymbol{j}\,. \tag{4.39}$$

Actually, Eqs. (4.38) are the energy and momentum conservation equation, respectively.

Expression (4.39) assumes the introduction of hydrodynamics in phonon transport equation related to the time derivative of the heat flux, which eventually leads to the prediction of second sound, *i. e.* the propagation of variations in the distribution function according to a wave equation, which has been observed experimentally in certain materials [91].

In steady-state, the time derivatives vanish, this means $D_{11} = D_{22} =\ /\ t\ \ 0$ and $\mathbf{j}/\ \mathbf{t} = \mathbf{0}$, then

$$\hat{\tau} = \ (R_{11}) - (R_{21} - D_{21})(R_{22} + N_{22})^{-1}(R_{12} - D_{12})\ ^{-1} \tag{4.40}$$

and Eq. (4.39) reduces to the Fourier law. Furthermore, in an homogeneous medium, the spatial derivatives included in $\mathbf{D}$, namely D_{12} and D_{21} vanish, then

$$\hat{\tau} = \ (R_{11}) - (R_{21})(R_{22} + N_{22})^{-1}(R_{12})\ ^{-1} \tag{4.41}$$

whose mean value is found after identifying the matrix terms (4.30) and (4.31), but note that the terms out of the diagonal R_{12} and R_{12} are not known *a priori*. If we consider two limiting cases, when N-processes are negligible and the opposite case, with some algebra it is possible to find suitable values for R_{12} and R_{21}. Let us find $\hat{\tau}$ in both cases:

- N-processes dominate:
  Since $N_{22} = 1/\ \tau_N$, when N_{22} , $\hat{\tau}$ $(R_{11})^{-1}$, hence we make the identification $R_{11} = \ \tau_R$. So in this limit
  $$\hat{\tau} \ = \ \tau_R^{-1}{}^{\ -1} \tag{4.42}$$

- N-processes negligible:
  When N_{22} 0, $\hat{\tau}$ $[(R_{11}) - (R_{21})(R_{22})^{-1}(R_{12})]^{-1}$. This term is in fact the first term of the inverse matrix R^{-1}, that is
  $$(R^{-1})_{11} = \ (R_{11}) - (R_{21})(R_{22})^{-1}(R_{12})\ ^{-1} \ . \tag{4.43}$$
  We have $R_{11} = R_{22} = \ \tau_R^{-1}$, so we need to set $(R_{21})^2 = (R_{12})^2 = R_{11}(R_{11} - 1/(R^{-1})_{11})$ to fulfill (4.43). Then,
  $$\hat{\tau} \ = \ \tau_R \ . \tag{4.44}$$

With all of this Eq.(4.41) becomes

$$\hat{\tau} \ = \ \tau_R \ \frac{\tau_N}{\tau_R \ + \ \tau_N} + (\ \tau_R^{-1}\ )^{-1} \frac{\tau_R}{\tau_R \ + \ \tau_N} \quad . \tag{4.45}$$

This leads to the expression of the thermal conductivity

$$= \frac{1}{3} c_v c^2 \ \hat{\tau} \ = \frac{1}{3} c_v c^2 \quad \tau_R \ (1 - \quad) + (\ \tau_R^{-1}\ )^{-1} \tag{4.46}$$

where we have expressed it in terms of

$$\equiv \frac{1}{1 + \ \tau_N \ / \ \tau_R} \tag{4.47}$$

which is a factor that allows us to determine the relative importance of R-processes against N-processes and viceversa. Then, the thermal conductivity can be seen as the combination of two contributions depending on the relative importance of N-processes against R-processes and viceversa. The main difference in both contributions is in the way of performing the average over the resistive processes. Note that when R-processes dominate τ_N τ_R ,

so $= 0$, and the thermal conductivity (4.46) reduces to the well-known kinetic expression (1.26)

$$= \frac{1}{3} c_v c^2 \ \tau_R \tag{4.48}$$

In the opposite case, if N-processes dominate $\tau_N \quad \tau_R$, so $= 1$ and the thermal conductivity (4.46) reduces to the kinetic expression differing only in the averaged relaxation-time

$$= \frac{1}{3} c_v c^2 (\ \tau_R^{-1} \ )^{-1} \tag{4.49}$$

where Guyer-Krumhansl denoted $\tau_z \equiv (\ \tau_R^{-1} \ )^{-1}$. This phenomenology gives rise to what Guyer and Krumhansl named as kinetic and Ziman transport regimes, corresponding to (4.48) and (4.49) respectively, where the Ziman regime is, in fact, an hydrodynamic regime for phonons.

To account for the surface effects on the thermal transport, it is required to analyze the phonon collisions against the system boundary separately in each regime. In the kinetic regime it is included as usually through the boundary scattering τ_B in the Mathiessen rule together with the other resistive processes considered, such that

$$\tau_R^{-1} = \tau_B^{-1} + \tau_U^{-1} + \tau_I^{-1} + \dots \tag{4.50}$$

However, in the hydrodynamic regime the viscosity against the walls of the system is affecting the whole phonon flux, therefore it cannot be considered as an independent scattering mechanism included in the Matthiessen rule. Instead, it is required to add a geometrical factor G in (4.49), such that the total thermal conductivity is

$$= \frac{1}{3} c_v c^2 \, [\ \tau_R \ (1 - \quad) + \tau_z G \ \ ] \tag{4.51}$$

where the geometrical factor was calculated in particular for a cylindrical wire, depending on its radius R, and is found by solving the transport equations (4.38) at first-order in the Ziman limit imposing that the heat current is zero at the walls and then averaging the thermal conductivity across the cylinder

$$G(R) = 1 - 2 \frac{J_1(iR/ \ )}{\frac{iR}{\ } J_0(iR/ \ )} \tag{4.52}$$

where J_0 and J_1 are Bessel's functions and $= c \ \ \overline{\tau_N \tau_z}/5$ is found to be the phonon mean-free path in this limit. Note that now, the τ_R included in τ_z accounts for the resistive processes through the Mathiessen rule excluding τ_B.

This model has opened a new line of thought about phonon behavior during thermal transport. Although this is a good starting point to model the thermal conductivity accounting for the N-processes in a more rigorous way, the main drawback of the Guyer-Krumhansl model is that in Eq. (4.46) is given in terms of mean values c_v, c, τ_R and τ_R^{-1} and τ_N in the framework of a Debye model (isotropic dispersionless phonons), and nowadays, as we have already discussed, it is very helpful using actual dispersion relations to provide a more accurate description of the effect of all the modes participating in the transport, including not only acoustic branches but also optical branches. Another drawback is that Eq. (4.51) is derived for a cylindrical wire, then at the time to calculate of a given sample, we are constricted to this geometrical shape. Nevertheless, this model has motivated us, in first place, to go beyond it and find a new formulation general for any geometry and material in the macro and the nanoscale, under a full dispersion relations framework, and in second place, to make converge the preceding methods (Variational method and relaxation-time approximation model) to take advantage of the strong points of both methodologies, as will be presented in the next Section.

4.6 Kinetic-collective model: A generalization of the Guyer-Krumhansl model

In this Section we present a new model which consist on a generalization of the Guyer-Krumhansl model and goes deeper into the role normal scattering on the thermal conductivity in semiconductor bulk, micro and nanoscale samples, and which is an original contribution of the present doctoral thesis.

Thermal conductivity as a function of temperature undergoes a smooth transition from a kinetic to a collective regime that depends on the relative importance of normal scattering events as compared to resistive processes. In this transition, the key point is changing the usual way of performing the average on the scattering rates. N-processes do not contribute to thermal resistance because they do not change phonon momentum (in contrast to resistive collisions), but they contribute to heat transport and they are crucial to determine the transition from the kinetic to the collective regime.

4.6.1 Resistive vs Normal scattering

As introduced in Chapter 3, phonons can relax by different mechanisms, mainly colliding with boundaries, impurities, and between them. All these mechanisms are resistive except some part of the phonon-phonon collisions: the normal scattering processes. Under small T the deviations from equilibrium, given by the Bose-Einstein distribution $n^0_{\boldsymbol{q}}$, are expected to be small. In that case, we can expand $n_{\boldsymbol{q}}$ and keep the first term in the expansion:

$$n_{\boldsymbol{q}} \quad n^0_{\boldsymbol{q}} + \frac{n_{\boldsymbol{q}}}{\quad_{\boldsymbol{q}}} \qquad n^0_{\boldsymbol{q}} + \frac{n^0_{\boldsymbol{q}}}{\quad_{\boldsymbol{q}}} \quad_{\boldsymbol{q}} = n^0_{\boldsymbol{q}} + \frac{n^0_{\boldsymbol{q}}(n^0_{\boldsymbol{q}}+1)}{k_B T} \quad_{\boldsymbol{q}} \quad . \tag{4.53}$$

Regarding the dominance of the N-processes, two limiting behaviors can be considered:

i) When resistive collisions are dominant and N-processes are negligible, momentum will be completely dissipated and its average value is zero. The only way to move the phonon distribution from equilibrium is by changing its temperature. In that case, the distribution function takes the form

$$n_{\boldsymbol{q}} = \frac{1}{e^{\hbar\omega_{\boldsymbol{q}}/k_B(T+\delta T)} - 1} \qquad \frac{1}{e^{\hbar\omega_{\boldsymbol{q}}/k_B T} e^{1-\delta T/T} - 1}. \tag{4.54}$$

Comparing with Eq. (4.53) an expression for $\quad_{\boldsymbol{q}}$ can be obtained

$$\quad_{\boldsymbol{q}} = \hbar\omega_{\boldsymbol{q}} \frac{T}{T}. \tag{4.55}$$

In this situation KM is the most suitable approach to use.

ii) When N-processes are dominant, the system will not be able to relax the momentum to zero (the quasi-momentum is conserved) and a displacement $\boldsymbol{u}$ of the distribution function in the direction of the thermal gradient is expected. The distribution function takes the form [34, 86]

$$n_{\boldsymbol{q}} = \frac{1}{e^{(\hbar\omega_{\boldsymbol{q}} - \boldsymbol{u}\cdot\boldsymbol{q})/k_B T} - 1} \tag{4.56}$$

which is in a non-equilibrium situation, with $\quad_{\boldsymbol{q}}$ given by

$$\quad_{\boldsymbol{q}} = \boldsymbol{u}\cdot\boldsymbol{q} \quad . \tag{4.57}$$

where $\boldsymbol{u}$ has dimensions of speed (recall that energy for phonons may be expressed as the product of momentum times the phase speed). In this case the VM approach must be used, as we will see.

Summing up, Eqs. (4.55) and (4.57) are the two forms of $\quad_{\boldsymbol{q}}$ expected for the distribution function in each approximation, KM and VM respectively, corresponding to two extreme

situations described above. However, both expressions of $_{\boldsymbol{q}}$ may yield equivalent expressions for the relaxation times. In Appendix C we show that the definition of the scattering rate in terms of $_{\boldsymbol{q}}$ holds in both situations, given by the dominance of N-processes over the resistive processes and viceversa.

4.6.2 Thermal conductivity regimes

Although thermal conductivity obtained within the KM and VM seems to be disconnected, from thermodynamic reasoning we show in this Section that both can be derived from the balance of entropy production. The main difference between both approaches resides in the way this balance is performed. The reason for this choice lies in the nature of normal scattering. Entropy generation is related to resistive collisions and normal scattering is not resistive. It is logical to think that entropy production can be modified when these kind of collisions are dominant.

Starting from this point, it is easy to demonstrate that a general expression for the thermal conductivity can be obtained by combining the distribution function in these two extreme situations: the first one where resistive processes are dominant, and the second one where normal processes are dominant.

The key point to notice is that N-processes, despite of being non-resistive, mix the different modes, affecting the balance between drift and collisions. If N-processes are not important and mode mixing is low, the entropy production balance should be fulfilled individually by each mode, that is, locally in momentum space. This leads to the thermal conductivity in the *kinetic regime*. On the other hand, when mode mixing is high (N-processes dominate) the entropy balance should be achieved globally, in this case we obtain the thermal conductivity in the *collective regime*. In Fig. 4.3 we show a sketch illustrating the phonon behavior in both limiting regimes. Depending on the intensity of the normal collisions we should select the local or the global version for the entropy production balance. Next, we specify both regimes of behavior and obtain the corresponding thermal conductivity contribution.

4.6.3 Kinetic regime

The density of entropy of a distribution of bosons is, in microscopic terms,

$$\frac{s_{\boldsymbol{q}}}{k_B} = n_{\boldsymbol{q}} \ln n_{\boldsymbol{q}} - (n_{\boldsymbol{q}} - 1) \ln(n_{\boldsymbol{q}} - 1) \quad . \tag{4.58}$$

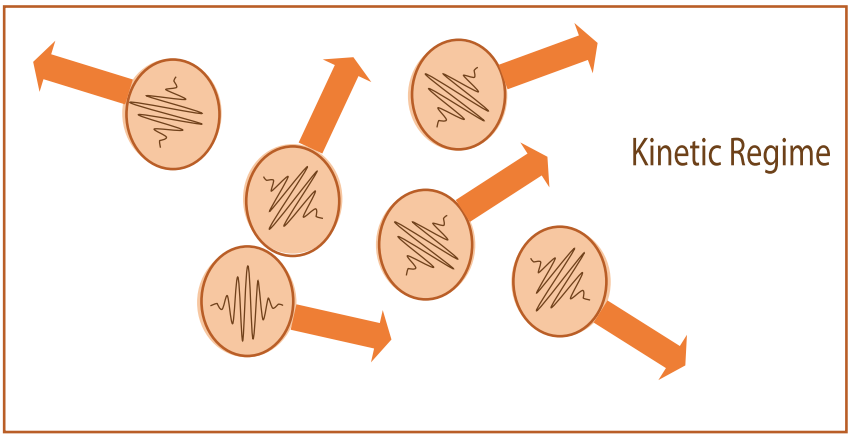

(a)

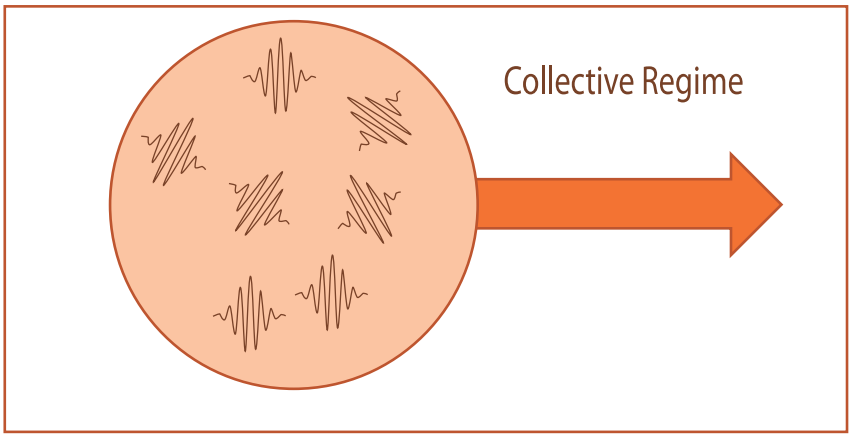

(b)

Figure 4.3: These sketches illustrate the behavior of the phonons in each regime: (a) In the kinetic regime N-processes are negligible. The phonon distribution is near equilibrium and resistive scatterings tend to bring it back to equilibrium. Each phonon mode contributes independently to the heat flux and so the equation of the entropy balance must be fulfilled individually by each mode. (b) In the collective regime N-processes dominate and the distribution is in non-equilibrium. Momentum is conserved and shared among the phononic modes through N-processes. The phonons behave as a collectivity, rising a total heat flux and so the equation of the entropy balance must be fulfilled globally.

The variation of entropy can be obtained from Eqs. (4.58) and (4.53), according to Ziman [36], if we take only linear terms in $_{\boldsymbol{q}}$ this can be written as

$$\dot{s}_{\boldsymbol{q}}|_{\text{scatt}} = \frac{s_{\boldsymbol{q}}}{t}\Big|_{\text{scatt}} = \frac{_{\boldsymbol{q}}}{T}\frac{n_{\boldsymbol{q}}}{t}\Big|_{\text{scatt}}, \tag{4.59}$$

Thermodynamically, the entropy variation can be also written in terms of the heat flux as

$$\dot{s}_{\boldsymbol{q}}|_{\text{driff}} = \frac{s_{\boldsymbol{q}}}{t}\Big|_{\text{driff}} = \boldsymbol{j}_{\boldsymbol{q}} \cdot {}_{\mathbf{r}}\frac{1}{T} = \frac{\boldsymbol{j}_{\boldsymbol{q}}^2}{_{\boldsymbol{q}}T^2} \tag{4.60}$$

where the heat flux contribution of mode $\boldsymbol{q}$ is

$$\boldsymbol{j}_{\boldsymbol{q}} = \hbar\omega_{\boldsymbol{q}}\boldsymbol{v}_{\boldsymbol{q}}(n_{\boldsymbol{q}} - n_{\boldsymbol{q}}^0) = \hbar\omega_{\boldsymbol{q}}\boldsymbol{v}_{\boldsymbol{q}}n_{\boldsymbol{q}}^0(n_{\boldsymbol{q}}^0 + 1)\frac{_{\boldsymbol{q}}}{k_B T} \tag{4.61}$$

and we have used (4.53) and the fact that the Fourier law holds per mode, that is $\boldsymbol{j}_{\boldsymbol{q}} = -\,_{\boldsymbol{q}}\,_{\mathbf{r}}T$, where $_{\boldsymbol{q}}$ is the thermal conductivity of mode $\boldsymbol{q}$.

Equating (4.60) and (4.59) leads to an expression giving the thermal conductivity of each mode

$$_{\boldsymbol{q}} = \frac{\boldsymbol{j}_{\boldsymbol{q}}^2}{T\,_{\boldsymbol{q}}\frac{\partial n_{\boldsymbol{q}}}{\partial t}\Big|_{\text{scatt}}}. \tag{4.62}$$

Integrating (4.62) over all modes yields total thermal conductivity in this kinetic regime

$$_{\text{kin}} = \int {}_{\boldsymbol{q}} d^3\boldsymbol{q} = \int \frac{\boldsymbol{j}_{\boldsymbol{q}}^2}{T\,_{\boldsymbol{q}}\frac{\partial n_{\boldsymbol{q}}}{\partial t}\Big|_{\text{scatt}}} d^3\boldsymbol{q} \tag{4.63}$$

and if we substitute Eq. (4.61) we finally obtain

$$_{\text{kin}} = \int \frac{\left(\hbar\omega_{\boldsymbol{q}}\boldsymbol{v}_{\boldsymbol{q}}n_{\boldsymbol{q}}^0(n_{\boldsymbol{q}}^0 + 1)\frac{\Phi_{\boldsymbol{q}}}{k_B T}\right)^2}{T\,_{\boldsymbol{q}}\frac{\partial n_{\boldsymbol{q}}}{\partial t}\Big|_{\text{scatt}}} d^3\boldsymbol{q} \tag{4.64}$$

4.6.4 Collective regime

In the second limiting case, phonons behave as a collectivity and each mode does not contribute to the entropy production individually but as a whole. In this case the entropy production balance should be achieved globally and the integration over the modes should be performed before equating terms. Thus, the total entropy production is on one side

$$\dot{s}_{\text{tot}}|_{\text{scatt}} = \int \dot{s}_{\boldsymbol{q}}|_{\text{scatt}}\, d^3\boldsymbol{q} = \int \frac{_{\boldsymbol{q}}}{T}\frac{n_{\boldsymbol{q}}}{t}\Big|_{\text{scatt}} d^3\boldsymbol{q} \tag{4.65}$$

and on the other side, we must account for a total heat flux, giving

$$\dot{s}_{\text{tot}}\big|_{\text{driff}} = \boldsymbol{j}_{\text{tot}} \cdot \quad {}_{\mathbf{r}} \quad \frac{1}{T} \quad . \tag{4.66}$$

Using the Fourier's law $\boldsymbol{j}_{\text{tot}} = - \quad {}_{\mathbf{r}}T$, we obtain

$$\dot{s}_{\text{tot}}\big|_{\text{driff}} = \frac{\boldsymbol{j}_{\text{tot}}^2}{T^2}. \tag{4.67}$$

being the global thermal conductivity in this regime. We denote it as $_{\text{coll}}$ and we obtain its expression by equating (4.65) and (4.67)

$$_{\text{coll}} = \frac{\boldsymbol{j}_{\text{tot}}^2}{T^2 \quad \frac{\boldsymbol{q}}{T} \frac{n_{\boldsymbol{q}}}{t}_{\text{scatt}} d^3\boldsymbol{q}} \quad , \tag{4.68}$$

where the total heat flux is

$$\boldsymbol{j}_{\text{tot}} = \quad \boldsymbol{j}_{\boldsymbol{q}} d^3\boldsymbol{q} = \quad \hbar\omega_{\boldsymbol{q}} \boldsymbol{v}_{\boldsymbol{q}} n_{\boldsymbol{q}}^0 (n_{\boldsymbol{q}}^0 + 1) \frac{\boldsymbol{q}}{T} d^3\boldsymbol{q} \quad . \tag{4.69}$$

By substituting this expression in Eq. (4.68), we have

$$_{\text{coll}} = \frac{\hbar\omega_{\boldsymbol{q}} \boldsymbol{v}_{\boldsymbol{q}} n_{\boldsymbol{q}}^0 (n_{\boldsymbol{q}}^0 + 1) \frac{\boldsymbol{q}}{k_B T} d^3\boldsymbol{q}}{T^2 \quad \frac{\boldsymbol{q}}{T} \frac{n_{\boldsymbol{q}}}{t}_{\text{scatt}} d^3\boldsymbol{q}}^{2} \quad . \tag{4.70}$$

This regime relies on a thermodynamic basis, and it can not be deduced from a framework where normal scattering is treated as a resistive mechanism of independent phonon modes, like in the Callaway model. After deriving the expression of the thermal conductivity in each regime, we need to choose a quantity allowing us to know whether we are in the local or global behavior, and in order to calculate the integrals in (4.64) and (4.70), we need to express them in terms of frequency and relaxation-times. This will be done in the next section.

4.6.5 Thermal conductivity in terms of frequency and relaxation times

We are now able to calculate the thermal conductivity from Eq. (4.64) for the kinetic regime and from Eq. (4.70) for the collective regime. In order to obtain numerical results, first we

need to express them in terms of the equilibrium distribution function and the relaxation times. Using (4.53) and (1.34) in Eq. (4.64), $_{\text{kin}}$ can be rewritten as

$$_{\text{kin}} = \quad \hbar\omega_{\boldsymbol{q}}\tau_{\boldsymbol{q}}\boldsymbol{v}_{\boldsymbol{q}}^2\frac{n_{\boldsymbol{q}}^0}{T}d^3\boldsymbol{q} \quad , \tag{4.71}$$

which is the usual expression for the thermal conductivity in the RTA (see Eq. (1.39)). (Note that, here and onward, we have omitted the sum $\sum_{\nu}$ and index ν for the phonon branch in the integrals for the sake of simplicity in the notation, but the integrals must be performed per phonon branch and the summing all the branches).

For (4.70), we can make the same substitutions to obtain

$$_{\text{coll}} = \frac{\quad_{\boldsymbol{q}}\boldsymbol{v}_{\boldsymbol{q}}\frac{n_{\boldsymbol{q}}^0}{T}d^3\boldsymbol{q}\quad^2}{\frac{\quad_{\boldsymbol{q}}^2}{\hbar\omega_{\boldsymbol{q}}}\frac{1}{\tau_{\boldsymbol{q}}}\frac{n_{\boldsymbol{q}}^0}{T}d^3\boldsymbol{q}} \quad . \tag{4.72}$$

The integrals $_{\text{kin}}$ and $_{\text{coll}}$ can be re-expressed in terms of frequency. This is done by integrating over the angular part of $d^3\boldsymbol{q} \equiv dqd, d$ and changing the integration variable $dq \quad D_\omega d\omega$, being D_ω the density of states. For the kinetic regime this leads to the expression

$$_{\text{kin}} = \frac{1}{3} \quad \hbar\omega\tau_\omega v_\omega^2\frac{n_\omega^0}{T}D_\omega d\omega \quad , \tag{4.73}$$

where now the frequency dependence is indicated with the subindex to not overload the notation, and for the collective regime

$$_{\text{coll}} = \frac{1}{3}\frac{\quad v_\omega q_\omega\frac{n_\omega^0}{T}D_\omega d\omega\quad^2}{\frac{q_\omega^2}{\hbar\omega}\frac{1}{\tau_\omega}\frac{n_\omega^0}{T}D_\omega d\omega} \quad , \tag{4.74}$$

where we have used the explicit form (4.57) to express $_{\boldsymbol{q}}$ in terms of the wavevector q_ω, which is the mean modulus of the wavevector for a given frequency, obtained from the dispersion relations.

As we have already pointed out, in both expressions (4.73) and (4.74) τ_ω is the same and accounts for the total relaxation time contributing to thermal resistance (the treatment of the boundary scattering in each regime will be detailed in the next Section). Then, we denominate it τ_{R_ω}. Finally, we need a quantity which accounts for the kind of regime the

phonon distribution is undergoing at the different temperatures. As we have commented, this is determined by the degree of mixing between modes. Since this is related to the dominance of normal with respect to resistive processes, a switching factor weighting the relative importance of these processes should be used. This factor can be calculated from a matrix representation following the Guyer-Krumhansl model [88] and turns out to be (4.47)

$$\equiv \frac{1}{1+\ \tau_N\ /\ \tau_R} \tag{4.75}$$

where τ_N is the relaxation time due to N-processes and τ_R is the relaxation time due to resistive processes. Both relaxation times τ_N and τ_R are averaged over all modes. This is calculated as

$$\tau_i \ = \frac{\hbar\omega\tau_{i_\omega}\dfrac{n^0_\omega}{T}D_\omega d\omega}{\hbar\omega\dfrac{n^0_\omega}{T}D_\omega d\omega} \tag{4.76}$$

with subindex i indicating N or R. Note that this is not an average over the phonon population n^0_ω, but rather on the energy exchanged in the collisions.

The general expression of the thermal conductivity must include this switching factor to account for all the intermediate regimes between the limiting regimes from kinetic to collective. Thus, according to (4.46) one has

$$= \ _{\text{kin}}(1- \ \ ) + \ _{\text{coll}} \tag{4.77}$$

In the kinetic (unmixed-mode) limit, $\tau_N >> \tau_R$, then 0 and $_{\text{kin}}$. In the collective (mixed-mode) limit, $\tau_N << \tau_R$, 1 and $_{\text{coll}}$, as it should be.

Different phenomenological behavior can be deduced from the mathematical difference in performing the averages in (4.73) and (4.74). These differences are equivalent to adding resistivities in series or parallel, if we interpret the scattering events on a particular mode as a resistance. This can give physical insight to interpret the thermal conductivity behavior in the different regimes. From Eq. (4.77) it can be understood why all models based on a single approach (KM or VM) fail when extended to a global model in a large range of temperatures. In such extension, they are used in an approximation where they are not supposed to be valid, in other words, since there are certain ranges of temperature where one approach is more suitable than the other, we cannot use only one approach to describe the behavior of in the whole range of temperatures. With (4.77), this fact is overcome thanks to the combination of both approaches. This way the applicability of the model is extended to the whole temperature range.

Another aspect we need to remark is the way to account for the phonon collisions against the system boundaries in both regimes. Let us discuss it next.

4.6.6 Size-effects on the kinetic and collective terms

In an infinite semiconductor sample at near room temperature one can consider that only impurities scattering and umklapp scattering participate significantly, then by means of the Matthiessen's rule

$$\tau_{R_\omega}^{-1} = \tau_{I_\omega}^{-1} + \tau_{U_\omega}^{-1} \quad . \tag{4.78}$$

Relaxation times allow to calculate a related term, the phonon mean free path , that is the product between the relaxation time of a mode and its group velocity $= v\tau$. If the size of the system is finite and the temperature is low, intrinsic mean free paths can be larger than the size of the system. In this case, boundary effects need to be included.

In the kinetic regime of the thermal conductivity, as the phonons behave individually, each mode experiences independently a scattering with the boundary. Then, an extra term considering this effect should be included in the kinetic term of Eq. (4.77) by using the Matthiessen's rule in combination with the intrinsic events, this is τ_{B_ω} the relaxation time due to boundary scattering

$$\tau_{R_\omega}^{-1} = \tau_{I_\omega}^{-1} + \tau_{U_\omega}^{-1} + \tau_{B_\omega}^{-1} \quad . \tag{4.79}$$

However, in the collective regime some caution has to be taken. In this regime a scattering rate is a quantity describing the distribution globally. In other words, one cannot assume an extra scattering term in each mode independently because the boundary is noticed by the whole phonon collectivity. Thermodynamically, this is the same situation as flow on a pipe. Carriers in the center of the pipe notice the boundary not by themselves but through the collisions with the rest of the particles. The net effect on the flow is the reduction of the flow on the surface. The usual solution for this situation is to assume that the flow on the surface is zero. This is feasible if surfaces are rough enough. Once imposed this extra assumption, a geometrical factor F (also called form factor) depending on the roughness and the transversal size of the system should be included in the collective term of Eq. (4.77). In the work by Guyer and Krumhansl [88] their form factor was calculated only for a system of cylindrical shape. In order to generalize the form factor to account for several geometries and so extend the range of validity of the collective term from bulk to small size samples, it is suitable to use an expression derived in a work by Alvarez *et al.* [92, 93] in the framework of the Extended

Irreversible Thermodynamics [78]

$$F(L_{\text{eff}}) = \frac{1}{2\pi^2}\frac{L_{\text{eff}}^2}{\ ^2} \qquad \overline{1 + 4\pi^2 \frac{\ ^2}{L_{\text{eff}}^2}} - 1 \tag{4.80}$$

being the phonon mean free path and L_{eff} the effective transversal length of the system. By geometrical considerations it can be deduced according to [12,36] (see Sec. 3.2.3). Regarding the mean free path, from the works by Alvarez *et al.* [14] and Guyer-Krumhansl [88] it can be easily deduced that $= v_g \quad \overline{\tau_N \quad \tau_R^{-1}}^{\ -1}$, reminding that mean relaxation times are calculated from Eq. (4.76).

The form factor $F(L_{\text{eff}})$ includes in its derivation higher-order terms into the BTE expansion, which can be important when the size of the samples are of the order of the phonon mean free path, and it has some advantages: it is analytical, it can be used for different geometries and it takes automatically into consideration the degree of non-equilibrium present in the sample, depending on the normal and resistive relaxation times. Further details can be found in Appendix B.

4.6.7 Total thermal conductivity in the Kinetic-Collective Model: a simple expression

Finally, the general expression of the thermal conductivity in the Kinetic-Collective model can be written as follows

$$= \ _{\text{kin}}(1 - \ ) + \ _{\text{coll}} \ F(L_{\text{eff}}) \tag{4.81}$$

entering Eq. (4.73) for $_{\text{kin}}$, Eq. (4.74) for $_{\text{coll}}$, Eq. (4.75) for , and Eq. (4.80) for $F(L_{\text{eff}})$. Note that if $/L_{\text{eff}} \quad 0$ (L_{eff}), then $F(L_{\text{eff}}) \quad 1$ and we recover Eq. (4.77). In the opposite limit, $/L_{\text{eff}}$ (L_{eff}), $F \quad L_{\text{eff}}/\pi \quad 0$. Note, that although we have followed a different way to derive the integral expressions of the thermal conductivity in each regime, the final equation can be seen as the generalization of the Guyer-krumhansl equation (4.46), valid any geometry, from the low to the high temperature range, in a realistic frame of phonon dispersion.

With this and using the calculated dispersion relations and density of states (see Chap. 2), and appropriate expressions for the relaxation times (obtained in Chap. 3), the model is ready to be applied to several samples in order to test its validity and its prediction power, which follows in the next Chapters.

4.7 Kinetic-Collective vs. Ballistic-Diffusive transport

As a last remark, it is worthy to note that, in the literature, the common way of discussing phonon transport is to differentiate between diffusive and ballistic transport. For example, transport in an infinite bulk system is always diffusive, while nanostructuring leads to the possibility of ballistic transport. This is because these regimes depend on the dominance of boundary scattering over the remaining scattering mechanisms. In contrast, in the kinetic-collective approach, the transport regime depends on the dominance of normal processes over resistive processes. Therefore, both descriptions are not mutually contradictory. That is, diffuse transport can be kinetic or collective, for instance, in the temperature interval where the thermal conductivity shows a peak, mass-defect scattering is the dominant process, and since it is a resistive process, we could describe the heat transport as diffusive-kinetic. On the other hand, at the temperature interval where the normal processes begin to participate in the transport, we could speak about a transition to a diffusive-collective regime. Similarly, the ballistic regime can be kinetic or collective. Since in the ballistic transport we are restricted to the range of low temperatures where the boundaries of the system shape the thermal conductivity, we would have a ballistic-kinetic regime. However, there is a special case observed in certain systems where normal processes gain importance over boundary collisions. It is then said that we are dealing with a Poiseuille phonon flow, and therefore we could also have a ballistic-collective regime.

Chapter 5

Applying the Kinetic-Collective model to silicon

In this Chapter, the Kinetic-Collective model is applied to calculate the thermal conductivity of silicon as a reference material, in order to test the validity of the model. Firstly, the model is tested on bulk Si with the natural isotopic composition, obtaining a very nice fit to experimental data. Then, with the same parameters, we predict the thermal behavior of an isotopically enriched Si sample to account for the effect of the mass-defect scattering on thermal conductivity. Finally, in order to account for size-effects, we calculate the thermal conductivity of several Si thin-films and nanowires whose effective sizes range from some microns to some tenths of nanometers. The model provides a good prediction of the thermal conductivity behavior with temperature for effective sizes above 30 nm with the same single expression. From the good agreement with experimental data obtained with the kinetic-collective model in nanometer sized samples, we can confirm that the model permits to establish the limit of classical theories in the study of the thermal conductivity in nanoscopic systems.

5.1 Inputs for the calculations

When calculating thermal properties of a material, it is desirable to simplify the theoretical expressions to get the maximum information in terms of the less number of variables. One of these simplifications is to assume isotropy. A medium is considered isotropic if the properties of the crystal do not depend on a certain crystallographic direction. In the case of Si, and other materials with the same lattice structure, the phase or group velocities are not so

anisotropic, and so it is usually to be considered isotropic. Although, as has been shown by Li *et al.* [39], there is little difference in the thermal conductivity of bulk Si along the crystallographic directions [100] and [001], if we assume isotropy, we may loose information and accuracy hidden in the properties depending on the phonon frequency. Since we are using in our calculation the Bond-charge model which accurately fit the dispersion relations in the whole Brillouin zone (see Chap. 2), we will take into account the existing anisotropy of a cubic material. Nevertheless, the assumption of an isotropic model would give a thermal resistivity of the same order of magnitude than that calculated by our model, specially in bulk, but in thin-films it has been seen that there is a difference of the 15% between results provided by both approaches, being more accurate the anisotropic model when comparing the results with experimental data [94].

In addition, we have opted for using the dispersion relations in the whole Brillouin zone rather than chose a certain direction, since we aim to reproduce experimental data on several samples (not only silicon samples in this Chapter, but also germanium, diamond and gray-tin samples in the following Chapter), where not always the direction of the crystal growth is specified, and this way, we can take into account the participation of each phonon branch (LA, TA1, TA2, LO, TO1 and TO2) in the thermal conductivity, as an average over the whole Brillouin zone. Moreover, this procedure is appropriate to study the implication of the whole phonon spectrum in the entire BZ, not in a single direction, in the heat transport, as we will see in the next Sections. This procedure has already been checked by Sellan et al. [94], who showed that using the dispersion relations of the full Brillouin zone, provides a more accurate description of all the modes participating in the transport, despite of being more time-consuming in the calculations. Group velocities $v(\omega_\nu)$ are always calculated from dispersion relations.

Once we have the dispersion relations and density of states, we keep them fixed when we change the size of the samples, so we can check the validity of bulk properties from bulk-size samples down to a certain effective size in the nanoscale, before quantum phenomenology appears.

Regarding the relaxation times, we use expressions (3.37), (3.38), (3.49) and (3.51) for τ_N, τ_U, τ_I and τ_B, respectively, which were introduced and discussed in Chap. 3, and here we summarize them in Table 5.1.

To calculate the thermal conductivity, we enter the dispersion relations, density of states, group velocities and relaxation times in the kinetic-collective equation (4.81), where the kinetic $_{\text{kin}}$ and the collective $_{\text{coll}}$ contributions are given by Eqs. (4.73) and (4.74) respectively; Eq.

Table 5.1: Relaxation times for non-resistive and resistive scattering processes. $_N$ and $_U$ are original contributions of the present thesis, while $_I$ and $_B$ are widely used in the literature. (See Chap. 3)

Non-resistive	**Expression**
Normal	$\tau_N(\omega_\nu) = \dfrac{1}{B_N T^3 \omega_\nu^2 [1 - \exp(-3T/\ _D)]} + \dfrac{1}{B_{N'} T}$

Resistive	**Expression**
Impurity	$\tau_I(\omega_\nu) = \dfrac{6}{\pi} \left(V \Gamma \omega_\nu^2 D(\omega_\nu) \right)^{-1}$
Umklapp	$\tau_U(\omega_\nu) = \dfrac{\exp(\ _U/T)}{B_U \omega_\nu^4 T [1 - \exp(-3T/\ _D)]}$
Boundary	$\tau_B(\omega_\nu) = L_{\text{eff}}/v(\omega_\nu)$

(4.75) is used for the switching factor and (4.80) for the form factor.

In Table 5.2 we detail the characteristics of the silicon samples used in this study: Two bulk samples with different isotopic composition but identical shape and size, these are natural occurring silicon ^{na}Si with composition (92.2%^{28}Si, 4.7%^{29}Si, 3.1%^{30}Si) and isotopically enriched silicon ^{iso}Si with composition (99.983%^{28}Si, 0.014%^{29}Si, 0.003%^{30}Si) from Ref. [65]. The other silicon samples, thin-films (TFs) and nanowires (NWs), have natural composition, but different shape and sizes.

5.2 Silicon thermal conductivity

In the following, we compare our calculations with the experimental data on the specified silicon samples in a large temperature interval $[1 - 1000]$K. The selected samples are chosen regarding their diversity of sizes, geometries and isotopic composition to account for both the

Table 5.2: Values of several properties for naturally occurring and for isotopically enriched Si bulk samples (^{na}Si and ^{iso}Si) and several thin-films (TFs) and nanowires (NWs): Γ is the mass-fluctuation calculated according to Eq.(3.48), the dimension of the cross-section is specified in each case (cross-section A for bulk, thickness h for TFs, diameter d for NWs) and the corresponding effective size L_{eff} calculated according to Sec.3.2.3. The samples and their corresponding thermal conductivity data are those from the indicated reference.

Sample	$\Gamma(\quad 10^{-5})$	Dimensions	L_{eff}	Reference
^{na}Si bulk	20.01	$A = 2.00 \quad 3.12\mathrm{mm}^2$	2.8mm	[65][1]
^{iso}Si bulk	$3.2 \quad 10^{-2}$	$A = 2.00 \quad 3.12\mathrm{mm}^2$	2.8mm	[65][2]
1.6μm TF	20.01	$h = 1.6\mu$m	3.6μm	[71]
830 nm TF	20.01	$h = 830$nm	1.87μm	[71]
420nm TF	20.01	$h = 420$nm	945nm	[71]
100nm TF	20.01	$h = 100$nm	225nm	[71]
30nm TF	20.01	$h = 30$nm	67.5nm	[71]
115nm NW	20.01	$d = 115$nm	115 nm	[8]
56nm NW	20.01	$d = 56$nm	56 nm	[8]
37nm NW	20.01	$d = 37$nm	37 nm	[8]
22nm NW	20.01	$d = 22$nm	22 nm	[8]

[1,2] Data courtesy of A. Inyushkin.

size-effects and the effect of isotopic disorder on the thermal conductivity. As a consequence of the obtained results, we discuss some novel aspects of phonon transport involving normal processes.

5.2.1 Bulk thermal conductivity: Kinetic and collective behavior

The first step is to calculate the thermal conductivity of bulk silicon with natural occurring isotopic composition ^{na}Si (see Table 5.2) and find suitable values for the only three adjustable parameters $B_N, B_{N'}$ and B_U, belonging to τ_N and τ_U (see Table 5.1), that provide the best fit to the experimental data (reminding that the remaining scattering rates τ_I and τ_B do not have adjustable parameters). The found values are shown in Table 5.3. The resulting thermal conductivity is shown in Fig. 5.1 in black dashed-line and compared to data (black symbols) from the work by Inyushkin *et al.* [65]. The agreement with data is very successful.

In Fig. 5.1 we also show the limiting curves corresponding to the pure kinetic $_{\text{kin}}$ (red dash-dot line) and pure collective regime $_{\text{coll}}$ (green dashed-line) for ^{na}Si according to Eqs. (4.73) and (4.74) respectively. It can be seen that in the low-temperature range the thermal conductivity is in the pure kinetic regime, since boundary scattering is expected to be the dominant process. As the temperature rises, N-processes begin to occur and gain importance against the resistive processes, so begins to separate from the pure kinetic regime and experiences a smooth transition towards the collective regime.

It is worthy to point out that, although both limits $_{\text{kin}}$ and $_{\text{coll}}$ contain only resistive terms in their integrals through τ_R, the thermal conductivity of the pure collective regime $_{\text{coll}}$ (see green line in Fig. 5.1) is significantly lower than the thermal conductivity of the pure kinetic regime $_{\text{kin}}$ (see red dashed-line in Fig. 5.1). This seems to be in contradiction with the fact that $_{\text{coll}}$ is governed by N-scatterings which have a non-resistive nature. Actually, the ability of N-processes at distributing the energy between modes enhances the resistive nature of the rest of the scattering mechanisms. In other words, the N-processes make sure that the presence of resistive collisions is noticed by all the modes of the collectivity by bringing about exchanges of energy between the modes. Therefore the thermal resistance increases, or inversely, the thermal conductivity decreases. This physics can be explained thanks to the different mathematical treatment of the relaxation times inside the integrals, interpreted in terms of serial and parallel resistivities in Sec. 4.6.5. Our model allows us to understand this unlike Callaway model and its derivatives, where normal scattering is considered inside the resistive integrals.

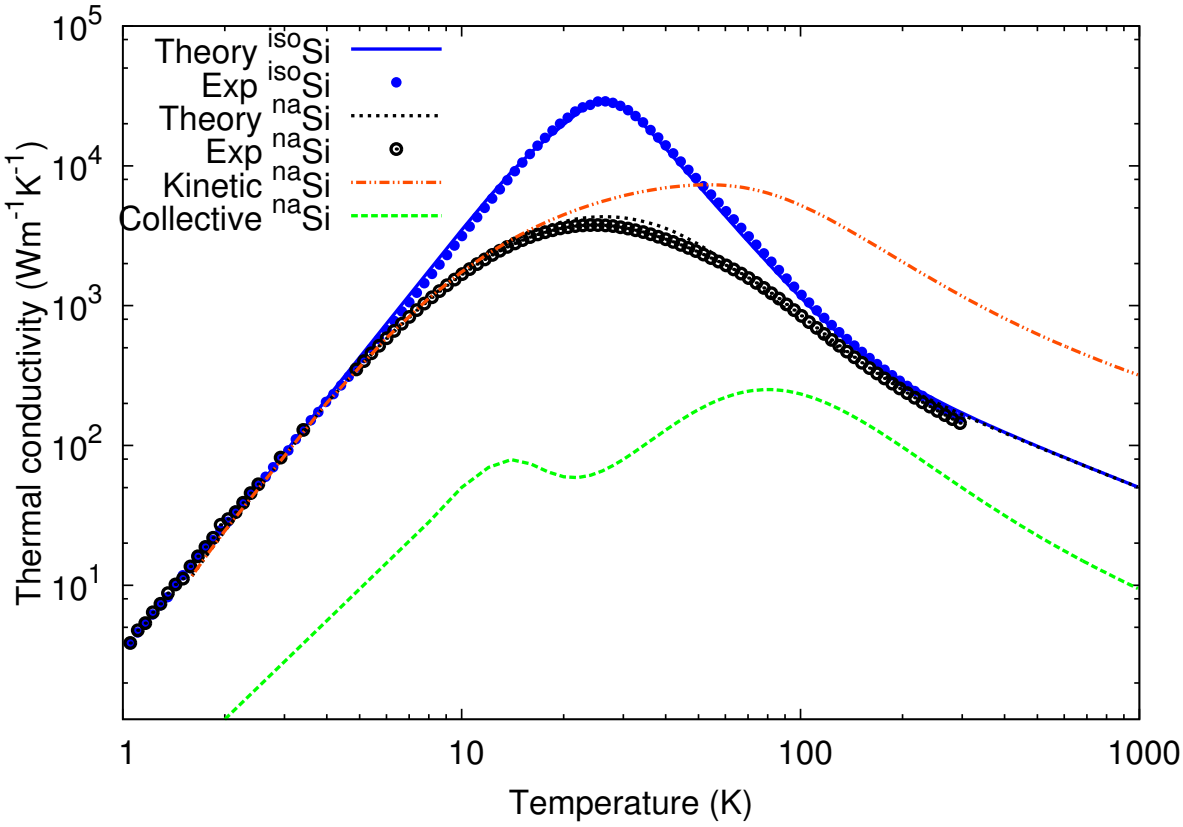

Figure 5.1: Total thermal conductivity as a function of temperature in a double logarithmic plot for $^{\mathrm{na}}Si$ *as a result of fitting Eq. (4.81) to experimental data from Inyushkin* et al. *[65], with fitting parameters shown in Table 5.3, and the prediction for* $^{\mathrm{iso}}Si$ *using the same parameters, onlychanging the mass-fluctuation factor. Pure kinetic* $_{\mathrm{kin}}$ *(4.73) and collective* $_{\mathrm{coll}}$ *(4.74) thermal conductivity regimes for* $^{\mathrm{na}}Si$ *are also plotted in dashed-lines.*

Table 5.3: Best-fit parameters for ^{na}*Si bulk.*

	B_U (s^{3}K^{-1})		B_N (sK^{-3})		B_N (s^{-1}K^{-1})	
Kinetic-collective model	2.8	10^{-46}	3.9	10^{-23}	4.0	10^{8}

Another remarkable behavior is the important presence of N-processes even at room temperature. One can expect Umklapp processes to dominate at high temperatures, but it can be seen that is not the case of bulk silicon at room temperature. It can be observed in Fig. 5.1, that the curves seem to suggest a change in the tendency at high temperatures. seems to tend to a more kinetic behavior at very high temperature. The temperature range where kinetic regime happens at high temperature will depend on the height of the dispersion relations that eventually determines the importance of Umklapp respect to normal scattering.

5.2.2 Predicting the effect of the isotopic composition on the thermal conductivity

In the work by Inyushkin *et al.* [65], two identical samples of silicon with natural composition were built in the shape of bars with square cross-section of the order of millimeters (see Table 5.3). One of the samples was isotopically enriched (^{iso}Si), and their respective mass-fluctuation factors were calculated using Eq. (3.48) and yield $\Gamma_{^{\mathrm{iso}}\mathrm{Si}} = \Gamma_{^{\mathrm{na}}\mathrm{Si}}/625$ (see Table 5.2). The thermal conductivity measurements on both samples show that their only difference is the peak, consequence of the dominating impurity scattering in this region, as can be seen in Fig. 3.8 (a) and Fig.5.1. Therefore, according to Inyushkin *et al.*, the thermal conductivity of ^{iso}Si should be predicted from the thermal conductivity of ^{na}Si by only changing the value of Γ. We have done this test with our model. Once we have fitted the bulk ^{na}Si, we recalculate introducing the corresponding value of Γ for ^{iso}Si (see Table 5.2). The result is shown in Fig. 5.1 (blue solid line). Note that the position of the peak for ^{na}Si is correctly fitted and for ^{iso}Si is correctly predicted (solid lines overlap experimental points in the plot) being the only change between both samples the calculated mass-fluctuation factor. This is a check of the consistency of our model and confirms the prediction given by Inyushkin *et al.* [65]. In the following section we have done the same test for Callaway and standard RTA models, obtaining worse results (see Fig. 5.7 in Sec. 6.3.2).

5.2.3 Predicting the effect of shape and size on the thermal conductivity: Thin-films and Nanowires

The TFs are those from the work by Asheghi *et al.* [71], with thicknesses and other characteristics reported in Table 5.2. Their respective effective lengths L_{eff} are calculated as explained in Sec. 3.2.3. Results for silicon TFs thermal conductivity are shown in Figs. 5.2 (a). Note that the calculations are the same as those performed for ^{na}Si bulk, without incorporating any further additional fitting parameter, only introducing the corresponding effective size for each sample.

Note also that all these samples may contain a certain concentration of gold impurities due to the fabrication process, according to [71], but we have kept the mass-fluctuation factor corresponding to the natural isotopic composition $\Gamma_{^{\text{na}}\text{Si}}$ for all the samples because there is no reported data to calculate Γ more accurately. Note also that at low temperatures the experimental data seem quite spread, this may indicate that some surface features (for instance roughness or back-scattering) are affecting the measures and should be taken into account in the theoretical modeling, however, no error bars are provided, and no additional information on the surface is given. Then, we focus here on the general trend of . Despite of this and the fact that a more precise value of Γ could improve the predictions, the resulting thermal conductivity of this set of TFs, with several thicknesses ranging from the micro to the nanoscale, is in overall good agreement with the experimental data. Our results also provide valuable information on the behavior of at low and high temperatures, where there is a lack of experimental measures, especially for the smallest samples (100 nm TF and 30 nm TF).

The NWs are those from the work by Li *et al.* [8], with diameters and other characteristics reported in Table 5.2. The samples are grown in the shape of cylinders using the VLS deposition technique, which assures to obtain a surface as smooth as possible [95]. Again, the NWs samples only differ from ^{na}Si bulk in the geometry and size, which are taken into account through L_{eff}, the other parameters remain the same as in the case of ^{na}Si bulk. In the case of cylindrical geometry, L_{eff} is equivalent to the diameter of the cylinder. The resulting thermal conductivities of this set of silicon NWs are shown in Fig. 5.2 (b). It can be observed that all curves are in good agreement with the experimental data with the exception of the thinnest NW (22 nm) and in some intermediate temperature region for the 37 nm NW, where bulk properties, mainly those arising from the bulk dispersion relations, may not be enough to describe the thermal transport at such small scale, and quantum effects should be taken into account to refine the predictions.

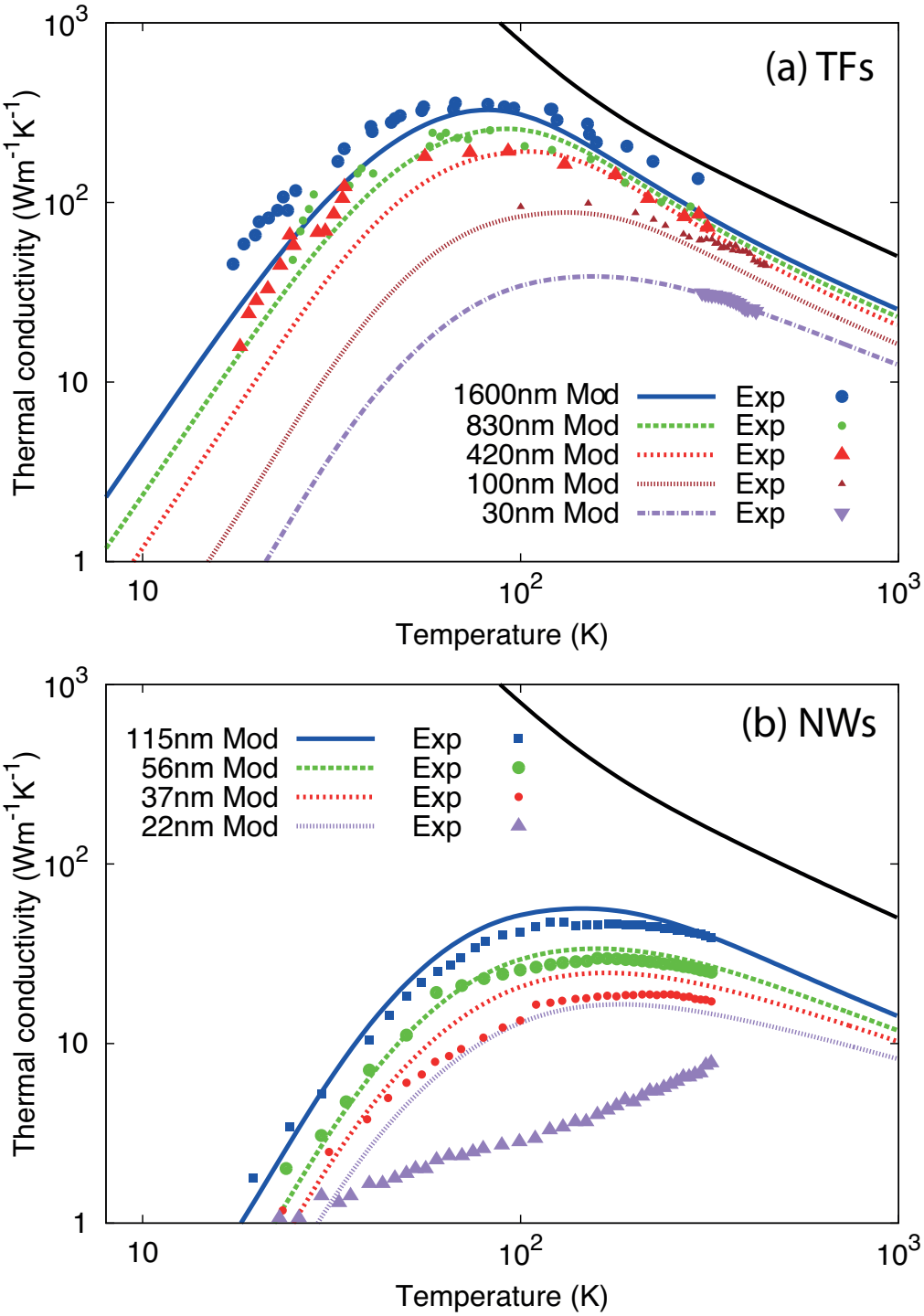

Figure 5.2: Thermal conductivity as a function of temperature in a double logarithmic plot of (a) Si TFs with several thicknesses and (b) several diameter Si NWs. In both plots, model predictions are shown in lines and experimental data are shown in symbols according to the legend; in addition the ^{na}*Si bulk thermal conductivity is plotted for reference (black solid line). Experimental data is extracted from [71] for TFs and from [8] for NWs .*

From the plots we can deduce that Eq. (4.81) is able to correctly describe thermal conductivity behavior for general geometries and sizes without the inclusion of quantum phenomenology above a certain threshold in the effective size, approximately L_{eff} >30 nm. Note that the thermal conductivity of the smallest TFs, 100nm and 30nm, is bigger than the thermal conductivity of the 115nm and 37nm NWs, because the L_{eff} of the thin-film is bigger of that of the nanowire (see Table 5.2), in other words, L_{eff}(30nmTF) = 67.5 nm is above the threshold and so it is correctly predicted. Then, for TFs quantum phenomenology is expected to appear for much thinner layers, probably below 15 nm.

5.2.4 Transition from the kinetic to the collective regime:

The smooth transition from one regime to another is determined by , shown in Fig. 5.3. In general, at very low temperatures, the boundary scattering present in τ_R is the dominant process, then we have τ_R τ_B τ_N and yields $= 0$, we are clearly in the kinetic regime $=$ $_{\text{kin}}$. For bulk samples at room temperature, we can easily calculate the ratio of τ_N/τ_U (neglecting the boundary and the impurity scattering mechanisms) and realize that it is of the order of 0.1, thus 1 (actually $= 0.9$) and we are in the collective regime, $_{\text{coll}}$. It can be observed in Fig. 5.3 that for ^{iso}Si the transition to the collective regime is sharper than for ^{na}Si. This is due to the fact that, for the bulk samples, the transition happens in the region of impurity scattering dominance, between 20 K and 100 K, because the probability of N-processes taking place increases as the temperature of the system raises.

This picture changes remarkably when the scale of the samples is shrunk and the size-effect begins to be the main cause of the drastic thermal conductivity reduction. It can be observed in Fig. 5.3, that the smaller the effective size of the sample is, the more kinetic the thermal conductivity becomes. This is reasonable and expected, since at small sizes, boundary scattering should contribute the most at thermal resistance, not only at low temperatures, but also up to room temperatures. Actually, $[0.4-0.5]$ for the 115 nm NW in the interval of temperatures [100-1000] K. In particular, $= 0.46$ at $T = 300$ K, which means that at room temperature the 46% of the total thermal conductivity belongs to the collective regime and the 54% to the kinetic regime. Both limits are shown in Fig.5.4.

5.2.5 Size-effects in the collective regime: $F(L_{\text{eff}})$

The size-effects in the collective regime are taken into account through the geometric factor $F(L_{\text{eff}})$ (see Eq.(4.80)), which depends on the effective size of the sample L_{eff}, or more precisely,

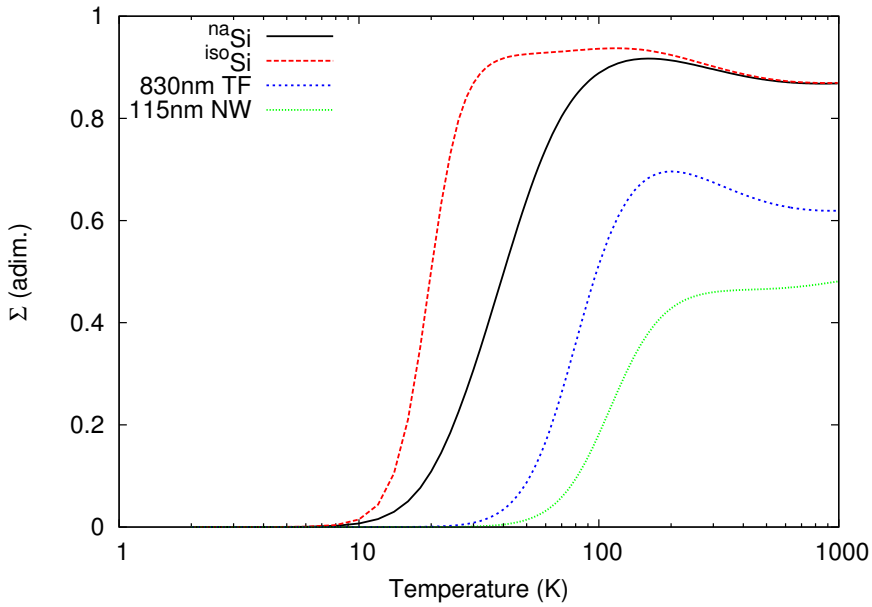

Figure 5.3: Switching factor Σ as a function of temperature in a semilogarithmic plot for $^{\mathrm{na}}Si$ *and* $^{\mathrm{iso}}Si$ *bulk, 830 nm TF and 115 nm NW.*

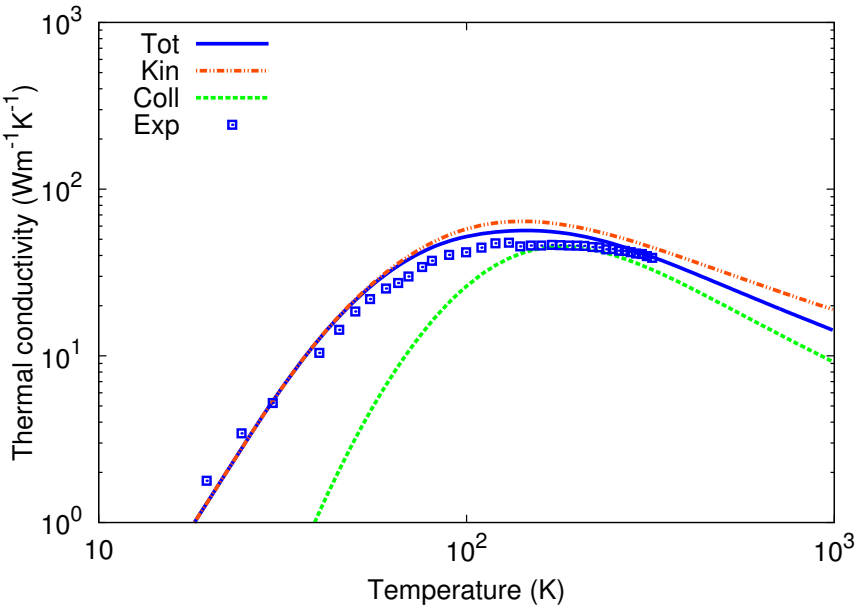

Figure 5.4: Predicted thermal conductivity as a function of temperature in a double logarithmic plot for the 115 nm NW (blue line) compared with experimental data from [8]. The pure kinetic $_{\mathrm{kin}}$ *and the collective* $_{\mathrm{coll}}$ *regimes are shown in red and green dashed-lines, respectively.*

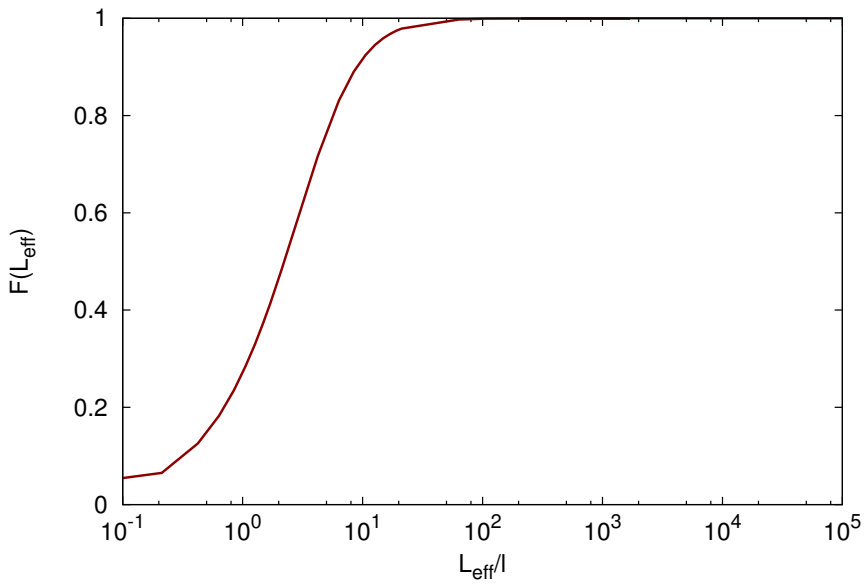

(a)

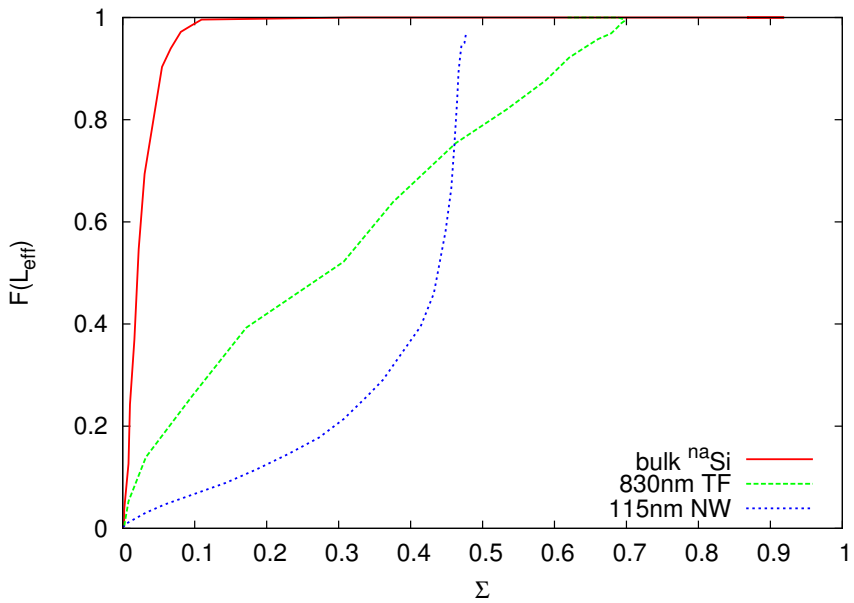

(b)

Figure 5.5: Size-effects in the collective flux: (b) Geometric factor $F(L_{\text{eff}})$ as a function of the inverse of the Knudsen number $L_{\text{eff}}/$ at T=300 K. (b) Geometric factor $F(L_{\text{eff}})$ vs switching factor Σ for three representative samples (bulk ^{na}Si, 830nm TF and 115nm NW).

on the Knudsen number $/L_{\text{eff}}$, and the temperature. $F(L_{\text{eff}})$ is required in the collective regime of Eq. (4.77), as explained in Sec.4.6.6, to account for surface effects and the geometry of the system due to hydrodynamics considerations. In the collective regime, the heat flux only feels the crystal boundaries in a region near the surface, but normal collisions allow that the inner flow also notices the surface. As a result, there is a hydrodynamic profile similar to the Poiseuille flow depending strongly on the effective size of the system. This can be observed in Fig. 5.5 (a), where we have plotted the behavior of $F(L_{\text{eff}})$ with $/L_{\text{eff}}$ at room temperature. As it can be observed in the plot, when the phonon mean-free path is much larger than the effective length of the sample, we have $F(L_{\text{eff}})$ 0. In this situation, if the size of the sample were small enough to give L_{eff} even when normal scattering is dominating the transport, the collective regime would be suppressed. However, this happens at small enough effective sizes, such as L_{eff} <30 nm, where quantum confinement is expected to appear [77]. In that case, the model should be modified to account for such quantum effects. The special case of materials with quantized transverse direction, like graphene, can be considered as 2-dimensional bulk systems with in-plane heat propagation, then L_{eff} should not be calculated with the thickness of the film, but with the width of the in-plane layer. On the other hand, when L_{eff} we have $F(L_{\text{eff}}) = 1$, this means that either the sample is very big, for instance bulk, or the temperature is high enough and the collective phonon flux does not feel the walls. From the plot we can see this happens for $L_{\text{eff}}/ > 10^2$ at room temperature.Nevertheless, the effect of $F(L_{\text{eff}})$ in the collective regime is observable as long as 1, since for 0 we are in a kinetic regime $_{\text{kin}}$, and both a negligible and non-negligible value of $F(L_{\text{eff}})$ would not be appreciated, *i. e.* $_{\text{coll}}$ is suppressed by 0, and therefore, this feature does not mask the final thermal conductivity. This can be seen in Fig. 5.5 (b), where we show $F(L_{\text{eff}})$ vs for bulk, 830nm TF and 115nm NW. Note that for the bulk $F(L_{\text{eff}}) = 1$ very quick, while for the NW never reaches this value, since viscosity against the walls is expected to play an important role at such reduced sizes

5.2.6 Global overview of the thermal conductivity

In Fig. 5.6 we show the global prediction achieved by our model; with this plot one can notice in a single view how the thermal conductivity works for the complete set of different size, shape and composition Si samples in the [1-1000]K temperature interval.

Obviously, our phenomenological expressions for the relaxation times cannot be used to obtain an extremely accurate fit. Further improvements of the model can be achieved by a

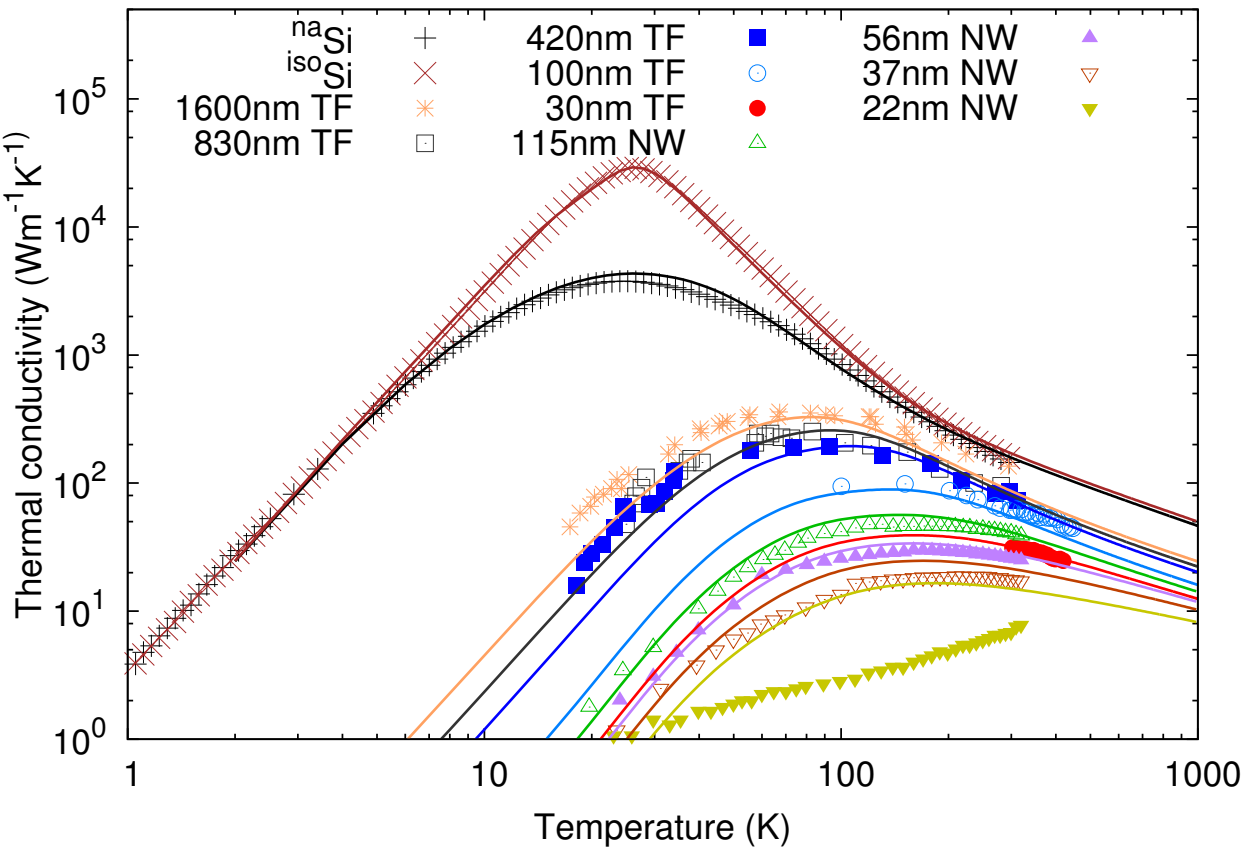

Figure 5.6: Thermal conductivity of all the silicon samples studied in this work (Bulk, thin films and nanowires). It can be seen that a very good global agreement is obtained at all ranges of size and temperature.

more precise treatment of scattering rates through *ab-initio* techniques, but we have demonstrated that some issues related to relaxation times come from their incorrect averaging. We can conclude that an appropriate treatment of the N-processes makes unnecessary the introduction of new terms in the expression of . Probably rough surfaces [70] would need additional considerations to improve the fit but this is out of the scope of the present work.

5.2.7 Comparison between standard RTA, Callaway and Kinetic-collective models

In order to show the improvement of our model over the standard RTA and the Callaway model [22], in this Section we compare our results with those obtained with these usual approaches. The procedure we have followed to fit ^{na}Si using the standard RTA and the Callaway model is the same as in our approach described in Sec.5.2. The same expressions for the relaxation times (see Table 5.1) are used in the three approaches (RTA, Callaway and Kinetic-collective) to highlight only the accuracy of the models. Note that in the RTA approach we have included the normal scattering rate in the Matthiessen rule together with the resistive scattering rates to account for the effect of such treatment of the N-processes on the conductivity, which can be found usually in the literature [26]. This is equivalent to the combined relaxation time τ_C in the Callaway model, and this way the first term of the thermal conductivity I_1 is equivalent to the RTA integral. The values of the fitting parameters that provide the best results for ^{na}Si in each approach, RTA and Callaway, are shown in Table 5.4 together with those values previously found for the Kinetic-collective model. Then, to test the prediction capability, we have calculated the thermal conductivity of the ^{iso}Si bulk and the 115 nm NW with the standard RTA and the Callaway model. This method highlights the predictive power of the used model regarding impurities present in the material (from ^{na}Si to ^{iso}Si changing only Γ), and regarding size-effects (from ^{na}Si to 115 nm NW changing only L_{eff}). The resulting thermal conductivities of these three samples obtained within the standard RTA and the Callaway model are shown in Fig. 5.7 compared to the results obtained within the Kinetic-collective model (already shown in Fig. 5.6).

As expected, RTA reproduces very well ^{na}Si in the low temperature range. Although for $T > 200$ K begins to slightly diverge from experimental data, in general the agreement is good. On the other hand, the prediction capability when we change the isotopic composition of the sample is poor: it underpredicts the ^{iso}Si peak and from this point forward. At the nanoscale it also fails in the prediction, as shown in the plot, the resulting of 115nm NW is

considerably underpredicted. Regarding the Callaway model, although is able to reproduce correctly the ^{na}Si sample, its prediction capability, though better than that provided by the RTA, is still poor. Contrarily to the RTA, the Callaway model overpredicts ^{iso}Si and the 115 nm nanowire. With this, we have shown two important points. First, it is relatively easy to provide a good fit to a single sample with any model. Second, the success in the prediction capability reveals the strength of the used model.

Usually, in the literature we can find two kind of works on lattice thermal conductivity. Firstly, there are some models focused on the prediction of the peak of the thermal conductivity providing fits to several bulk samples with natural and enriched isotopic composition in the whole or in a partial temperature range, but they are not checked at the nanoscale [27]. In contrast, we can find models focused on the fitting to nanoscale samples giving a good agreement with measurements, but they are not checked at reproducing the thermal conductivity of other isotopic composition bulks [26, 28]. Since providing a good fit at the peak region for both bulks (^{na}Si and ^{iso}Si) is very difficult, most of the published models for the thermal conductivity avoid the temperature interval corresponding to the peaks. Normally they show fits and predictions for $T > 50$ K or $T > 100K$, *i.e.* higher temperatures than that of the peak. With four simple and representative scattering events (boundary, impurities, normal and umklapp) our model is able to provide a very satisfactory prediction from the macro to the nanoscale in the whole range of temperatures.

5.2.8 Effect of N-processes on the thermal conductivity

In view of the poor prediction capability of the standard RTA and Callaway model, and since we think it is due of the incorrect treatment of the N-processes, we have made a test. It consist of neglecting τ_N in the thermal conductivity calculation within the RTA and the Callaway model. Therefore, in RTA thermal conductivity (see Eq. (1.39)) we use a pure

Table 5.4: Best-fit parameters for ^{na}Si bulk with the standard RTA, Callaway and Kinetic-collective model.

	B_U (s^{3}K^{-1})		B_N (sK^{-3})		B_N (s^{-1}K^{-1})	
Kinetic-collective model	2.8	10^{-46}	3.9	10^{-23}	4.0	10^{8}
Callaway model	1.4	10^{-46}	3.5	10^{-24}	1.0	10^{7}
standard RTA	1.9	10^{-45}	9.3	10^{-23}	3.2	10^{5}

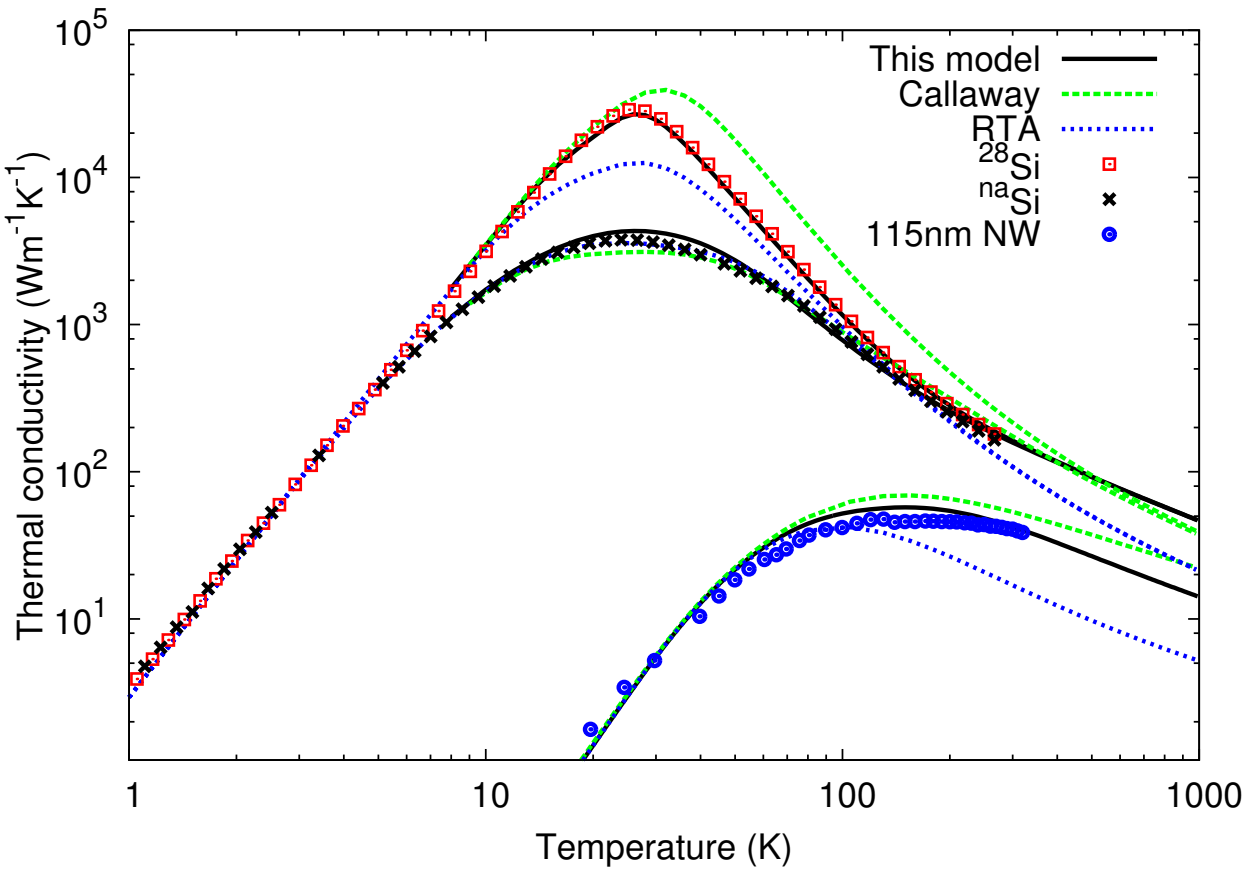

Figure 5.7: Thermal conductivity as a function of temperature for $^{\mathrm{na}}Si$ *and* $^{\mathrm{iso}}Si$ *bulk, and the 115 nm NW. We show the best fit provided by the standard RTA and the Callaway models against the Kinetic-Collective model.*

resistive relaxation time $\tau_R = (\tau_B^{-1} + \tau_I^{-1} + \tau_U^{-1})^{-1}$, according to the Matthiessen rule. In the Callaway model, if we neglect τ_N, we have $\tau_C = \tau_R$, and the second term . I_2 is vanished, so we recover the RTA expression (see Sec. 4.2.1). The result of these calculations, with the same B_U parameters used before in each case (see Table 5.4), allows us to check how the thermal conductivity is affected when τ_N are removed. In Fig. 5.8 we show fitted with τ_N (from the previous Section, see Fig.5.7) compared to the curve obtained without τ_N. As it can be observed in plot (I), at low temperatures, the RTA thermal conductivity with and without τ_N provides the same result (the curves are overlapped), as it is expected, since τ_B is the dominant scattering mechanism. If we remind our Kinetic-collective result (see Fig.5.1), at this temperature region the total thermal conductivity belongs to the pure kinetic regime,

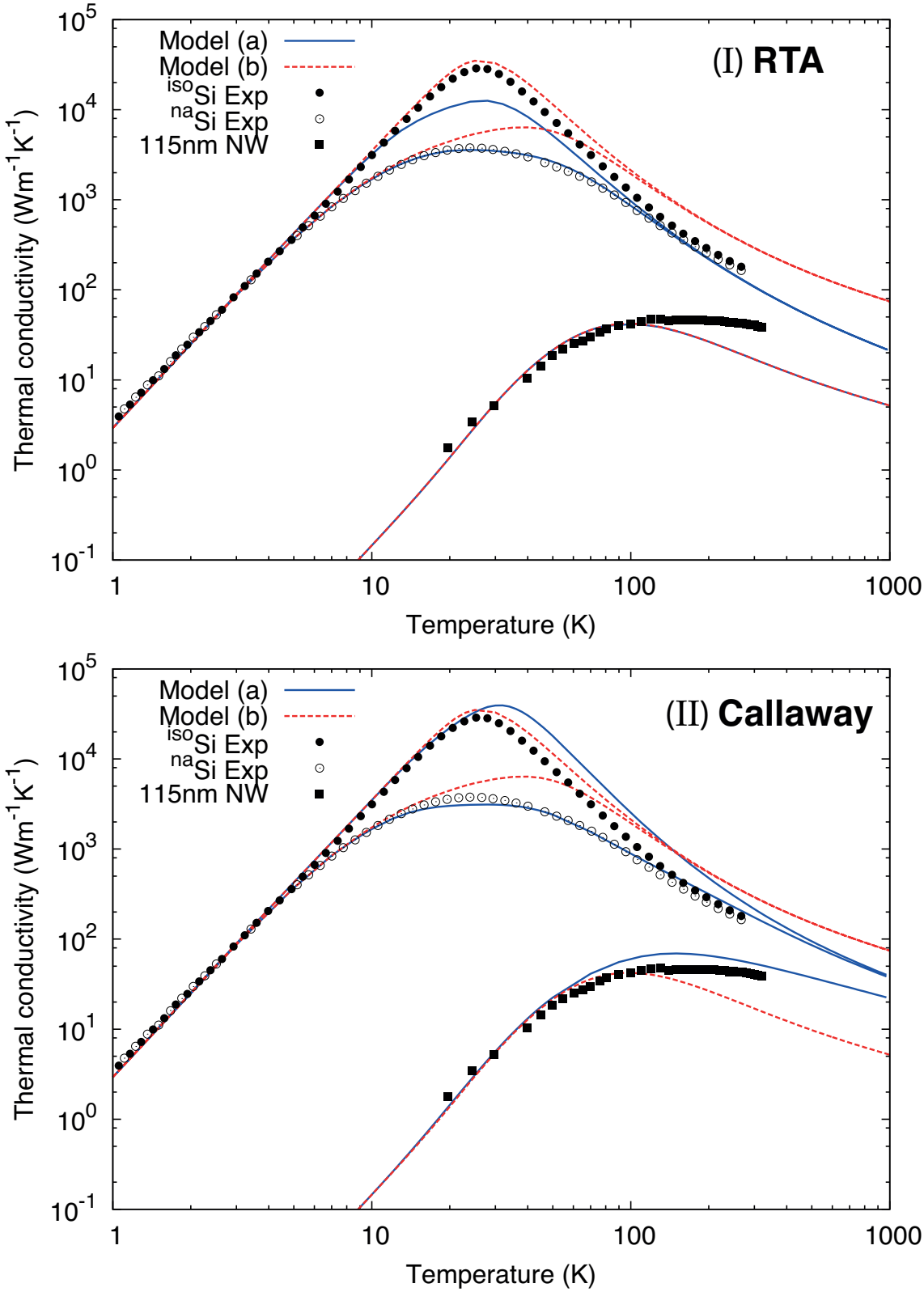

Figure 5.8: Thermal conductivity for the three representative samples ^{na}Si *and* ^{iso}Si *bulk, and 115nm NW as a function temperature calculated using: (I) the RTA model and (II) the Callaway model. In each plot, model (a) (blue lines) indicates that* $_N$ *are included in the calculations, as already shown in Fig.5.7; and model (b) (red dashed-lines) shows the result of removing* $_N$.

which is, in fact, the RTA. As the temperature increases, it can be seen that N-processes begin to play a role in the transport, since the curves without τ_N (red dashed-lines) diverge considerably from the curves with τ_N (blue lines) for the both bulk samples. In the nanowire both curves are the same in the whole range of temperatures, since τ_B is the limiting scattering mechanism in the Matthiessen rule due to the very small L_{eff}, then, the effect of τ_N is masked when including them in the Matthiessen sum together with the other resistive scatterings. Regarding the Callaway model, plot (II), the effect of removing τ_N in both bulks means we are calculating with the pure RTA (red dashed-lines), however the refinement of the RTA made by Callaway by including the correction . I_2 affects specially at the nanoscale. We can observe in the plot that the effect of this correction due to τ_N is to raise the thermal conductivity from the purely resistive RTA prediction (neglecting τ_N). Actually, this test on the effect of τ_N over the RTA and the Callaway model is an analogy we have done to compare with the effect of τ_N in our model, since our limit $_{\text{kin}}$ corresponds to the maximum effect of removing τ_N, *i. e.* it is a purely resistive RTA result, and $_{\text{coll}}$ corresponds to the maximum effect that τ_N can induce in the thermal conductivity.

5.3 Behavior of the relaxation times with frequency

Let us now discussed some important aspects of the behavior of the relaxation times τ_N, τ_U, τ_I and τ_B with frequency and temperature (see Table 5.1): i) To study the whole frequency spectrum, we have selected two branches: the longitudinal acoustic (LA) and the longitudinal optic (LO), since representing the 6 phonon branches would complicate the plots. With the LA we study the behavior of low-frequency phonons, and with LO the high-frequency phonons. ii) To study the behavior at high and low temperature, we have selected $T = 300$K and $T = 30$K respectively. iii) To compare the behavior of the relaxation times at the macro and the nanoscale we have chosen two representative samples: bulk ^{na}Si and the 115 nm diameter NW. Since they have different effective sizes and the only size-dependent relaxation time is τ_B, both samples will have identical τ_N, τ_U and τ_I and the size-effect will be highlighted through τ_B.

This frame is represented in Fig. 5.9 and Fig. 5.10 for the LA and the LO branches respectively.

Let us begin with the low-frequency phonons. In Fig. 5.9 we show the frequency dependence of τ_N, τ_U, τ_I and τ_B for the LA branch at low 5.9 (a) and high 5.9 (b) temperatures, for bulk ^{na}Si and the 115 nm diameter NW. At $T = 30$ K the bulk thermal conductivity exhibits

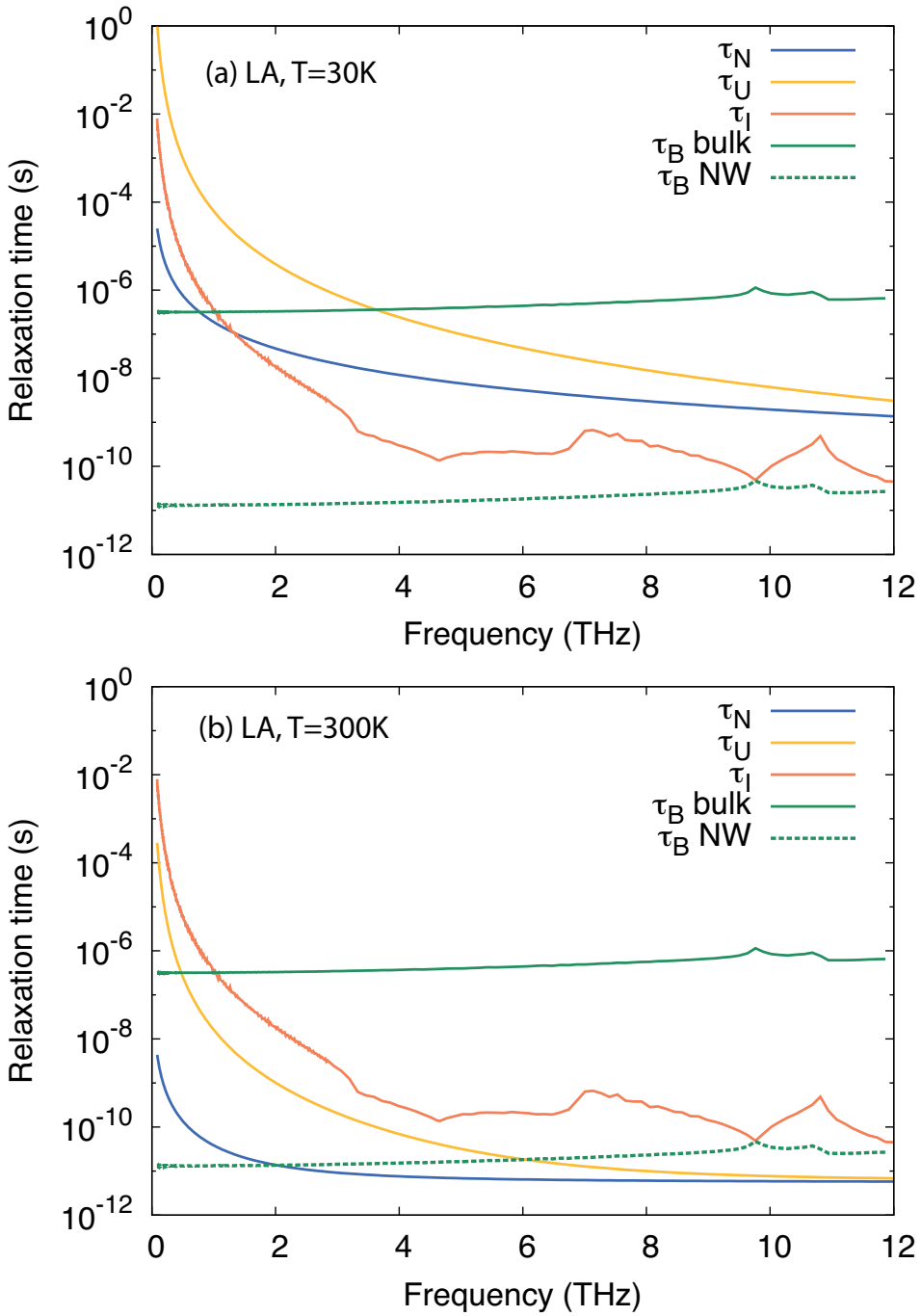

Figure 5.9: Behavior of phonon relaxation times $_N$, $_U$, $_I$ and $_B$ with the frequency for the LA branch at several temperatures: (a) T=30 K, (b) T=300 K. To highlight the size-effect we have plotted the set of relaxation times for two samples: bulk $^{\mathrm{na}}Si$ and the 115 nm diameter NW. Note that both samples have identical $_N$, $_U$ and $_I$, but they have different $_B$ due to their different sizes (indicated in the legend).

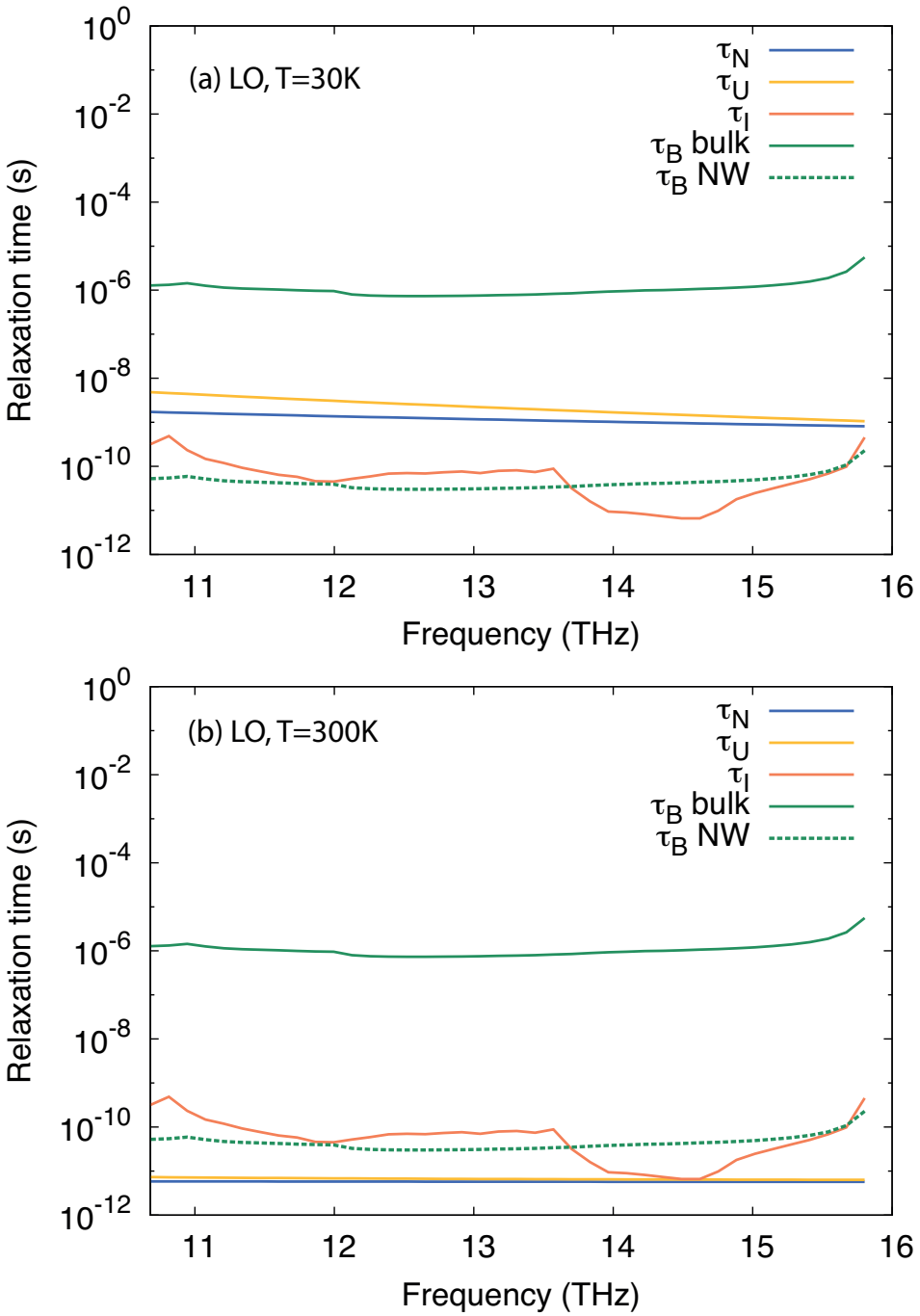

Figure 5.10: Behavior of phonon relaxation times $_N$, $_U$, $_I$ and $_B$ with the frequency for the LO branch at several temperatures: (a) T=30 K, (b) T=300 K. To highlight the size-effect we have plotted the set of relaxation times for two samples: bulk $^{\mathrm{na}}Si$ and the 115 nm diameter NW. Note that both samples have identical $_N$, $_U$ and $_I$, but they have different $_B$ due to their different sizes (indicated in the legend).

the peak and τ_I is expected to be the dominant scattering process. This can be observed in 5.9 (a), since τ_I has the smallest values for the whole range of acoustic frequencies, except for the modes under 2 THz, which are still dominated by τ_B. On the other hand, we can see that for the NW the situation is different. As expected τ_B is the dominating scattering due to the small values of L_{eff}. When the temperature increases, we can observe in 5.9 (b) that now, the dominant scattering mechanism is τ_N, for both Bulk and NW, except for the short-frequency modes in the NW (below 2THz) where τ_B is still the dominating process. Note that now, for both bulk and NW, τ_U plays an important role. In the bulk, τ_U is clearly the dominant resistive scattering and for frequencies above 6THz, becomes comparable to τ_N, though higher, this makes 1, we are in the collective regime. In the NW, even at room temperature, the size-effects still play an important role, as we can observe in the plot, τ_B for modes below 6THz τ_B is the limiting scattering, while for higher modes τ_U dominates.

Let see what happen with optic phonons. In Fig. 5.10 we show the frequency dependence of τ_N, τ_U, τ_I and τ_B for the LO branch at low 5.10 (a) and high 5.10 (b) temperatures, again for bulk ^{na}Si and 115 nm NW. At $T = 30$ K the dominating scattering is also τ_I, as for the acoustic modes. However, for the NW the situation chafes respect to the LA branch. Now, the boundary scattering combined with the impurity scattering are the dominating processes, since τ_B and τ_I are of the same order of magnitude. At room temperature the situation changes remarkably. For both samples, bulk and NW, Umklapp and normal scattering are of the same order of magnitude. τ_U is the dominating resistive scattering, as expected, but higher than τ_N, since we are in a collective regime. Recall that when $\tau_N << \tau_R$, we have

$_{\text{coll}}$.

5.4 Spectral thermal conductivity

Until now, we have described the behavior of the thermal conductivity at different temperature intervals, but it is also important to study how the phonons with different frequencies participate in the thermal transport at a given temperature. For this purpose, it is very useful to represent the spectral thermal conductivity (ω_ν) per phonon branch[1], which is in fact the

[1]Let us now indicate the phonon branch dependence with the subindex .

integrand of the thermal conductivity integral expression

$$= \sum_{\nu} \qquad (\omega_\nu) d\omega \tag{5.1}$$

where following the Kinetic-collective model, from Eq. (4.81) we have

$$(\omega_\nu) = \ _{\text{kin}}(\omega_\nu)(1 - \ ) + \ _{\text{coll}}(\omega_\nu) F(L_{\text{eff}}) \ . \tag{5.2}$$

Recalling the expressions for $_{\text{kin}}$ and $_{\text{coll}}$, see Eqs. (4.73) and (4.74), we can express the spectral thermal conductivity in each regime in terms of a phonon diffusion coefficient equivalent to the relaxation-time times the velocity square, that is, ($\equiv \tau v^2$. Therefore, in the kinetic regime we have

$$_{\text{kin}}(\omega_\nu) = \frac{1}{3}\hbar\omega_\nu(\ _{\text{kin}}(\omega_\nu)\frac{n^0(\omega_\nu)}{T} D(\omega_\nu) \tag{5.3}$$

where the kinetic diffusion coefficient is

$$(\ _{\text{kin}}(\omega_\nu) \equiv \tau_{\text{R}}(\omega_\nu) v^2(\omega_\nu) \tag{5.4}$$

where $v(\omega_\nu)$ is the group velocity obtained from the dispersion relations and $\tau_{\text{R}}(\omega_\nu)$ is the effective relaxation time that we have already employed in the previous calculations and it is obtained with the Matthiessen rule as

$$\tau_{\text{R}}(\omega_\nu) = \left(\tau_I^{-1}(\omega_\nu) + \tau_U^{-1}(\omega_\nu) + \tau_B^{-1}(\omega_\nu)\right)^{-1} \ . \tag{5.5}$$

It is important to notice that ($_{\text{kin}}(\omega_\nu)$ is frequency dependent through the relaxation time and velocity, since in the kinetic regime, each mode contributes independently to thermal resistance, so we have a diffusion coefficient per mode. However, in the collective regime the phonon collectivity must be considered as a whole, raising a global (frequency independent) diffusion coefficient ($_{\text{coll}}$ obtained as a result of averaging the relaxation time and velocity in the "collective" fashion. This is equivalent to rewrite (4.74) as

$$_{\text{coll}}(\omega_\nu) \equiv \frac{1}{3}\hbar\omega_\nu(\ _{\text{coll}}\frac{n^0(\omega_\nu)}{T} D(\omega_\nu) \tag{5.6}$$

with

$$(\ _{\text{coll}} = \frac{\sum_{\nu} \quad v(\omega_\nu) q_\nu \frac{n^0(\omega_\nu)}{T} D(\omega_\nu) d\omega \quad ^2}{C_v \sum_{\nu} \quad \frac{q_\nu^2}{\hbar\omega_\nu} \frac{1}{\tau_{\text{R}}(\omega_\nu)} \frac{n^0(\omega_\nu)}{T} D(\omega_\nu) d\omega} \ . \tag{5.7}$$

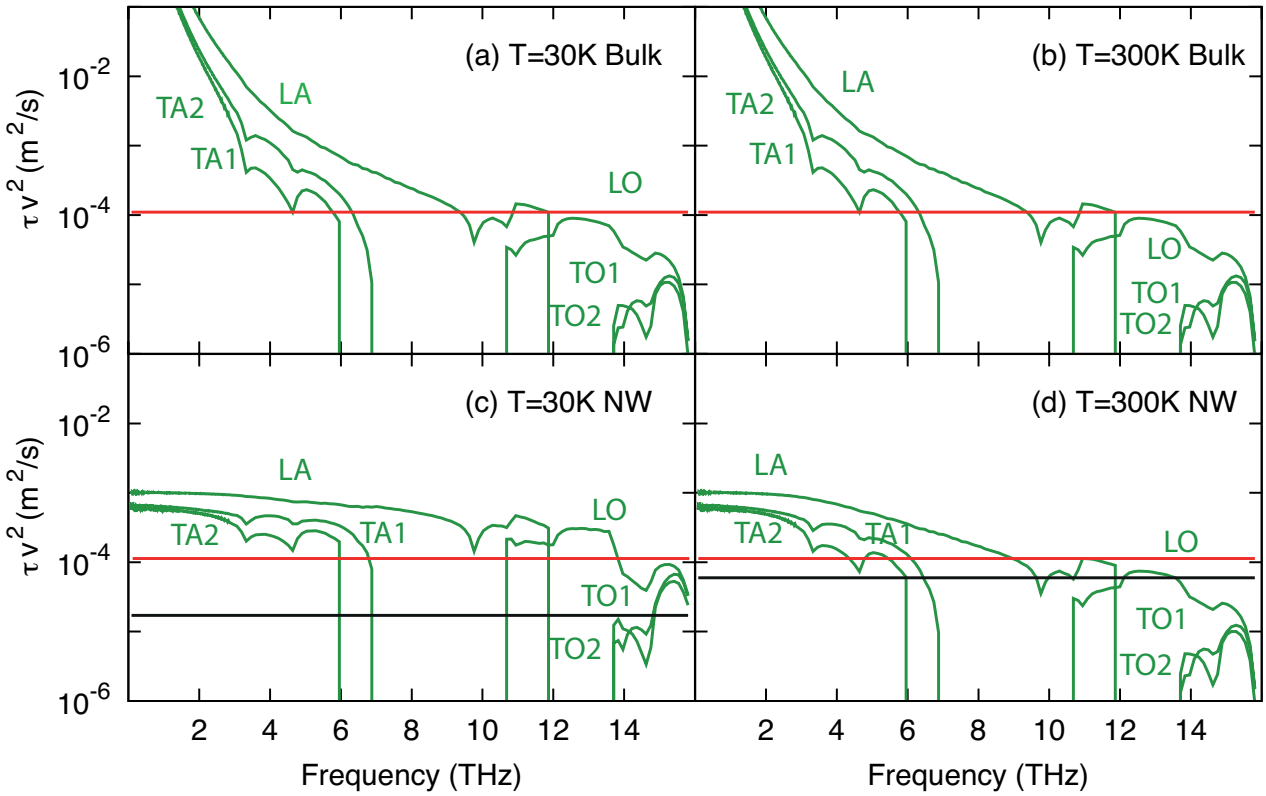

Figure 5.11: Kinetic (green lines) and collective (red lines) phonon diffusion coe cients in terms of frequency for Si bulk (^{na}Si sample) at low and room temperature: T =30 K (a) and T =300 K (b); and for the 115nm NW at the same temperatures: T =30 K (c) and T =300 K (d). Note that the kinetic diffusion coe cient is a frequency dependent quantity, and therefore we show the values for each branch: longitudinal acoustic (LA), transversal acoustic (TA1 and TA2), longitudinal optic (LO) and transversal optic (TO1 and TO2), while the collective diffusion coe cient is a mean value for the whole phonon collectivity, only depending on T.

Recall that τ_R is the resistive relaxation time excluding the boundary scattering

$$\tau_{\mathrm{R}}(\omega_\nu) = (\tau_I^{-1}(\omega_\nu) + \tau_U^{-1}(\omega_\nu))^{-1}. \tag{5.8}$$

and $C_v = \sum_\nu \hbar\omega_\nu \frac{n^0(\omega_\nu)}{T} D(\omega_\nu) d\omega$ is the specific heat. Summing up, the main difference between (5.4) and (5.7) is that the first is a per-mode expression and consequently depends on frequency while the second is a frequency averaged constant.

In Fig. 5.11 (a),(b) we show the obtained diffusion coefficients ($\equiv \tau v^2$ for the two transport regimes (5.4) and (5.7) in terms of frequency at the same temperatures. For this, we have used the same relaxation times expressions and the other inputs specified in 5.1. We can observe the strong frequency-dependence of the kinetic diffusion coefficient for the different branches (green lines), while the collective term is a constant (red line), shorter than the kinetic one for low-frequency modes while for high frequencies it is larger. Diffusion coefficient gives the capacity of a mode to carry energy from one point to another. This means that the collective transport tends to enhance the contribution of high-energy modes and reduce that of the low-energy modes in the transport process. Note that ($_{\mathrm{kin}}(\omega)$ is shorter for the NW than for bulk due to the size-effect through τ_B, while ($_{\mathrm{coll}}$ is the same for bulk and NW, as τ_{R} used in Eq.(5.7) does not include τ_B.

The effect of the diffusion coefficient on thermal conductivity can be seen in Fig. 5.12 where we have plotted the total spectral densities of the thermal conductivities in the kinetic (5.3) and collective (5.6) regime accounting for all the branches, that is, green dotted line represents $\sum_\nu {}_{\mathrm{kin}}(\omega_\nu)$, let us call it $_{\mathrm{k}}$ and red dashed-line $_{\mathrm{coll}}(\omega_\nu)$, let us call it $_{\mathrm{c}}$. We can observe that in the low-frequency range the kinetic contribution is dominant and in the high-frequency range the dominance is inverted. In a middle temperature region the contributions cross. The dominance of collective term at high frequencies appears clearly in the plot, but it could be hidden at low temperatures by the effect of the specific heat per mode $\hbar\omega_\nu \frac{n^0(\omega_\nu)}{T} D(\omega_\nu)$ in Eq.(5.6), since at such temperatures the phonon population is very small.

The values of the kinetic and collective contributions need to be weighted by , giving the fraction of the total avalaible flux in each regime that is actually contributing to the thermal transport at a given temperature. This can be also observed in Fig. 5.12 where we have plotted the kinetic $_{\mathrm{k}}(1-\ )$ (filled curve in green) and the collective $_{\mathrm{c}}$ (filled curve in red). As we know, takes values between 0 and 1 depending on the importance of N-processes over the rest of the resistive scattering mechanisms. When $= 0$, that is, when resistive scattering is dominant, we recover the usual kinetic expression. In that case green line is full

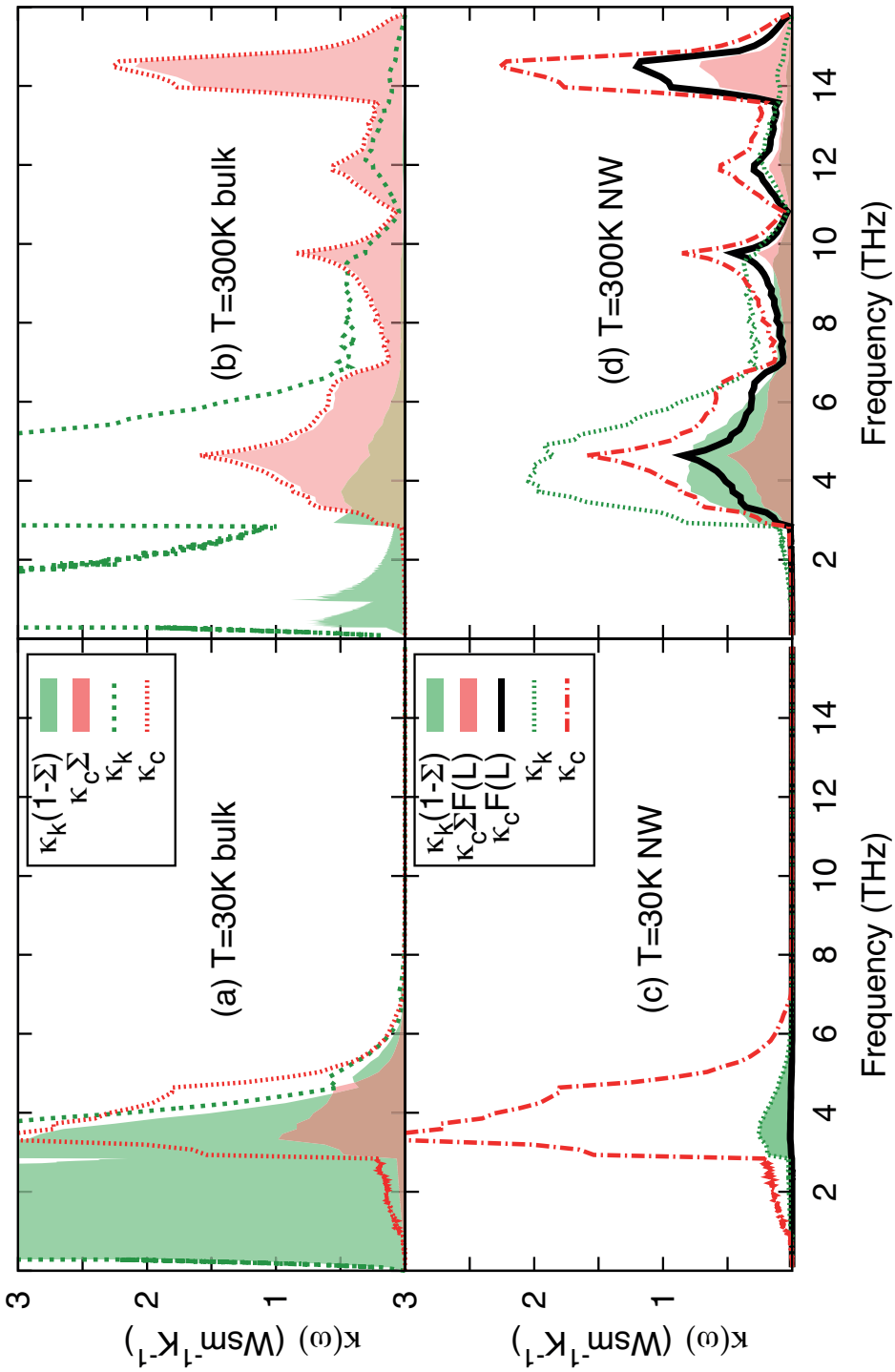

Figure 5.12: Spectral thermal conductivity contributions in terms of frequency of both regimes at low $T = 30K$ and room temperature $T = 300K$ for Si bulk (a),(b) and 115nm NW (c),(d), respectively. In all the plots pure kinetic $_{\mathrm{k}}$ and collective $_{\mathrm{c}}$ regimes (shortened in the legend as $_{\mathrm{k}}$ and $_{\mathrm{c}}$ respectively) are shown in dashed-lines, the reduction due to Σ is shown for each regime with filled curves. For the NW the effect of $F(L_{\mathrm{eff}})$ in the collective regime is also shown (solid line), for the bulk is omitted for the sake of simplicity, since $F(L_{\mathrm{eff}}) = 1$ at both temperatures (see Fig. 5.5). Note that in (a) and (b) the peaks of $_{\mathrm{k}}$ appear cut because are out of scale.

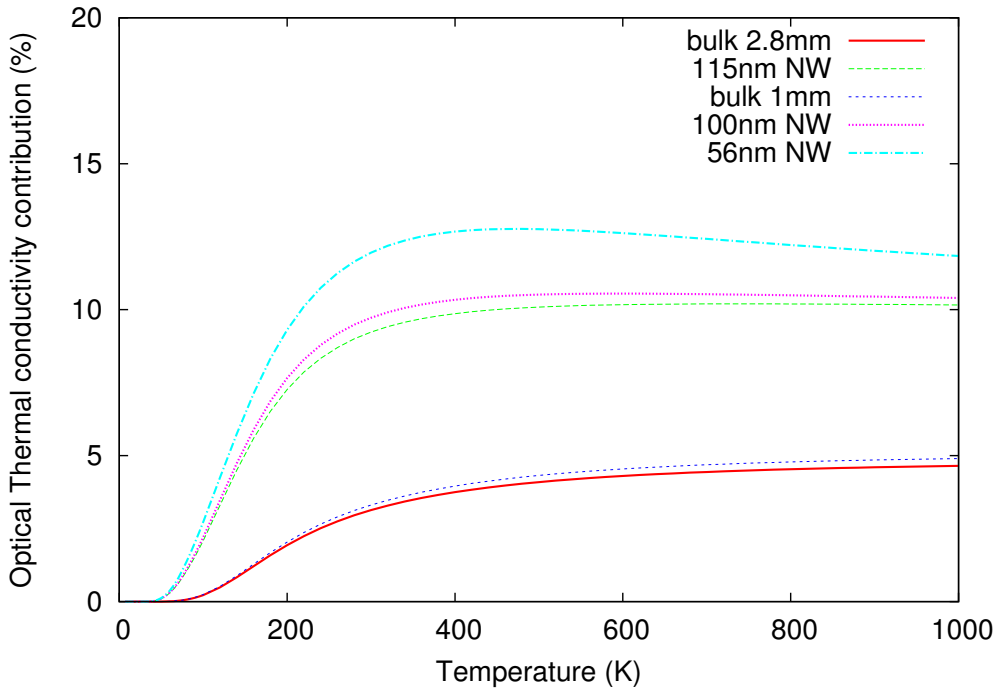

Figure 5.13: Normalized thermal conductivity contribution due to optical phonons for several sample sizes.

and red line empty. When N-process is dominant = 1 and we are in the pure collective regime (red dashed-line is full and green dotted-line empty). Particularly, for bulk ^{na}Si we obtain = 0.31 at $T = 30$ K, *i.e.* the 69% of the kinetic phonons are contributing to , while from the collective phonons the 31% of them are participating. At $T = 300$K we have = 0.92, now only the 8% of the kinetic phonons is participating against the 92% of the collective phonons. In the case of the NW, we have = 0.002 at $T = 30$K , this indicates that clearly the transport is kinetic (99.8%, note the the kinetic curve is completely filled) and = 0.46 at $T = 300$K, this indicates that at room temperature we are in an intermediate regime where 46% of the collective phonons are participating together with the 54% of the kinetic phonons (note that both curves are half-filled)[2].

From observing Figs. 5.11 and 5.12 one can see that the high-frequency modes (corresponding to the optic branches) have an important contribution in the collective regime, while in the kinetic regime they are inhibited. From this, we deduce that the effect of the N-processes may be to enhance the contribution of the optic phonons in the thermal con-

[2]The filled part of the kinetic regime is behind the collective one and is not appreciated in this figure.

ductivity. The general believe is that their contribution is so small that can be neglected in the thermal conductivity integral, so when using the RTA or the Callaway-like models only acoustic branches are usually considered. Other authors have indicated, that their contribution, though small, should not be disregarded. Actually, according to Tian et al., their contribution is specially significant at the nanoscale [96]. In Fig. 5.13 we show the contribution of the optical phonons to the total conductivity. Similar results were found by Tian *et al.* with *ab-initio* methods [96]. Our model predicts a contribution of the 15% for the 115nm NW, in agreement with Tian *et al.* The agreement between such different approaches may indicate that indeed, optical phonons are an important feature in nanostructures. However, the *ab-initio* methodology followed in [96] is not able to provide a physical interpretation of this phenomena, while our model let us infer that the source of such contribution may lie in the effect of N-process in the thermal transport. Note that, our kinetic regime is in fact equivalent to the RTA with a τ_R and that in this regime, as seen in the plot, there is no optic phonons population, it appears only in the collective regime, where N-process dominate the transport. Although this hypothesis should be further studied and maybe some experimental evidence would be of great help to support our explanation, we can conclude that our model has let us to shed some light on this important topic.

Chapter 6

Applying the Kinetic-Collective model to group-IV semiconductors.

As we have shown in the previous Chapter, the Kinetic-collective model has been tested on bulk Si, with different isotopic compositions, and Si thin-films and nanowires. The agreement of our theoretical predictions with experimental data from bulk to nanoscale in those silicon samples in the whole range of temperatures is remarkable [77]. This good result on silicon has motivated us, in first place, to check the robustness of the model by applying it to other materials than silicon. We have stressed our attention into other materials with the same lattice structure as silicon, under the hypothesis that, since they have the same diamond structure, only differing in the value of the lattice parameter, their dispersion relations are, roughly, similar or even proportional in certain regions of the **q**-space, (as can be seen in Figs. (2.5-2.8) in Chap. 2), and this proportionality could be extended to the behavior of phonon-phonon interactions. These materials with the same diamond structure are the group-IV element semiconductors introduced in Chapter 2: silicon, germanium, gray-tin and diamond itself. This way, the validity of the Kinetic-collective model is checked to be extended to a family of semiconductor materials without any additional phenomenology.

On the other hand, one of the drawbacks of phenomenological models is the inclusion of adjustable parameters to fit individually the thermal conductivity of each material [24,27,97]. This individual fitting can be interpreted as a lack of predictive power in the model, if the obtained values keep no relation between them. Therefore, our motivation is, in second place, to predict the thermal conductivity of a set of samples of several materials without fitting individually each sample but globally all of them. This global approach, and the large

reduction in the fitting parameters, will stress the accuracy of the Kinetic-collective model predictions.

6.1 Relations between phonon-phonon relaxation times expressions

Let us discuss in this Section some aspects of the phonon-phonon relaxation times to be able, eventually, to obtain theoretically the values of parameters B_N, B_N and B_U involved in phonon-phonon relaxation time expressions. In Table 6.1 we summarize the relaxation time expressions that we will use along this Chapter. Note that we use expressions for the Umklapp, normal and boundary scattering, (3.38), (3.37) and (3.51) respectively, are those which were introduced and discussed in Chap. 3 and used previously in Chap. 5 (see Section 3.2 and Table 5.1). On the contrary, we use now for the impurity scattering the expression provided by Klemens (3.50) instead of that provided by Tamura, and we will discuss later this choice.

The exact functional form of phonon-phonon relaxation times $\tau_U(\omega_\nu)$ and $\tau_N(\omega_\nu)$ (let us drop the ω_ν dependence here and onward for the sake of simplicity) is a matter of great discussion. However, as we discussed in Sec. 3.2, τ_U and τ_N exhibit a behavior such that $\tau_{U/N}^{-1} \quad B\omega^a T^b$, where the dependence on frequency and temperature relies on empirical values of the exponents a and b, and the presence of an adjustable parameter B is required. Generally, the B parameters have appeared in the literature as fitting parameters, forgetting the information they may hide. In an early work by Leibfried and Schlömann [60], it appears for the first time a semiempiric expression to calculate B_U and B_N in terms of some properties of the material with the dependence on frequency and temperature. Later recovered by Morelli *et al.* [27], this expression is written for both parameters belonging to Umklapp and normal processes, that we denote with the subindex U/N for brevity, as

$$B_{U/N} \quad \frac{k_B}{\hbar}^{\;b} \; \frac{{}^2\hbar V^{\,(a+b-2)/3}}{M v_g^{(a+b)}} \tag{6.1}$$

where k_B is the Boltzmann constant, $\hbar$ the Planck constant, the Grüneisen parameter and M the atomic mass, being a, b the exponents of frequency and temperature respectively. This expression can be used to relate the parameters of several materials with an expected similar behavior of the phonon-phonon interactions.

Table 6.1: Relaxation times for non-resistive and resistive scattering processes. $_N$ *and* $_U$ *are original contributions of the present thesis, while* $_I$ *and* $_B$ *are widely used in the literature. (See Chap. 3)*

Non-resistive	Expression
Normal	$\tau_N(\omega_\nu) = \dfrac{1}{B_N T^3 \omega_\nu^2 [1 - \exp(-3T/\ _D)]} + \dfrac{1}{B_{N'} T}$

Resistive	Expression
Impurity	$\tau_I(\omega_\nu) = \left(\dfrac{V\Gamma}{4\pi v^3(\omega_\nu)} \omega_\nu^4\right)^{-1}$
Umklapp	$\tau_U(\omega_\nu) = \dfrac{\exp(\ _U/T)}{B_U \omega_\nu^4 T [1 - \exp(-3T/\ _D)]}$
Boundary	$\tau_B(\omega_\nu) = L_{\text{eff}}/v(\omega_\nu)$

In our specific case for Umklapp scattering Eq. (3.38), we have from

$$\tau_U^{-1} \quad \omega^4 T^1 \tag{6.2}$$

therefore $a = 4$ and $b = 1$, and entering these exponents in Eq. (6.1) we have

$$B_U = \frac{k_B\ ^2 V}{M v_g^5} \qquad (s^3 K^{-1})\,. \tag{6.3}$$

Analogously, for normal scattering Eq. (3.37) we have: i) at low temperatures

$$\tau_N^{-1} \quad \omega^2 T^3 \tag{6.4}$$

therefore $a = 2$ and $b = 3$, and entering these exponents in Eq. (6.1) we have

$$B_N = \frac{k_B^3\ ^2 V}{\hbar^2 M v_g^5} \qquad (sK^{-3})\,, \tag{6.5}$$

and ii) at high temperatures ,

$$\tau_N^{-1} \quad \omega^0 T^1 \tag{6.6}$$

therefore $a = 0$ and $b = 1$, and entering these exponents in Eq. (6.1) we have

$$B_N = \frac{k_B \ ^2}{M v_g V^{1/3}} \qquad , \quad (s^{-1}K^{-1}) \tag{6.7}$$

Since K_B and $\hbar$ are constants, B_U, B_N and B_N depend exclusively on material's properties $, v_g, V$ and M. Note that B_U, B_N and B_N depend on frequency indirectly through the group velocity and on temperature through the Grüneisen parameter. They have dimensions of time and temperature, but each of them has different units and magnitudes because they belong to different scattering rate functional forms.

Now we can express the B parameters for each material of our group in terms of the values of one of them through a conversion factor. Let us take Si as the reference material, since we have already worked with it. Starting from the values $B_{U,Si}, B_{N,Si}$ and $B_{N,Si}$ that provide the best fit for naturally occurring Si (^{na}Si), we can calculate the respective values for the other materials as

$$B_{U/N,x} = f_x B_{U/N,Si} \tag{6.8}$$

and

$$B_{N,x} = f_x B_{N,Si} \tag{6.9}$$

where x denotes the material: $Ge, C, \ \text{-}Sn$, being

$$f_x = \frac{[\ ^2V/Mv^5]_x}{[\ ^2V/Mv^5]_{Si}} \tag{6.10}$$

the conversion factor for both parameters: B_N in the low-temperature term of τ_N, and B_N in τ_U; and

$$f_x = \frac{^2/MvV^{1/3}{}_x}{[\ ^2/MvV^{1/3}]_{Si}} \tag{6.11}$$

is the conversion factors for the parameter B_N in the high-temperature term of τ_N. Calculated values of f_x and f_x are given in Table 6.3.

6.2 Inputs for the calculations

In Chapter 2, we have presented the family of group-IV semiconductors with diamond lattice structure and calculated their dispersion relations and density of states using the Bond-charge

Table 6.2: Materials properties: Debye temperature Θ_D, atomic mass M, atomic volume V, mean zone-center velocity $\bar{v}$, and Umklapp extinction temperature Θ_U.

Material	$_D$ (K)	M (g mol^{-1})	V (m^3)	$\bar{v}$ (m/s)	$_U$ (K)
Si	645	28.086	20.01 10^{-30}	6272	126
Ge	375	72.63	22.75 10^{-30}	3923	70
C	1850	12	5.67 10^{-30}	13746	405
-Sn	230	118.69	34.05 10^{-30}	2769	37

model (see Figs. 2.5 -2.8). Another important characteristic of each material arising from the dispersion relations is the Debye temperature $_D$. The higher the phonon branches are in frequency, the higher $_D$ is expected. It is worthy then to calculate the specific heat c_v from the obtained dispersion relations for each material and check the increasing values of $_D$. Calculated molar specific heats for C, Si, Ge and $-$Sn where obtained in Chap. 2, see also Fig. 2.9, where the Debye temperature for each material is marked with a grid in the plot, the values are reported in Table 6.2. Note that the values keep a proportionality between them and correspond to tabulated values in the literature [3].

To calculate the conversion factors we need the values of the Grüneisen parameter , atomic volume V, atomic mass M and group velocity v_g for each material. Regarding V and M we have used the standard values used in the literature for each material, reported in Table 6.2. The Grüneisen parameter varies with frequency and temperature and is a current subject of study. However, since we are interested in using a proportionality rule, according to Ehrenreich *et al.* [98], the same mean value $= 0.7$ can be used for all the group-IV materials considered here. Regarding the group velocity v_g, we also need a mean value v as input for the conversion factors. We have calculated the mean value $\bar{v}$ at the zone-center of the Brillouin zone from the dispersion relations using the common expression [15, 36]

$$\bar{v} = [2/3v_T + 1/3v_L]^{-1} \tag{6.12}$$

where v_T and v_L are the mean values at the zone-center of the BZ of the transversal and longitudinal branches respectively, obtained from our calculated BCM dispersion relations. The found values are shown in Table 6.2 and are in very good agreement with both experimental and other theoretical calculations of the group velocity at the zone-center of the BZ [99].

With this, we can calculate the conversion factors for each material in terms of the reference values of the Si given in Table 5.3 using Eqs. (6.10) and (6.11) entering the values of the

Table 6.3: Conversion factors f_x and f_x calculated from Eqs. (6.10) and (6.11) for each material.

Parameter	Factor	-Sn	Ge	Si	C
$B_{U/N}$	f_x	24.01	4.60	1	0.013
B_N	f_x	0.45	0.59	1	1.158

Table 6.4: Values of Γ, cross-section A and effective size L_{eff} for Si, Ge, C and -Sn samples with natural and enriched isotopic compositions.

Sample	Γ		A (mm^2)		L_{eff}(mm)	Reference
^{na}Si	20.01	10^{-5}	2.00	3.12	2.8	[65]
^{28}Si	3.2	10^{-7}	2.00	3.12	2.8	[65]
^{na}Ge	58.7	10^{-5}	2.46	2.50	2.78	[24]
$^{70/76}$Ge	1.53	10^{-3}	2.02	2.00	2.25	[24]
^{70}Ge99.99	1.8	10^{-7}	2.20	2.50	2.63	[24]
^{70}Ge96.3	7.57	10^{-5}	2.50	2.50	2.8	[24]
^{na}C	7.54	10^{-5}	$\sim$1	1	0.82	[100]
^{13}C	6.94	10^{-6}	1	2	1.58	[101]
^{na}Sn	33.46	10^{-5}	2.5	2.5	2.8	-

material properties summarized in Table 6.2. The obtained values of f_x and f_x for $x = Ge, C,$ $-Sn$ are given in Table 6.3.

We have chosen the most representative set of samples of bulk Si, Ge and C with several isotopic compositions, whose thermal conductivity measurements can be found repeatedly in the literature. Analogously to what we did in the previous Chapter for the set of Si samples, we have summarized in Table 6.4 the values of the mass-fluctuation factor, cross-section and effective size, as well as the reference to the work where the experiment can be found. In the case of naturally occurring -Sn there is a lack of experimental measurements on thermal conductivity, to the best of our knowledge, therefore we have chosen random values for the cross-section. Note that the samples ^{na}Si and ^{28}Si are those we have already studied in the previous Chapter.

Table 6.5: Best-fit parameters for ^{na}Si bulk

	B_U (s^3K^{-1})		B_N (sK^{-3})		B_N ($s^{-1}K^{-1}$)	
Kinetic-collective model	2.8	10^{-46}	2.2	10^{-23}	3.7	10^8

6.3 Thermal conductivity of group-IV semiconductors

In this Section, we show the thermal conductivity predictions of our set of nine samples of group-IV semiconductors with several isotopic compositions and we discuss the results. We have first calculated the thermal conductivity of ^{na}Si using Eq. (4.77) entering into it the relaxation times given in Table 6.1. The values of the normal and Umklapp relaxation times parameters providing the best fit to ^{na}Si experimental data $B_{U,Si}$, $B_{N,Si}$ and $B_{N,Si}$ are given in Table 6.5. Note that the value of $B_{U,Si}$ is the same as in the previous fit from Chap. 5, but the values of $B_{N,Si}$ and $B_{N,Si}$ are slightly different (see Table 6.5). This is due to the fact that we have used different expression for τ_I (Klemens' vs. Tamura's formula). While working with other materials, we realized that the Klemens' expression provided a better prediction for germanium. We still do not know exactly the nature of this behavior, but we believe that it has to be with the flat phonon branches at the boundary of the BZ and the density of states.

The resulting is shown in Fig. 6.1 together with measurements from [65]. Secondly, as we did in Sec. 5.2, we have calculated for the other naturally occurring samples using the conversion factors given in Table 6.3 to calculate the B parameters as explained in Sec. 6.1. The obtained for ^{na}C, ^{na}Ge and ^{na}Sn are shown in Figs. 6.1(b)-(d) respectively, and compared with experimental data from [24] for germanium and from [100] for diamond. Thermal conductivity prediction for naturally occurring -Sn still awaits for experimental evidence.

Finally, the isotopic effect on thermal conductivity is also considered. The thermal conductivity of isotopically enriched samples (^{13}C, ^{28}Si, $^{70/76}$Ge, ^{70}Ge99.99, and ^{70}Ge96.3) is calculated in each case by only changing the value of Γ and L_{eff} for the corresponding samples reported in Table 6.4. The predictions are shown in Figs. 6.1 (a)-(c) and compared with experimental data from [24, 65, 101].

These results are better than one could expect, as it is known that some of the materials properties (like V or) may depend on T. This may lead to consider that our phenomenological expressions are only valid to obtain general trends of the behavior of . However,

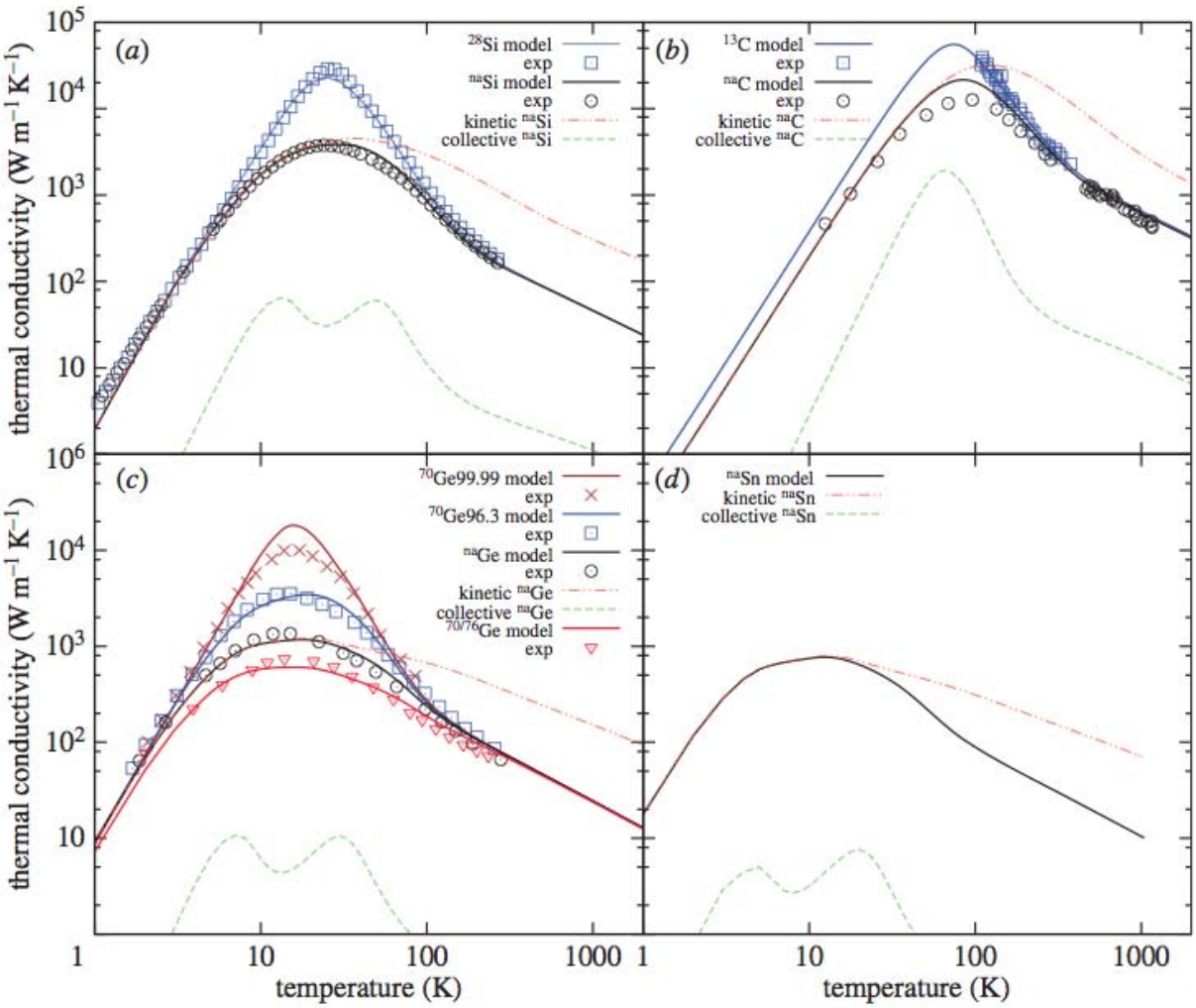

Figure 6.1: Thermal conductivity of the set of group-IV semiconductors. The fit for ^{na}Si (solid line) is shown in (a). Predictions (solid lines) are shown for ^{28}Si in (a), for diamond samples in (b), for Ge samples in (c) and for -Sn in (d). The kinetic (dashed-dot lines) and collective (dashed lines) contributions are plotted for each naturally occurring samples. Experimental data from [65] for Si, from [24] for Ge and from [100, 101] for C appear in symbols.

the agreement between our theory and the experiments is remarkably good. Note that we have not considered the effect of dislocations in ^{70}Ge99.99 and neither unknown impurities in ^{na}C, reported by their authors in each case. For these samples the predictions slightly differ from experiments in the temperature region where exhibits the peak, as it is logical since dislocations and impurities are known to affect the peak of the thermal conductivity.

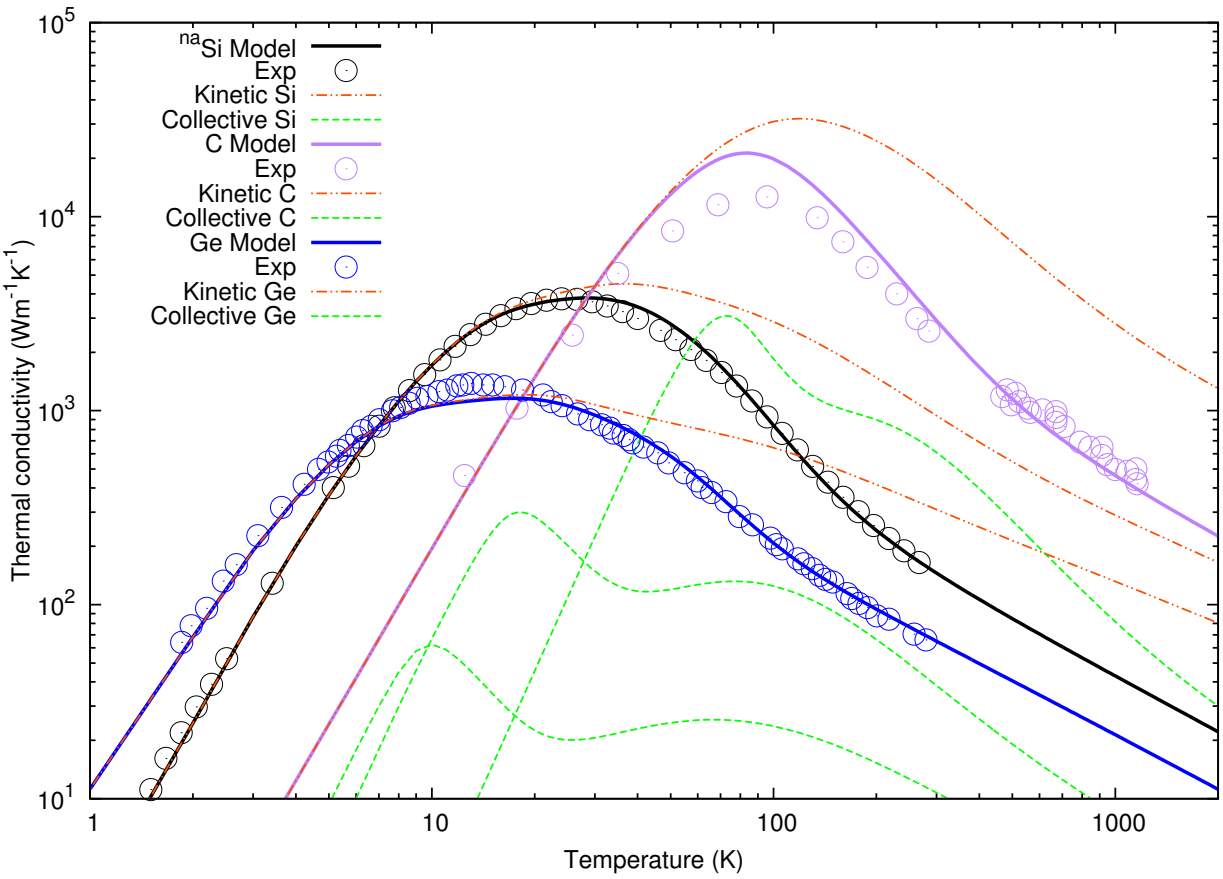

Figure 6.2: Thermal conductivity as a function of temperature for the naturally occurring samples. Fit for ^{na}Si *(solid black line) and predictions for* ^{na}C *(solid purple line) and* ^{na}Ge *(solid blue line) compared to experimental data (symbols). The kinetic (dashed-dotted orange lines) and collective (dashed green lines) contributions are plotted for each sample. Note that they decrease from C to Ge.*

In Fig. 6.2 are also plotted the kinetic and the collective limits for naturally occurring samples ^{na}Si, ^{na}C and^{na}Ge. From them, it can be seen that as T rises, makes a transition from a purely kinetic to a collective behavior. At low temperatures resistive boundary scattering is dominant and consequently the thermal transport is kinetic. As the temperature increases, normal scattering is starting to be important and the collective behavior appears making the total thermal conductivity separate from a pure kinetic regime. The importance of the collective contribution is very similar in all the samples. The only difference between them is the temperature at which this behavior begins to be experienced. As we discussed in

Sec. 5.2, the insufficient attention to this transition in usual theoretical models may be the cause for the difficulties in trying to obtain the same predictions by using, for instance the Callaway model.

6.3.1 Transition from the kinetic to the collective regime:

To study the differences in the transition from one regime to another between Si, Ge, C and Sn, we show in Fig. 6.3 the behavior with temperature of the switching factor for the naturally occurring samples. Again, as we have observed with silicon in the previous Chapter, at very low temperatures, the boundary scattering present in τ_R behaves as τ_B L_{eff} τ_N and yields $= 0$. Therefore, we are in the pure kinetic regime $_{\text{kin}}$. At room temperature, 1 (actually $= 0.86$ for ^{na}Si[1]) and we are in the collective regime, $_{\text{coll}}$. It can be observed in Fig. 6.3 that the transition to the collective regime is very similar for Ge and Sn. For diamond the transition begins at a temperature higher than for the others. This is due to the fact that the transition happens in the region of impurity scattering dominance, and the peak of diamond occurs at much higher temperature than for the others.

To account for the effect of impurities in the transition, let us take Ge as an example, since we have a complete set of experimental data in the whole range of temperature including samples with thermal conductivity higher and lower than the thermal conductivity of the natural occurring sample. In Fig. 6.4 we show for the set of Ge samples with different isotopic compositions. We can observe that the sample with highest Γ, that is $^{70/76}$Ge, experiences the transition in a wider interval of temperatures T $[10, 300]K$. This is translated as a flatter peak in the thermal conductivity (see Fig.6.1 (c)). On the contrary, in the sample with the smallest Γ, that is ^{70}Ge99.99, the transition happens in a more narrow interval of temperature, T $[8, 80]K$, and the peak of the thermal conductivity is sharper. This means that the higher the isotopic purity is, the more abrupt and quick the transition from the kinetic to the collective regime, and consequently, the sharper the thermal conductivity peak. In terms of relaxation times, this situation is explained, because if Γ is very high, τ_I is very small and becomes the dominating scattering process or at least is competing with τ_U during a wider range of temperature, this slows down the transition.

[1]Note that in the previous Chapter, the value was 0.9, not much error is induced with this new set of parameters.

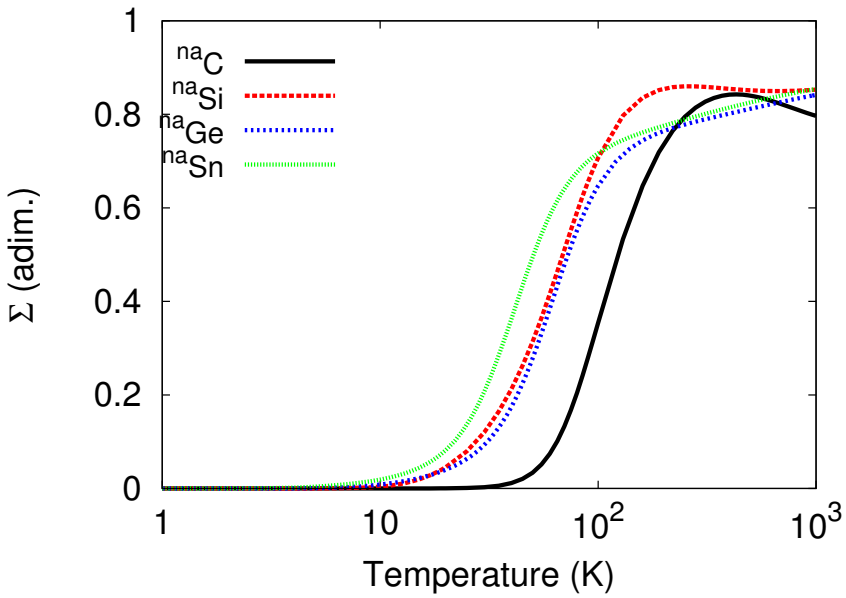

Figure 6.3: Switching factor Σ as a function of temperature in a semilogarithmic plot for the naturally occurring samples.

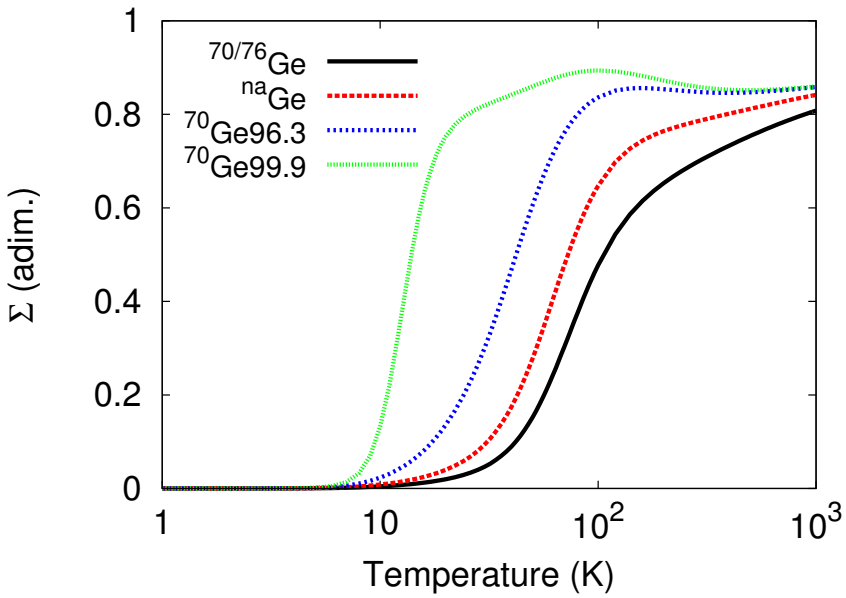

Figure 6.4: Switching factor Σ as a function of temperature in a semilogarithmic plot for the set of germanium samples with several isotopic compositions.

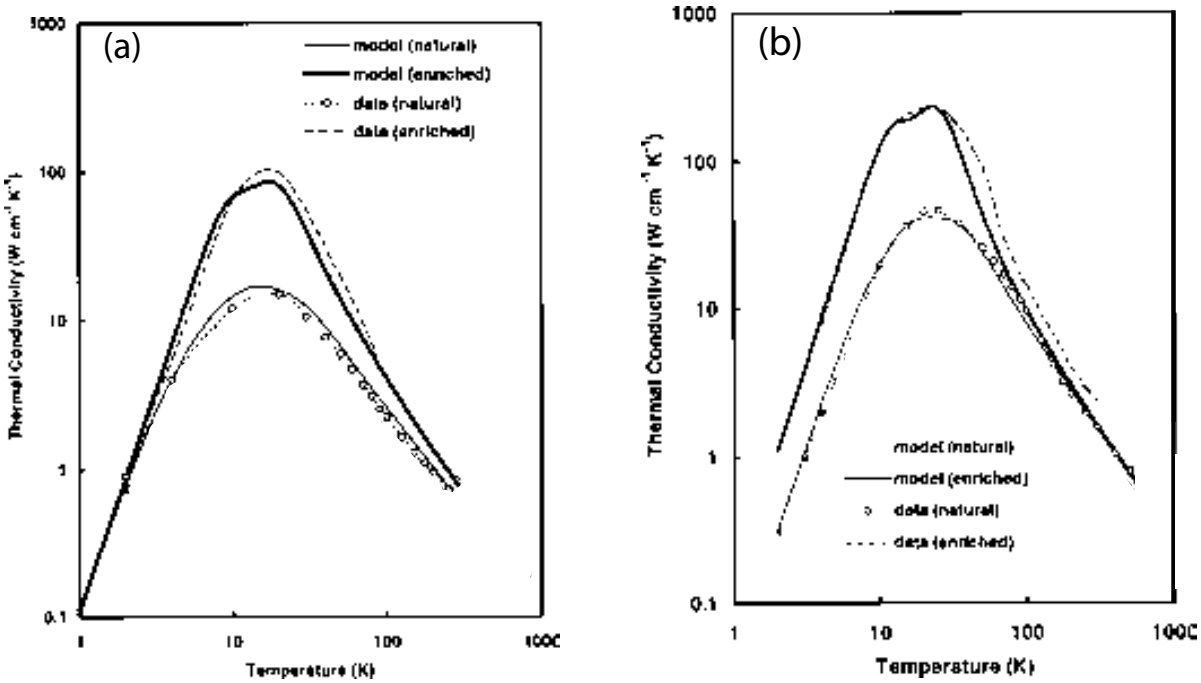

Figure 6.5: Thermal conductivity of natural and enriched (a) germanium and (b) silicon, calculated with Morelli's model, compared to experimental measures from [24, 74, 102]. The isotopic composition of the Ge and Si samples are $^{\mathrm{na}}Ge$, $^{70}Ge99.99$, $^{\mathrm{na}}Si$, ^{28}Si, *from Table 6.4, but note that the Si samples differ in size. Figures extracted from [27].*

6.3.2 Comparison with other models

It is worthy to compare our model and results with previous works aiming to fit a set of materials with a single model using a single set of relaxation times. Morelli *et al.* presented quite recently a paper with this objective [27]. They calculated the thermal conductivity of Ge, Si, C, SiC, BN and GaN using a Debye-Callaway formula taking into account transversal and longitudinal acoustic branches. Let us focus on Ge, Si and C to compare with our model. The set of relaxation times they proposed is the following:

$$\tau_{U,i}^{-1} = B_{U,i}\omega^2 T \exp\left(- \quad {}_{D,i}/3T\right) \tag{6.13}$$

where $i = L, T$ denotes the phonon branch.

$$\tau_{N,L}^{-1} = B_{N,L}\omega^2 T^3 \quad \text{and} \quad \tau_{N,T}^{-1} = B_{N,T}\omega T^4 \tag{6.14}$$

$$\tau_{I,i} = \quad \frac{V\Gamma}{4\pi v_i^3}\omega_j^4 \quad {}^{-1} \tag{6.15}$$

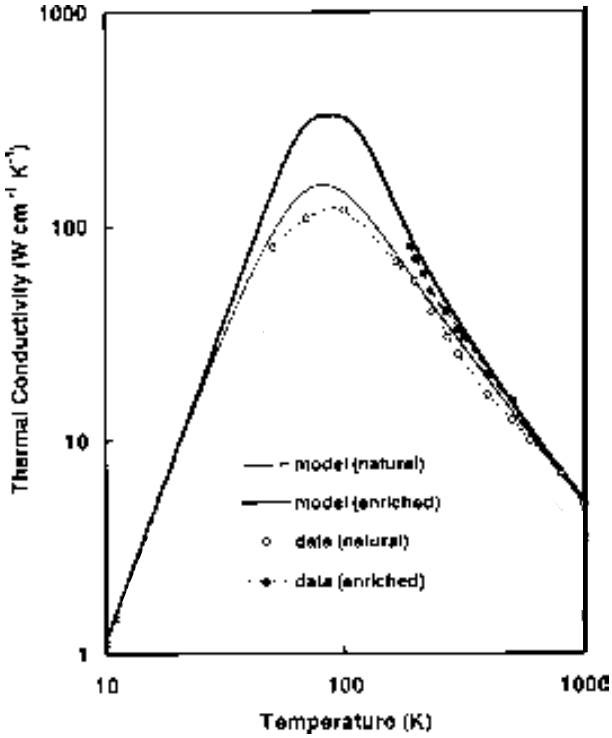

Figure 6.6: Thermal conductivity of natural and enriched diamond, calculated with Morelli's model, compared to experimental measures from [103]. The isotopic composition of the C samples are $^{\mathrm{na}}C$ *and*^{13}C *from Table 6.4. Figures extracted from [27].*

$$\tau_{B,i} = d/v_i \tag{6.16}$$

d is the effective diameter of the sample which is fitted to the experimental data. From Eq. (6.1) they obtain the values of the parameters $B_{U,T}, B_{U,L}, B_{N,T}, B_{N,L}$ in terms of mean values for the Grüneisen parameter and velocity for each branch $_T$, $_L$, v_T and v_L. The values $_T$, $_L$ are fitted for each material. Therefore, they have three adjustable parameters $_T$, $_L$ and d which are fitted individually to each material using the naturally occurring sample, this raises a total of 9 fitting parameters in the model. The isotopically enriched samples are then predicted changing the value of Γ, as usual. We show in Figs.6.5 and 6.6 the results provided by Morelli *et al.* [27]. Note that the naturally occurring samples are well fitted, but for the isotopically enriches samples are not correctly predicted, specially in silicon. Similar modeling techniques have been used with diamond. See for instance the work by Barman and Srivastava [97], where they also fit individually each parameter to each diamond sample with different isotopic composition. The work by Morelli *et al.* is valuable because they study

the dependence of the phonon-phonon relaxation time parameters in term of the properties of the material. The main drawback of the Morelli's model that they use Eq. (6.1) to fit individually each material's thermal conductivity, while we use Eq. (6.1) to related the material's parameters between them. Consequently our model let us not only to reduce the number of free adjustable parameters, but to improve the prediction power.

From these results it can be deduced that usual relaxation times expressions are good enough to calculate thermal conductivity, and that some of the issues when fitting experimental values could be related to the phenomenological model. Further improvements of the model can be achieved by a more precise calculation of the B as a function varying with temperature or even with frequency, as $B(\omega, T) \qquad (\omega, T)/v(\omega)$. In conclusion, we have shown that using a kinetic-collective model, the thermal conductivity can be predicted for a group of samples of several materials without additional fitting parameters. The model allows to interpret the behavior of the thermal conductivity as a transition from a kinetic to a collective regime. The transition happens as normal scattering gains importance versus resistive scatterings. The results shed light on the understanding of the phonon-phonon interaction in this kind of samples.

Chapter 7

Applying the Kinetic-collective model to Bi_2Te_3

In this Chapter we apply the Kinetic-collective model to a well-known thermoelectric material: bismuth telluride (Bi_2Te_3). Bi_2Te_3 is a highly anisotropic material with a lattice structure considerably different from that of the group-IV materials examined in the previous Chapter. As a consequence, the values of its thermal conductivity vary significantly when samples built along different crystallographic orientations are measured [104]. This fact is clearly an advantage at the time to tailor the thermoelectric properties of this material. In a collaboration between the Group of Nanomaterials of the Autonomous University of Barcelona (GNaM) and the Institute of Microelectronics of CSIC-Madrid, some p-type Bi_2Te_3 nanowires with diameters d=350 nm and d=120 nm have been grown oriented in the direction [110]. The finality of this testing NWs is to study their thermoelectric efficiency to eventually fabricate a thermoelectric module made of p-type and n-type NW arrays embedded in a matrix. For this preliminary study, theoretical predictions of the behavior with size of the NWs' thermal properties are desirable. Our role in this collaboration is to predict the thermal conductivity of such NWs. Having tested previously our model on other materials, as shown in Chap. 5 and 6, this analysis on Bi_2Te_3 is a check that the model is consistent for different material atomic structures, and we can provide, at least, a reliable picture of the global trend of the thermal conductivity behavior with size and temperature. This way, our model intends to be a concise tool for both theoretical and experimental researchers.

Table 7.1: Bi_2Te_3 properties: Debye temperature Θ_D, atomic mass M, atomic volume V, and Umklapp extinction temperature Θ_U.

Material	$_D$ (K)	M (g mol^{-1})	V (m^3)	Γ	$_U$ (K)
Bi_2Te_3	160	800.7	174.03 10^{-30}	8.21 10^{-5}	4

Table 7.2: Values of Γ, diameter d for NWs, and the effective size L_{eff} for naturally occurring Bi_2Te_3 samples.

Sample	Γ	dimensions	L_{eff}
Bulk	8.21 10^{-5}	-	-
350nm NW	8.21 10^{-5}	$d = 350$ nm	350 nm
120nm NW	8.21 10^{-5}	$d = 120$ nm	120 nm

7.1 Inputs for the calculations

Some properties of the Bi_2Te_3 required for the thermal conductivity calculation are summarized in Table 7.1. The properties of the samples appear in Table 7.2. The dispersion relations along [110] were obtained in Chap. 2 (see Fig.2.11), where we also show the obtained density of states (see Fig.2.13) and the specific heat (see Fig.2.14). On the other hand, the relaxation times deserve a little discussion. Since the lattice structure of the Bi_2Te_3 is different from the diamond structure, the expressions for τ_N (3.37) and τ_U (3.38) must be modified accordingly.

7.1.1 Relaxation times expressions

Preliminary measurements with the 3-ω method at room temperature carried out by our collaborators show that $_{350\text{nmNW}} = 1.37 \pm 0.2$ Wm^{-1}K^{-1} (see Ref. [105]) and $_{120\text{nmNW}} = 0.7 \pm 0.2$ Wm^{-1}K^{-1}, while for the bulk $_{\text{bulk}} = 2.4 \pm 0.2$ Wm^{-1}K^{-1}. Note that the lack of experimental measurements along with a wider range of temperatures for the bulk sample increases the the uncertainty of the predictions, because the behavior of the phonon-phonon interactions in this type of material is still very unclear and to the best of our knowledge there are no feedback from *ab-initio* techniques providing expressions for τ_U and τ_N, unlike the case of silicon. Nevertheless, in this work, as a first approximation, we suggest to use the following expressions for the relaxation times. For the boundary scattering we maintain the usual Casimir expression

$$\tau_B(\omega_\nu) = L_{\text{eff}}/v(\omega_\nu) \quad , \tag{7.1}$$

as we did in the previous Chapters for the other materials. For the impurity scattering we use, as in the case of Silicon, the expression given by Tamura [64], since it accounts for the density of states in the given direction

$$\tau_I(\omega_\nu) = \frac{6}{\pi}\left(V\Gamma\omega_\nu^2 D(\omega_\nu)\right)^{-1} \quad , \tag{7.2}$$

although this expression should be taken with caution, since in its derivation some approximations were made regarding the cubic lattice structure of diamond-like materials. The normal and Umklapp relaxation times requires further discussion. As we know, their dependence with frequency and temperature is such that $\tau_{U/N} \quad \omega^a T^b$. For the normal scattering we suggest to use, for analogy, the expression used for Si, but the appropriate values of the frequency and temperature exponents are $a = 3$ and $b = 2$ for the crystal structure of Bi_2Te_3 at low temperatures, according to the values tabulated by Herring [58]. Thus,

$$\tau_N(\omega_\nu) = \frac{1}{B_N T^2 \omega_\nu^3 [1 - \exp(-3T/\ \ _D)]} + \frac{1}{B_{N'} T} \quad . \tag{7.3}$$

For the Umklapp scattering, the situation is slightly different. Note that the Debye temperature of Bi_2Te_3 is very low ($_D$=160 K). Room temperature (T=300 K) is well above $_D$, so it can be considered in the range of high-temperatures. At this range, the Umklapp scattering is expected to behave, as in the case of normal scattering, as $\tau_U^{-1} \quad B_U T$. Since the thermal conductivity is very low, it is expected to be dominated by the Umklapp collisions. Furthermore, the Umklapp extinction temperature $_U$ is found to be very low (4 K). From this reasoning, we suggest to use the expression

$$\tau_U = \frac{\exp(\ \ _U/T)}{B_U T[1 - \exp(-3T/\ \ _D)]} \quad . \tag{7.4}$$

Recently, Cahill and collaborators [106] have proposed similar empiric expressions for τ_U and τ_N following the work by Morelli *et al.* we have discussed in the previous Chapter [27]. For the Umklapp relaxation time they use the same expression as Morelli used for diamond-like materials, that is

$$\tau_{U,i} = (B_{U,i} T\omega^2 \exp(\ \ _{D,i}/3T))^{-1} \quad . \tag{7.5}$$

with $i = T, L$ indicating the acoustic branch. However, they use different exponents a, b than those used by Morelli for the normal relaxation time, being

$$\tau_{N,i} = (B_{N,i} T\omega^2)^{-1} \quad , \tag{7.6}$$

Table 7.3: Fitting parameters for Bi_2Te_3 bulk.

	B_U (s^3K^{-1})		B_N (sK^{-3})		B_N ($s^{-1}K^{-1}$)	
This model	7.0	10^5	0.75	10^{-32}	4.0	10^5

but no reasoning is given for such choice.

7.2 Bi_2Te_3 thermal conductivity

According to the procedure followed along this work, we have first calculated the thermal conductivity of the bulk sample. The values of the fitting parameters B_U, B_N and B_N providing a reasonable tendency of the thermal conductivity with temperature, in agreement with the available experimental data, are shown in Table 7.3. The resulting curve for (T) is shown in Fig. 7.1. Next, by changing the value of L_{eff} by those corresponding to the NWs (see Tab. 7.2), we obtain their thermal conductivity, also shown in Fig.7.1, being in reasonable agreement with data at room temperature.

As expected, the thermal conductivity is very near to the pure kinetic regime, since this material has a very low thermal conductivity (very resistive). This is a hint to believe that along the considered temperature intervals, the dominating scattering mechanism is the Umklapp scattering. As we discussed in the previous Section, as the temperature reaches the Debye temperature the probability of resistive three-phonon processes to occur is very high, and according to Pomeranchuk [107], even four-phonon processes should be taken into account since their probability to happen increases when we exceed the Debye temperature.

Note that, due to the different synthesis and characterization techniques [108], it is still not clear how much reduction may suffer the thermal conductivity when nano structuring this material, specially at the 50-100nm size-scale [109]. Actually, in the literature we can find very different values of the thermal conductivity for such small wires. On one hand, values of an order of magnitude lower than bulk [110]. On the contrary, values near those of bulk [111]. Therefore, it is very difficult to figure out a theoretical way to predict which type of system will have more desirable thermoelectric efficiency. While awaiting more experimental data on the reported nanowires, our theoretical thermal conductivity predictions on the behavior of with temperature and size may provide useful information to experimentalist, and it is a useful tool to study the potential thermoelectric interest of these NWs, as we will discuss in the next Section.

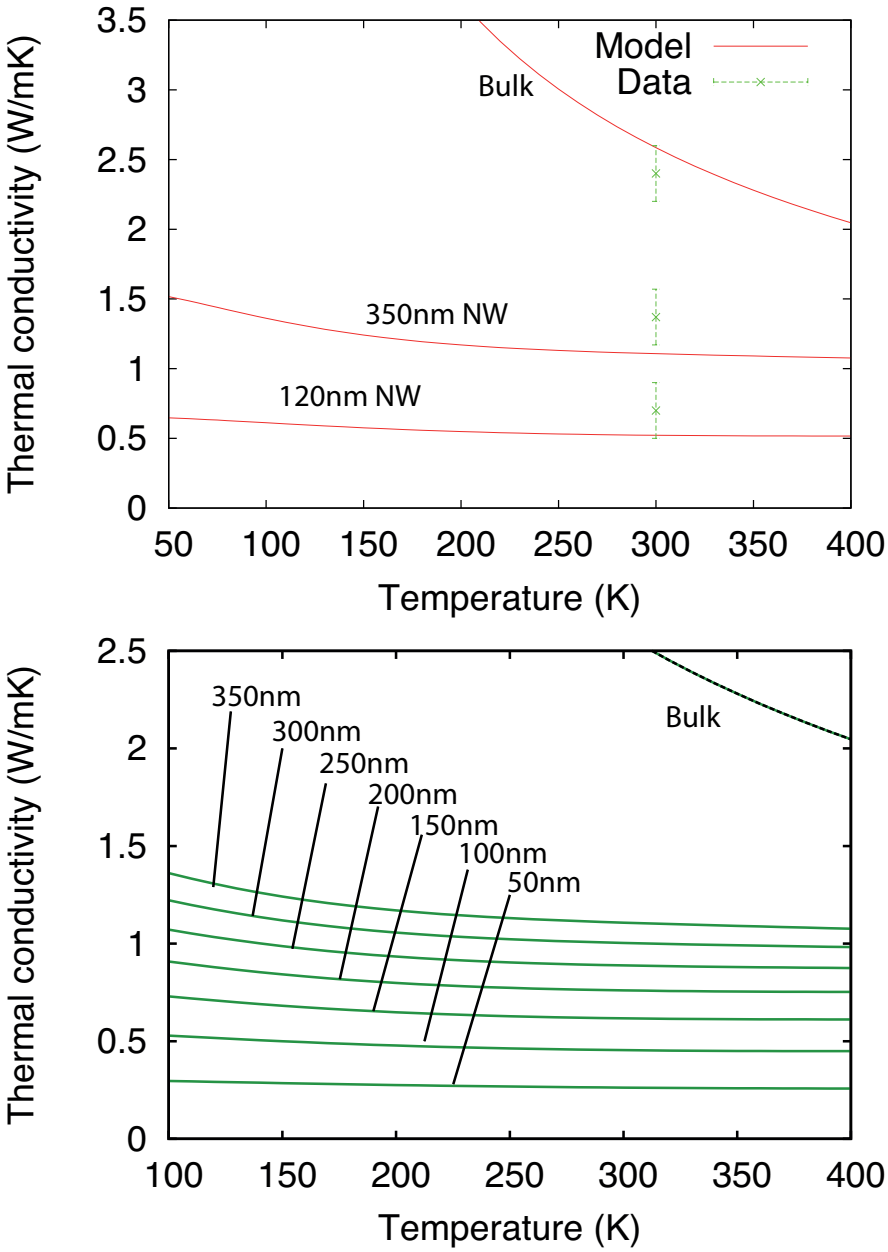

Figure 7.1: (a) Thermal conductivity of bulk Bi_2Te_3 and NWs with several diameters oriented in the crystallographic direction-[110] compared to experimental experimental measurements (symbols). (b) Thermal conductivity prediction of a set of NWs with diameters ranging from 350 nm to 100 nm. Bulk is also shown for reference.

7.3 Thermoelectric applications

We assume a thermoelectric nanowire of radius r and length L whose ends are kept at temperatures T_H and T_L (High and Low temperatures, respectively). As a consequence of Seebeck effect, the temperature difference produces a voltage difference, which may be the source of an electric current. The maximum efficiency of the thermoelectric energy conversion is

$$_{max} = \frac{T_H - T_L}{T_H} \frac{\overline{1 + ZT_{av}} - 1}{\overline{1 + ZT_{av}} + T_L/T_H}, \tag{7.7}$$

with T_{av} the average temperature $T_{av} = \frac{1}{2}(T_H + T_L)$. Thus, the thermoelectric figure of merit

$$Z = S^2 \quad / \tag{7.8}$$

with S the Seebeck coefficient, the electrical conductivity and the thermal conductivity, is the key material parameter in the expression for the efficiency. As it is well known, one of the ways of enhancing the value of Z is by reducing the thermal conductivity, which is the sum of the phonon and the electron (and hole) contributions, $_p$ and $_e$ respectively.

We will take into consideration an important effect: The increase of the efficiency as a result of a reduction of the thermal conductivity due to size-effects.

Therefore, reducing r reduces the phonon effective conductivity and enhances the value of Z. Since the electronic mean free path is usually much shorter than that of phonons, we will consider that $_e$ is not modified by the radius. In addition, $_p >> _e$, so we will consider $_e$ as a constant value indirectly included in the fitting of $_p$ to the bulk data. If one considers only the r dependence of the thermal conductivity, one has that the smaller the radius, the higher value of Z, and there is not a finite optimal nanowire radius. To study the enhancement of ZT due to the reduction of , we have simulated the 350 nm and 120 nm diameter NWs with COMSOL Multiphysics. The nanowires have the same length 20 μm, and the bottom of the nanowire is fixed at room temperature. The calculations are made are under vacuum conditions to avoid heat dissipation. Further, we have assumed bulk values for S and for the sake of simplicity, since for these nanoscale sizes they are expected not to vary significantly, but in general both will depend on the size as well. In Fig. 7.2 we show the calculated value of the figure of merit as a result of the predicted .

If we apply an electric voltage to the NW, then a temperature difference is generated between the ends of the NW and viceversa. This is the thermoelectric effect. In Fig 7.3 we show the results of the simulation of the ΔT generated for an applied voltage ranging

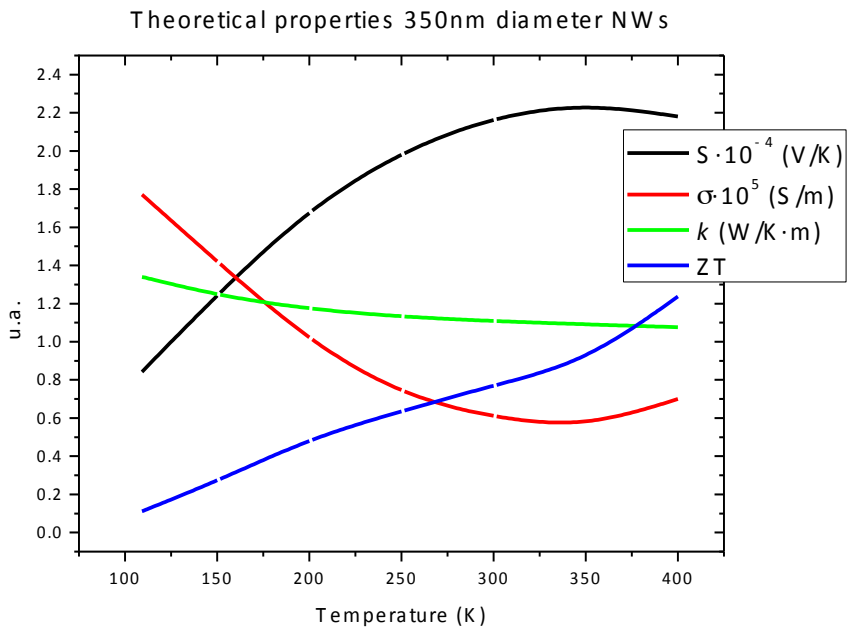

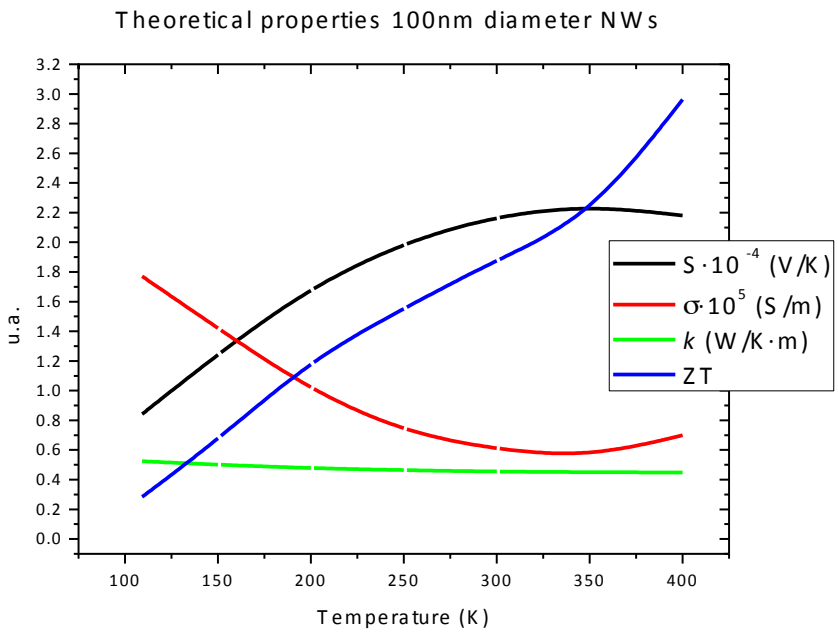

Figure 7.2: Bi_2Te_3 thermal properties for 350 nm and 100 nm NWs at several temperatures. S and are taken from bulk as it is not expected to change for these NWs' diameter range. is calculated with the BCM. ZT calculated with Eq. (7.8) Courtesy of M.M. Rojo.

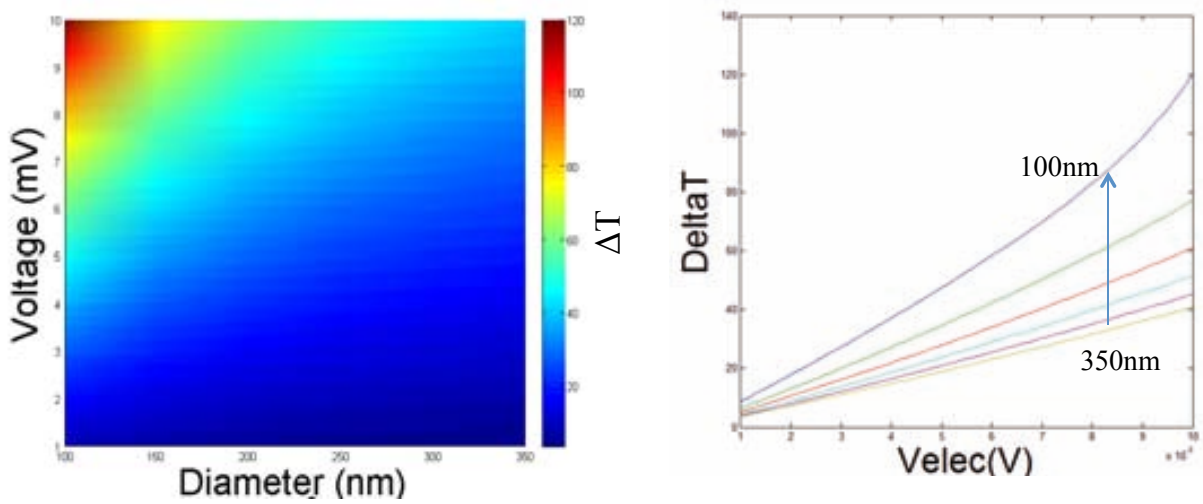

Figure 7.3: Voltage vs temperature difference for the several NWs with diameters ranging from 350 nm to 100nm. Courtesy of M.M. Rojo.

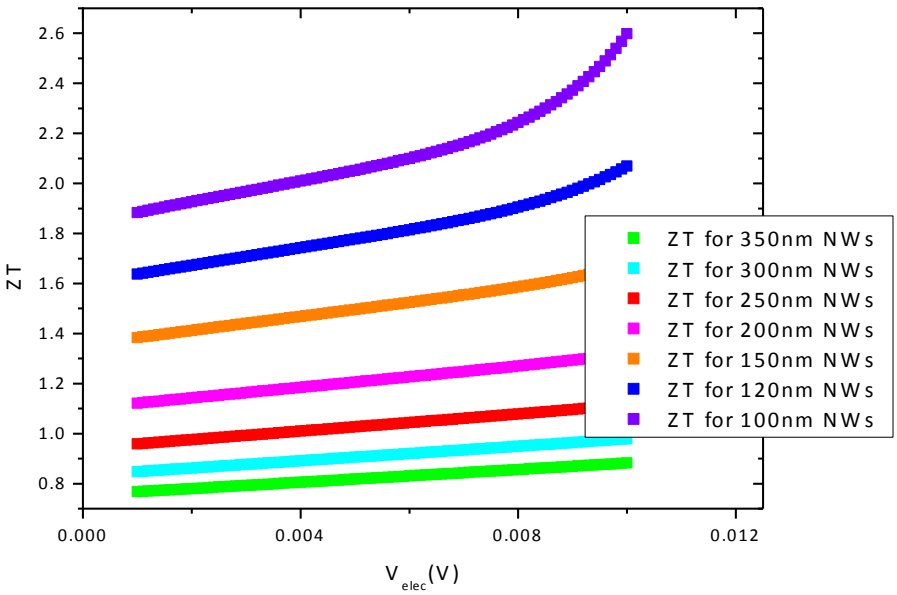

Figure 7.4: ZT calculated with with Eq. (7.8 entering the values shown in Fig. 7.2 with T being the average temperature corresponding to the temperature difference generated by the corresponding voltage, for the set of NWs with diameters ranging from 350 nm to 100nm.Courtesy of M.M. Rojo.

from [1-10] mV, for different diameters of the NWs. With this, we can calculate the ZT_{av} in terms on the voltage for each NW. The results are shown in Fig.7.4. In the plot we can observe that the figure of merit ZT is expected to increase above 1.6 for the 100nm NW under certain values of the applied voltage across the sample, while the 350nm NW remains near bulk values. Although this preliminary study is a first approximation in ideal conditions, it is a good starting point for further research. A refinement in the calculations will include measured values of the electric conductivity and Seebeck coefficient in the nanowires, and taking into account the electronic contribution to the thermal conductivity by using a simple model which could provide reliable values at the nanoscale.

Chapter 8

Conclusions

In this last Chapter we stress and summarize the main conclusions of this Ph.D. Thesis:

1. **Thermal transport regimes**
   Whereas the role of resistive scattering (Umklapp, impurities, boundaries) is well-known and it is the basis of most current models of thermal conductivity, the role of normal scattering has been much more confuse and elusive. This work shows that a key point for an accurate description of the thermal conductivity of semiconductor materials in the whole range of temperatures is taking into account the effect of normal processes on the phonon collective behavior. The consequence of the well-defined incorporation of normal processes, followed by the theoretical formulation by Guyer and Krumhansl, led us to stablish two well differentiated thermal transport regimes: the kinetic and the collective, depending on which scattering mechanism (resistive or normal) is dominating the transport. Here, for the first time, a complete study of the thermal conductivity in terms of these two thermal transport regimes is developed and implemented in several materials.

2. **The Kinetic regime**
   In the kinetic regime N-processes are negligible. Each phonon mode contributes independently to the heat flux and so the equation of the entropy production balance must be fulfilled individually by each mode.

3. **The Collective regime**
   In the collective regime N-processes dominate. Momentum is conserved and shared among the phononic modes through N-processes, this enhances the effect of the resistive

processes. The phonons behave as a collectivity, rising a total heat flux and so the equation of the entropy production balance must be fulfilled globally.

4. **Switching factor**
   We have included a switching factor (Eq. (4.75)) that determines the transport regime in terms of the normal and resistive mean scattering times. The continuos transition between both regimes happens as normal scattering gains importance versus resistive scatterings. Such a switching factor was already proposed by Guyer and Krumhansl, but it had not been applied since then. Here, we have further clarified its physical meaning and practical relevance.

5. **Higher-order non-equilibrium effects**
   We have also included higher-order non-equilibrium effects through an analytical function $F(L_{\text{eff}})$ (Eq. 4.80) in the collective term of the thermal conductivity to generalize the model to any kind of samples depending on its geometry and characteristic size. This factor, which was not considered by Guyer and Krumhansl, improves the agreement with the experimental data. It has also a conceptual interest, because in principle, the Knudsen number acts as an indicator of when high-order effects should be considered.

6. **Thermal conductivity in the Kinetic-collective model**
   The expression of (Eq. (4.81)) given by the Kinetic-collective model is valid for all ranges of temperatures. This expression is obtained by combining both the variational method and the relaxation-time approximation approaches under entropic considerations. This equation provides a new insight into the underlying physics of thermal transport. It introduces a thermodynamic perspective at a mesoscopic level that allows us to understand the differences in phonon behavior in terms of the average of the phonon-phonon processes.

7. **Predictions of thermal conductivity for bulk materials**
   We have applied the Kinetic-collective model to calculate the thermal conductivity of a number of bulk samples of group IV semiconductors with different isotopic compositions without additional fitting parameters. The model allows us to interpret the behavior of the thermal conductivity in terms of temperature as a transition from a kinetic to a collective regime. The results can shed light to the understanding of the phonon-phonon interaction in this kind of samples.

8. **Predictions of thermal conductivity at the nanoscale**
   Our thermal conductivity predictions of silicon thin-films and nanowires, and bismuth telluride nanowires with characteristic sizes above 30 nm are in good agreement with experimental data. We show that confinement or quantum effects are not necessary to understand the lattice thermal transport above these sizes and that the difficulty of prediction at the nanoscale seems to be closely related to the thermodynamic treatment of phonon-phonon interactions. At the same time, this allows us to establish a lower limit for classical models, where bulk properties are enough to understand the phenomenology. Only below this limit, of the order of a few tens of nanometers, confinement effects may play a role.

9. **Role of optic phonons in thermal transport**
   By studying the spectral density of the thermal conductivity in silicon bulk and nanowires, we have confirmed with our phenomenologic model, what other molecular dynamics model predicted: a contribution of about 15% of the optical phonons in the thermal conductivity in nanowires. Further, we have shown that the cause may be their enhancement through N-processes.

10. **Relaxation times**
    We have proposed new expressions for phonon-phonon scattering rates which contain only 3 adjustable parameters. We have found that for a family of materials with the same lattice structure (group-IV) they are related between them through some material properties. This makes possible to calculate their values instead of fitting them.

11. **Lattice dynamics**
    A considerable part of the computational effort of this thesis has been the explicit calculations of the dispersion relations and the corresponding density of states of the materials we have studied. Although it is not an original result, it has required a much time-consuming effort, but using realistic dispersion relations in the thermal conductivity integral it is a required step to study the participation in the thermal transport of the whole frequency spectrum of phonons.

12. **Overall conclusion**
    We have shown that an accurate treatment of N-processes not only leads to a correct description of the thermal conductivity of samples made of a given material with sizes ranging from macroscale down to nanoscale, but also provides an accurate description of

the thermal conductivity of several materials with both similar and different characteristics. Although the model may have some limits of application (not valid for extremely reduced samples), it is expected to be general.

13. **Publications**
The results of this research have been presented in the following publications:

- C. de Tomas, A. Cantarero, A.F. Lopeandia, F.X. Alvarez, "From kinetic to collective behavior in the thermal transport on semiconductors and semiconductor nanostructures." *J. Appl. Phys.* **115**, 164314 (2014).
- C. de Tomas, A. Cantarero, A.F. Lopeandia, F.X. Alvarez, "Thermal conductivity of group IV semiconductors from a kinetic-collective model." *Proc. Roy. Soc. A* **470**, 2169 (2014).
- C. de Tomas, A. Cantarero, A.F. Lopeandia, F.X. Alvarez, "Lattice thermal conductivity of Si nanowires". *J. Thermoelectricity*, **4**, 11 (2013).
- C. de Tomas, A. Cantarero, A.F. Lopeandia, F.X. Alvarez, "The role of optic phonons in thermal transport" (submitted).

14. **Open perspectives**
The open problems which could be explored with our method and concepts are:

(a) Application to other kinds of materials, as NGa, PbTe, and others, deserving much current attention because of their interest in thermoelectric conversion.

(b) Application to more complicated geometries, as for instance, porous Si or porous Ge phononic crystals or to SiGe superlattices. Application to functionally graded systems, *i. e.* to continuously inhomogeneous systems along the heat flux direction, trying to improve the ZT values in thermoelectric energy conversion.

(c) Effects of quantum confinement when the size of the nano system becomes comparable to the thermal wavevector of phonons by using the dispersion relations of the nanosystem instead those of the bulk.

(d) To find an accurate description of backscattering effects of phonons against rough surfaces on the thermal conductivity.

Appendix A

The Ewald's method is a mathematical treatment of the Coulomb's sum with the purpose of accelerating the convergence of the series (an alternate series, slowly convergent) and was derived by P.P. Ewald in the works [40, 41].

The Coulomb matrix is defined as

$$C_{\alpha\beta}(\boldsymbol{q};\quad) = \sum_{\boldsymbol{l}'} \quad {}_{\alpha\beta}(\boldsymbol{l}\quad,\boldsymbol{l}\quad)e^{i\boldsymbol{q}\cdot(\boldsymbol{r}_{\boldsymbol{l}\kappa}-\boldsymbol{r}_{\boldsymbol{l}'\kappa'})} \tag{8.1}$$

where $\boldsymbol{l}$ is a reference lattice, since we calculate the energy per unit cell (actually, we can take $\boldsymbol{l} = 0$). The force coefficients

$$_{\alpha\beta}(\boldsymbol{l}\quad,\boldsymbol{l}\quad) = ez_{\kappa}\frac{{}^{2}/}{x_{\alpha,\boldsymbol{l}\kappa}\quad x_{\beta,\boldsymbol{l}'\kappa'}}, \tag{8.2}$$

are the derivative of the electrostatic energy or, extracting the factor ez_{κ}, the derivatives of the electrostatic potential due to the charge $ez_{\kappa'}$ on the point where the charge ez_{κ} is located, times ez_{κ}. This is also denominated interaction energy. The sum is performed over all the atoms in the reference cell and all other atoms in the whole crystal.

Explicitly, the interaction energy (per unit cell) can be written as:

$$U^{Coulumb}(\boldsymbol{l}) = \frac{1}{4\pi\ {}_{0}}\sum_{\substack{\boldsymbol{l}'\kappa'\\ \kappa}}\frac{e^2 z_{\kappa}z_{\kappa'}}{|\boldsymbol{r}_{\boldsymbol{l}\kappa}-\boldsymbol{r}_{\boldsymbol{l}'\kappa'}|} \tag{8.3}$$

The Coulomb potential due to the charge $ez_{\kappa'}$ is

$$/^{\mathrm{C}}(\boldsymbol{r}-\boldsymbol{r}_{\boldsymbol{l}'\kappa'}) = \frac{1}{4\pi\ {}_{0}}\frac{ez_{\kappa'}}{|\boldsymbol{r}-\boldsymbol{r}_{\boldsymbol{l}'\kappa'}|} \tag{8.4}$$

Let us consider a Gaussian charge distribution

$$^{\mathrm{G}}(\boldsymbol{r}-\boldsymbol{r}_{\boldsymbol{l}'\kappa'}) = ez_{\kappa'}\ \ \frac{}{\pi}\ \ {}^{3/2}e^{-\eta|\boldsymbol{r}-\boldsymbol{r}_{\boldsymbol{l}'\kappa'}|^2} \tag{8.5}$$

In order to check the value of the charge corresponding to this distribution let us take the origin of coordinates at $\boldsymbol{r}_{\boldsymbol{l}'\kappa'}$.

$$q = \quad {}^{\mathrm{G}}(\boldsymbol{r})d^3\boldsymbol{r} = ez_{\kappa'}4\pi\ \ \frac{}{\pi}\ \ {}^{3/2}\quad {}_{0}\quad r^2e^{-\eta r^2}dr = ez_{\kappa'}\frac{4}{\pi}\quad {}_{0}\quad {}^{2}e^{-\zeta^2}d \tag{8.6}$$

The integral in can be obtained after integration by parts,

$$_0 \quad {}^2 e^{-\zeta^2} d \;=\; \begin{matrix} u = & du = d \\ dv = \; e^{-\zeta^2} d & v = -\dfrac{1}{2} e^{-\zeta^2} \end{matrix} \;= \frac{1}{2} \quad _0 \quad e^{-\zeta^2} d \;= \frac{\overline{\pi}}{4} \tag{8.7}$$

i.e. $q = ez_{\kappa'}$. The idea of Ewald is to add and subtract the point charge by an equivalent charge distribution in the way:

$$/^{\mathrm{C}} = /^{\mathrm{G}} + \left(/^{\mathrm{C}} - /^{\mathrm{G}}\right) \equiv /^{\mathrm{G}} + /^{\mathrm{H}} \tag{8.8}$$

The first potential is due to the Gaussian distribution and the second to the difference between the original Coulomb potential and the one corresponding to the Gaussian distribution. Actually, we need the second derivative of the potentials. Let us work first with the first potential $/^{\mathrm{G}}$ and arrive to a final expression for the Coulomb matrix corresponding to this contribution. In order to find the derivatives it is more convenient to expand the potential in a Fourier series as:

$$/^{\mathrm{G}}(\boldsymbol{r} - \boldsymbol{r}_{l'\kappa'}) = \sum_{\boldsymbol{\tau}} /^{\mathrm{G}}(\boldsymbol{\tau}) e^{i\boldsymbol{\tau}\cdot(\boldsymbol{r}-\boldsymbol{r}_{l'\kappa'})} \tag{8.9}$$

Thus,

$$_{\alpha\beta}(\boldsymbol{l} \;\; , \boldsymbol{l} \quad) = ez_{\kappa} \sum_{\boldsymbol{\tau}} \tau_\alpha \tau_\beta /^{\mathrm{G}}(\boldsymbol{\tau}) e^{i\boldsymbol{\tau}\cdot(\boldsymbol{r}-\boldsymbol{r}_{l'\kappa'})} \tag{8.10}$$

Now, we need the Fourier transform component of the potential. This is obtained through the Poisson equation, expanding both the potential and charge density in Fourier series:

$$\boldsymbol{\nabla}^2 \sum_{\boldsymbol{\tau}} /^{\mathrm{G}}(\boldsymbol{\tau}) e^{i\boldsymbol{\tau}\cdot(\boldsymbol{r}-\boldsymbol{r}_{l'\kappa'})} = -\sum_{\boldsymbol{\tau}} \tau^2 /^{\mathrm{G}}(\boldsymbol{\tau}) e^{i\boldsymbol{\tau}\cdot(\boldsymbol{r}-\boldsymbol{r}_{l'\kappa'})} = -\frac{1}{_0} \sum_{\boldsymbol{\tau}} \quad ^{\mathrm{G}}(\boldsymbol{\tau}) e^{i\boldsymbol{\tau}\cdot(\boldsymbol{r}-\boldsymbol{r}_{l'\kappa'})} \tag{8.11}$$

Since the Fourier components are orthogonal,

$$/^{\mathrm{G}}(\boldsymbol{\tau}) = \frac{1}{_0 \tau^2} \quad ^{\mathrm{G}}(\boldsymbol{\tau}) \tag{8.12}$$

We need to calculate the Fourier component of the Gaussian distribution. From the book of Born&Huang [Eq. (22.22), p. 216],

$$^{\mathrm{G}}(\boldsymbol{\tau}) = \frac{1}{v_a} \quad _{\mathrm{cell}} \quad ^{\mathrm{G}}(\boldsymbol{r}) e^{-i\boldsymbol{\tau}\cdot\boldsymbol{r}} d^3\boldsymbol{r} = \frac{1}{V} \quad _{\mathrm{whole\,space}} \quad ^{\mathrm{G}}(\boldsymbol{r}) e^{-i\boldsymbol{\tau}\cdot\boldsymbol{r}} d^3\boldsymbol{r} \tag{8.13}$$

since we are dealing with a continuous distribution in the whole space (V is the total volume of the crystal and v_a the unit cell volume).

$$^{\mathrm{G}}(\boldsymbol{\tau}) = ez_{\kappa'} \quad \frac{}{\pi} \quad ^{3/2} \frac{2\pi}{V} \quad _0 \quad r^2 dr e^{-\eta r^2} \quad ^{+1}_{-1} \quad e^{i\tau r\zeta} d \;= ez_{\kappa'} \quad \frac{}{\pi} \quad ^{3/2} \frac{2\pi}{i\tau V} \quad _0 \quad r dr e^{-\eta r^2} e^{i\tau r} - \text{c.c.} \tag{8.14}$$

If we change r by $-r$ in the second integral, the integral to calculate becomes

$$\int_{-\infty}^{\infty} r dr e^{-\eta r^2} e^{i\tau r} = \frac{i\tau}{2} \frac{\sqrt{\pi}}{\eta^{3/2}} e^{-\tau^2/4\eta} \tag{8.15}$$

This is the Fourier transform (in one dimension) of the function $re^{-\eta r^2}$. The final result is

$$\phi^{\mathrm{G}}(\boldsymbol{\tau}) = \frac{ez_{\kappa'}}{V} e^{-\tau^2/4\eta} \tag{8.16}$$

and the potential

$$\varphi^{\mathrm{G}}(\boldsymbol{\tau}) = \frac{ez_{\kappa'}}{V\varepsilon_0 \tau^2} e^{-\tau^2/4\eta} \tag{8.17}$$

From (8.18),

$$\Phi^{\mathrm{G}}_{\alpha\beta}(\boldsymbol{l}, \boldsymbol{l}') = \frac{e^2 z_\kappa z_{\kappa'}}{\varepsilon_0} \sum_{\boldsymbol{\tau}} \frac{\mathcal{T}_\alpha \mathcal{T}_\beta}{\tau^2} e^{-\tau^2/4\eta} e^{i\boldsymbol{\tau}\cdot(\boldsymbol{r}_{\boldsymbol{l}\kappa} - \boldsymbol{r}_{\boldsymbol{l}'\kappa'})} \tag{8.18}$$

The Coulomb matrix becomes

$$C^{\mathrm{G}}_{\alpha\beta}(\boldsymbol{q}; \eta) = \frac{e^2 z_\kappa z_{\kappa'}}{\varepsilon_0} \sum_{\boldsymbol{\tau}} \frac{\mathcal{T}_\alpha \mathcal{T}_\beta}{\tau^2} e^{-\tau^2/4\eta} e^{i(\boldsymbol{\tau}+\boldsymbol{q})\cdot(\boldsymbol{r}_\kappa - \boldsymbol{r}_{\boldsymbol{\kappa}'})} \sum_{\boldsymbol{l}'=1}^{N} e^{i(\boldsymbol{\tau}+\boldsymbol{q})\cdot(\boldsymbol{r}_{\boldsymbol{l}} - \boldsymbol{r}_{\boldsymbol{l}'})} \tag{8.19}$$

The summation

$$\sum_{\boldsymbol{l}'} e^{i(\boldsymbol{\tau}+\boldsymbol{q})\cdot(\boldsymbol{r}_{\boldsymbol{l}} - \boldsymbol{r}_{\boldsymbol{l}'})} = N \tag{8.20}$$

if $\boldsymbol{\tau} + \boldsymbol{q}$ belongs to the reciprocal lattice, otherwise

$$\sum_{\boldsymbol{l}'} e^{i(\boldsymbol{\tau}+\boldsymbol{q})\cdot(\boldsymbol{r}_{\boldsymbol{l}} - \boldsymbol{r}_{\boldsymbol{l}'})} = 0 \tag{8.21}$$

This can be written in a close form as

$$\sum_{\boldsymbol{l}'=1}^{N} e^{i(\boldsymbol{\tau}+\boldsymbol{q})\cdot(\boldsymbol{r}_{\boldsymbol{l}} - \boldsymbol{r}_{\boldsymbol{l}'})} = N \sum_{\boldsymbol{\tau}'} \delta_{\boldsymbol{\tau}', \boldsymbol{\tau}+\boldsymbol{q}} \tag{8.22}$$

The final expression of the Coulomb matrix is

$$C^{\mathrm{G}}_{\alpha\beta}(\boldsymbol{q}; \eta) = \frac{e^2 z_\kappa z_{\kappa'}}{v_a \varepsilon_0} \sum_{\boldsymbol{\tau}} \frac{(\tau_\alpha + q_\alpha)(\tau_\beta + q_\beta)}{|\boldsymbol{\tau} + \boldsymbol{q}|^2} e^{-|\boldsymbol{\tau}+\boldsymbol{q}|^2/4\eta} e^{i\boldsymbol{\tau}\cdot(\boldsymbol{r}_\kappa - \boldsymbol{r}_{\boldsymbol{\kappa}'})} \tag{8.23}$$

We still need to calculate the contribution of

$$\varphi^{\mathrm{H}}(\boldsymbol{r} - \boldsymbol{r}_{\boldsymbol{l}'\kappa'}) = \varphi^{\mathrm{C}}(\boldsymbol{r} - \boldsymbol{r}_{\boldsymbol{l}'\kappa'}) - \varphi^{\mathrm{G}}(\boldsymbol{r} - \boldsymbol{r}_{\boldsymbol{l}'\kappa'}) \tag{8.24}$$

Let us take, for the moment, the origin of the coordinates system in $\boldsymbol{r}_{\boldsymbol{l}'\kappa'}$. The expression we have to calculate is

$$/^{\mathrm{H}}(\boldsymbol{r}) = \frac{1}{4\pi \quad {}_0} \quad \frac{ez_{\kappa'}}{r} - \quad \frac{{}^{\mathrm{G}}(\boldsymbol{r} - \boldsymbol{r}\ )}{|\boldsymbol{r} - \boldsymbol{r}\ |} d^3\boldsymbol{r} \tag{8.25}$$

Writing explicitly the charge distribution,

$$/^{\mathrm{H}}(\boldsymbol{r}) = \frac{ez_{\kappa'}}{4\pi \quad {}_0} \quad \frac{1}{r} - \quad \frac{}{\pi} \quad {}^{3/2} \quad \frac{e^{-\eta|\boldsymbol{r}-\boldsymbol{r}'|^2}}{|\boldsymbol{r} - \boldsymbol{r}\ |} d^3\boldsymbol{r} \tag{8.26}$$

Let us call $\boldsymbol{R} = \boldsymbol{r} - \boldsymbol{r}\ $. We can imagine a sphere of radius r. The contribution of the charge within this sphere can be written as the contribution of a point charge located at the origin of coordinates, divided by $4\pi \ {}_0 r$ (from Gauss' Law). Thus, the previous equation can be transformed into

$$/^{\mathrm{H}}(\boldsymbol{r}) = \frac{ez_{\kappa'}}{{}_0} \quad \frac{}{\pi} \quad {}^{3/2} \quad \frac{1}{r} \quad {}_0 \quad R^2 e^{-\eta R^2} dR - \frac{1}{r} \quad {}_0^{\ r} R^2 e^{-\eta R^2} dR - \quad {}_r \quad Re^{-\eta R^2} dR \tag{8.27}$$

and thus

$$/^{\mathrm{H}}(\boldsymbol{r}) = \frac{ez_{\kappa'}}{{}_0} \quad \frac{}{\pi} \quad {}^{3/2} \quad \frac{1}{r} \quad {}_r \quad R^2 e^{-\eta R^2} dR - \quad {}_r \quad Re^{-\eta R^2} dR \tag{8.28}$$

The first integral,

$${}_r \quad R^2 e^{-\eta R^2} dR = \begin{matrix} u = R & du = dR \\ dv = Re^{-\eta R^2} dR & v = -\frac{1}{2} e^{-\eta R^2} \end{matrix} = \frac{r}{2} e^{-\eta r^2} + \frac{1}{2} \quad {}^{3/2} \quad {}_{\overline{\eta} r} \quad e^{-\zeta^2} d \tag{8.29}$$

The second integral has a primitive,

$${}_r \quad Re^{-\eta R^2} dR = v = -\frac{1}{2} e^{-\eta R^2} \quad {}_r \quad = \frac{1}{2} e^{-\eta r^2} \tag{8.30}$$

The expression for the potential is finally

$$/^{\mathrm{H}}(\boldsymbol{r}) = \frac{ez_{\kappa'}}{4\pi \quad {}_0 r} \frac{2}{\overline{\pi}} \quad {}_{\overline{\eta} r} \quad e^{-\zeta^2} d \quad = \frac{ez_{\kappa'}}{4\pi \quad {}_0 r} \mathrm{erfc}(\quad {}^{-} r) \tag{8.31}$$

The force constant

$${}^{\mathrm{H}}_{\alpha\beta}(\boldsymbol{l}\ \ , \boldsymbol{l}\ \ \ ) = ez_\kappa \frac{{}^2/}{x_{\alpha,\boldsymbol{l}\kappa} \quad x_{\beta,\boldsymbol{l}'\kappa'}} = -ez_\kappa \frac{{}^2/}{x_{\alpha,\boldsymbol{l}\kappa} \quad x_{\beta,\boldsymbol{l}\kappa}} = -ez_\kappa \frac{{}^2/}{X_\alpha \quad X_\beta} \tag{8.32}$$

where X_α is the cartesian component of $\boldsymbol{R} = \boldsymbol{r}_{\boldsymbol{l}\kappa} - \boldsymbol{r}_{\boldsymbol{l}'\kappa'}$

$$\overset{\mathrm{H}}{\alpha\beta}(\boldsymbol{l} \quad , \boldsymbol{l} \quad) = \frac{e^2 z_\kappa z_{\kappa'}}{4\pi \quad {}_0} \frac{\quad {}^2}{X_\alpha \quad X_\beta} \frac{\mathrm{erfc}(\quad {}^{-}R)}{R} \tag{8.33}$$

We need to calculate the derivatives of the complementary error function. Let us call

$$H(\quad {}^{-}R) = \frac{\frac{2}{\overline{\pi}} \quad \int_{\overline{\eta}R}^{\quad} e^{-\eta\varsigma^2} d}{R} \tag{8.34}$$

$$H \; (\quad {}^{-}R) = \frac{2}{R} \quad \frac{\overline{\quad}}{\pi} e^{-\eta R^2} - \frac{\mathrm{erfc}(\quad {}^{-}R)}{R^2} \tag{8.35}$$

The second derivative,

$$H \; (\quad {}^{-}R) = \frac{4 \quad {}^{3/2}}{\overline{\pi}} e^{-\eta R^2} + \frac{4}{R} \quad \frac{\overline{\quad}}{\pi} e^{-\eta R^2} + \frac{2}{R^3} \mathrm{erfc}(\quad {}^{-}R) \tag{8.36}$$

$$\frac{{}^2 H}{X_\alpha \quad X_\beta} = \frac{\quad}{X_\alpha} \quad \frac{R}{X_\beta} H \quad = \frac{{}^2 R}{X_\alpha \quad X_\beta} H \; + \frac{R}{X_\alpha} \frac{R}{X_\beta} H \tag{8.37}$$

$$\frac{R}{X_\alpha} = \frac{X_\alpha}{R} \tag{8.38}$$

$$\frac{{}^2 R}{X_\alpha \quad X_\beta} = \frac{\quad}{X_\alpha} \quad \frac{X_\beta}{R} \quad = \frac{\alpha\beta}{R} - \frac{X_\alpha X_\beta}{R^3} \tag{8.39}$$

$$\frac{{}^2 H}{X_\alpha \quad X_\beta} = \quad \frac{\alpha\beta}{R} - \frac{X_\alpha X_\beta}{R^3} \quad H \; + \frac{X_\alpha X_\beta}{R^2} H \tag{8.40}$$

Appendix B

The solution of the Boltzmann equation may be expanded in terms of higher-order derivatives of the classical hydrodynamic variables (Chapman-Enskog approach) or of higher-order fluxes (Grad approach). In this first case, the expansion parameter is , or equivalently $\tau c \cdot$. Since is of the order of $1/R$ with R the radius of the system, the ratio $/R$, *i. e.* the Knudsen number, may reach values equal or higher than 1. In this case, it seems logical that the solution of the Boltzmann equation should not be truncated at first-order.

From a mesoscopic approach, some authors have proposed to modify the thermal conductivity in terms of thermodynamic variables. This kind of models let us introduce in a more natural way non-equilibrium effects in situations where fluxes or gradients are high. The inclusion of these non-equilibrium effects cannot be easily made when using a microscopic approach, since the integral expressions are based mainly on equilibrium distribution functions and these are not valid in non-equilibrium situations. From this point of view, the best and most natural approach to include non-equilibrium effects are non-equilibrium thermodynamic models. In this work we include these effects using the framework of the Extended Irreversible Thermodynamics (EIT) [78].

When the system we are studying is very far from equilibrium it begins to be important considering higher order terms in the fluxes equations. While the Guyer-Krumhansl formalism stops at second order in the heat flux equation, the EIT goes beyond by including these terms as a consequence of non-local effects, which become more and more important when the size of our samples is smaller and smaller.

According to [78], non-local effects are included as a hierarchy of fluxes $J^{(0)}, J^{(1)}, J^{(2)}, \ldots, J^{(n)}$ with the vector $J^{(1)}$ standing for the heat flux $\boldsymbol{j}$, the second order tensor $J^{(2)}$ standing for the flux of the heat flux, etc. and being $J^{(0)} \equiv \quad T^{-1}$. Thus, we can write

$$T^{(-1)} - \quad {}_1\dot{J}^{(1)} + \cdot {}_1 \quad J^{(2)} = \mu_1 J^{(1)} \tag{8.41}$$

and generalizing

$$\cdot {}_{n-1} \quad J^{(n-1)} - \quad {}_n\dot{J}^{(n)} + \cdot {}_n \quad J^{(n+1)} = \mu_n J^{(n)} \tag{8.42}$$

being ${}_i, \cdot {}_i, \mu_i$ phenomenological coefficients related to the relaxation times, correlations lengths and transport coefficients respectively. If we consider an infinite number of fluxes and apply the Fourier's transform to the previous equations we obtain the following expres-

sion of the heat flux

$$\hat{\mathbf{j}}(\omega,\mathbf{q}) = -i\mathbf{q}\ \ (\omega,\mathbf{q})\hat{T}(\omega,\mathbf{q}) \tag{8.43}$$

where upper hats designate Fourier's transforms and $\ (\omega,\mathbf{q})$ is the following continued-fraction for the $\omega,\mathbf{q}$-dependent effective thermal conductivity

$$(T,\omega,\mathbf{q}) = \frac{{}_0(T)}{1+i\omega\tau_1+\frac{q^2\ell_1^2}{1+i\omega\tau_2+\frac{q^2\ell_2^2}{1+i\omega\tau_3+\frac{q^2\ell_3^2}{1+i\omega\tau_4+\dots}}}} \tag{8.44}$$

where ${}_0(T)$ is the bulk thermal conductivity in a hydrodynamic regime, that is ${}_{\text{coll}}$, $\tau_n = {}_n/\mu_n$ is the relaxation time and ${}_n$ is the correlation length defined through ${}^2_n = \cdot\,{}^2_n/\mu_n\mu_{n+1}$. Assuming that all the relaxation times and all the correlation lengths are equal ($\tau_1 = \cdots = \tau_n = \tau$ and ${}_1 = \cdots = {}_n = \ /2$) independently of the order of the flux, the continued fraction (8.44) reduces to the asymptotic limit

$$(T,\omega,\mathbf{q}) = \ {}_0(T)\frac{-(1+i\omega\tau)+\sqrt{(1+i\omega\tau)^2+q^2\ {}^2_2}}{\frac{1}{2}q^2\ {}^2_2} \tag{8.45}$$

this way, with this expression, we are considering an infinite number of terms.
In the steady state approximation $\omega = 0$, yielding

$$(T,q) = \ {}_0(T)\frac{\sqrt{1+q^2\ {}^2_2}-1}{\frac{1}{2}q^2\ {}^2_2} \tag{8.46}$$

and identifying $q = 2\pi/L_{\text{eff}}$ we finally have the expression

$$(T,\ /L_{\text{eff}}) = \ {}_0(T)\frac{L^2_{\text{eff}}}{2\pi^2\ {}^2}\qquad\sqrt{1+4\pi^2\frac{{}^2}{L^2_{\text{eff}}}}-1 \tag{8.47}$$

where we call

$$F(L_{\text{eff}}) = \frac{L^2_{\text{eff}}}{2\pi^2\ {}^2}\qquad\sqrt{1+4\pi^2\frac{{}^2}{L^2_{\text{eff}}}}-1 \tag{8.48}$$

a function depending only on the mean free path $\ $ and the dimension of the system through L_{eff}.

Appendix C

Let us show with a little algebra, that the definition of scattering rate is valid in both the RTA and the VM. In general, the collision term in the Boltzmann equation can be written, for elastic scattering, as

$$\frac{n_{\boldsymbol{q}}}{t}_{\text{scat}} = \frac{{}_{\boldsymbol{q}} - {}_{\boldsymbol{q}'}}{k_B T} P_{\boldsymbol{q}}^{\boldsymbol{q}'} d\boldsymbol{q} \,. \tag{8.49}$$

where $P_{\boldsymbol{q}}^{\boldsymbol{q}'}$ are the scattering transition rates from mode $\boldsymbol{q}$ to $\boldsymbol{q}'$ when the distribution functions correspond to equilibrium [36].

The integral (8.49) is expressing the fact that the relaxation process out of equilibrium is modified by the terms ${}_{\boldsymbol{q}} - {}_{\boldsymbol{q}'}$, *i. e.* they depend on the displacement with respect to equilibrium of the different colliding particles. Expression (8.49) can be generalized for an arbitrary number of colliding particles as

$$\frac{n_{\boldsymbol{q}}}{t}_{\text{scat}} = \frac{1}{k_B T} \quad {}_{\boldsymbol{q}} + \sum_{i=1}^{n} {}_{\boldsymbol{q}_i} - \sum_{j=1}^{m} {}_{\boldsymbol{q}'_j} \quad P_{\boldsymbol{q}\boldsymbol{q}_1 \ldots \boldsymbol{q}_n}^{\boldsymbol{q}'_1 \ldots \boldsymbol{q}'_m} \Big|_{\substack{i=1 \\ j=1}}^{\substack{m \\ n}} d\boldsymbol{q}_i d\boldsymbol{q}_j \quad , \tag{8.50}$$

where $\boldsymbol{q}$ collides with $\{\boldsymbol{q}_i\}$ giving as a result the modes $\boldsymbol{q}_j$. Expression (8.50) shows the main complexity of solving the BTE equation. The scattering term requires the actual distribution function inside an integral expression establishing BTE as an integro-differential equation. To reach an analytical solution, the approaches we have presented, RTA and VM, are usually based on the fact that the distribution used in the integral does not modify significantly the final result in some limiting situations. In RTA we assume that the system is close enough to equilibrium that the differences between using the actual form of the distribution or the equilibrium form in the collision integral (8.50) is small. This is equivalent to say that the only mode out of equilibrium is that with wavevector $\boldsymbol{q}$ and that the other modes stay in equilibrium. Thus

$${}_{\boldsymbol{q}_i} = {}_{\boldsymbol{q}'_j} = 0 \qquad \boldsymbol{q}_i = \boldsymbol{q}, \quad \boldsymbol{q}_j = \boldsymbol{q} \quad . \tag{8.51}$$

In this case,

$$\frac{n_{\boldsymbol{q}}}{t}_{\text{scat}} = \frac{{}_{\boldsymbol{q}}}{k_B T} \quad P_{\boldsymbol{q}\boldsymbol{q}_1 \ldots \boldsymbol{q}_n}^{\boldsymbol{q}'_1 \ldots \boldsymbol{q}'_m} \Big|_{\substack{i=1 \\ j=1}}^{\substack{m \\ n}} d\boldsymbol{q}_i d\boldsymbol{q}_j \quad . \tag{8.52}$$

If we substitute Eq. (4.53) in (8.52) we have

$$\frac{n_{\boldsymbol{q}}}{t}_{\text{scat}} = \frac{n_{\boldsymbol{q}} - n^0_{\boldsymbol{q}}}{n^0_{\boldsymbol{q}}(n^0_{\boldsymbol{q}}+1)} \quad P^{\boldsymbol{q}'_1 \cdot\cdot \boldsymbol{q}'_m}_{\boldsymbol{q}\boldsymbol{q}_1 \ldots \boldsymbol{q}_n} \quad \sum_{\substack{i=1 \\ j=1}}^{\substack{m \\ n}} d\boldsymbol{q}_i d\boldsymbol{q}_j \quad . \tag{8.53}$$

Thus, we can define the relaxation time $\tau_{\boldsymbol{q}}$ of mode $\boldsymbol{q}$ as

$$\frac{1}{\tau_{\boldsymbol{q}}} = \frac{1}{n^0_{\boldsymbol{q}}(n^0_{\boldsymbol{q}}+1)} \quad P^{\boldsymbol{q}'_1 \cdot\cdot \boldsymbol{q}'_m}_{\boldsymbol{q}\boldsymbol{q}_1 \ldots \boldsymbol{q}_n} \quad \sum_{\substack{i=1 \\ j=1}}^{\substack{m \\ n}} d\boldsymbol{q}_i d\boldsymbol{q}_j \tag{8.54}$$

and so, we obtain the BTE solution in the well known RTA approach

$$\frac{n_{\boldsymbol{q}}}{t}_{\text{scat}} = -\frac{n_{\boldsymbol{q}} - n^0_{\boldsymbol{q}}}{\tau_{\boldsymbol{q}}} \quad . \tag{8.55}$$

We can make a similar assumption when normal scattering is the dominant relaxation process. The only change is that the distribution function to which the actual distribution function will relax is that given by Eqs. (4.56)-(4.57). In that case, the condition (8.51) cannot be fulfilled locally by each mode, but in the linear regime not much error is made in Eq. (8.50) [36] if we consider that

$$_{\boldsymbol{q}_i} P^{\boldsymbol{q}'_1 \cdot\cdot \boldsymbol{q}'_m}_{\boldsymbol{q}\boldsymbol{q}_1 \ldots \boldsymbol{q}_n} d\boldsymbol{q}_i = \quad _{\boldsymbol{q}'_j} P^{\boldsymbol{q}'_1 \cdot\cdot \boldsymbol{q}'_m}_{\boldsymbol{q}\boldsymbol{q}_1 \ldots \boldsymbol{q}_n} d\boldsymbol{q}_i = 0 \qquad i, j \quad . \tag{8.56}$$

This condition leads to the same result as that obtained near equilibrium (8.53)-(8.54), since condition (8.56) applied to Eq. (8.50) cancels all the terms except the first one, as condition (8.51) also holds. Thus, we can use the same expression for the scattering rates in both limiting situations, near equilibrium and in non-equilibrium, despite of the very different nature of the two situations. Note that by using Eqs. (4.54)-(4.55) and (4.56)-(4.57) in Eq. (8.56) we are not stating that resistive processes are suppressed. In fact, $P^{\boldsymbol{q}'_1 \cdot\cdot \boldsymbol{q}'_m}_{\boldsymbol{q}\boldsymbol{q}_1 \ldots \boldsymbol{q}_n}$ are the transition rates for all the resistive scattering processes. We are only considering that the collision integral (8.56) does not change significantly when one uses the actual form of the distribution function or the proposed approximations in the corresponding regimes.

Bibliography

[1] H. Rauh, R. Geick, H. Kohler, N. Nucker, and N. Lehner. Generalised phonon density of states of the layer compounds bi_2se_3,bi_2te_3, sb_2te_3, and $bi_2(te_{0.5}se_{0.5})_3$, $(bi_{0.5}sb_{0.5})_2te_3$. *Journal of Physics C: Solid State Physics*, 14:2705, 1981.

[2] B. Qiu and X. Ruan. Molecular dynamics simulation of lattice thermal conductivity of bismuth telluride using two-body interatomic potentials. *Physical Review B*, 80:165203, 2009.

[3] D. M. Rowe. *CRC Handbook of thermoelectricity.* CRC Press, 1995.

[4] W. Weber. New bond-charge model for the lattice dynamics of diamond-type semiconductors. *Physical Review Letters*, 33:371, 1974.

[5] J. Fourier. *Théorie Analytique de la chaleur.* Firmin Didot Père et Fils, Paris, 1822.

[6] R. E. Peierls. *Annalen der Physik*, 3:1055, 1929.

[7] H. B. G. Casimir. Note on the conduction of heat in crystals. *Physica*, 5:595, 1938.

[8] D. Li, Y. Wu, P. Kim, L. Shi, P. Yang, and A. Majumdar. Analysis of lattice thermal conductivity. *Applied Physics Letters*, 83:2934, 2003.

[9] M. Wingert, Z. C. Y. Chen, E. Dechaumphai, J. Moon, J. Kim, J. Xiang, and R. Chen. Thermal conductivity of ge and ge-si core-shell nanowires in the phonon confinement regime. *Nano Letters*, 11:5507, 2011.

[10] I. Ponomareva, D. Srivastava, and M. Menon. Thermal conductivity in thin silicon nanowires: phonon confinement effect. *Nano Letters*, 7:1155, 2007.

[11] A. A. Balandin, S. Ghosh, W. Bao, I. Calizo, D. Teweldebrhan, F. Miao, and C. N. Lau. Superior thermal conductivity of single-layer graphene. *Nano Letters*, 8:902, 2008.

[12] Z. M. Zhang. *Nano/microscale heat transfer.* McGraw-Hill Nanoscience and Technology, 2007.

[13] M. Prunnila and J. Meltaus. Acoustic phonon tunneling and heat transport due to evanescent electric fields. *Physical Review Letters*, 105:125501, 2010.

[14] F. X. Alvarez and D. Jou. Memory and nonlocal effects in heat transport: from diffusive to ballistic regimes. *Applied Physics Letters*, 90:083109, 2007.

[15] N. W. Ashcroft and N. D. Mermin. *Solid state physics.* Saunders College, Philadelphia, 1976.

[16] G. Chen. *Nanoscale energy transport and conversion.* Oxford University Press, 2005.

[17] G. P. Srivastava. *The physics of phonons.* Adam Hilger, Bristol, Philadelphia and New York, 1990.

[18] P. Debye. Zur theorie der spezifischen wärmen. *Annalen der Physik*, 39:789, 1912.

[19] C. Kittel. *Introduction to Solid State Physics.* John Wiley and Sons, 1996.

[20] A. Einstein. Die plancksche theorie der strahlung und die theorie der spezifischen wärme. *Annalen der Physik*, 22:180, 1907.

[21] P. Brüesch. *Phonons: Theory and experiments I.* Springer Berlin Heidelberg, 1982.

[22] J. Callaway. Model for lattice thermal conductivity at low temperatures. *Physical Review*, 113:1046, 1959.

[23] M. G. Holland. Analysis of lattice thermal conductivity. *Physical Review*, 132:2461, 1963.

[24] M. Asen-Palmer, K. Bartkowski, E. Gmelin, M. Cardona, A. P. Zhernov, A. V. Inyushkin, A. Taldenkov, V. I. Ozhogin, K. M. Itoh, and E. E. Haller. Thermal conductivity of germanium crystals with different isotopic compositions. *Physical Review B*, 56:9431, 1997.

[25] J. Zou and A. Balandin. Phonon heat conduction in a semiconductor nanowire. *Journal of Applied Physics*, 89:2932, 2001.

[26] P. Chantrenne, J.L. Barrat, X. Blase, and J.D.Gale. An analytical model for the thermal conductivity of silicon nanostructures. *Journal of Applied Physics*, 97:104318, 2005.

[27] D. T. Morelli, J. P. Heremans, and G. A. Slack. Estimation of the isotope effect on the lattice thermal conductivity of group iv and group iii-v semiconductors. *Physical Review B*, 66:195304, 2002.

[28] N. Mingo. Calculation of si nanowire thermal conductivity using complete phonon dispersion relations. *Physical Review B*, 68:113308, 2003.

[29] B. Allison. `http://www.smf.phy.cam.ac.uk`.

[30] H. Fröhlich. Long-range coherence and energy storage in biological systems. *International Journal of Quantum Chemistry*, 11:641, 1968.

[31] J. de Launay. *Solid state physics II.* Ed. F. Seitz and D. Turnbull, New York: Academic, 1956.

[32] J. W. Rohlf. *Modern physics physics from A to Z.* Wiley, 1994.

[33] Hyperphysics. `http://hyperphysics.phy-astr.gsu.edu/hbase/hph.html`.

[34] R. Berman. *Thermal conduction in solids.* Oxford University Press, 1976.

[35] R. E. Peierls. *Quantum theory of solids.* Oxford University Press, 1955.

[36] J. M. Ziman. *Electrons and phonons.* Clarendon Press, Oxford, 1979.

[37] H. Struchtrup. *Macroscopic transport equations for rarefied gas flows.* Springer Verlag, Berlin Heidelberg, 2005.

[38] L. Boltzmann. Weitere studien über das wärmegleichgewicht unter gasmolekülen. *Sitzungsberichte der Akademie der Wissenschaften, Wien*, 66:275, 1872.

[39] W. Li, N. Mingo, L. Lindsay, D. A. Broido, D. A. Stewart, and N. A. Katcho. Thermal conductivity of diamond nanowires from first-principles. *Physical Review B*, 85:195436, 2012.

[40] P. P. Ewald. Zur begründung der kristalloptik. *Annalen der Physik*, 54(519), 1917.

[41] P. P. Ewald. The calculation of optical and electrostatic grid potential. *Annalen der Physik*, 64(253), 1921.

[42] W. Weber. Adiabatic bond charge model for the phonons in diamond, si, ge, and gray-sn. *Physical Review B*, 15:4789, 1977.

[43] J. Camacho and A. Cantarero. Phonon dispersion of wurtzite cds: the bond charge model. *Physica Status Solidi (b)*, 215:181, 1999.

[44] R. Tubino, L. Piseri, and G. Zerbi. Lattice dynamics and spectroscopic properties by a valence force potential of diamond-like crystals: C, si, ge, and sn. *The Journal of Chemical Physics*, 56:1022, 1972.

[45] K. Kunc. Lattice-dynamics of several compounds having zinc blend structure. *Annales de Physique*, 8:22, 1973-74.

[46] A. Valentin, J. See, S. Galdin-Retailleau, and P. Dollfus. Study of phonon modes in silicon nanocrystals using the adiabatic bond charge model. *Journal of Physics: Condensed Matter*, 20:145213, 2008.

[47] W. Setyawan and S. Curtarolo. High-throughput electronic band structure calculations: Challenges and tools. *Computational Material Science*, 49:299, 2010.

[48] J.L. Warren, J.L. Yarnell, G. Dolling, and R.A. Cowley. Lattice dynamics of diamond. *Physical Review*, 158:805, 1967.

[49] G. Nilsson and G. Nelin. Study of the homology between silicon and germanium by thermal-neutron spectrometry. *Physical Review B*, 6:3777, 1972.

[50] D. Price, J. Rowe, and R. Nicklow. Lattice Dynamics of Grey Tin and Indium Antimonide. *Physical Review B*, 3:1268, 1971.

[51] B. Huang and M. Kaviany. Ab initio and molecular dynamics predictions for electron and phonon transport in bismuth telluride. *Physical Review B*, 77:125209, 2008.

[52] J. R. Wiese and L. Muldawer. *Journal Physics and Chemistry of Solids*, 15:13, 1960.

[53] M. H. Francombe. Structure-cell data and expansion coefficients of bismuth telluride. *British Journal of Applied Physics*, 9:415, 1958.

[54] P. Debye. *Der Vorträge über die kinetische Theorie der Materie und Elektrizität.* Teubner, Berlin, 1914.

[55] P. Carruthers. Theory of thermal conductivity of solids at low temperatures. *Reviews of Modern Physics*, 33:92, 1961.

[56] L. Van Hove. *Physica*, 21:517, 1955.

[57] I. Pomeranchuk. On the thermal conductivity of dielectrics. *Physical Review*, 60:820, 1941.

[58] C. Herring. Role of low-energy phonons in thermal conduction. *Physical Review*, 95:954, 1954.

[59] P. G. Klemens. The thermal conductivity of dielectric solids at low temperatures (theoretical). *Proceedings of the Royal Society (London)*, A208:108, 1951.

[60] G. Leibfried and E. Schlömann. Heat Conduction in Electrically Insulating Crystals. *Nachrichten Akad. Wiss. Göttingen. Math. Phys. Klasse. 2a*, 71, 1954.

[61] A. Ward and D. A. Broido. Intrinsic phonon relaxation times from first-principles studies of the thermal conductivities of si and ge. *Physical Review B*, 81:085205, 2010.

[62] M. Kazan, G. Guisbiers, S. Pereira, M. R. Correia, P. Masri, A. Bruyant, S. Volz, and P. Royer. Thermal conductivity of silicon bulk and nanowires: Effects of isotopic composition, phonon confinement, and surface roughness. *Journal of Applied Physics*, 107:083503, 2010.

[63] P. G. Klemens. The scattering of low-frequency lattice waves by static imperfections. *Proceedings of the Royal Society A*, 68:1113, 1955.

[64] S. Tamura. Model for lattice thermal conductivity at low temperatures. *Physical Review B*, 27:858, 1983.

[65] A. V. Inyushkin, A. N. Taldenkov, A. M. Gibin, A. V. Gusev, and H. J. Pohl. On the isotope effect in thermal conductivity of silicon. *Physica Status Solidi (c)*, 1:2995, 2004.

[66] A. V. Inyushkin. Thermal conductivity of isotopically modified silicon: Current status of research. *Inorganic Materials*, 38:427, 2002.

[67] C. R. Tellier and A. J. Tosser. *Size effects in thin films.* Elsevier, Amsterdam, 1982.

[68] M. I. Flik and C. L. Tien. Size-effect on the thermal conductivity of high-t thin-film semiconductors. *Journal of Heat Transfer*, 112:872, 1990.

[69] A. L. Moore, S. K. Saha, R. S. Prasher, and L. Shi. Phonon backscattering and thermal conductivity suppression in sawtooth nanowires. *Applied Physics Letters*, 93:083112, 2008.

[70] A. I. Hochbaum, R. Chen, R. D. Delgado, W. Liang, E. C. Garnett, M. Najarian, A. Majumdar, and P. Yang. Enhanced thermoelectric performance of rough silicon nanowires. *Nature*, 451:163, 2008.

[71] M. Asheghi, M. N. Touzelbaev, K. E. Goodson, Y. K. Leung, and S. S. Wong. Temperature-dependent thermal conductivity of single-crystal silicon layers in soi substrates. *Journal of Heat Transfer*, 120:30, 1998.

[72] P. G. Klemens. Thermal resistance due to point defects at high temperatures. *Physical Review*, 119:507, 1960.

[73] P. B. Allen. Improved callaway model for lattice thermal conductivity. *Physical Review B*, 88:144302, 2013.

[74] C. J. Glassbrenner and G. A. Slack. Thermal conductivity of silicon and germanium from 3k to the melting point. *Physical Review*, 134:A1058, 1964.

[75] K. C. Hass, M. A. Tamor, T. R. Anthony, and W. F. Banholzer. Lattice dynamics and raman spectra of isotopically mixed diamond. *Physical Review B*, 45:7171, 1992.

[76] T. H. Geballe and G. W. Hull. Isotopic and other types of thermal resistance in germanium. *Physical Review*, 110:773, 1958.

[77] C. De Tomas, A. Cantarero, A. F. Lopeandia, and F. X. Alvarez. From kinetic to collective behavior in thermal transport on semiconductors and semiconductor nanostructures. *Journal of Applied Physics*, 115:164314, 2014.

[78] D. Jou, J. Casas-Vazquez, and G. Lebon. *Extended Irreversible Thermodynamics.* Springer, Berlin, 1993.

[79] M. Kohler. Behandlung von nichtgleichgewichtsvorgngen mit hilfe eines extremalprinzips. *Zeitschrift für Physik*, 124:772, 1948.

[80] M. Kohler. Transporterscheinungen im elektronengas. *Zeitschrifstung der Physik*, 125:679, 1949.

[81] E. H. Sondheimer. The theory of the transport phenomena in metals. *Proceedings of the Royal Society A*, 203:75, 1950.

[82] D.A. Broido, M. Malorny, G. Birner, N. Mingo, and D.A. Stewart. Intrinsic lattice thermal conductivity of semiconductors from first principles. *Applied Physics Letters*, 91(23):231922, 2007.

[83] L. Lindsay, D. A. Broido, and T. L. Reinecke. Phonon-isotope scattering and thermal conductivity in materials with a large isotope effect: A first-principles study. *Physical Review B*, 88:144306, 2013.

[84] G. Fugallo, M. Lazzeri, L. Paulatto, and F. Mauri. Ab initio variational approach for evaluating lattice thermal conductivity. *Physical Review B*, 045430:88, 2013.

[85] L. Lindsay, D. A. Broido, and T. L. Reinecke. Ab initio thermal transport in compound. *Physical Review B*, 87:165201, 2013.

[86] J. A. Krumhansl. Thermal conductivity of insulating crystals in the presence of normal processes. *Proceedings of the Royal Society*, 85:921, 1965.

[87] R. A. Guyer and J. A. Krumhansl. Solution of the linearized phonon boltzmann equation. *Physical Review*, 148:766, 1966.

[88] R. A. Guyer and J. A. Krumhansl. Thermal conductivity, second sound, and phonon hydrodynamic phenomena in nonmetallic crystals. *Physical Review*, 148:778, 1966.

[89] R. A. Guyer and E. M. Hogan. The thermal conductivity of oriented single crystals of hcp helium 4. *Solid State Communication*, 5:909, 1967.

[90] C. C. Ackerman and R. A. Guyer. Three-phonon processes in solid helium crystals. *Solid State Communications.*, 5:671, 1967.

[91] L. P. Mezov-Deglin. *Soviet Physics - JETP*, 22:47, 1966.

[92] F. X. Alvarez and D. Jou. Size and frequency dependence of effective thermal conductivity in nanosystems. *Journal of Applied Physics*, 103:094321, 2008.

[93] F. X. Alvarez, D. Jou, and A. Sellitto. Phonon hydrodynamics and phonon-boundary scattering in nanosystems. *Journal of Applied Physics*, 105:014317, 2009.

[94] D. P. Sellan, J. E. Turney, A. J. H. McGaughey, and C. H. Amon. Cross-plane phonon transport in thin films. *Journal of Applied Physics*, 108:113524, 2010.

[95] M. Shao, D. Duo Duo Ma, and S.T. Lee. Silicon nanowires synthesis, properties, and applications. *European Journal of Inorganic Chemistry*, page 4264, 2010.

[96] Z. Tian, K. Esfarjani, J Shiomi, A.S. Henry, and G. Chen. On the importance of optical phonons to thermal conductivity in nanostructures. *Journal of Applied Physics*, 99:053122, 2011.

[97] S. Barman and G. Srivastava. Temperature dependence of the thermal conductivity of different forms of diamond. *Journal of Applied Physics*, 101:123507, 2007.

[98] H. Ehrenreich, F. Seitz, D. Turnbull, and G. Slack. The Thermal Conductivity of Nonmetallic Crystals. *Solid State Physics*, 34:1, 1979.

[99] A. Ward, D. A. Broido, D. A. Stewart, and G. Deinzer. Ab initio theory of the lattice thermal conductivity in diamond. *Physical Review B*, 80:125203, 2009.

[100] D. Onn, A. Witek, Y. Qiu, T. Anthony, and W. Banholzer. Some aspects of the thermal conductivity of isotopically enriched diamond single crystals. *Physical Review Letters*, 68:2806, 1992.

[101] L. Wei, P.K. Kuo, R.L. Thomas, T. Anthony, and W. Banholzer. Thermal conductivity of isotopically modified single crystal diamond. *Physical Review Letters*, 70:3764, 1993.

[102] T. Ruf, R. W. Henn, M. Asen-Palmer, E. Gmelin, M. Cardona, H.-J. Pohl, G. G. Devyatych, and P. G. Sennikov. Thermal conductivity of isotopically enriched silicon. *Solid State Communication*, 115:243, 2000.

[103] J. R. Olson, R. O. Pohl, J. W. Vandersande, A. Zoltan, T. R. Anthony, and W. F. Banholzer. Thermal conductivity of diamond between 170 and 1200 k and the isotope effect. *Physical Review B*, 47:14850, 1993.

[104] T. M. Tritt and M. A. Subramanian. Thermoelectric materials, phenomena, and applications: a bird's eye view. *MRS Bulleting*, 31:188, 2006.

[105] M. Muoz-Rojo, S. Grauby, O. Caballero-Calero, and M. Martin-Gonzalez. Fabrication of bi2te3 nanowire arrays and thermal conductivity measurement by 3w-scanning thermal microscopy. *Journal of Applied Physics*, 113:054308, 2013.

[106] C. Chiritescu, C. Mortensen, D. G. Cahill, and P. Zschack. Lower limit to the lattice thermal conductivity of nanostructured bi2te3-based materials. *Journal of Applied Physics*, 106:073503, 2009.

[107] I. Pomeranchuk. *J. Phys. (U.S.S.R.)*, 6:237, 1942.

[108] M. Muoz-Rojo, O. Caballero-Calero, A. F. Lopeandia, J. Rodriguez-Viejo, and M. Martin-Gonzalez. Review on measurements techniques of transport properties of nanowires. *Nanoscale*, 5:11526, 2013.

[109] B. Qiu, L. Sun, and X. Ruan. Lattice thermal conductivity reduction in bismuth telluride quantum wires with smooth and rough surfaces: A molecular dynamics study. *Physical Review B*, 83:035312, 2011.

[110] D.A. Borca-Tasciuc, G. Chen, A. Prieto, M.S. Martin-Gonzalez, A. Stacy, T. Sands, M.A. Ryan, and J. P. Fleurial. Thermal properties of electrodeposited bismuth telluride nanowires embedded in amorphous alumina. *Applied Physics Letters*, 85:6001, 2004.

[111] A. Mavrokefalos, A.L. Moore, M. T. Pettes, L. Shi, W. Wang, and X. Li. Thermoelectric and structural characterizations of individual electrodeposited bismuth telluride nanowires. *Journal of Applied Physics*, 105:104318, 2009.